AC SELF-BEARING MOTORS WITH A BRIDGE CONFIGURED WINDING

WEE KEONG KHOO

Doctor of Philosophy

THE UNIVERSITY OF ASTON IN BIRMINGHAM

August 2002

The University of Aston in Birmingham

AC Self-Bearing Motors with a Bridge Configured Winding

Wee Keong Khoo

Doctor of Philosophy

2002

SUMMARY

Magnetic levitation bearings eliminate friction, wear and the need for lubrication and so have high speed capability and potential for vibration control. One noteworthy development in the realm of magnetic levitation is the self-bearing or bearingless motor – an electromagnetic machine that supports its own rotor by way of magnetic forces generated by windings on its stator. Accordingly, various winding schemes have been proposed to accomplish the task of force production.

This thesis proposes a novel concept of winding based on a bridge connection for polyphase self-bearing rotating electrical machines with the following advantages:

- the connection uses a single set of windings and thus power loss is relatively low when compared with self-bearing motors with conventional dual set of windings.
- the motor and levitation controls are segregated such that only one motor inverter is required for the normal torque production and levitation forces are produced by using auxiliary power supplies of relatively low current and voltage rating. The usual way of controlling the motor is retained.
- there are many variant winding schemes to meet special needs.
- independent power supplies for levitation control offer redundancy for fault tolerance.

This thesis dwells specifically on the conceptual design and implementation of the proposed single set of windings scheme. The new connection has been verified to exhibit the characteristics of a self-bearing motor via coupled-field finite element analysis: results are crosschecked analytically. Power loss and other aspects such as cost, design and implementation are compared to support the newly proposed connection as a potential alternative to present designs.

Keywords: SELF-BEARING MOTOR, BEARINGLESS MOTOR, MAGNETIC BEARING, MAGNETIC LEVITATION, MAGNETIC SUSPENSION, BRIDGE CONNECTION.

To my family

and

Ingrid Caroline Hayes

ACKNOWLEDGEMENTS

I am profoundly indebted to my principal supervisor, Prof. W.T. Norris, for his patie enthusiasm and unwavering supervision that propelled me through this research. Not has he guided me within the subject of electrical engineering but also enlightened me on British literatures and history.

My gratitude is extended to Dr. Roger Fittro and Prof. Seamus Garvey for their unse and never ceasing contributions even after leaving the department. It has been my privi to collaborate with them since the very first day of my research in Aston.

I am also grateful to Dr. Nagi Fahmi who offered me his invaluable advice and gene help during the course of my research.

Last but not least, I thank the School of Engineering and Applied Science for funding providing the facilities for this research.

CONTENTS

(I) LIST OF SYMBOLS AND ABBREAVIATIONS

Symbols	Description
$A_{coilside}$	coil side area (m^2)
A_{cond}	area of a copper conductor (m^2)
A_p	cross-sectional area of a pole (m^2)
A_{slot}	slot area (m^2)
B, B_{Gap}	magnetic flux density (T)
B_0	permanent magnet remanence (T)
B_0	flux density adjacent to the insulation between laminations (T)
B_{AG}	air gap flux density due to motor current and permanent magnet (T)
B_{AGMax}	maximum air gap flux density due to motor current and permanent magnet (T
B_{Lev}	levitation-producing component of magnetic flux density (T)
$B_{Lev(X)}$	levitation flux density in x-direction (T)
$B_{LevMax(X)}$	maximum levitation flux density in x-direction (T)
$B_{Lev(Y)}$	levitation flux density in y-direction (T)
$B_{LevMax(Y)}$	maximum levitation flux density in y-direction (T)
B_{MC}	flux density produced by motor current (T)
B_{MCMax}	maximum flux density produced by motor current (T)
B_n	normal component of magnetic flux density (T)
B_{PM}	permanent magnet flux density (T)
B_{PMMax}	maximum permanent magnet flux density (T)
B_t	tangential component of magnetic flux density (T)
B_{Torq}	torque-producing component of magnetic flux density (T)
$B_{TorqMax}$	maximum flux density of the torque component (T)
$B_{Total(Y)}$	total magnetic flux density in the air gap, y-direction (T)
C_f	coil fill factor
d	lamination thickness (m)
E_e	bus voltage (V)
E_f	field excitation voltage (V)
$E_{\phi\text{-}n}$	phase to neutral generated voltage (V)
f	frequency (Hz)
f	force slew rate (N/s)
F, F_0	force (N)
F_{max}	maximum force (N)
F_{min}	minimum force (N)
F_{mm}	magnetomotive force (A)
F_{mml1}	levitation MMF 1 (A)
F_{mml2}	levitation MMF 2 (A)
F_{mmlR}	resultant of levitation MMFs 1 and 2 (A)
F_{mmr}	maximum fundamental rotor MMF (A)
F_{mms}	maximum fundamental stator MMF (A)
F_D	disturbance force (N)
F_{net}	net force (N)
F_s	step input force (N)
F_x	force in the x-direction (N)
F_y	force in the y-direction (N)
g	gravity (m/s^2)
g_{max}	maximum air gap length (m)
g_{min}	minimum air gap length (m)

g_n	air gap size at tooth number n (m)
g_o	air gap size (m)
g_x	air gap size in x-direction (m)
g_z	air gap size in z-direction (m)
G_s	sensor gain (V/m)
H	magnetic field intensity (A/m)
H_n	normal component of magnetic field intensity (A/m)
H_{PM}	magnetic coercivity (A/m)
H_t	tangential component of magnetic field intensity (A/m)
I	current (A)
I_{0L}	bias current of the left bearing (A)
I_{0R}	bias current of the right bearing (A)
I_B	bias current (A)
I_K	vector sum of motor and levitation currents
I_{Lev}	levitation current (A)
I_{LevMax}	maximum levitation current (A)
I_{MC}	motor current (A)
I_{MCMax}	maximum motor current (A)
I_n	current in n coil (A)
i_p , I_p	perturbation current (A)
i_{pxL_n}, i_{pxR_n}	perturbation currents for x-direction in the left and right bearing respectively (A). $n=1, 2$ denotes diametrically opposite poles of each bearing.
i_{pyL_n}, i_{pyR_n}	perturbation currents for y-direction in the left and right bearing respectively (A). $n=1, 2$ denotes diametrically opposite poles of each bearing.
i_{pz}	perturbation current for axial or z-direction
I_{RMS}	root mean square current (A)
j	complex number operator $=\sqrt{-1}$
K_i, K_I	actuator gain (N/A)
$K_{i_{pxL}}$	actuator gain in x-direction for a left bearing (N/A)
$K_{i_{pz}}$	actuator gain in z-direction (N/A)
K_p	proportional controller gain
K_T	torque constant (Nm/A)
K_x	open loop stiffness or negative stiffness in x-direction (N/m)
K_{xL}	open loop stiffness in x-direction of the left bearing (N/m)
K_y	open loop stiffness or negative stiffness in y-direction (N/m)
K_z	open loop stiffness or negative stiffness in z-direction (N/m)
K_{zL}	open loop stiffness in z-direction of the left bearing (N/m)
l	rotor length or axial length (m)
l	mean path of the flux loop (m)
l_{coil}	approximate length of one turn of coil (m)
l_h	axial length between the centre of the rotor and the centre of the cone (m)
l_{PM}	permanent magnet radial thickness (m)
L	inductance (H)
L_{Bridge}	inductance of a single bridge (H)
L_c	coil inductance (H)
$L_{Mtrphase}$	inductance in motor phase coils (H)
m	mass (kg)
M_{Lev}	matrix of MMF drop due to levitation current
M_{MC}	matrix of MMF drop due to motor current
M_{PM}	matrix of an equivalent MMF drop due to permanent magnet
n	integer

n	tooth number
N	north magnetic pole
N	number of coil turns
$N_{coilside}$	number of coil side
N_{Lev}	number of turns of the levitation coil
N_m	motor winding
N_{MC}	number of turns of the motor coil
N_{PPL}	pole-pair number of the levitation-producing component
N_{PPT}	pole-pair number of the torque-producing component
N_S	number of stator teeth
N_{slot}	number of conductor per slot
N_x	position control winding for x-direction
N_y	position control winding for y-direction
p	number of pole-pairs
P	power (W)
P_{loss}	power loss (W)
r	rotor radius (m)
r_{cond}	radius of a copper conductor (m)
r_{sta_i}	stator inner radius (m)
r_{sta_o}	stator outer radius (m)
R	resistance (Ω)
R_{Bridge}	resistance of a single bridge connection (Ω)
R_c, R_{coil}	coil resistance (Ω)
R_e	external circuitry resistance (Ω)
R_K	resistance of the copper per coil side (Ω)
R_{Lev}	reluctance matrix due to levitation field
R_{MC}	reluctance matrix due to motor field
$R_{Mtrphase}$	resistance of a single phase (Ω)
R_{PM}	reluctance matrix due to permanent magnet field
s	Laplace operator
S	south magnetic pole
t	time (s)
T	torque (Nm)
T_d	derivative controller gain
T_i	integral controller gain
T_{max}	maximum torque (Nm)
T_{min}	minimum torque (Nm)
v_0	initial velocity (m/s)
V	supply voltage (V)
V_{Bridge}	voltage across bridge (V)
$V_{\phi\text{-}n}$	phase to neutral supply voltage (V)
W	stored energy (J)
W_T	total stored energy (J)
x	rotor displacement in the horizontal or x-direction (m)
x_0	maximum permissible rotor displacement (m)
X	reactance (Ω)
X_d	direct-axis reactance (Ω)
X_q	quadrature-axis reactance (Ω)
y	rotor displacement in the vertical or y-direction (m)
z	rotor displacement in the axial or z-direction (m)

α	cone angle in a conical magnetic bearing (°)
β	sensitivity of the air gap to rotor displacement
γ	desired angle of lateral force (rad or °)
δ	load angle (rad or °)
ε	eccentricity (m)
θ	angular position (rad or °)
θ	power factor angle (rad or °)
θ_h	half angle between two poles (°)
θ_{l1}	angle of levitation MMF axis 1 measured from the horizontal axis (rad or °)
θ_{l2}	angle of levitation MMF axis 2 measured from the horizontal axis (rad or °)
θ_{lr}	angle between levitation MMF axis 1 and resultant MMF axis (rad or °)
θ_{lR}	angle of resultant of levitation MMF axes 1 and 2 measured from the horizontal axis (rad or °)
θ_x	angle of rotation about x-axis (rad)
θ_y	angle of rotation about y-axis (rad)
λ	phase angle of the air gap flux density due to motor current and permanent magnet (rad or °)
μ	magnetic permeability = $\mu_0\mu_r$ (H/m)
μ_0	permeability of free space (H/m)
μ_{PM}	relative permeability of permanent magnet
μ_r	relative permeability
μ_{rot}	relative permeability of rotor
μ_{sta}	relative permeability of stator
ρ	coil resistivity (Ωm)
σ	electrical conductivity (S/m)
σ_n	normal stress (N/m^2)
σ_t	tangential stress (N/m^2)
σ_y	y-direction component of stress (N/m^2)
φ_e	electrical torque angle (rad or °)
φ_m	mechanical torque angle (rad or °)
Ψ	flux linkage (Wb)
Ψ_T	total flux linkage (Wb)
ω	electrical angular frequency (rad/s)
ω_s	rotor speed (rad/s or rpm)

Abbreviations	**Description**
2D	2-Dimensional
AC	Alternating Current (A)
AMB	Active Magnetic Bearing
DC	Direct Current (A)
DS	Dual Set of Windings
DSP	Digital Signal Processing
EMF	Electromotive Force (V)
FEA	Finite Element Analysis
GUI	Graphical User Interface
LVAD	Left Ventricular Assist Devices
MAGLEV	Magnetic Levitation

MMF	Magnetomotive Force (A)
MST	Maxwell Stress Tensor
NASA	National Aeronautics & Space Administration
PI	Proportional and Integral
PID	Proportional, Integral and Derivative
pu	per unit
RMS	Root Mean Square
SS	Single Set of Windings
UMP	Unbalanced Magnetic Pull (N)
VW	Virtual Work

(II) LIST OF FIGURES AND TABLES

Table	**Title**	**Page**

CHAPTER 1

INTRODUCTION

1.1 Definition of the research area of interest

The term "self-bearing motor" is related to an electrical machine that levitates its own rotor. In addition to the normal torque-producing function it produces a lateral or radial force perpendicular to the axis which provides the levitation and can counter rotor unbalance. The main theme of this thesis is to present a novel concept of winding connection for polyphase self-bearing rotating machines. This first chapter is an introduction to magnetic bearings and self-bearing motors and their applications.

1.2 A vignette history of electric machinery and magnetic suspension

Prior to the 18th century the natural phenomenon of magnetism was thought as a separate entity from that of electricity [Cra31]. Hans Christian Oersted (1777-1851) first found a connection between electricity and magnetism in the year 1820 [Bri99a]. While working in Copenhagen he discovered that a compass needle was deflected when brought close to the vicinity of a current carrying conductor [Cra31]. This astonishing discovery stirred up interest among the scientific community. One of them, Andre-Marie Ampere (1775-1836), demonstrated that a pair of parallel conductors either repel or attract each other depending on the relative direction of current flow and that a small current carrying coil acted like a magnetic dipole.

The following year had seen the birth of a remarkable invention from a British philosopher, Michael Faraday (1791-1867). Faraday conceived that a magnetic pole could move in continuous circular motion around a conductor carrying current. By a clever arrangement Faraday successfully put forward the world's first electric motor in 1821. Such a simple apparatus forms the basis of today's advanced electric motors. About 10 years later Faraday made another discovery, namely electromagnetic induction, in which a changing magnetic field induces an electromotive force in an electrical circuit (Faraday's law). It is believed that an American professor Joseph Henry (1799-1878) observed the same phenomenon a year before Faraday but did not published his discovery, and thus lost the distinction for

American science [Tay96]. Nevertheless, Henry made numerous contributions to electromagnets and electric motors.

James Clerk Maxwell (1831-1879) was one of the greatest mathematicians ever lived. Having understood Faraday and other scientists' discoveries, Maxwell established one of the most elegant theories of all time uniting electricity and magnetism into the concept of the electromagnetic field [Eve75]. His theory paved the way and enhanced many technological developments in the 19th century physics. Together with the profound basic physics discoveries made in the past, many primitive electromagnetic structures have evolved into what we have today such as modern electric machinery, transformer, electromagnetic suspension system, magnetic bearing, electromagnetic launch system, etc.

While they were many concepts of electric motor proposed in the 19th century, it was Nikola Tesla (1856-1943) who first conceived the idea of utilising a rotating magnetic field, the basis of most alternating current machinery [Bri99b]. His discovery of polyphase alternating current systems holds more advantages than that of its rival direct current in revolutionising the modern use of electricity and power distribution.

Today a dozen or more modern types of electric motor are found in households and factories. From a miniature motor of a digital disc player to the world's largest drive and motor system at NASA's National Transonic Facility Wind Tunnel [ABB97], their usage is ever increasing in countless applications. The rapid development of drives and control systems over the past few decades have also encouraged the innovation of more technological breakthrough products. One invention that stirred up a lot of excitement was unveiled very recently – the Segway Human Transporter, a futuristic two-wheel scooter which uses gyroscopic and tilt sensors to achieve dynamic stabilisation [Seg01]. The component that propels this self-balancing vehicle is undoubtedly the electric motor!

Simple linear or rotary magnetic actuators are one of the earliest applications of electromagnetism. An important area that opened up the possibilities of utilising magnetic suspension in the last century was the ground transportation industry. It is believed that Graeminger [Gra11], [Jay81], [Sin87] was the first to propose suspending a vehicle below a steel rail by a controlled DC electromagnet mounted on the vehicle itself. A decade later in 1922 an alternative configuration incorporating gyro motors was suggested by Anschuz-Kaempfe [Ans23]. However, it was Kemper [Kem37] who first used active control system

with capacitive or inductive sensing methods for vehicle suspension. At that time many limitations such as poor magnetic material properties and inability to control the currents quickly had somewhat hampered the development of sophisticated systems.

With the advent of solid-state power electronics and development of advanced magnetic materials, the design of practical systems capable of supporting hundreds of tonnes and travelling more than 300 km/h has become more viable [Sin87]. Many research works on magnetically levitated trains (MAGLEV) have been pursued over the last few decades but there were no large-scale and high-speed commercial projects. One of the reasons was that MAGLEV is a relatively new transportation technology and therefore it is extremely difficult to compete with a more mature technology such as conventional railway trains [Goo99]. The world's first MAGLEV carriage in Birmingham, England connecting its airport terminal and the nearby rail line was shut down only recently after about eleven years of operation. It became too expensive to maintain. Despite all the criticisms, China has taken a bold step recently by constructing the world's first commercial high speed MAGLEV in Shanghai [AP01]. This multi-million dollars project is expected to complete in 2003 and will encourage more commercial levitated trains to be constructed elsewhere in the world.

Early use of permanent magnet to suspense or relieve the load of the shaft or spindles have been reported since the beginning of the 20th century [Eve1900], [Fau39]. High speed suspension that evolved from Kemper's development was mostly researched in the University of Virginia in the 1940's [Bea37], [BYM46]. Since then numerous projects on rotor suspension by magnetic bearings were reported but many were hindered by the then high cost and size of control system components. With the availability of more sophisticated control components, active control of magnetic bearings has become more practicable. One admirable project undertaken by NASA in the early 1970s was the use of magnetic suspension systems for satellite momentum flywheels [HL79].

In recent years the research and development of magnetic bearings have been very competitive and many potential applications have been identified [MOFN97]. One example is the aerospace industry where magnetic bearings will be utilised extensively in future commercial and military aircrafts [HE99]. There is supporting evidence that the current trend of the aerospace technology is shifting towards the so-called "more-electric aircraft"

[Wei00]. Other areas of application include commercial electronic products, semiconductor and manufacturing industries and medical equipments.

Magnetic suspension is an exotic technology. The demand for more high performance suspension systems is ever increasing and coupled with the rapid advances of solid-state electronics, measurement and control devices, such a technology will continue to induce more promising innovations in the future.

1.3 A general introduction to magnetic bearings and self-bearing machines

1.3.1 Conventional bearings

Conventional bearings such as rolling element and oil film bearings have long been employed to provide support to the rotor in rotating machinery. Rolling element bearings consist of an inner race, an outer race and a cage to support and guide the rolling elements (balls, cylinders or taper pins). These mechanical rolling elements have physical metal to metal contact with the inner and outer races. Oil film bearings, however, have no rolling elements but rely on lubricant viscosity to form a supporting fluid wedge. Circulation of lubricants is usually provided to cool the bearing system during operation.

Rolling element bearings have limitations due to the physical contact made with the machine components. They cannot operate beyond certain surface speed limitations. Oil film bearings also have speed limits due to losses and they are not suitable to be incorporated into manufacturing processes that are sensitive to contamination. Regular maintenance of these bearings is unavoidable because of wear and lubrication requirements.

1.3.2 Magnetic bearings

The disadvantages posed by conventional bearings have opened the door to alternative approaches in certain applications which require higher rotational speed and extreme reliability. Active magnetic bearings (AMB) are a non-contacting technology employed to perform the same task as conventional bearings but with advantages due to their active nature. The active nature of magnetic bearings offers control of rotor vibration, diagnostics and load measurement capabilities [KC96]. Among the advantages are: elimination of

friction, wear and lubrication; high speed capability; ability to operate in higher temperatures; potential for vibration control; and longer life.

The elimination of mechanical contact implies the rotor can be rotated at much higher speeds because of the absence of friction. Such high speed operation is highly desirable in applications such as aerospace, hydro-electric and machine tools applications. Furthermore, no lubrication is needed and this eliminates the necessity of coolers and associate piping system. The absence of lubricants also means magnetic bearings can be used in vacuum and clean room environments such as in the semiconductor industries. Other applications include: turbo generators, gas turbine engines, pumps, flywheels for energy storage, optical choppers, artificial heart and blood pumps. High reliability and low maintenance cost are expected in processes that incorporate magnetic bearings.

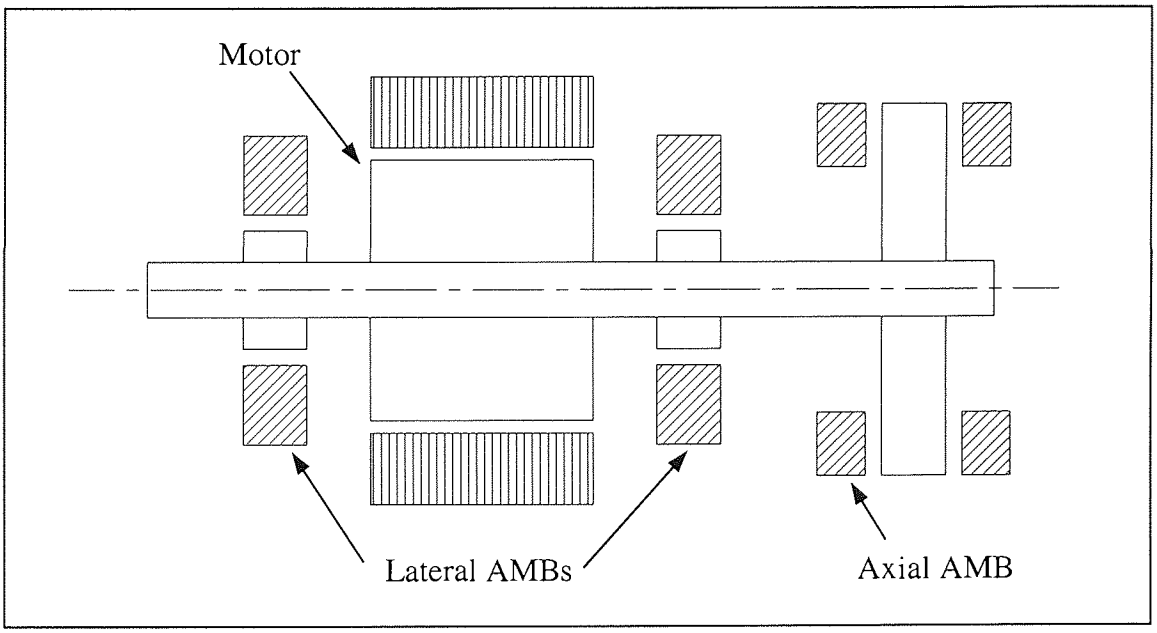

Figure 1.1: Configuration of a motor and magnetic bearings system.

In order to levitate and position a rotor, the magnetic forces must be exerted along five axes, usually two perpendicular axes at each rotor end and a fifth axis along the rotor axis, as shown in figure 1.1. Lateral magnetic bearings are responsible for the levitation of the shaft in the plane of the two perpendicular axes. Many writers used the terms "radial bearing" or "radial force" but we use the term "lateral" in this thesis.

1.3.2.1 Construction of active magnetic bearings (AMBs)

The construction of a lateral magnetic bearing is similar to that of the stator of an electric machine where stacked laminations of ferromagnetic material are used to reduce the effect of eddy current losses. The way they usually operate is by injecting currents into the coils wound around the poles such that a net attractive force is created to minimise the displacement of the rotor. Axial or thrust bearing is used to counteract axial forces in both directions. It is comprised of two stators sandwiching the rotor disc with a clearance gap. The stator is usually solid instead of laminated in order to avoid complicated manufacturing process and it has circumferential slots filled with coils. The flux paths for both lateral and axial AMBs are shown in figure 1.2.

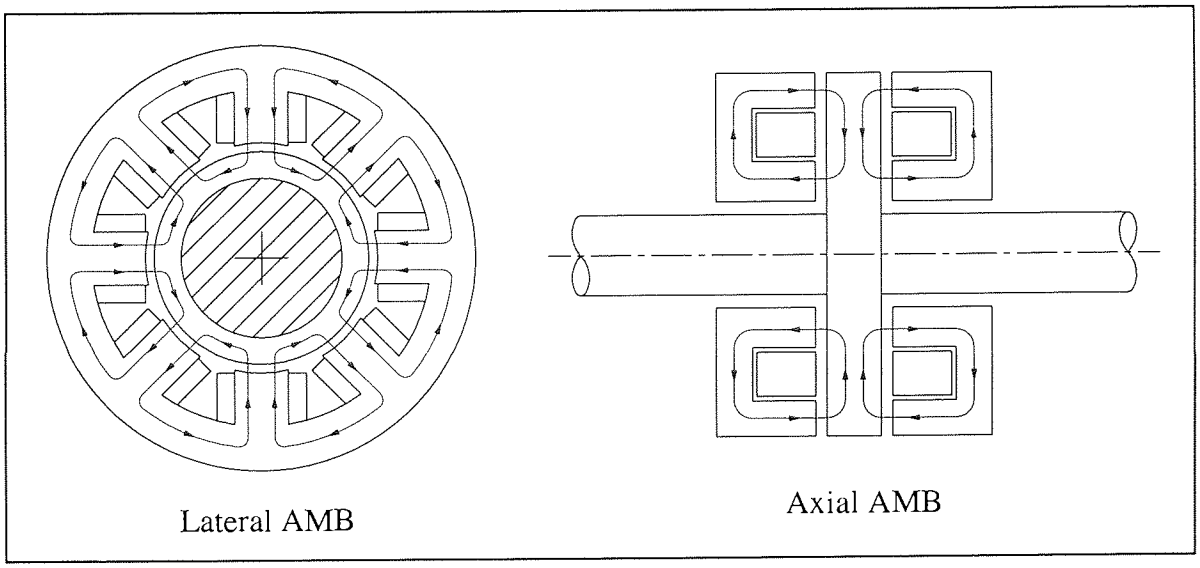

Figure 1.2: Flux paths of radial and axial AMBs.

1.3.2.2 Control system

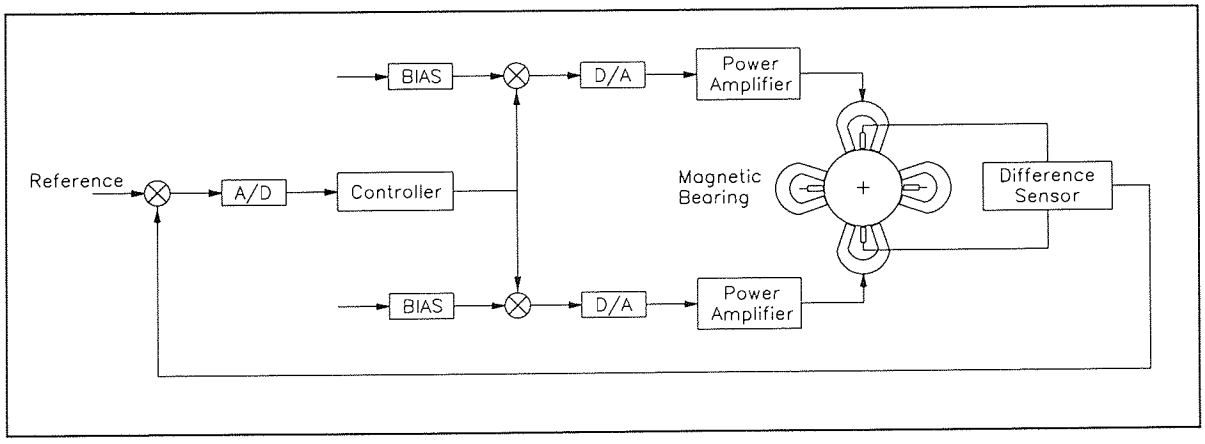

Figure 1.3: A general control loop of an active magnetic bearing system.

Figure 1.3 illustrates a general block diagram of a simple active magnetic bearing system. The attractive force for each horseshoe electromagnet is proportional to the square of the current I and inversely proportional to the square of the air gap size g_0, i.e.

$$F = \frac{\mu_0 N^2 I^2 A_p}{4 g_0^{\ 2}} \tag{1.1}$$

where μ_0 is the permeability of free space; A_p is the cross-sectional area of the pole; and N is the number of turns of winding coil.

Feedback control is indispensable for active magnetic bearings because they are inherently unstable. Sensors measure the position and orientation of the rotor and these signals pass through anti-aliasing filters to eliminate high frequency noise. The controller then processes the filtered signals and sends request for current to the power amplifiers which in turn drive the coils. The use of bias current is very common so that the net force produced is approximately linear with the varying coil current. To position the rotor, the current in one of the coils is increased from the bias current while the opposing current coil is decreased. These exciting currents are proportional to the amount of rotor deviation from its concentric position. With an appropriate controller command, the rotor displacement can be minimised even when the system is subjected to dynamic loading.

1.3.2.3 Conical magnetic bearings

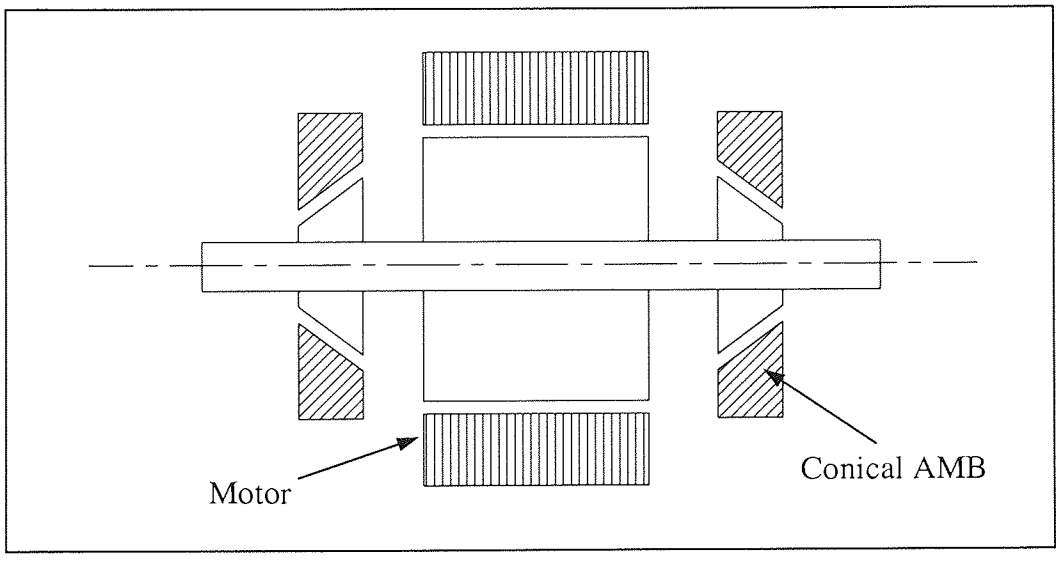

Figure 1.4: Conical magnetic bearings.

As mentioned previously, a five degree-of-freedom model is typically used to represent the forces experienced by the rotating machine. This model suggests that two lateral bearings, one on each end (constraining in x- and y-directions), and one axial (actuating in the z-direction) bearing must be employed to achieve full stabilisation of the rotating shaft. Another possible implementation of magnetic bearings is to employ two conical magnetic bearings as depicted in figure 1.4. In this configuration, the control force is segregated into a lateral and an axial component by the angle of the conical bearing and thus, the axial or thrust bearing is no longer needed. Conical bearings are especially advantageous in applications where space is at a premium but the performance capacity may be limited because of the split in the lateral and axial forces.

1.3.3 Self-bearing motors

Where bearings are required in the same context as electromagnetic torque production, it is natural to consider self-bearing or bearingless machines. The self-bearing machine is an innovation which integrates magnetic bearings and an electric machine into a single compact unit. Thus, a self-bearing machine suspends the rotor and generates torque simultaneously.

Typically, in an active magnetic bearing system, the rotating force driving the shaft is provided by other mechanisms such as a motor. Such a configuration results in a rather long axial shaft length and a long shaft decreases the critical speed which in turn complicates the control task [CDFR94]. A self-bearing motor can have a shorter shaft than a motor and bearing configuration, thus higher speed operations are possible. In addition to the advantages that conventional magnetic bearings possess, the self-bearing motor has fewer components and therefore a reduction of cost is possible.

The principle of operation behind a self-bearing motor is to create an unbalanced flux distribution in the air gap by means of supplying additional currents to the windings. This unbalanced flux distribution in the air gap interface between the stator and rotor gives rise to a net lateral force between the components. The essential requirement as we show later for lateral force productions is to superimpose the torque and force-producing flux components that have a pole-pair number differing by 1 in the air gap. By appropriately controlling these

additional currents the magnitude and direction of force exerted on rotor may be varied as desired. Chapter 3 describes the mechanisms of force production in a greater detail.

Figure 1.5 illustrates two common configurations of a self-bearing motor. As in the case of a motor with magnetic bearings, the rotor of the self-bearing motor must be constrained by magnetic force along five axes. Therefore, two segments of self-bearing motors and an axial magnetic bearing are required for full stabilisation control. An alternative configuration with 2 independent degrees of freedom can be realised when the motor stack length is made to be much shorter than its diameter. This configuration is known as a disc-shaped self-bearing motor. The axial and angular displacement of this class of self-bearing motor is controlled in a passive manner. More information with regard to the passive stabilisation of a disc self-bearing motor can be found in chapter 3.

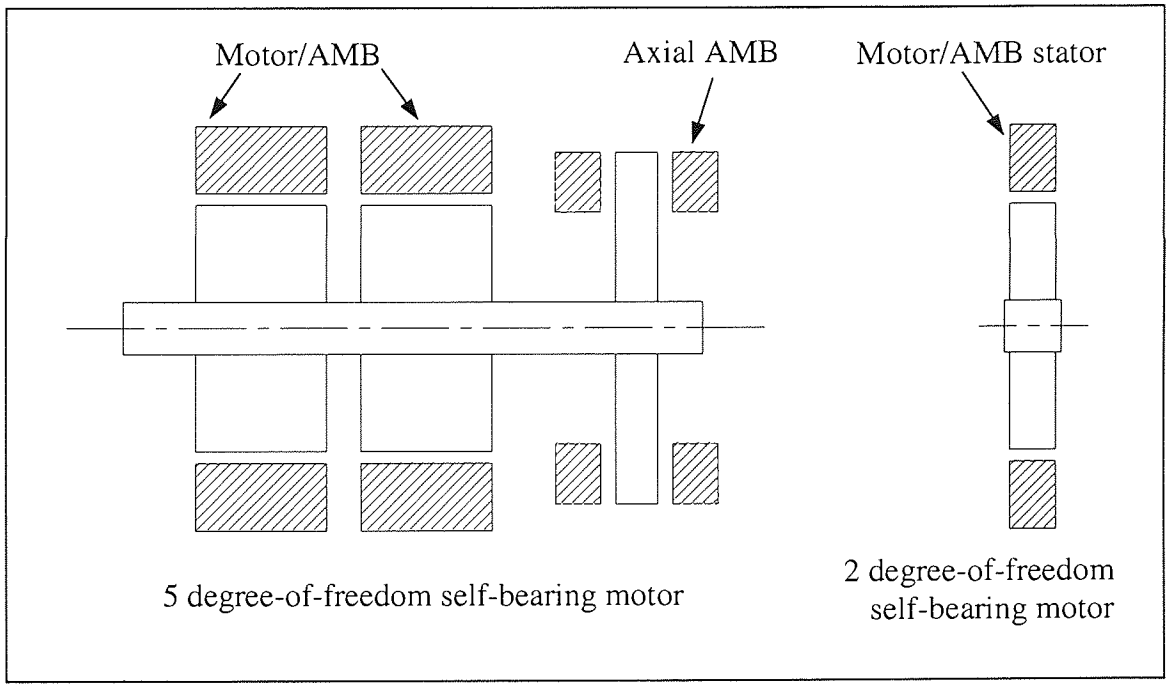

Figure 1.5: Two possible configurations of self-bearing motor.

1.3.3.1 Applications of self-bearing motors

Perhaps some of the most popular applications of a self-bearing motor are the blood pumps, artificial hearts and left ventricular assist devices (LVAD). In these medical devices the impeller is magnetically levitated and rotated simultaneously to create a fluid pumping action [SB97], [Har96], [SBF+00]. The self-bearing motor can also be used in canned motor pumps employed in the pharmaceutical and chemical industries [Gem96]. In the

semiconductor industry, self-bearing motors play a role of supporting a rotatable platform in the wafer processing chamber [NJL+98]. A prototype bearingless bubble bed reactor with a totally magnetic suspended impeller was also built for efficient supply of oxygen to growing cells [SBWR98]. To summarise, it can be seen that the development of self-bearing motor is very much driven by the demand in specific applications.

1.3.4 Issues related to magnetic bearings and self-bearing motors

There are several drawbacks associated with magnetic bearings and self-bearing motors. In particular, the initial setting up cost for an active control system is much higher and more complex than a conventional motor with mechanical bearings. Furthermore magnetic bearings are not as stiff as their mechanical counterpart. The fact that the stator of the self-bearing motor performs two functions, namely levitation and rotation, means its performance capability may be limited. This is attributable to the limited current capacity of its windings. For a given performance the self-bearing motor will have more copper losses than a standard motor as a result of the additional current supplied for levitation. One aim of the scheme proposed in the thesis is to have lower losses than in earlier designs. Nevertheless, the aforementioned disadvantages can be outweighed by the distinct advantages that magnetic bearings and self-bearing motors posses in many applications.

1.4 Organisation of thesis

This thesis can be generally divided into 3 major sections namely: (1) background and the state of the art; (2) the newly proposed concept; and (3) general applications and summary. Chapters 1-3 provide the necessary background of self-bearing motors to the reader. With the understanding of the basic concepts the reader is then invited to proceed to chapters 4-7 which emphasise the principles behind the operation of the newly proposed machine. Finally the remaining chapters are devoted to discuss its applications to other machines and further improvements to be attempted. A more detail breakdown of contents is as follows.

Chapter 1 introduces a brief history of electric machinery and magnetic suspension, and further expands to the general aspects and applications of magnetic bearings and self-bearing motors. Literature review of some early designs of self-bearing motors is described

in chapter 2. Some disadvantages of the presently available machines are discussed to assist in identifying the problem definitions and aims of this research. Chapter 3 discusses the mechanisms and principles of lateral force and torque production in a self-bearing motor. Among the related aspects included within this chapter are: unbalanced magnetic pull; numerical examples of lateral force production; passive stabilisation; and the effect of saliency on force and torque production.

Chapter 4 unveils a novel concept of producing lateral forces and torque using only a single set of windings. The properties of such a connection and advantages over its predecessor windings are also presented in this chapter. Chapter 5 focuses on the ANSYS finite element simulations performed to validate the proposed connection scheme. In particular, a 3-phase permanent magnet synchronous motor is chosen as an example. The proposed self-bearing motor windings scheme is then compared with other conventional windings in chapter 6. This is done via finite element analysis with the performance and power loss parameters are chosen as a basis of comparison. Chapter 7 outlines the levitation and torque control system for the proposed self-bearing motor.

In chapter 8 the application of the newly proposed scheme to other electrical machines is discussed. A design study of a motor to drive a vacuum pump is presented in chapter 9 where the ratings of the self-bearing motors and levitation power supplies are estimated from the required force slew rate and dynamics of the system. Also included in this chapter is the initial control system design incorporating a PID controller, and the system response to step and impulse inputs are investigated. Chapter 10 concludes the thesis, summarises the accomplishments and proposes further work to be undertaken. Appendices supplement the thesis in aspects related to magnetic bearings, suggestion for experimental work and finite element modelling techniques.

CHAPTER 2

STATE OF THE ART OF SELF-BEARING MOTORS

This chapter reviews and examines some of the self-bearing motors published in patents, journals and technical conferences over the last few decades. More emphasis is given to the windings design irrespective of the type of self-bearing motors or application. From an understanding of the presently available connection schemes, the problem definition and specific aims of the research are identified which lead to a new concept of self-bearing motor windings being proposed.

2.1 Winding schemes

It is believed that one of the first recorded proposals of an electric motor having the function of a radial magnetic bearing was by Hermann [Her73], [Her74] in 1973. Another early known motor with uses magnetic forces to restore and dampen rotor motion was invented by Meinke and Flachenecker [MF74]. Since then many motor designs with combined magnetic bearings have been invented but it was not until 1988 that the technical term "bearingless motor" was used [Bos88]. The terms "bearingless" and "self-bearing motor" have the same meaning and will be used interchangeably hereafter. Furthermore, the term "levitation" will be used frequently to mean producing a lateral force.

From the windings perspective self-bearing motors can be broadly categorised into 2 groups, namely: dual set of windings configuration (figure 2.1(a)); and single set of windings configuration (figures (b) and (c)). The former category refers to any self-bearing machine that incorporates two separate sets of windings; the primary set carries the motor currents while the secondary set carries levitation currents. For a self-bearing machine to fall in the latter category, however, all its windings must carry motor currents at any operating cycle, although some windings may be selectively used to carry levitation currents. Both former and latter configurations have relative merits of their own depending on the applications.

Several types of self-bearing machines with such windings have been proposed in the literature, for example induction, stepping, reluctance and permanent magnet synchronous

motors. Most patented self-bearing machines are of a generic type but some are specifically designed to fit certain applications. The following subsections describe some of the presently designs of self-bearing motor winding in a greater detail.

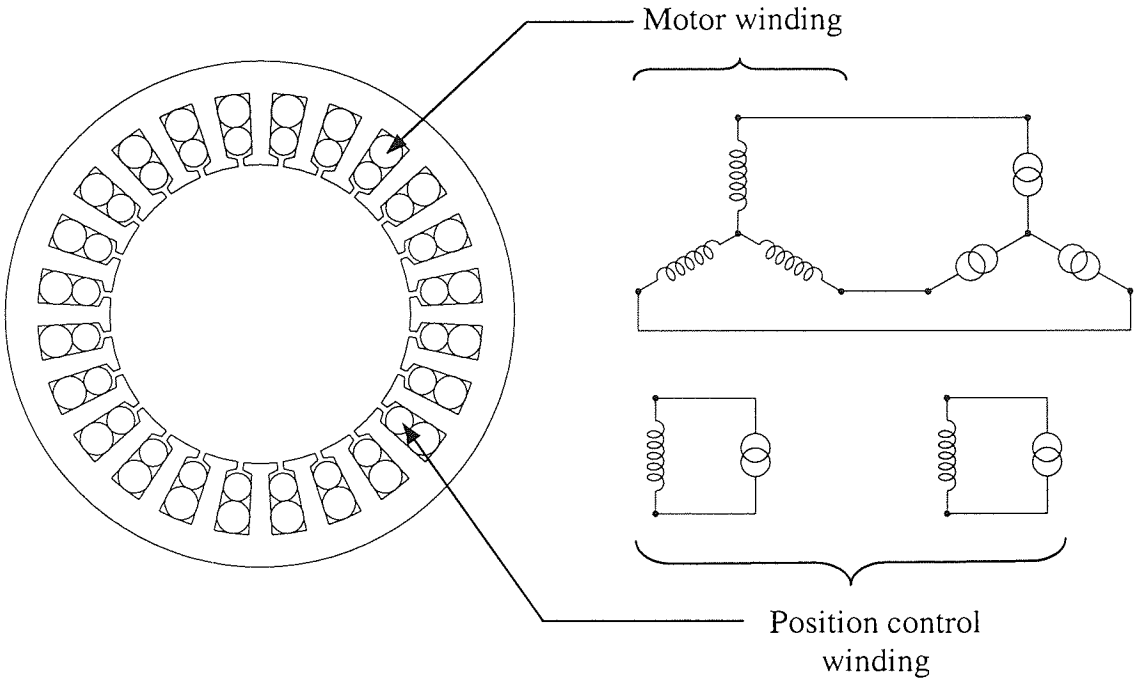

Selected references: [CCF90], [CDFR94], [CFA+97], [CFM96], [CRF91], [FCM96a], [FCM96b], [Hig86], [OCFR96], [OGS98], [OMD+96], [OMS+98], [Wil87].

Figure 2.1(a): Dual set of windings arrangement.

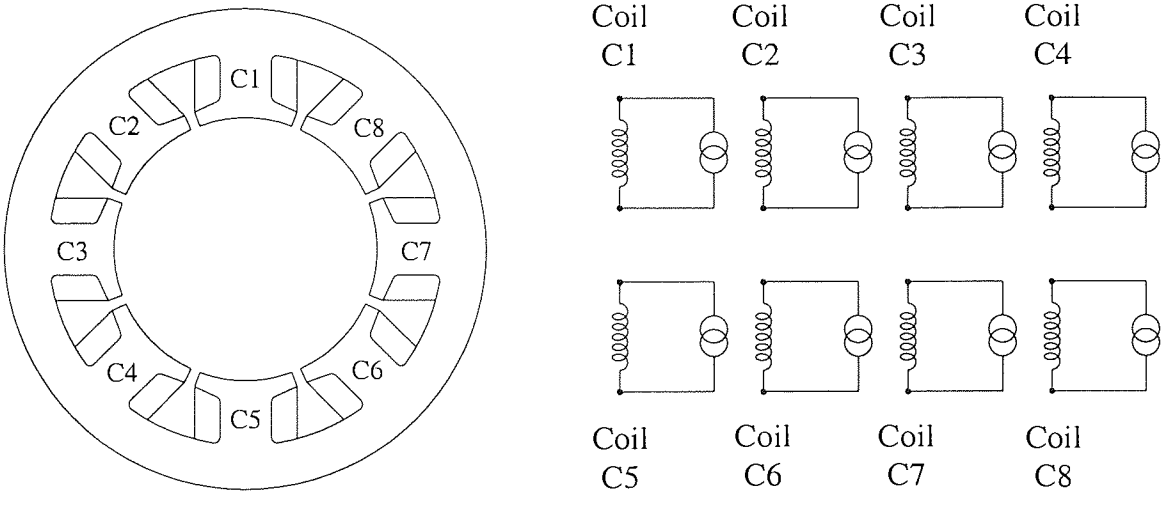

Selected references: [ODO95], [Ohi92], [OMO96], [PLRC94].

Figure 2.1(b): Single set of windings arrangement with a power supply driving each coil.

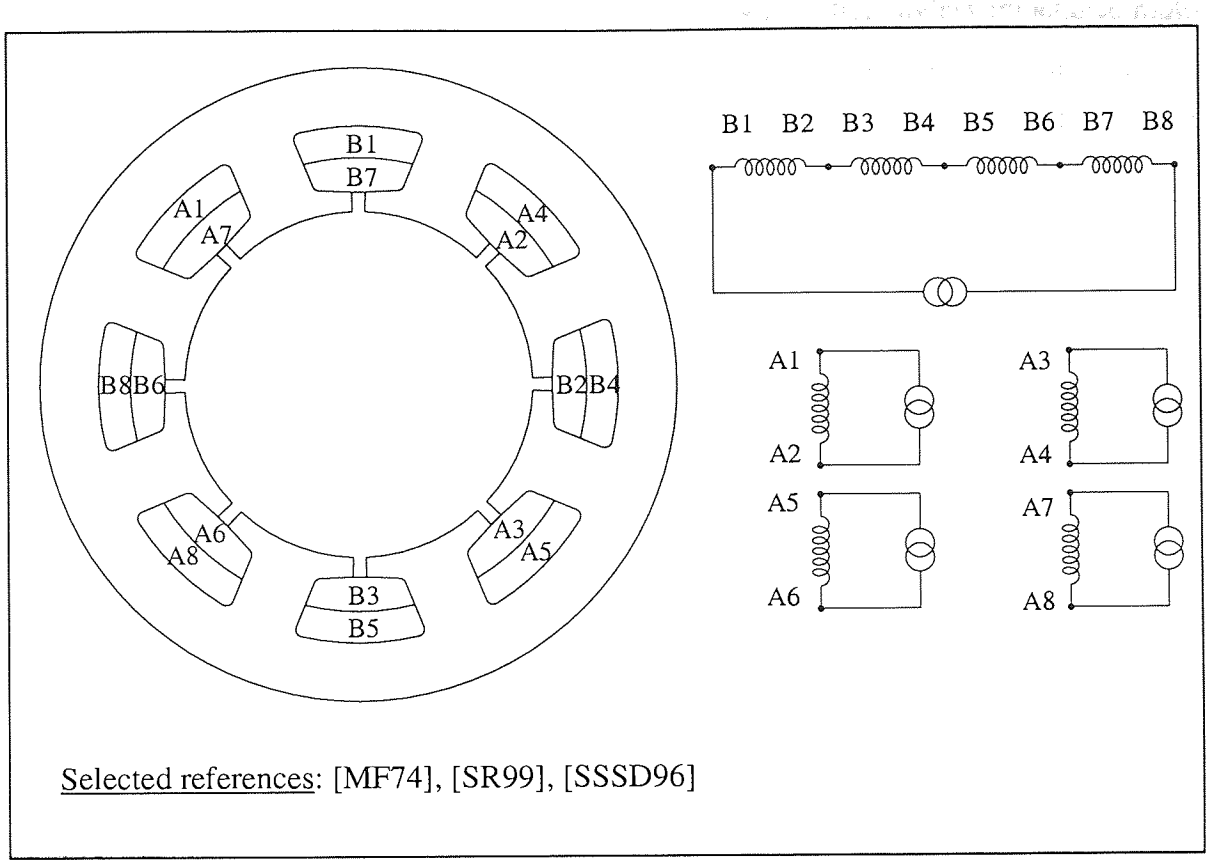

Figure 2.1(c): Single set of windings arrangement (split winding scheme).

2.1.1 Dual set of windings self-bearing rotating machines

Early designs of self-bearing motors involved the use of two sets of windings for the production of lateral force and torque. One set of windings is the conventional motor winding for torque production and the other set, known as position control windings, generate lateral forces. In the absence of levitation currents in the position control windings, the flux distribution is the air gap created solely by the motor windings. However, when the levitation currents are excited, the flux distribution in the air gap is unbalanced and thus exerts a net lateral force on the rotor.

Higuchi [Hig86] proposed a stepping self-bearing motor that comprises four electromagnet blocks forming the stator and a rotor with circumferential teeth. Each electromagnet has two layers of concentrated coils; the outer layer constitutes the position control windings whereas the inner layer forms the motoring windings. Such a connection scheme makes use of a specially built stator.

Chiba et al. [CCF90], [CRF91], [CDFR94] developed 4-pole bearingless reluctance motors that utilise a conventional stator but with added 2-pole position control windings. It is shown that the mutual inductances between the windings are related to lateral force production, and the magnitude of this force is proportional to the product of motor and levitation currents. As a result, the contribution of motor currents to lateral force production is very substantial in any bearingless reluctance motor.

Bearingless induction motors having two sets of windings were also proposed by Chiba et al. [CDFR94], [CFA+97]. Little was mentioned with regard to its windings because the windings scheme is essentially similar to what they had proposed for other machines. A more detail description of windings from Chiba et al. can be found in [CFM96]. This patent discloses a high speed rotary induction machine with additional position control windings fitted in the stator. The cage conductors of the rotor are designed such that the mutual inductance between the conductors and position control windings is zero in order to avoid excessive heating.

Another bearingless induction machine with a second set of windings to levitate the squirrel-cage rotor was disclosed by Satoh et al. [SOM98]. In this machine the magnetic flux distribution in the air gap is detected by integrating the counter-electromotive voltage induced in the stator windings. The authors addressed the difficulty of controlling the levitated rotor when a low frequency component is detected at an attenuated level. To substitute and compensate for the attenuated flux, the stator winding is supplied with a corrective current.

Williamson [Wil87] disclosed a method of constructing polyphase bearingless machines with an auxiliary set of windings to exert a non-rotating lateral force on the rotor. The additional windings maybe arrange in any convenient way to generate the required levitation field. This levitation field rotates at the same direction and frequency as the main field and has pole number differing by two.

Osama et al. [OGS98] disclosed a more compact bearingless machine with simplified fabrication techniques. This invention also has a separate position control windings wound in the stator. The whole induction machine assembly comprises two stator and two rotor segments and an axial bearing to accomplish stable levitation. When the two rotor segments are offset with respect to their stators, the resultant machine is capable of generating axial

forces to counter the axial movement of the rotor. Therefore the use of axial bearing can be eliminated by such an arrangement. A single rotor segment extending from one stator segment to another may be used for permanent magnet and synchronous machines since there is no current flow in the rotor.

A variable-speed dynamotor having magnetic bearing capability for suppressing vibrations and controlling the damping of the rotor was devised by Fukao et al. [FCM96a]. This machine does not require the stator to be structurally modified, but only needs an additional winding to be wound around the stator. The same authors also proposed another rotating machine with position control windings [FCM96b]. It includes a circuit for sensing the rotor displacement based on the induced voltage or current and the magnitude and speed of the rotating magnetic field.

Perhaps one of the most extensively reported machines in the literature is the permanent magnet self-bearing motor. This particular class of machine comes in various flavours such as disc-shaped motor, exterior-rotor configuration, hybrid type motor, slotless stator, etc. and with different topologies. Some selected examples with dual set of windings are discussed as follows.

Ooshima et al. [OCFR96], [OMD+96] presented a few permanent magnet bearingless motors with an additional set of windings for rotor displacement control. The authors reported that the lateral force is proportional to the mutual inductance between motor and levitation windings, and the equivalent MMF current contributed by surface-mounted permanent magnets. Having thick permanent magnets would decrease the derivative of the mutual inductance but concurrently increase the equivalent MMF current. Based on the authors' development, they suggested an optimal design of using thin permanent magnets and small air gap. To further increase the radial forces, Ooshima et al. [OMS+98] employed a buried permanent magnet type rotor.

An integrated magnetic levitation and rotation system for semiconductor wafer processing was proposed by Nichols et al. [NJL+98]. Accordingly, the stator assembly has permanent magnets to levitate and passively centre a ring-shape rotor along the vertical axis. By energizing the stator position control coils, the interaction of fluxes generated by the control coils and DC flux produced by permanent magnets give rise to an active lateral position

control. Torque is developed when the polyphase drive coils wound on the stator plates are excited.

Casemore and Stephens [CS99] designed a toothless permanent magnet self-bearing motor for smooth torque applications. A toothless machine has a larger air gap size because of the additional equivalent air gap introduced by the low permeability of the permanent magnets, and the motor and levitation control windings. As a consequence this machine has a relatively low bearing capacity and is particularly suited for low-gravity environments such as space-based systems.

A hybrid AMB type self-bearing motor that uses DC magnetic flux for lateral force control was designed by Okada et al. [OSUO98]. The assembly has a two degree-of-freedom rotor and consists of two segments, i.e. one segment is the permanent magnet self-bearing motor with two sets of windings and the other is a hybrid type magnetic bearing. The former and latter are joined together by a permanent magnet assembly that produces the bias flux. Unlike other self-bearing machines that require a pole-pair difference of 1, this machine requires a minimum number of 3 pole-pairs to ensure control independence of levitation and torque. The authors claimed that a simpler construction and control system is possible with this design.

Another variant of hybrid type self-bearing machine was also proposed by Kanebako and Okada [KO00]. The improved features are that both segments comprise a self-bearing motor and the whole assembly does not require any bias from permanent magnets. Each pole piece of the stator has 2 sets of concentrated coils; one for levitation and the other for torque control. Kim et al. [KSKO00] constructed a short span hybrid type self-bearing motor with an exterior rotor assembly for potential use in artificial heart pump. The rotor is actively controlled in two orthogonal axes by energising the levitation windings while other motions rely on passive stabilisation.

2.1.2 Single set of windings self-bearing rotating machines

It is possible to achieve an equivalent magnetic field distribution in the air gap with only one set of windings. Predetermined currents of different amplitude and phase are injected into the same set of windings to generate a superimposed magnetic field, and this resultant

field gives rise to torque and levitation. Usually the method of superposition of currents requires a number of power electronic devices to drive the independently wound stator coils. Here currents are summed electrically in a controller before injecting into the terminal windings. Using a single set of windings for two functions is a more efficient solution and it presents an important concept in moving towards an integrated design. Several machines with a single set of windings according to the aforementioned definition are discussed below.

Meinke and Flachenecker [MF74] patented an electromagnetic drive assembly with a magnetically supported rotor. The windings arrangement concerned is of a single set type where all three pairs of toroidally wound coils are excited appropriately to drive the rotor. In order to stabilise the rotor, the requisite magnetic forces are generated by superimposing additional levitation currents into some motor coils. Another interesting feature of this machine is that part of the coils can also be used to form inductive sensors for sensing the rotor displacement.

A connection scheme resembling that of Meinke and Flachenecker was devised by Santisteban et al. [SSSD96], [SR99] for their bearingless induction motors. The windings are distributed within the stator forming a two-phase induction machine and a total of five inverters are required to drive the windings. Another name associated with this type of windings arrangement is known as "split windings".

A magnetic bearing device employing a rotating magnetic field was developed by Ohishi [Ohi92]. In this machine, all coils wound on the stator are independently controlled by separate units of power amplifier. The rotor has surface mounted permanent magnets and is connected to a drive shaft of an external rig. Levitation is achieved by sequentially energising the coils so that a rotating magnetic field is produced to oppose and attract the polarities of the permanent magnets on the rotor. Okada et al. also applied the similar concept in the development of permanent magnet synchronous and induction bearingless motors [ODO95], [OMO96]. One significant conclusion made by the authors was that the torque and levitation control in an induction bearingless machine is inevitably coupled.

Preston et al. [PLRC94] reported an integrated magnetic bearing and switched reluctance machine. The stator poles are wound with separately excitable phase windings and each winding is energised with a combination of phase winding and magnetic bearing currents.

The force generated in each winding has a tangential and radial component to rotate and levitate the salient pole rotor respectively.

Another machine that uses the principle of superposition of currents was constructed by Maurio and Thaxton [MT98]. The 4-pole stator windings of the permanent magnet synchronous machine are split in half to form 2-pole magnetic bearing windings and 4-pole motor windings. The windings are injected with the superimposed currents having polarity relationship with the permanent magnets in the rotor so as to produce torque and levitation. These current signals are summed electrically in a controller before being injected into the windings.

Mishkevich et al. [MTZ96] proposed a method of damping and counteracting mechanical vibrations of an induction motor by means of inducing unbalanced forces on the motor shaft. The stator coils are divided into a four groups of star-connected coils in which each group is separately excited by a power supply unit. By providing exciting currents to all the four groups of coils, the required four-pole rotating field is generated. Additionally, two sets of levitation fields (two-pole) that rotate at different frequencies and opposing each other are generated by selectively exciting the groups of 3-phase coils with appropriate frequency and phase relationships.

The aforesaid self-bearing machines are of polyphase windings. Low cost single-phase permanent magnet bearingless motors for applications such as pump, fan or blower have also been investigated. Amrhein and Silber [AS98], [SA98] dealt with the design of bearingless motors with a single set of concentrated coils wound on the interior and exterior type rotors. The torque and force-producing component of currents are superimposed before being supplied to the four concentrated coils of the assembly. Nenninger et al. [NAS00] built a bearingless motor with fractional pitch windings for a better force control, but there is a reduction in average torque production.

2.2 Disadvantages associated with current designs

On examination of the presently available designs for self-bearing rotating machines, we can comment as follows:

- The purpose of employing two sets of windings is to superimpose two fields of different magnitude and pole number in the air gap, so as to generate torque and levitation simultaneously. It is evident that these machines are not cost effective - they require extensive additional manufacturing effort to accommodate secondary windings.

- The dual set of windings configuration has a relatively high power loss for a given motor performance, and also a poor specific power rating. This is attributable to the presence of secondary windings in the stator and so the number of turns of the primary windings has been limited.

- All existing designs with single set of windings require the use of more than one high-rated power-switching component for the normal torque-producing function. Some machines demand the same number of power supplies as the number of stator teeth because each concentrated coil is independently excited. The fact that all drive units must carry identical and in-phase currents to generate the main field means that they are relatively high-rated drive units. There is usually a high setting up cost associated with this control method. Moreover, this windings scheme is impractical to implement in machines with a large number of teeth, for instance 24, 36 or more teeth. It is preferable to use just one power supply unit to drive the self-bearing machine as in the case of a conventional electric machine.

- Some of them do not take advantage of the fact that by utilising the interaction between torque-producing fields and levitation-producing fields, the additional losses in the machine due to levitation requirements can be very small.

2.3 Main aims of research

In view of the limitations described above, a new set of specifications for general AC self-bearing rotating machines can be derived:

- The primary objective of the present research is to provide a rotating electrical machine that is capable of generating torque and lateral forces, utilising only a single set of windings. The same conductors within the set of windings must carry currents

from the torque and lateral force-producing components simultaneously. In addition, the conductors carrying both components of current must present in all stator slots for an efficient use of iron.

- A further object is to provide a self-bearing rotating electrical machine that uses its phase windings, so connected to form independent current loops such that separate and independently controlled inverters or supplies can be used for the torque and lateral force productions. This self-bearing machine benefits from needing only one standard drive (or supply) for the normal torque-producing function.

- It also required that relatively low-rated power electronic devices be used for the achievement of lateral force. Using such low power electronic devices may allow some redundancy fault tolerance. In the presence of other suitable rotor support means, these low-rating power supplies can be switched off and the motor driven by the conventional power supply described above.

- Another object of the research is to provide a self-bearing machine that has minimal dependence of the machine torque on the commanded lateral force.

- It is mandatory that the proposed windings scheme can be implemented in any polyphase machines such as two-phase, three-phase or higher phase machines. It is also desirable to have other variants of connection based on the proposed concept. Thus, it will provide flexibility in the detail design.

2.4 Summary of principal matters

The idea of levitating a rotor via additional windings in the motor has been extensively reported in the literature. Such a design leads to disadvantages related to poor torque capacity, higher copper loss, increase in the machine size and so high cost. Various self-bearing motors with a single set of windings have also been developed. Although they have relatively lower losses than their rivals with dual set of windings, the manner in which their windings are connected require more power supply units than is necessary for the normal torque-producing function. This could increase the initial cost of setting up a self-bearing drive system and render such an investment unattractive.

In retrospect, the development of self-bearing machines is driven by two important factors. One is the desire in better performance self-bearing machines and the other is being driven by the demand in specific applications. In this research the former direction is taken as a motivation. The main aim is to present an AC electrical rotating machine that is capable generating torque and lateral forces, utilising only a single set of windings. The proposed winding connection will also benefit from: requiring only one standard power supply unit for its normal motor operation; the possibility of relatively low-ratings for the additional power supply units used for producing lateral force; and the feasibility of extension to any polyphase machine.

CHAPTER 3

MECHANISMS OF LATERAL FORCE AND TORQUE PRODUCTION

The understanding of lateral force and torque production mechanisms is crucial in the study and development of self-bearing electrical machines. It is the aim of this chapter to discuss how lateral forces could be exploited in the machine by using its own torque-producing component of flux. This chapter begins by introducing the components of stresses necessary for force and torque development in magnetic bearings and conventional electrical motors before proceeding to the principle of lateral force production in self-bearing machines. Other related factors such as unbalanced magnetic pull; passive stabilisation; and the effect of saliency in force and torque production are also included in this chapter.

3.1 Maxwell stresses

Lateral force and torque developments in electrical machines can generally be computed by means of the Virtual Work Method or Maxwell's stresses. The former evaluates force and torque based on stored energy in the magnetic field: the fact that it relates to circuitry parameters makes this method attractive. The latter is a macroscopic field theory used to describe stresses developed at the boundary of an air space in which the magnetic field energy exists. Since Maxwell's stresses provide a greater insight into the internal workings of how mechanical force is developed, this method will be utilised to shed more light on our discussion about lateral force and torque production in self-bearing motors. For simplicity the succeeding treatment and discussion assume that: (1) the ferromagnetic material is of infinite permeability such that all the energy is stored in the air gaps and the flux crosses the iron/air boundary orthogonally; (2) leakage and fringing are small and can be neglected; and (3) the effects of slotting is negligible.

Magnetic flux traversing through the boundaries between air and iron gives rise to mechanical stresses at the corresponding boundaries. In the following discussion, the general term "iron/air boundary" is used to represent the surface of both stationary and rotary members of the machine. Two general cases that constitute the principal stresses are illustrated in figure 3.1. Tensile stresses arise as a result of the flux impinging the iron/air boundary at right angles, whereas compressive stresses are developed when the flux is

crossing parallel to the iron/air boundary. These stresses are essentially a normal component with respect to the ferromagnetic surfaces, which plays an important role in the operation of linear-motion magnetic actuators, such as magnetic bearings.

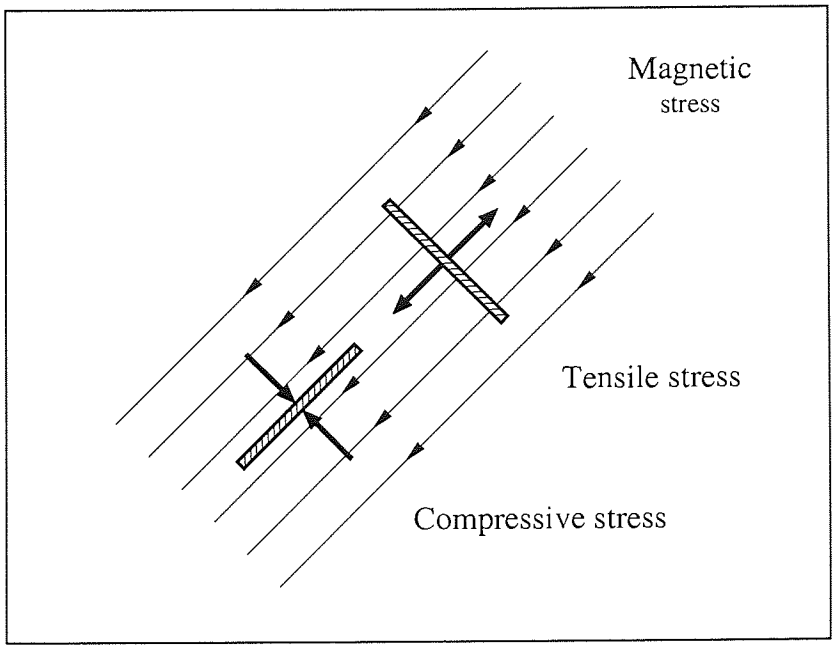

Figure 3.1: The principal stresses on ferromagnetic surfaces.

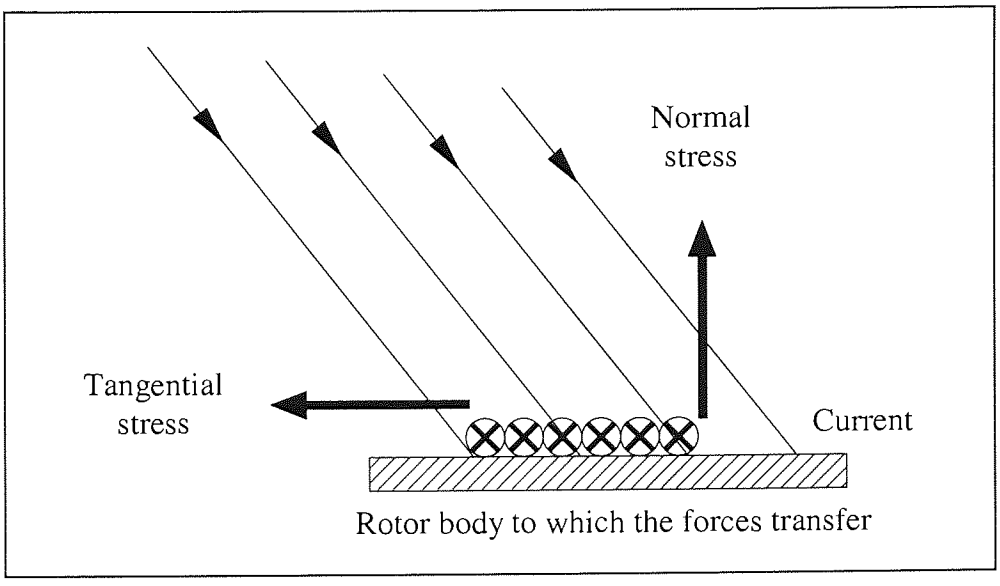

Figure 3.2: Tangential stresses developed as a result of an MMF source introduced on the iron surface.

For rotary operation tangential stresses are indispensable. In order to create tangential stresses at the iron/air boundary it is a necessity for the magnetic flux to cross the bounding surface at an angle other than 90°. Such a consequence is possible if the iron is provided

with an additional source of current to influence the existing field, for example by introducing current windings or mount permanent magnets on the bounding surface. Such an effect is illustrated in figure 3.2. The total torque developed is then the summation of all the mechanical stresses on the bounding surface of interest.

3.1.1 Relationship between mechanical stresses and magnetic fields

It is useful at this stage to relate mathematically the mechanical stresses to the magnetic flux density B and magnetic field intensity H. These equations reference can be applied at any arbitrary point embracing the iron/air boundaries:

$$\text{Tangential stress, } \sigma_t = B_n H_t \tag{3.1}$$

$$\text{Normal stress, } \quad \sigma_n = \frac{1}{2}\left(B_n H_n - B_t H_t\right) \tag{3.2}$$

The subscripts n and t refer to normal and tangential quantities respectively. As far as the normal field is concerned, current excitation on either the stationary or rotary member would contribute the same effect to its opposite member, i.e. H_n created at the surface of the excited stator would also give approximately the same H_n on the rotor surface. Thus H_n is essentially constant and uniform across the air gap. H_t varies approximately linear across the gap from a maximum value at a surface with a local MMF source to zero on the opposite side. Strictly speaking, at either the stator or rotor surfaces, the resultant tangential component is contributed by the local MMF source alone.

If a local air gap has currents of the same polarity on stator and rotor surfaces, the normal field components act in the same direction whereas tangential field components are mutually opposed. Anywhere in between the bounding surfaces, the resultant H_n and H_t are derived from the vector summation of both MMF sources, if the machine is doubly excited. With these important field properties, the mechanism of torque and lateral force productions in any electromagnetic structures can be better understood.

3.1.2 Torque and force development in electric machinery and magnetic bearing

Consider a singly excited machine with a salient-pole rotor shown in figure 3.3. The solid rotor has two cylindrical pole faces subtending the same angle as the stator. When the coil is

energised a transfer of energy from the electrical source to the magnetic field in the air gap occurs. Apparent from figure 3.3 is the fact that H_t is zero on the rotor surfaces because of the absence of a local excitation. Therefore the tangential stress t_t is zero according to equation (3.1) and so no torque is produced. In accordance to the aforementioned properties, the normal components H_n are developed at the cylindrical pole surfaces and flat edges of the respective salient-pole rotor. The normal components on the cylindrical faces produce attractive forces of equal magnitude but in opposite direction. Such forces do not give rise to a net lateral force nor do they contribute to torque production. On the flat edges, however, the normal components H_n yield forces that act circumferentially and tend to restore the rotor to its equilibrium position. Such a torque-producing mechanism forms the basis for reluctance and stepping motors.

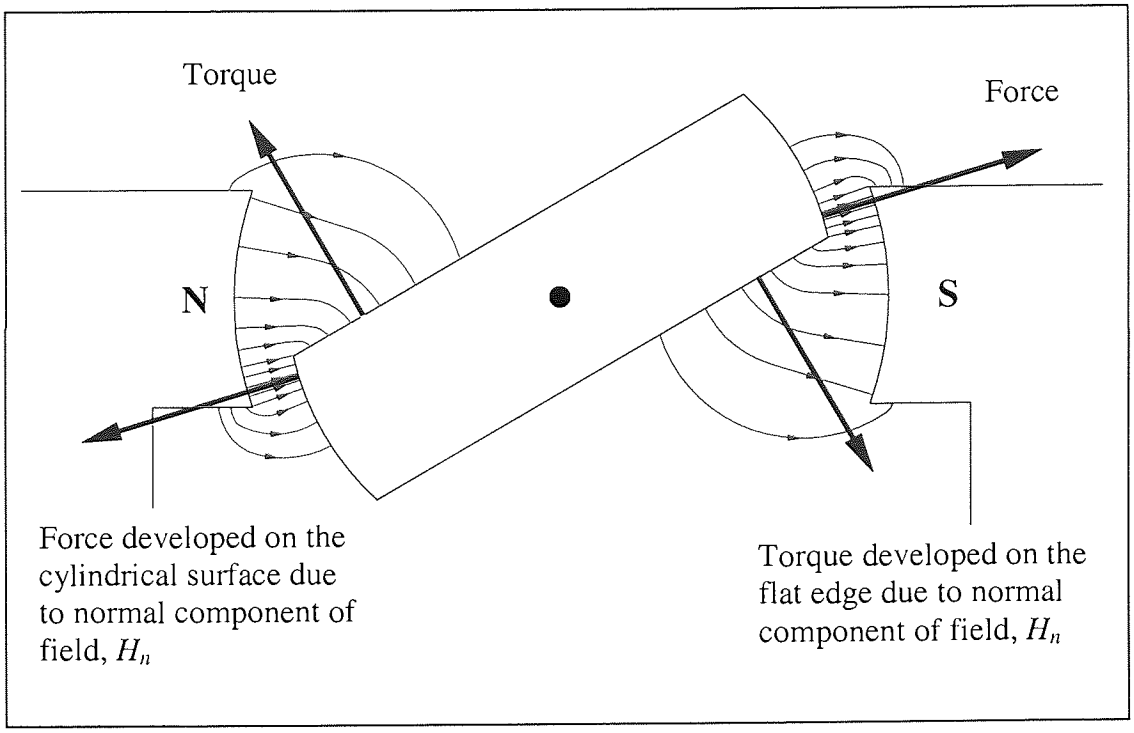

Figure 3.3: A flux plot in the air gap during torque production.

For the case of a cylindrical rotor H_t is zero around the rotor's periphery and thus contribute nothing to torque. As a remedy the cylindrical rotor must incorporate an MMF source in order to produce the necessary tangential stresses, for instance, a permanent magnet rotor used in an AC brushless motor, a DC excited field winding incorporated in a three-phase synchronous machine and a squirrel-cage rotor which relies on the induced voltage employed in an induction machine. It is also apparent from equation (3.1) that torque is also generated on the stator itself. Since the stator is required to be stationary the torque generated will be transmitted to the base where it is mounted.

In practical lateral magnetic bearings shown in figure 1.2 of chapter 1, the journal is not excited by any means and so the normal components of flux H_n generated by the stator enter or emerge the rotary member at right angle. These normal components H_n result in a local force directed toward each stator pole. By appropriately varying the coil currents such that an unbalanced flux distribution is created in the circumferential air gap, a net lateral force on the rotor is generated toward the direction where flux is most concentrated.

An accurate evaluation of force and torque would require finite element analysis since they are dependent upon the actual geometry of the motor. Further, it is a subject of debate as to whether virtual work or Maxwell's stresses methods is more appropriate for computing force and torque. In virtual work method, torque is evaluated from the variation of the total magnetic energy of the system with respect to the rotor angular displacement, whereas Maxwell's stresses method computes the surface integral placed in the air gap enclosing the rotor. Each method has its own advantages and disadvantages from the aspect of accuracy and implementation [BWR99], [Cou83], [DRM98]. In most cases the virtual work method is more preferable in 2D and 3D finite element field solutions. With some assumptions approximate expressions for force and torque can be obtained for verification purposes by analysis.

3.2 Principle of lateral force production

This section describes how self-bearing motors produce lateral forces.

3.2.1 Unbalanced magnetic pull (UMP)

The unbalanced magnetic pull (UMP) phenomenon in conventional electrical machines is somewhat analogous to the lateral force effect in self-bearing motors. UMP is a natural occurrence where there is any eccentricity of the rotor with respect to the stator bore due to manufacturing tolerances, rotor whirl, or bearing defects. The consequences associated with UMP are noises, excessive vibrations, electrical losses at the rotor surface, etc. While the UMP is highly undesirable in conventional motors, the understanding of the basic UMP concepts is a good starting point for study of self-bearing motors.

The pattern in which the flux is distributed around the air gap periphery of a machine dictates whether or not an UMP may happen. Figure 3.4 compares the flux distributions established in the air gap for the cases where the rotor is concentric and eccentric with respect to the stator. For the purpose of discussion, the rotor is assumed to have its own MMF distribution. When the rotor is held concentric with respect to the stator, the normal and tangential forces acting on the rotor surface are balanced. Any arbitrary diametrically opposite points on the rotor surface have the same magnitude but in opposite direction of force, as indicated in the perfect sine wave flux plot. However, when rotor eccentricity occurs the flux distribution is no longer sinusoidal but distorted as shown in figure 3.4. Such a distortion of flux density waveform causes an UMP towards the smaller air gap.

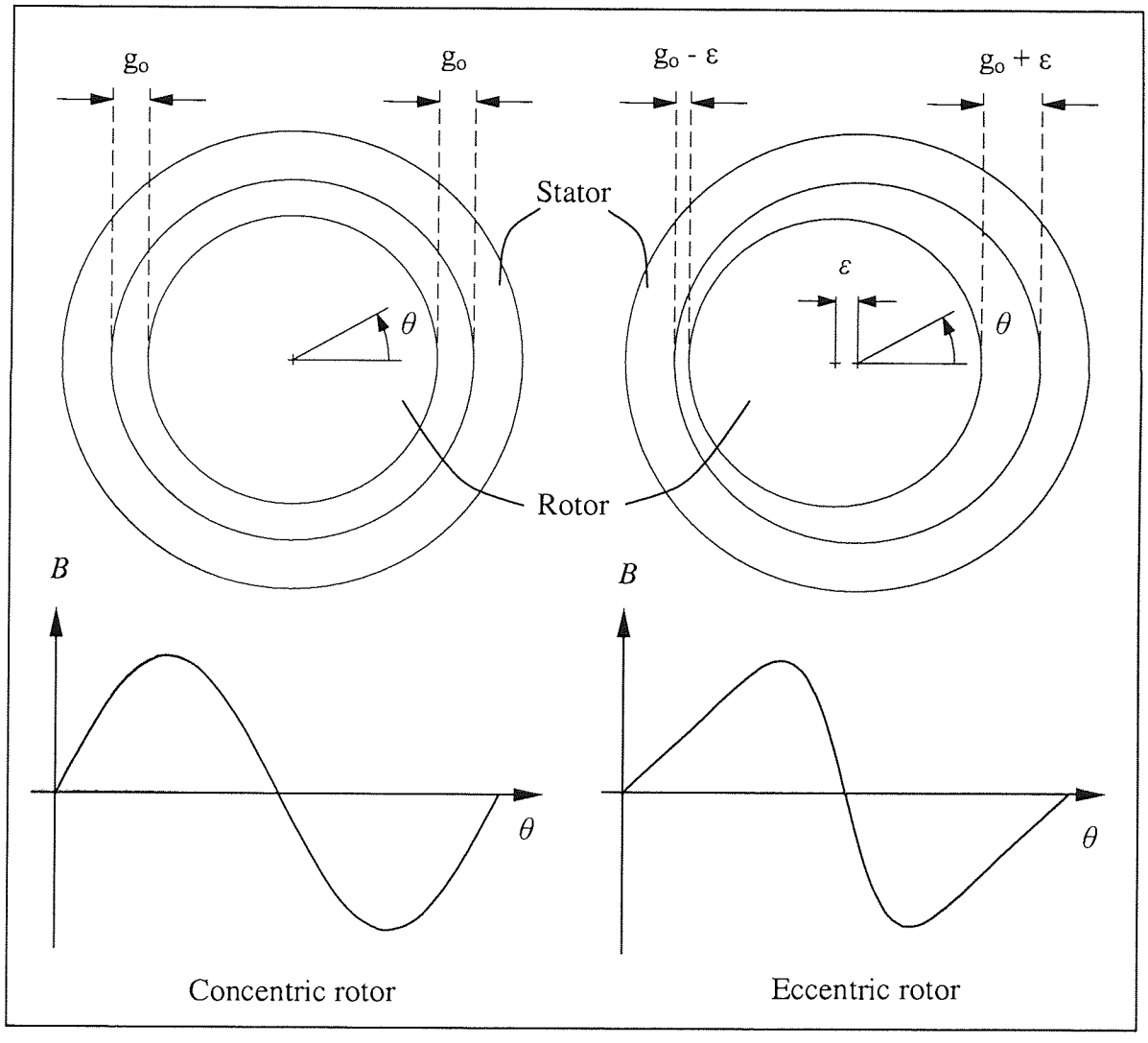

Figure 3.4: Flux distributions in machines with a concentric and eccentric rotor.

The main difference between lateral force production in self-bearing motors and UMP in conventional motors is that the former is being controlled actively to suppress vibrations or support the rotary member. UMP may be reduced by increasing the flux excitation such that

tooth saturation causes the reluctance path around the narrower air gap to increase [Dor99]. The mechanism of force production, however, is similar for both cases and it varies with both amount of eccentricity and angular position of the rotor. Consider a general expression of lateral force production in magnetic bearings:

$$F = K_I I_p + K_x x \tag{3.3}$$

where K_I and K_x are the actuator gain and open-loop stiffness respectively.

Note that the open-loop stiffness is negative when a displacement of rotor results in a transverse force in the same direction. When the rotor is concentric with respect to stator ($x=0$), the second term in expression (3.3) disappears, yielding a force expression which only relates to the perturbation current, I_p. Here current I_p is supplied sufficiently to balance the weight of the rotor. As soon as the rotor deviates, the second term is no longer insignificant and current I_p has to be increased to overcome the rotor weight and magnetic pull. Thus, the second term in expression (3.3) resembles the UMP condition. Furthermore, additional fields with pole-pair numbers differing by one from the machine main field are generally used to model and simulate the effect of UMP [Dor99]. This modelling method is consistent with the mandatory requirement of producing lateral forces in self-bearing motors.

3.2.2 Lateral force production in self-bearing motors

The concept of the natural occurrence of UMP can be exploited in a self-bearing machine where the flux distribution in the air gap is deliberately unbalanced to achieve rotor positioning. Figure 3.5 illustrates how lateral forces may be generated by supplying additional currents to unbalance the existing motor flux density in the air gap. This particular example is essentially a reluctance motor in which its salient-pole rotor is not excited. It is understood from the properties of magnetic field that no tangential stresses exist on the rotor because H_t is zero. Consequently the stator alone contributes the overall motor flux. It is assumed that the four-pole motor field is created by the stator windings alone but similar principle can also be applied for the case where both stator and rotor contribute the motoring MMFs.

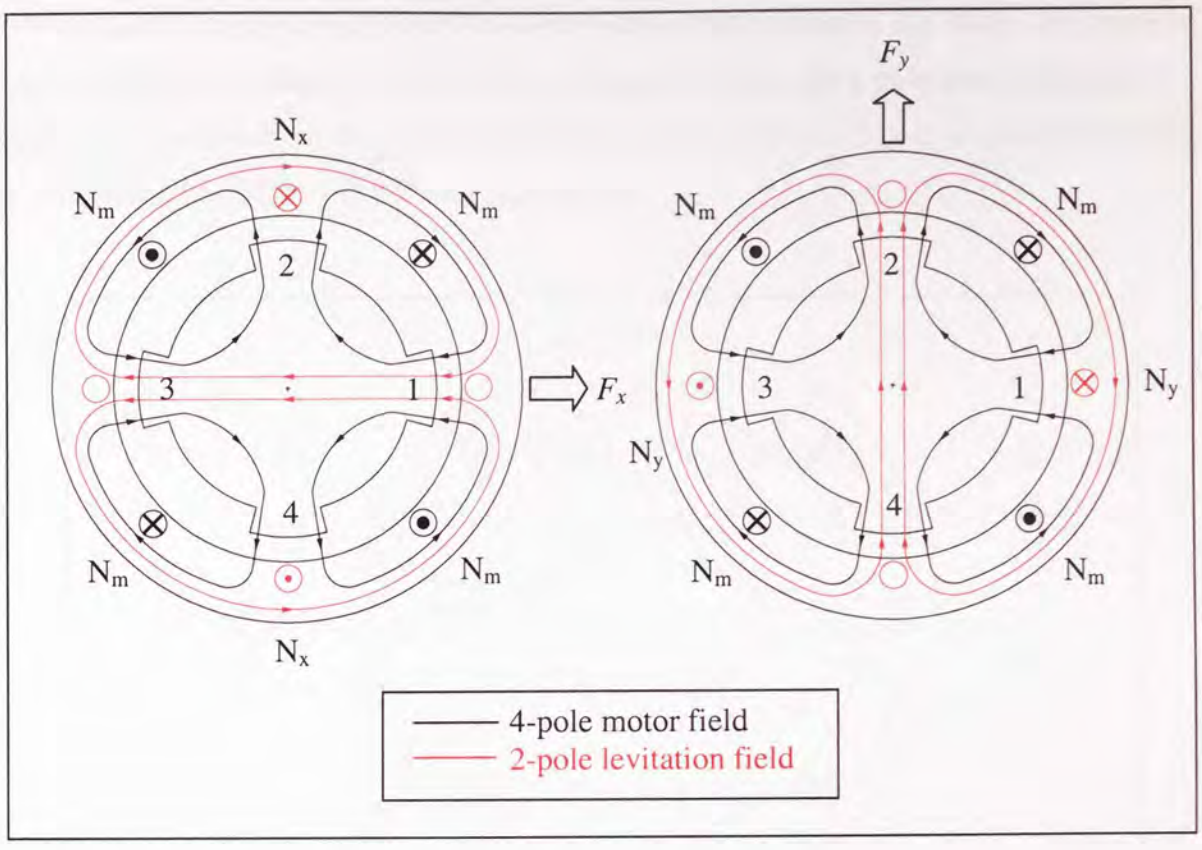

Figure 3.5: Levitation by means of unbalanced flux distribution.

The additional currents are hereto referred as levitation or bearing currents, and are supplied to the position control windings. Referring to figure 3.5, the designated four-pole flux is produced by the motoring current in the stator winding N_m. When there are no currents supplied in the position control windings N_x and N_y, the flux densities at the air gap of poles *1*, *2*, *3* and *4* are equal to each other. To produce a net lateral force in the positive *x*-direction, the four-pole magnetic field is deliberately unbalanced by the current in the N_x winding. In effect a two-pole levitation field is produced and causes the flux density at pole *3* to decrease while the flux density at pole *1* increases. As a result a net lateral force F_x is exerted on the rotor as shown in figure 3.5. Likewise, exciting the current in N_y winding at that particular instant gives rise to a vertical force F_y. Therefore, a net lateral force in any arbitrary direction can be produced since it is merely a linear combination of the two independently excited position control windings N_x and N_y.

It is apparent that the superimposed levitation field is of a pole-pair different to the motoring field. If one were to use a 4-pole levitation field is in addition to the motoring field, the torque is either enhanced or subdued, depending on the relative magnitude and phase relationships. No levitation is produced under such a circumstance. However, a six-pole

levitation field imposed will result in a net lateral force between the stator and rotor as shown in figure 3.6. Thus, it is important to recognise that only a pole-pair difference of 1 between the fields can produce a net lateral force in the machine. These observations above are proved mathematically in the next sub-section.

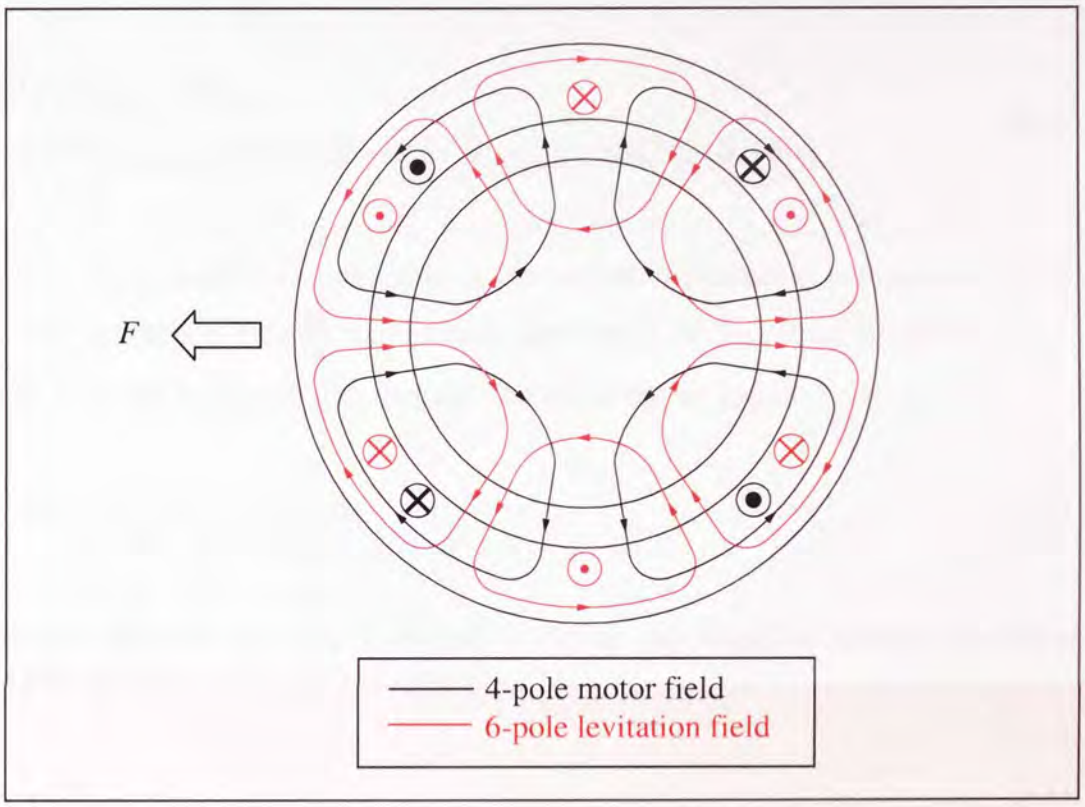

Figure 3.6: Lateral force production by superimposing a six-pole levitation field to a four-pole motor field.

3.2.3 Mathematical derivation of lateral force expressions

In all magneto-mechanical devices, the forces (and torques) can be considered to arise as the integration of Maxwell stresses in the air gaps and these stresses are, in turn, proportional in magnitude to the square of flux density. The following shows how a general lateral force expression can be derived for a generic self-bearing machine.

Assume that the magnetic circuit is linear and that the distribution of rotor MMF remains unchanged by the presence of a levitation MMF field. We can consider $B_{Torq}(\theta)$ to represent the rotating magnetic field on any cylindrical surface concentric with the machine axis and passing through the air gap:

$$B_{Torq}(\theta) = B_{TorqMax} \sin(N_{PPT}\theta - \omega t) \tag{3.4}$$

In this expression, N_{PPT} is the number of pole pairs of the torque-producing component of flux and ω is a frequency. Let the additional rotating magnetic field in the air gap for levitation purposes be denoted:

$$\begin{aligned} B_{Lev}(\theta) &= B_{Lev(X)} + B_{Lev(Y)} \\ &= B_{LevMax(X)} \sin(N_{PPL}\theta - \omega t) + B_{LevMax(Y)} \cos(N_{PPL}\theta - \omega t) \end{aligned} \tag{3.5}$$

where N_{PPL} is the number of pole pairs of the levitation-producing component of flux. We restrict our discussion here to the vertical component of $B_{Lev}(\theta)$ of expression (3.5), i.e. $B_{Lev(Y)}(\theta)$. Then the total magnetic flux distribution in the air gap is:

$$B_{Total(Y)}(\theta) = B_{Torq}(\theta) + B_{Lev(Y)}(\theta) \tag{3.6}$$

Accordingly, Maxwell stresses developed in the air gap interface between the stator and rotor is proportional to $B_{Total}(\theta)$ in expression (3.6):

$$\sigma_Y = \frac{1}{2\mu_0}\left(B_{Torq} + B_{Lev(Y)}\right)^2 \tag{3.7}$$

The corresponding Maxwell force developed on the infinitesimal area of the rotor surface is:

$$dF_x = \sigma_Y \times lrd\theta \tag{3.8}$$

where l and r are the length and radius of the rotor respectively. The total Maxwell forces exerted on the rotor in the y-direction can then be computed by integrating the stresses in equation (3.7) around the air gap:

$$\begin{aligned} F_y &= lr\int_0^{2\pi} \sigma_Y \sin\theta.d\theta \\ &= \frac{lr}{2\mu_0}\int_0^{2\pi}\left(B_{Torq} + B_{Lev(Y)}\right)^2 \sin\theta.d\theta \end{aligned} \tag{3.9}$$

To produce a net lateral force, i.e. F_y is non-zero, the pole-pair difference between the torque and levitation flux-producing component must be 1, namely:

$$N_{PPL} = N_{PPT} \pm 1 \tag{3.10}$$

Further manipulation of equations (3.9) and (3.10) leads to that of Okada [ODO95], [OMO96]:

$$F_Y = \frac{1}{2\mu_0} \pi l r B_{TorqMax} B_{LevMax(Y)} \tag{3.11}$$

In a similar manner the levitation force in the x-direction can be derived as:

$$F_X = \frac{1}{2\mu_0} \pi l r B_{TorqMax} B_{LevMax(X)} \tag{3.12}$$

3.2.4 Implications of the force expressions

The general force expressions in (3.11) and (3.12) suggest that the force exerted on the rotor is simply proportional to the product of maximum motor and levitation flux densities. Because most practical electric machines operate with moderately high flux densities in the order of 0.8 T in the air gap for their normal torque-producing function, it transpires that relatively small asymmetries in the distribution of magnetic flux in the air gap can result in relatively large net transverse forces between rotor and stator. Experience suggests that for a given machine flux density B_{Torq}, the additional flux B_{Lev} required to sufficiently overcome gravity force on the rotor may be 100 times smaller than B_{Torq}. This is perhaps easier to comprehend by considering the following examples:

Case (1): A small 4kW motor with B_{Torq_Max}=1.2 T, rotor mass, m=8 kg, l=0.11 m, and r=0.0445 m;

The vertical force required to balance the rotor is: $F_Y = \frac{1}{2\mu_0} \pi l r B_{TorqMax} B_{LevMax(Y)}$

$$8\times 9.81=\frac{1}{2\times 4\pi\times 10^{-7}}\times\pi\times 0.11\times 0.0445\times 1.2\times B_{LevMax(Y)}$$

$$B_{LevMax(Y)}=0.0107 \text{ Tesla}$$
$$<<1.2 \text{ Tesla } (B_{Torq\_Max})$$

Case (2): An induction machine with B_{Torq_Max}=1.2 T, rotor mass, m=900 kg, l=0.87 m, and r=0.2 m;

$$900\times 9.81=\frac{1}{2\times 4\pi\times 10^{-7}}\times\pi\times 0.87\times 0.2\times 1.2\times B_{LevMax(Y)}$$

$$B_{LevMax(Y)}=0.0338 \text{ Tesla}$$
$$<<1.2 \text{ Tesla } (B_{Torq\_Max})$$

Thus, in the absence of any substantial torque-producing component of magnetic flux, the level of levitation flux required to exert lateral forces is considerably higher than otherwise.

Both force expressions (3.11) and (3.12) apply to any arrangement of coils in the stator and rotor so long as the necessary B_{Torq} and B_{Lev} are produced. Equally important is the fact that torque and force-producing flux components must have a pole-pair number differing by 1 in order to obtain a lateral force.

3.2.5 Contribution of tangential stresses in lateral force development

From a cursory inspection of expression (3.2), if a rotor is excited the resultant normal stress tends to be smaller, giving a less lateral force. Further, when the tangential and normal field components are equal, i.e. at 45° to each other, the normal stress is found to be zero and thus no levitation force is obtained.

In the studies of UMP the contribution of tangential stresses to a lateral magnetic pull is much less than the normal stresses, and can therefore be neglected under normal circumstances [BD73]. Even a machine with concentric rotor and under full-load conditions, as mentioned by Gray [Gra89a], the normal field H_n is much greater than the tangential field H_t. Self-bearing machines also possess a similar characteristic. In the foregoing development the lateral forces are derived as a result of normal components of stresses on

the rotor surface. Tangential components of stresses also exist but they are insignificant in contributing lateral forces when compared to their normal counterparts. We therefore neglect the effect of tangential stresses on lateral force production.

3.3 Passive stabilisation of a disc-shaped self-bearing motor

The previously discussed mechanisms of lateral force and torque production involve the use of active control to stabilise the rotary member. This particular section describes another class of rotor support which is commonly found in disc-shaped or short span self-bearing motors, namely passive stabilisation.

A conventional rotor-bearing system has five independent degrees of freedom and its minimum configuration is typically composed of two radial magnetic bearings and a thrust bearing to provide full stabilisation active control. The length of such a rotor is much greater than its diameter in general. In applications where the thickness of the motor must be made as thin as possible, active control of two degrees of freedom can be implemented. In particular, disc or pancake self-bearing motors have such a configuration and so they have fewer components than conventional magnetic bearing systems.

The approach is to make the diameter of the rotor much greater than its axial length. It is also essential to ensure that the axial lengths of both stator and rotor are approximately equal. This model can be thought as reducing the axial length of between two magnetic bearings until they are adjacent to each other. It is then possible to eliminate the need for active control of the other three degrees of freedom. The disc self-bearing motor requires active control of rotor suspension in the x- and y-directions only. The axial control in the z-direction, however, is of a passive type. Maxwell stress tensors forms the basis for an explanation of passive stabilisation in disc-shaped self-bearing motors.

Figure 3.7 illustrates how magnetic flux acts to stabilise the tilting rotor. Magnetic flux lines behave like elastic strings and have tendency to shorten themselves. They also tend to make 90° at the boundaries between the air and the stator or rotor because of high permeability of the magnetic material. When the stator and rotor are aligned, flux lines are approximately straight and the magnetic reluctance is minimised. When an external torque is exerted on the rotor, causing it to be displaced angularly in a clockwise direction, the flux lines are curved as shown in figure 3.7. Because flux lines tend to be as straight and short as possible, a

restoring torque is generated and acts in a counter clockwise direction to move the rotor back to its equilibrium position.

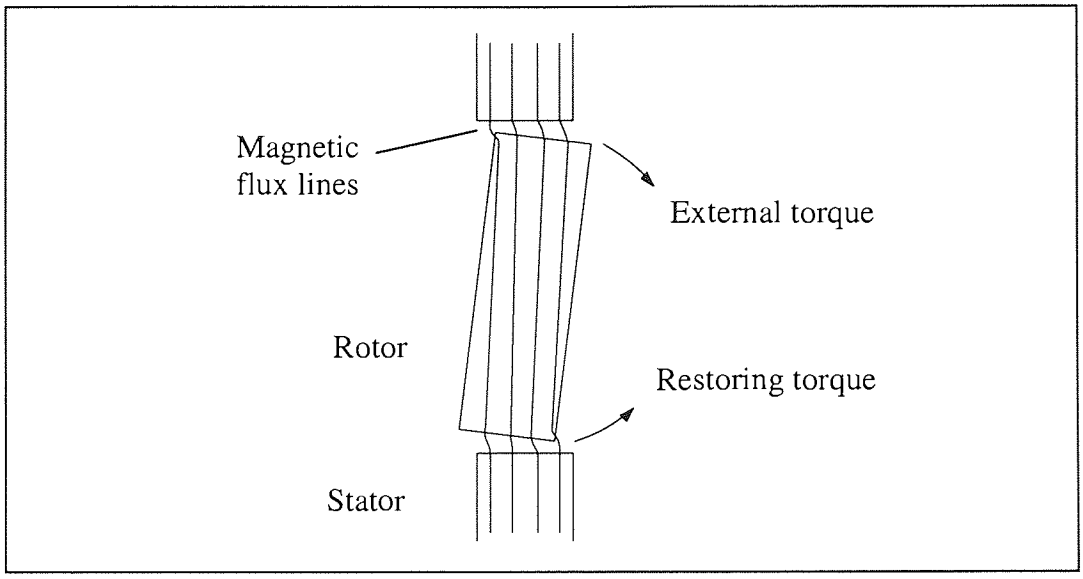

Figure 3.7: Magnetic flux in a disc-shaped self-bearing motor (side view).

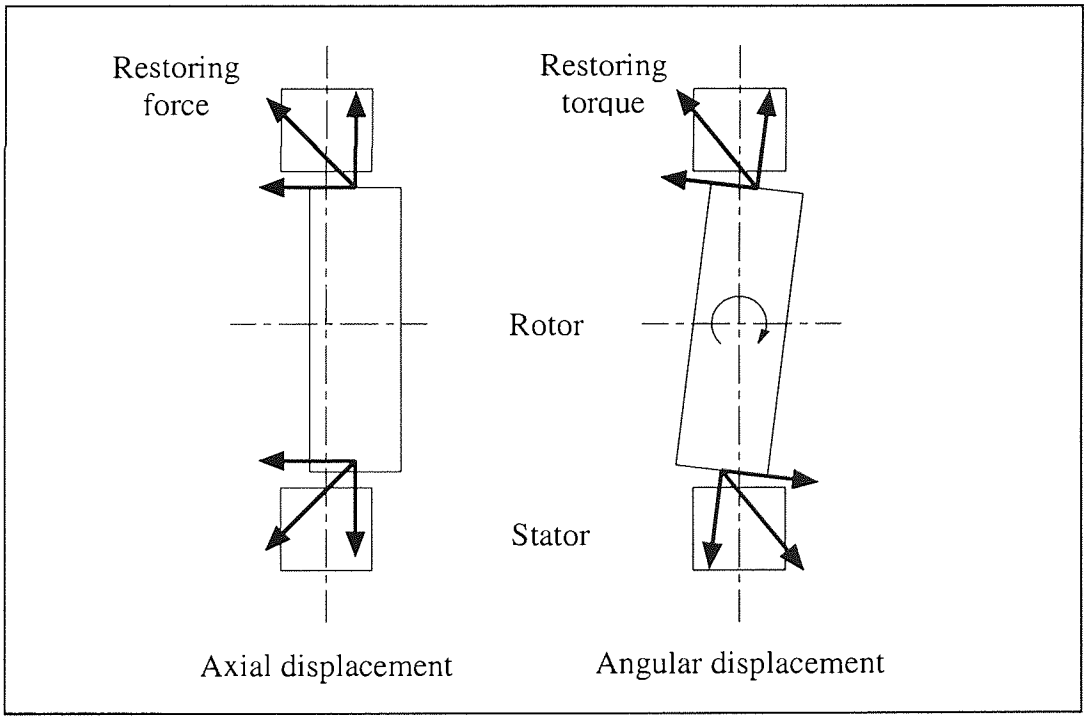

Figure 3.8: Passive stabilisation of a disc-shaped self-bearing motor.

Passive stabilisation of a disc-shaped self-bearing motor can be divided into two types, namely axial displacement and angular displacement, as shown in Figure 3.8. The aforementioned properties and restoring torque also apply to the case of axial displacement of rotor. As is often the case, insufficient damping of rotor motion exists when employing passive stabilisation methods. This can be compensated by other means; for example, fluid

in a driven pump can provide an additional hydraulic damping during its normal operation [UCO+98].

3.4 The effect of saliency on torque and lateral force production in self-bearing machines

The term "saliency" in electrical machine parlance relates to the physical protrusions of ferromagnetic material around the periphery of a rotor and/or inner boundary of a stator. Such a construction gives rise to a non-uniform air gap between the stator and rotor. It is often exploited to improve the performance of electrical machines, simplify the construction and also for economical reasons. For example, in a large synchronous machine, the effect of salient-pole rotor is to increase the maximum torque capability. Not all machines, however, can benefit from the concept of saliency. If a salient-pole rotor were used in a large induction machine, the undesirable effects such as noise, vibration and a zero averaged oscillating power flow would result [WM68].

The presence of saliency in stator construction is inevitable unless a toothless or slotless stator is employed. Teeth or pole pieces in a stator act as flux guides to channel the necessary fluxes to and from the rotor across the air gap boundary. When the stator coils are excited the flux traversing into or out of each tooth is essentially constant across the tooth area (or pole face). The apparent effect of having a toothed stator is that the overall flux distribution around the air gap periphery is no longer a pure sinusoid, but a "stepped" sinusoidal waveform. Nevertheless with an appropriate design methodology adopted such as increasing the number teeth, skewing the stator teeth, incorporating a distribution windings scheme, etc., the resultant flux distribution can be made to approximate to an ideal sinusoidal waveform.

Since the stator is more or less standard from the aspects of design and construction, it is the aim of this section to confine the discussion to saliency in rotor and its effect on torque and lateral force generation.

3.4.1 The effect of saliency on torque production

One analytical method to reason the effect of saliency on torque production is by considering the basic stored energy principles. Hawes [Haw73] derived torque equation based on the fundamental MMF's of a salient-pole synchronous machine. Here the irregularities in the air gap are ignored and the effective radius of the air gap is assumed constant for simplicity. The torque produced is found by differentiating the total stored energy W_T in the air gap with respect to mechanical angle θ_m:

$$T = \frac{\partial W_T}{\partial \theta} \tag{3.13}$$

$$\begin{aligned} T = &-p\mu_0 rl\left[\frac{1}{g_{\min}}\left(\frac{\pi}{2}+1\right)+\frac{1}{g_{\max}}\left(\frac{\pi}{2}-1\right)\right]F_{mms}F_{mmr}\sin\varphi_m \\ &-2p\mu_0 rl\left[\frac{1}{g_{\min}}-\frac{1}{g_{\max}}\right]F_{mms}{}^2\sin\varphi_m.\cos\varphi_m \end{aligned} \tag{3.14}$$

where:

p	:number of pole-pairs	l	:axial length in the air gap
μ_0	:permeability of air	g_{min}	:minimum air gap length
r	:rotor radius	g_{max}	:maximum air gap length
F_{mms}	:maximum fundamental stator MMF		
F_{mmr}	:maximum fundamental rotor MMF		
φ_m	:angle between fundamental stator MMF axis and rotor MMF axis		

The negative sign in expression (3.14) above refers to the fact that the torque acts to align the stator and rotor magnetic axes. For a cylindrical rotor, $g_{min}=g_{max}=g_0$ and so the second term, disappears, yielding a simpler torque equation:

$$T = -\frac{p\mu_0\pi rl}{g_0}F_{mms}F_{mmr}\sin\varphi_m \tag{3.15}$$

Thus, the first term is a torque expression for the cylindrical rotor and the second term accounts for saliency in the rotor. The second term is also known as reluctance torque. When the saliency of the rotor is apparent, g_{min} is not equal to g_{max}. It is evident from

equation (3.14) that provided $sin\ \varphi_m$ and the product $sin\ \varphi_m.cos\ \varphi_m$ are both positive or both negative, saliency increases the torque of the motor.

The effect of saliency on torque production can also be explained in terms of electrical circuitry parameters. In a synchronous machine the permeance along the direct axis (polar axis) is significantly greater than that of the quadrature axis (interpolar axis) and so the direct-axis reactance X_d is greater than the quadrature-axis reactance X_q. This is a key feature which accounts for differences in performance in electrical machines. A general expression relating reactances, terminal power and load angle can be derived from a phasor diagram with armature resistance neglected [FKU92]:

$$P = \frac{E_f E_e}{X_d} \sin\delta + E_e^2 \left(\frac{X_d - X_q}{2X_d X_q} \right) \sin 2\delta \qquad (3.16)$$

where:

P	:power per phase	X_d	:direct-axis reactance
E_f	:field excitation voltage	X_q	:quadrature-axis reactance
E_e	:bus voltage	δ	:load angle

The total torque is then:

$$T = \frac{3P}{\omega_s} \qquad (3.17)$$

where ω_s is the rotor speed.

Expression (3.16) is analogous to expression (3.14) in which the first term is applicable to the cylindrical gap machine and the second term introduces the effect of saliency. No reluctance torque will be established if the direct and quadrature-axis reactances are equal in magnitude. In comparison with the cylindrical rotor torque, the reluctance torque is independent of the field excitation voltage and of double frequency sinusoid. As illustrated in figure 3.9, the effect of saliency is to increase the maximum torque capability of the machine. This effect is more pronounced when the field excitation voltage is relatively small. The salient-pole machine is also stiffer because the gradient of the plot is steeper and

this characteristic improves the prospects for transient stability [Gra89b]. By varying the load angle δ, making E_f leads E_e or E_f lags E_e, the synchronous machine can be operated as a generator or motor respectively.

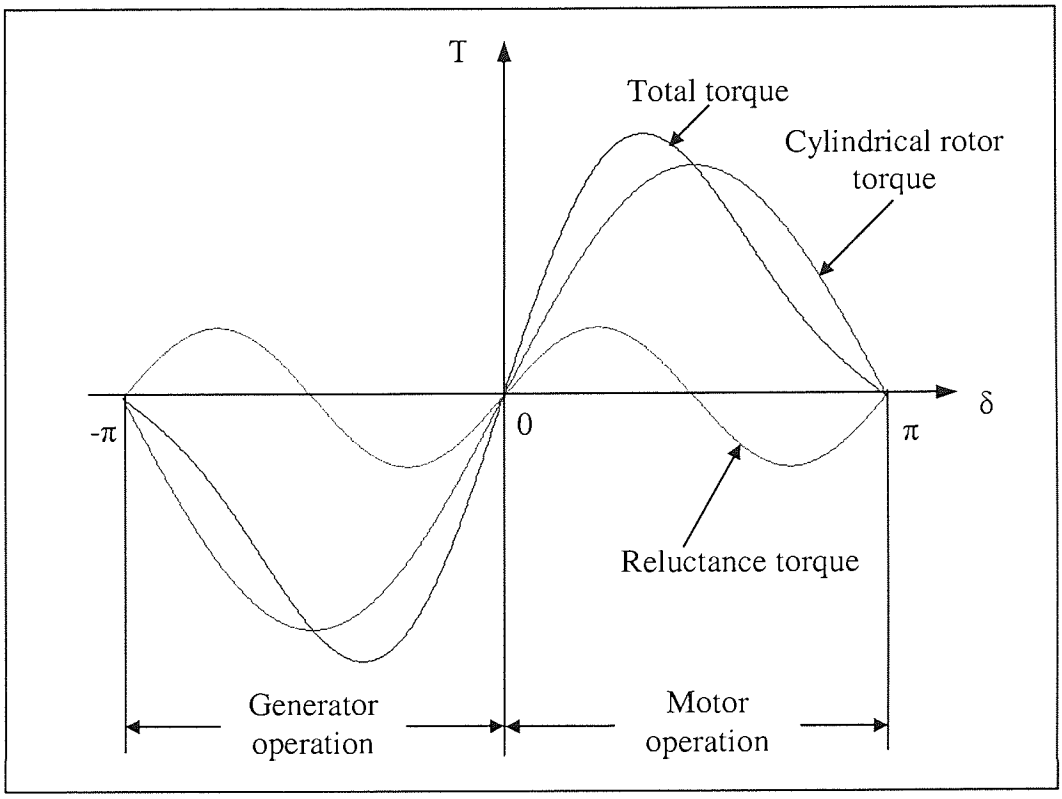

Fig. 3.9. Torque variation with load angle δ for a three-phase salient-pole synchronous machine.

3.4.2 The effect of saliency on lateral force production

Lateral force production in magnetic bearings is derived from the integration of normal stresses σ_n around the air gap enclosing the rotor journal. The surface area of the journal presented to the stator is important in determining the magnitude of lateral force developed. Maximum surface area is obtained when a cylindrical journal is used. For a salient-pole journal with the same air gap size (measured from its protruding poles), minimum reluctance paths are present at the pole surface while maximum reluctances are found elsewhere of the journal. Such a variant in the reluctance paths gives rise to an increase of effective air gap size when compared to the cylindrical case. In effect the lateral force developed on the rotating journal has been reduced. For this reason it is uncommon to incorporate salient-pole journals in magnetic bearing systems.

The levitation concept of self-bearing machines is somewhat different from magnetic bearings in the sense that the former rely considerably on the presence of motoring flux. Unlike magnetic bearings, saliency in self-bearing machines could offer the prospect of lateral force production since they utilise two set of fields namely, motor and levitation fields. As shown in figure 3.5, the motor fluxes traverse across the air gap entering the rotor at its salient-pole face, emerge at the other salient pole crossing the air gap again and back to the stator. If an additional set of field windings is provided such that the fluxes at one pole of the rotor is increased while the diametrically opposite pole is decreased, the rotor will be accelerated towards the gap where the field is stronger. Thus, saliency plays a role in reluctance self-bearing machines.

For other machines that do not rely entirely on saliency for torque production, it is debateable whether saliency could provide improvements such as increasing or supplementing the force production, simplifying control methods, etc. Consider two permanent magnet self-bearing motors with concentric rotors shown in figures 3.10(a) and (b). Both machines are identical except the fact that one has a cylindrical rotor whereas the other has a salient-pole rotor. Each stator excites two different currents of magnitude and phase namely, motor current and levitation current. Levitation is achieved by superimposing a two-pole levitation field supplied by the levitation current to the four-pole motor fields created by the motor currents and permanent magnets.

For a permanent magnet machine the motor fluxes are contributed predominantly by its permanent magnets. Therefore, by injecting currents of appropriate magnitude and phase in relation to the field created by the magnets, an upward lifting force is produced as shown in figure 3.10(a). Note that the two-pole levitation field also unbalances the four-pole field generated by the motor currents. Because the reluctance paths across all the air gaps are equal and the motor flux density is relatively small, the interaction between the fields generated by motor and levitation currents is small. This lateral force acts in the positive x-direction as depicted in figure 3.10(a). Since this force is much smaller than the vertical force produced by the interaction of permanent magnets and levitation current, the net lateral force is still very much in the vertical direction. However, when the motor current is increased, the direction of the resultant lateral force is no longer vertical, but at a direction defined by the vector summation of both forces.

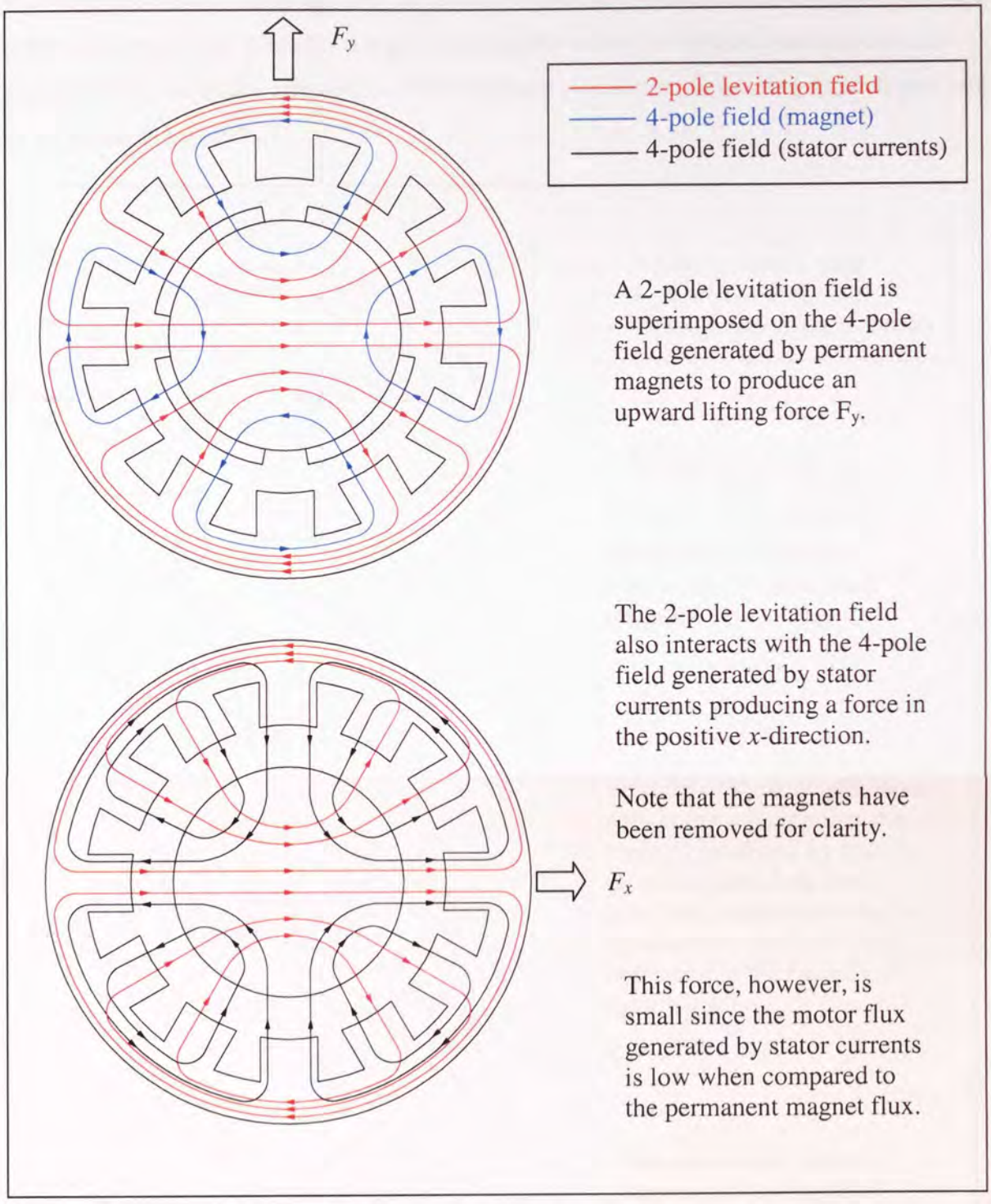

Figure 3.10(a): Lateral force production in a cylindrical rotor machine.

With the same currents applied to the machine with a salient-rotor, the magnitude and direction of force due to the interaction between permanent magnets and levitation fields is similar to that of the cylindrical rotor machine. This is shown in figure 3.10(b). However, the force at positive x-direction created by the interaction between motor and levitation fields is now substantial because of the low reluctance paths at the protruded poles. Even a small motor current excitation will result in large force exerted in the horizontal axis. This

particular force will dominate over the intended vertical force if the motor currents are further increased. This scenario is highly undesirable since the intended vertical direction of force has been seriously affected. A finite element simulation supporting these arguments can be found in appendix C.

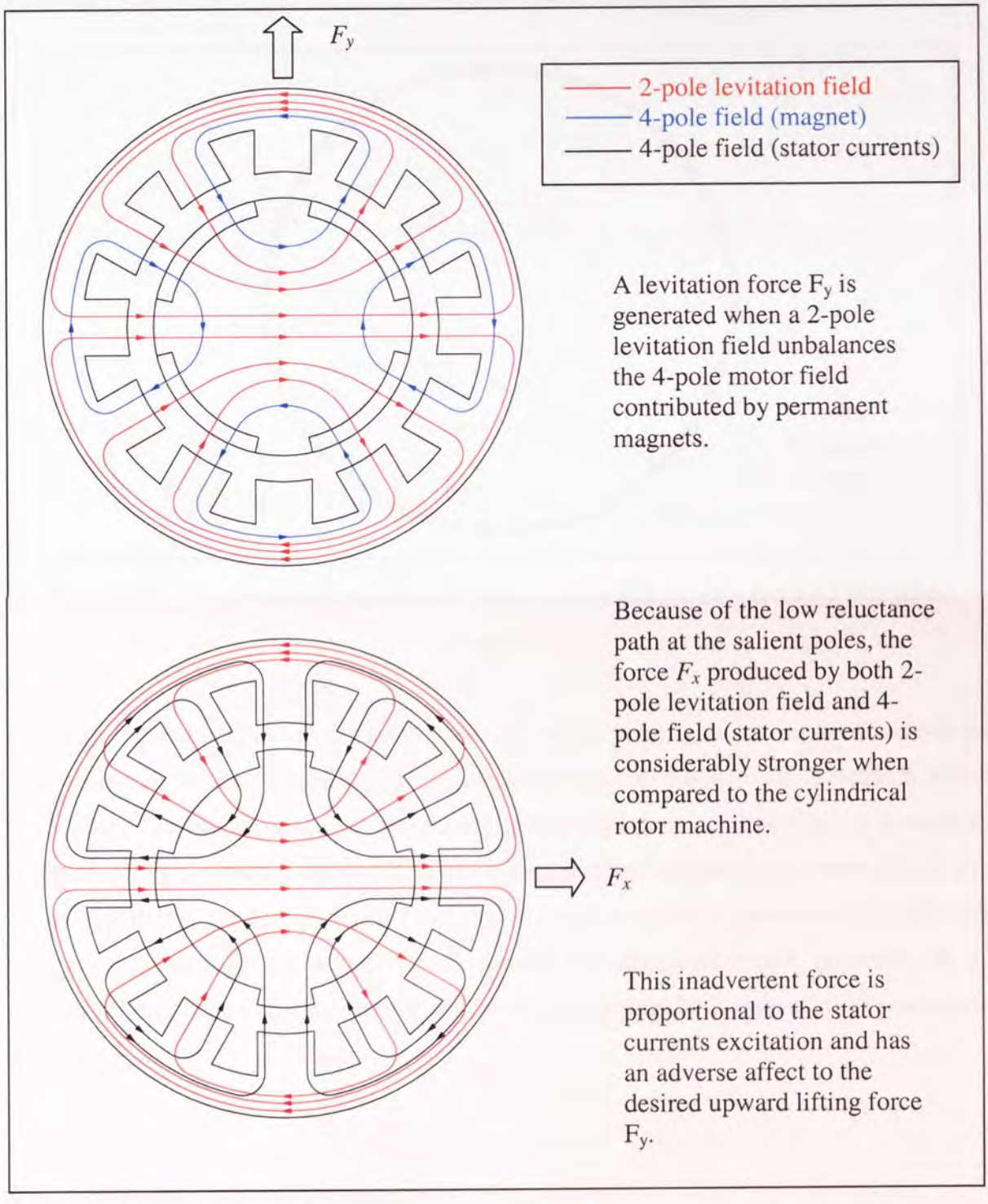

Figure 3.10(b): Lateral force production in a salient-pole rotor machine.

One way of correcting the force control is by switching the levitation currents as if it is a reluctance motor in figure 3.5. Since lateral forces are exerted only at the salient poles of the

rotor, it is necessary to supply both motor and levitation currents simultaneously to the appropriate stator teeth where the salient poles are present at any operating instant. The disadvantage associated with this control method is that the abundant flux provided by permanent magnets is not being used at all. Furthermore, controlling the permanent magnet motor as a reluctance motor tends to give rise to more torque ripple.

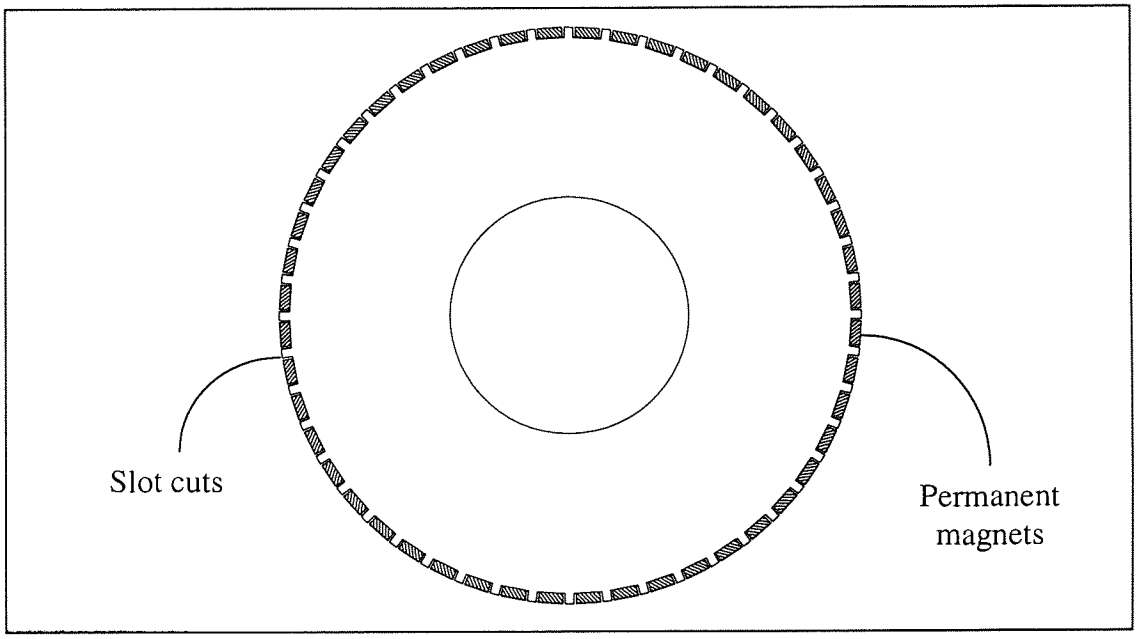

Figure 3.11: A permanent magnet rotor with multiple slot cuts for housing permanent magnets.

Although the example above disfavours saliency in self-bearing motors, it does not rule out completely all forms of saliency to be implemented for the sake of increasing torque production. The salient-pole rotor considered previously has a small number of protrusions and each protrusion face is relatively large causing sharper irregularities around the air gap. As an alternative, a rotor with small slot cuts for accommodating permanent magnets and evenly spread around its periphery will reduce the unwanted forces generated at the protrusions by the interaction of motor and levitation currents. This type of rotor is shown in figure 3.11.

3.5 Summary of principal matters

In any self-bearing machines, lateral force and torque arise as the integration of Maxwell's normal and tangential stresses respectively in the air gaps. When an additional field of a pole-pair differing by one is superimposed on the existing motor field, a net lateral force is

produced between stator and rotor. On the other hand, exciting motor currents with the same pole-pair as the motor field will give rise to a rotational torque. Thus, to generate torque and lateral forces simultaneously in an electrical machine, the essential requirement is to apply torque and force-producing flux components that have a pole-pair number differing by one.

The lateral forces exerted on the rotor are proportional to the product of maximum motor and levitation flux densities. The usual design practices for electric motors result in relatively high flux densities in the air gap for their normal torque-producing function. It is intuitively obvious that a relatively small amount of additional flux can create a significant net transverse force between rotor and stator. Therefore, the presence of torque-producing component of magnetic flux can be advantageously used to exert lateral forces with addition of a minimum amount of levitation flux.

An active control of two degrees of freedom can be implemented if the rotor diameter is very much greater its axial length, such as in disc-shaped or short span self-bearing motors. Other degrees of freedom are stabilised passively. In particular, the axial and angular displacements rely on the properties of Maxwell stress tensor to restore the rotor to its equilibrium position.

Saliency is very often exploited in electrical machines to increase torque capability. This is possible because of the established reluctance torque in addition to the cylindrical rotor torque. In magnetic bearings, however, salient-pole journals are not used because the variation of reluctance path around the air gap increases the effective air gap size. Such an increase in air gap causes a reduction of lateral forces exerted on the rotating journal.

The principle of lateral force production in self-bearing machines is different from that of magnetic bearings because the former rely on additional flux superimposed to unbalance the motor flux distributions. While saliency is important for torque and force production in reluctance self-bearing machines, it could have undesirable effects in other types of machine such as an AC permanent magnet self-bearing motor. In permanent magnet self-bearing motors the fluxes contributed by the magnets and levitation current are utilised for the achievement of force production. The presence of saliency could lead to unwanted lateral forces to be exerted on the protruded poles because of the interaction of motor and levitation fields, and thereby affecting the intended vertical direction of force. Such a consequence could be reduced if an appropriate rotor design methodology is adopted.

CHAPTER 4

AC SELF-BEARING MOTOR WITH A SINGLE SET OF WINDINGS

In the foregoing chapters, background and essential aspects of self-bearing machines were presented to lead the reader to the heart of the thesis. This chapter, as the main contribution of the research, unveils a novel concept of producing lateral forces and torque in a rotating electrical machine utilising only a single set of windings and minimal addition of power electronic devices. It begins by describing how the new winding connection scheme is derived along with its general properties before proceeding to other variants of the connection. The advantages of such a connection over conventional self-bearing motor windings are discussed at the end of this chapter.

4.1 Principal aims of research revisited

We saw in chapter 2 how the presence of a secondary set of windings limits the capacity of the self-bearing machine. Using a single set of windings conventionally connected, however, requires more power electronic devices to switch the necessary motor and levitation currents, and this may be expensive. It is the principal aim of this research to investigate the use of a single set of windings for carrying both motor and levitation currents simultaneously so as to achieve a net lateral force in any desired arbitrary direction in addition to its normal torque production. The presently proposed scheme requires only one standard motor drive for its torque generation and relatively low power rated supplies for switching levitation currents. Hereafter, the term "levitation current" is used interchangeably with the term "bearing current" and the power electronic device that switches this current is also known as a "bearing inverter" or "bearing supply".

4.2 General observations of flux distribution in the air gap

Most electrical machines are conventionally connected such that lateral forces are balanced even if an unbalanced supply is applied. This is achieved by using parallel connection of coils on diametrically opposite sides of the machine so that if one of these sees an unusually high or low current, its partner also sees this and the increase in net lateral force is zero. The

windings of virtually all AC electrical machines are organised into two or more separate phases. Each phase is an independent circuit which can carry current even if the other phases are open circuit. Each phase has two terminals. Sometimes, the ends of phases are connected together inside a machine but most commonly, all phase ends are brought out to the terminal box.

Since the excitation currents dictate how flux is distributed or changed around the air gap periphery, it is perhaps appropriate to examine first the distribution properties of the motor and levitation fields before formulating some possible winding connections. A simple 4-pole motor that uses an additional 2-pole levitation field to exert lateral forces on rotor is considered. It is assumed that each stator tooth has a single coil wound and independently excited to produce the required flux distributions. The rotating fields produced by motor and levitation currents are studied separately and crosschecked to determine how the coils should be arranged in the stator slots.

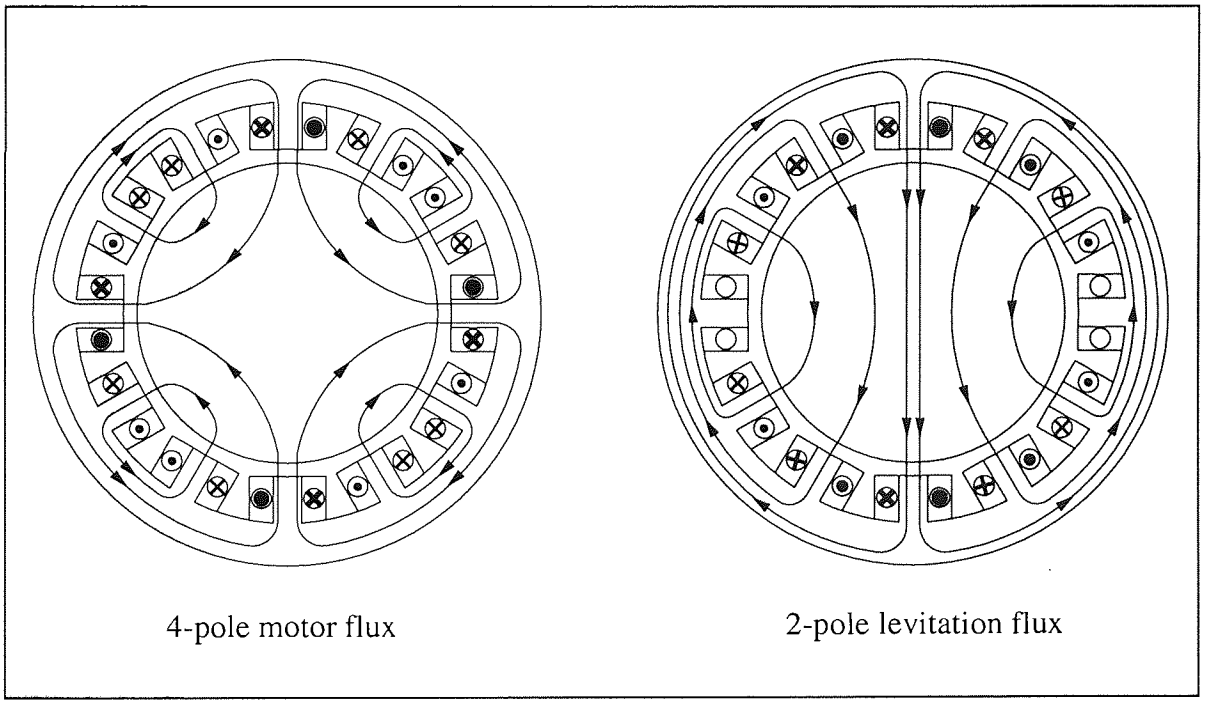

Figure 4.1: Flux distributions for a 4-pole motor and 2-pole levitation fields.

Figure 4.1 illustrates that if the motor flux is considered exclusively, a round trip along the air gap periphery gives four changes in magnetic polarity. These polarity changes are not abrupt but involve some transitional change so that ideally the waveform would be sinusoidal. It can be seen that for a 4-pole motor, diametrically opposite teeth spanning 180° produce the same magnitude and direction of motor flux density. This is as true as saying

that conductors in the diametrically opposite slots are carrying the same magnitude of currents and in the same direction. Now if the 2-pole levitation flux is considered solely, as shown in figure 4.1, diametrically opposite stator conductors carry the same magnitude of levitation currents but in the opposite direction.

As a design aid, the properties of diametrically opposing teeth or slots in relation to the pole number, flux density and current density are deduced first. Accordingly, a $4(1+n)$ pole flux gives rise to the same magnitude and direction of flux densities at diametrically opposite teeth, whereas a $2(1+2n)$ pole flux produces the same magnitude but opposite direction of flux densities. Here n is an integer $0, 1, 2, 3$, etc. The same rule also applies to the current carrying conductors: the same magnitude and direction of current densities at diametrically opposite slots generate a $4(1+n)$ pole field, whereas the same magnitude but opposite direction of current densities generate a $2(1+2n)$ pole field. This general observation can be summarised as shown in Table 4.1 below.

Flux distribution	Magnitude of flux or current	Direction of flux or current	Pole numbers
$4(1+n)$ pole	Same magnitude	Same direction	4, 8, 12, etc.
$2(1+2n)$ pole	Same magnitude	Opposite direction	2, 6, 10, etc.

Table 4.1: Attributes of diametrically opposite teeth and conductors in the stator.

In general the attributes listed in table 4.1 applies to any self-bearing machines where if a $4(1+n)$ pole field is chosen as the motor field, the levitation field must form a $2(1+2n)$ pole field and vice versa. A useful piece of information can be extracted from this table. It is evident that diametrically opposite teeth and conductors have the same magnitude attributes for both $4(1+n)$ and $2(1+2n)$ pole fields. This suggests a possibility of using the same excitation source (having output terminals + and -) for the coils at diametrically opposite teeth. The term "same excitation source" here means same DC link, rectifier and utility supply and as a whole represents one unit of power supply or inverter. Therefore, diametrically opposite coils can be connected either in series or parallel to a common inverter.

It appears that the same excitation source can be used for supplying both motor and levitation currents in the diametrically opposite coils by considering the magnitude attribute listed in table 4.1. Unfortunately the direction attribute in table 4.1 imposes a limitation to our inclination to incorporate the same source and same set of conductors for producing motor and levitation currents. For a 4-pole motor, a pair of diametrically opposite coils connected in series or parallel to a single excitation source would give the same magnitude and polarities if the torque-producing component of current were excited. If the same source were to supply a levitation-producing component of current, the same magnitude and polarities would be obtained. Thus, the required 2-pole levitation field cannot be produced and this implies that a separate source is inevitable.

The review in chapter 2 showed that self-bearing machines with a single set of windings require a number of motor supplies for their normal torque production. By making use of the aforementioned properties, the stator coils can be physically connected such that only one unit of motor inverter is needed to drive the self-bearing motor. Furthermore, from the previous chapter, it is shown that the amount of levitation flux needed for producing lateral forces is very small compared to the main motor flux. Hence, relatively low current and low voltage bearing inverters can be employed to switch levitation currents. This new connection scheme is discussed in the next section.

4.3 The "bridge" connection: A novel connection scheme for AC self-bearing rotating electrical machines

It is not uncommon in machine design to find that phases comprise several parallel groups of windings. The stator windings proposed in this thesis comprise a number of independent phases and each phase may be split into two or more parallel groups. For simplicity of description, we assume that this number is two but the extension to higher numbers is straightforward. Each group further comprises a series connection of coils. For simplicity of description again, we assume that there are two coils per group but the extension to higher numbers is possible. Since all electrical machines have distinct phases with 2 ends to every phase, we can consider only one phase as shown in figure 4.2.

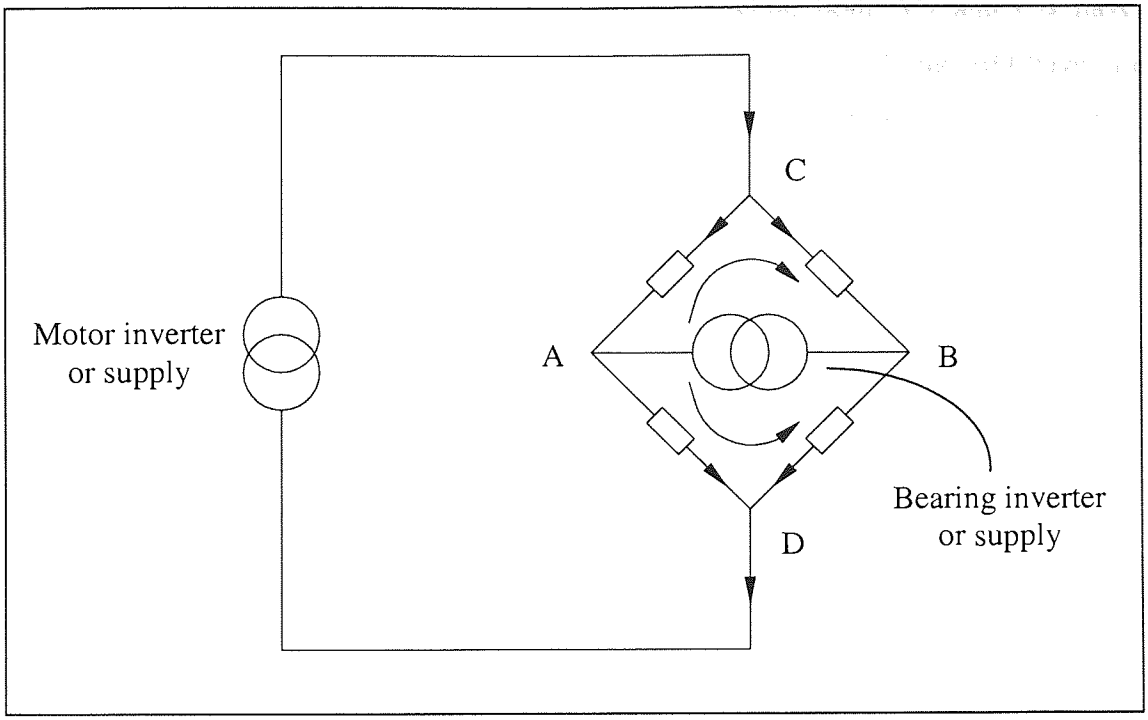

Figure 4.2: A fundamental connection scheme for coils in one phase of the new self-bearing machine (The "bridge" connection).

The principal feature of the winding is that the currents responsible for torque production are divided into two parallel paths in each phase. By injecting additional current between the mid points of each path in a bridge-like configuration, a net lateral force is generated. The currents flowing in arms "CA", "CB", "AD" and "BD" are expected to be very substantial compared with the levitation current flowing in the branch "AB". Similarly, the voltage drop across "AB" is expected to be very small compared with the full voltage rating for the phase "CD". Referring to the total current flowing across "CD" as the main machine current, it is evident from symmetry that if the impedances of branches CA, CB, AD, BD are the same, the voltage drop across CD is independent of the current through AB and vice versa.

Each branch of the bridge-like configuration can be regarded as a coil wound around a single stator tooth. To conform to the properties observed in table 4.1, coils must be so wound or connected to either:

- produce the same magnetic polarity when a motor current is supplied across the parallel paths CD. In this manner the polarities created at one pair of coils as a result of bearing current excitation are guaranteed to be opposite of the other pair, i.e.

branches CA and BD have the same polarity while both AD and CB have the opposite polarity respect to CA and BD. Since branches CA and BD have similar attributes they can be conceived as a group. Likewise, branches AD and CB are conceived as another group and these two groups of coils must be placed diametrically opposite to each other according to the properties listed in table 4.1.

- or produce the same magnetic polarity for a pair of parallel coils and the opposite polarity for the other parallel pair when a motor current is injected at points C and D. Injection of levitation current will now result in the same polarity for all coils in the bridge. This configuration can be thought as having the previous connection scheme being reversed inside out. Each parallel pair of coils with the same polarity form a group and these two groups of coils are placed diametrically opposite to each other.

The schematics of the connection and arrangement of coils for both cases are shown in figures 4.3(a) and 4.3(b). The magnetic polarities as a result of motor and levitation excitations are labelled at the exterior and interior of the bridges respectively. These polarities are interchanged when a reverse direction of current is flowing in the coils.

The issue about impedance mismatch in the connection can be resolved by ensuring that the voltage rating of the bearing inverter must be sufficient to withstand the voltage that will exist across it. With this implementation, unbalanced currents that arise from the mismatch coil impedance can be prevented from flowing into the bearing inverter. The current that the bearing inverter injects must be trimmed accordingly to take account of the impedance mismatch.

The proposed connection scheme is hereby referred to as the "bridge" connection. For practical applications of such a connection, the fundamental bridge connection in figure 4.2 must be extended to permit generation of the necessary motor and levitation fields in the air gap. The subsequent sections of the thesis describe in a greater detail of how extensions and other variants may be implemented.

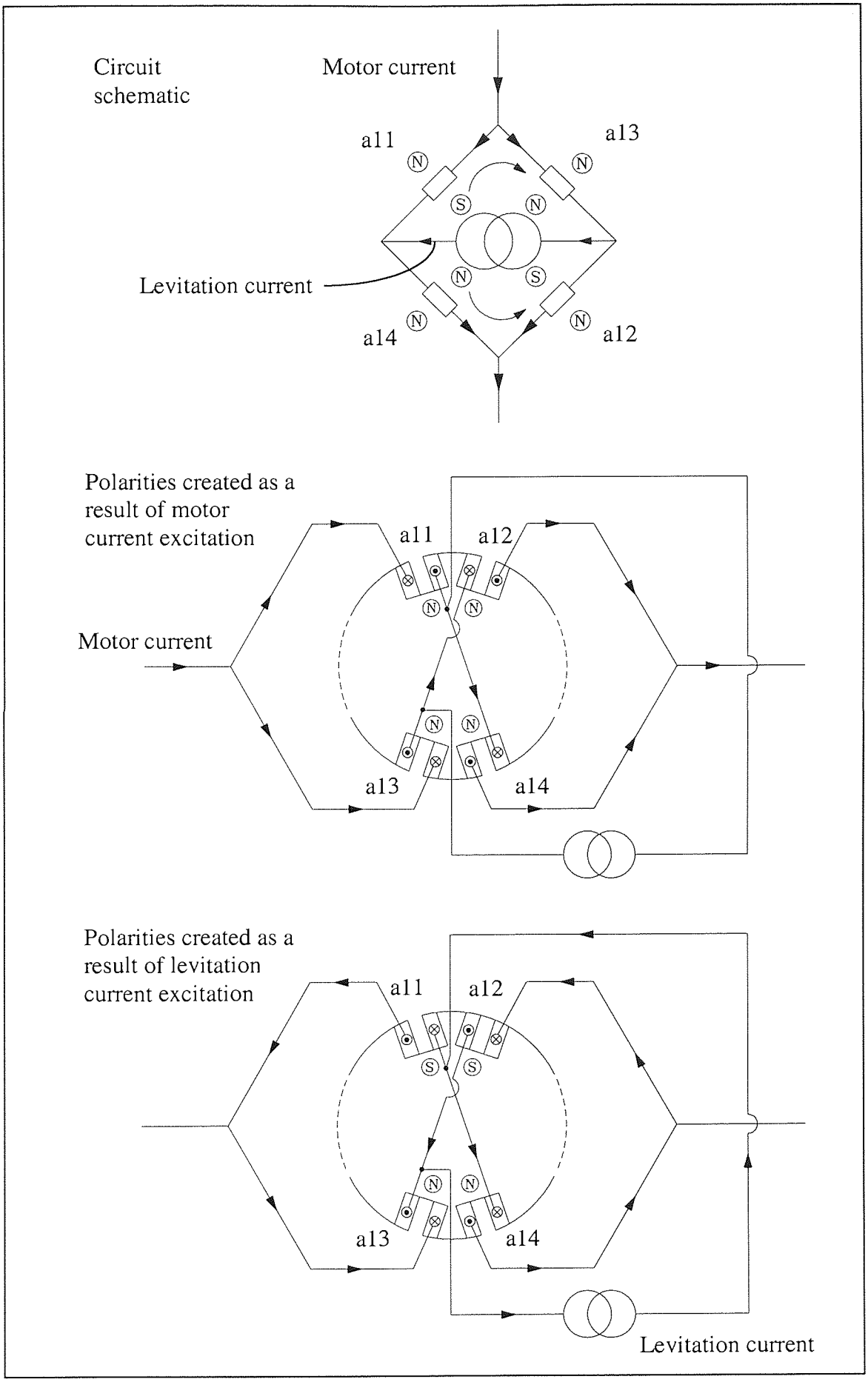

Figure 4.3(a): A schematic of connection to obtain the properties listed in table 4.1.

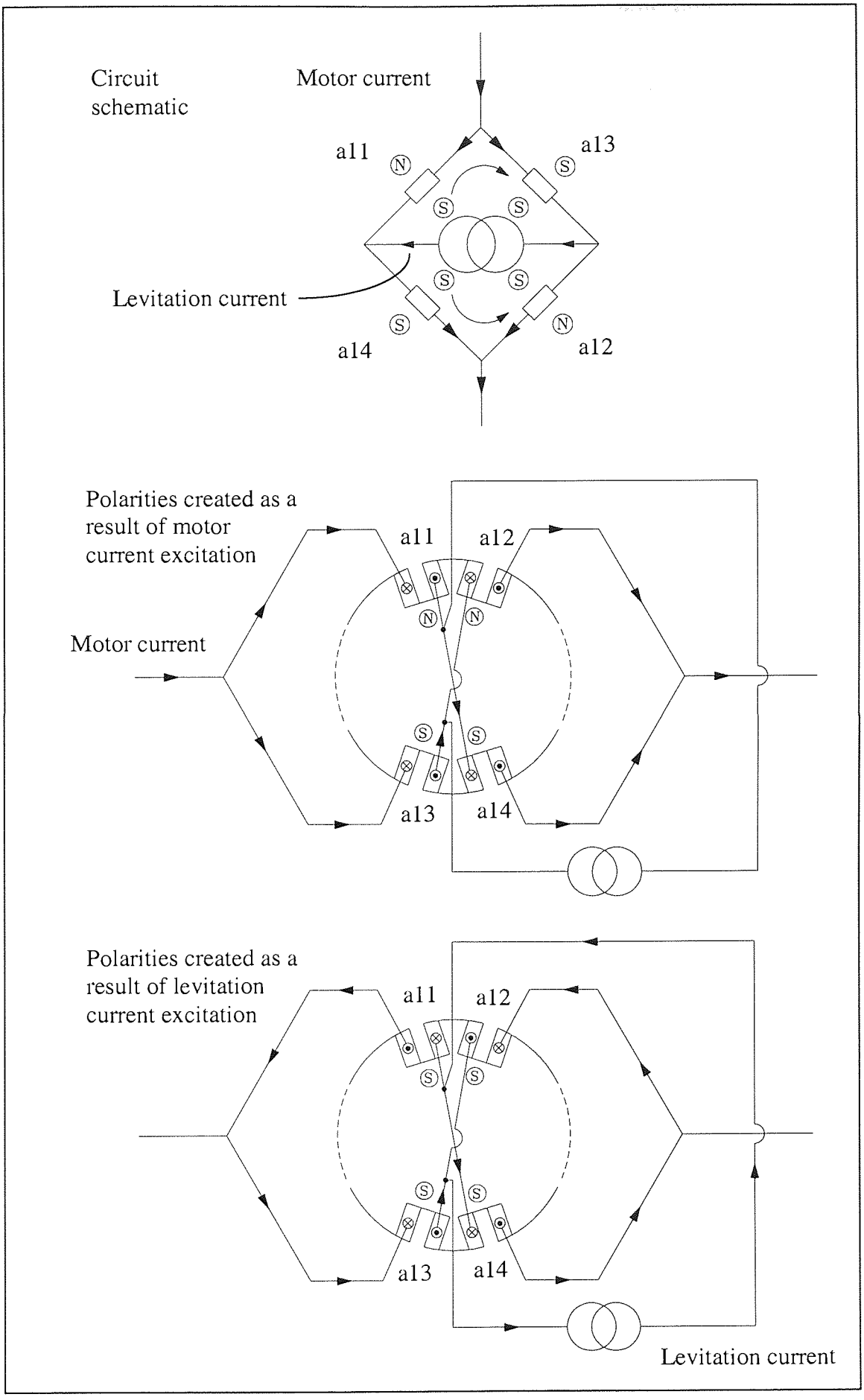

Figure 4.3(b): An alternative connection to obtain the properties listed in table 4.1.

4.4 General extensions and other variants of the bridge connection

The significance of the bridge connection is that it can be easily extended to higher phases and concurrently serving to offer locations for injecting bearing currents. Such a configuration in figure 4.2 can be regarded as a building block where any extensions required can be accomplished by linking the motor currents injection points. For instance, point D (in figure 4.2) of a bridge can be linked to point C of another bridge, etc. Two main variants of the bridge connection are explained namely, concentrated windings and "equivalent" distributed windings, and in addition each variant has two types of connection.

4.4.1 Concentrated winding (Type I)

In its simplest configuration the bridge connection scheme in figures 4.2 and 4.3 must be extended to form two bridges which requires a single phase motor supply and two bearing supplies At this juncture we simply consider the self-bearing motor to be a generic machine. This single phase 4-pole self-bearing motor having 8 stator teeth and its coils connection are illustrated in figure 4.4.

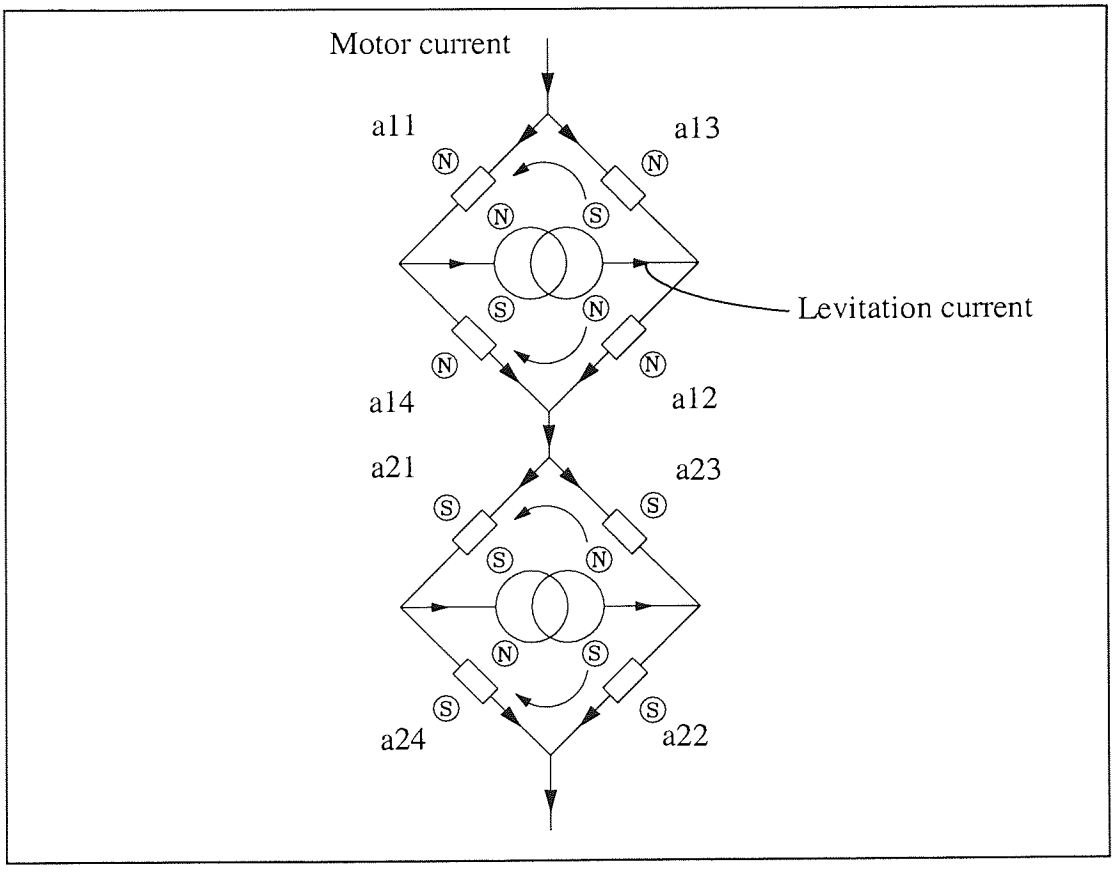

Figure 4.4: Coils connection of a single-phase self-bearing motor.

Coils are arranged such that the set of 4 coils in the top bridge ("a11", "a12", "a13" and "a14") gives an N polarity while the other set of coils in the bottom bridge ("a21", "a22", "a23" and "a24") gives an S polarity when a positive motor current flows in the direction as shown. The motor polarities as well as the levitation polarities are designated at the exterior and interior of the connected bridges respectively. Each bearing supply generates a 2-pole levitation field of its own and is controlled independently from the other. When both bearing supplies are activated the corresponding MMF axes are orthogonal to each other as shown in figure 4.5. This results in a linear combination of MMFs for producing lateral forces in any arbitrary directions.

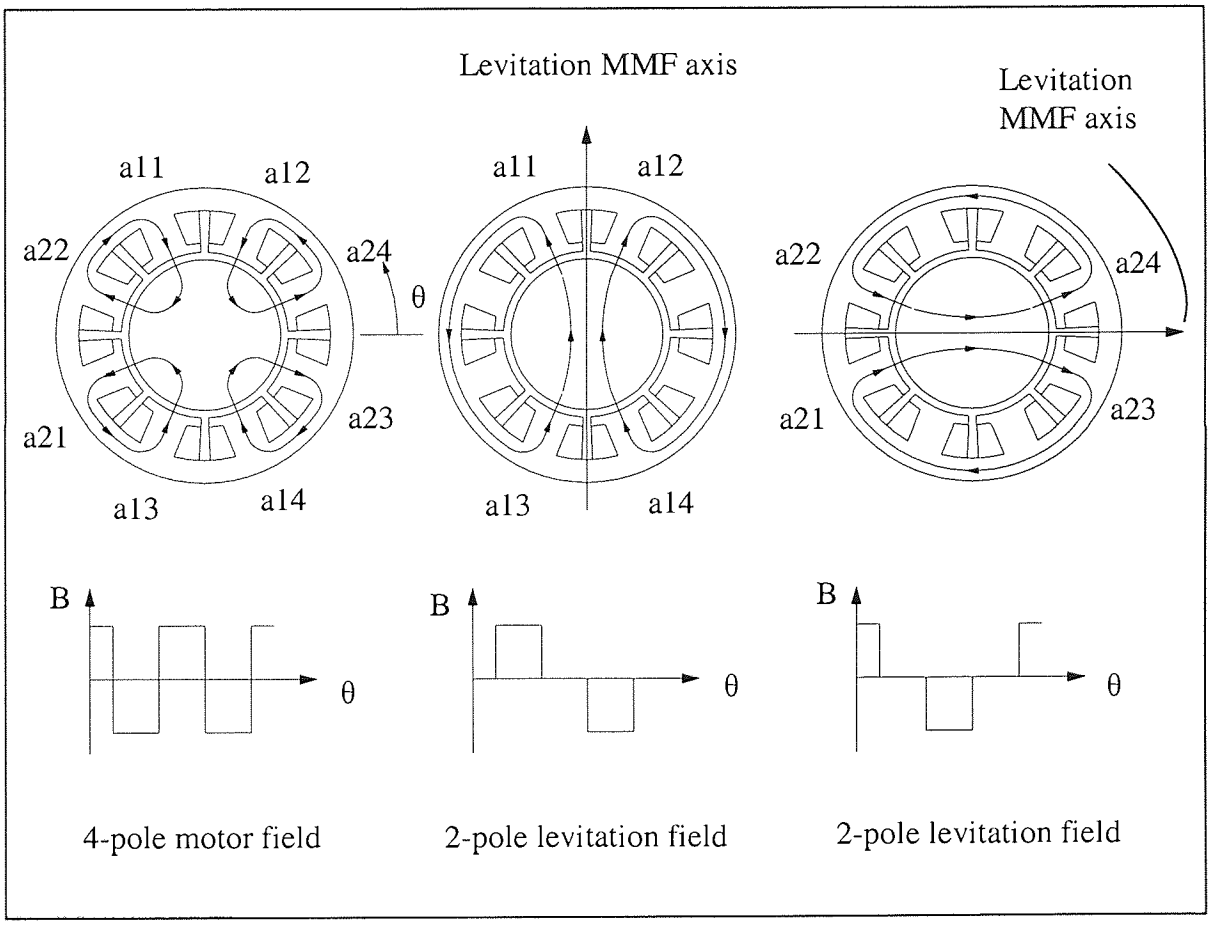

Figure 4.5: Motor and levitation flux distributions of a connection shown in figure 4.4.

Since the motor has a relatively small number of stator teeth and operates on a single-phase supply, the space distribution of flux in the air gap at any operating instant is of a square waveform. A direct consequence of such a machine is that the generated torque is not smooth but with serious ripples. Therefore, it seems that a higher number of phases and a larger number of stator teeth are preferable to reduce the torque ripple in the machine.

The connection in figure 4.4 can be conveniently extended to form a three-phase star connection, yet retaining the number of pole of the motor and levitation fields, as shown in figure 4.6. Accordingly, there are 8 coils per phase and so a 24-tooth stator is needed to accommodate all three-phase coils. In what follows, the description of coils arrangement is confined to phase "a" coils since the connections of phases "b" and "c" are similar to that of phase "a".

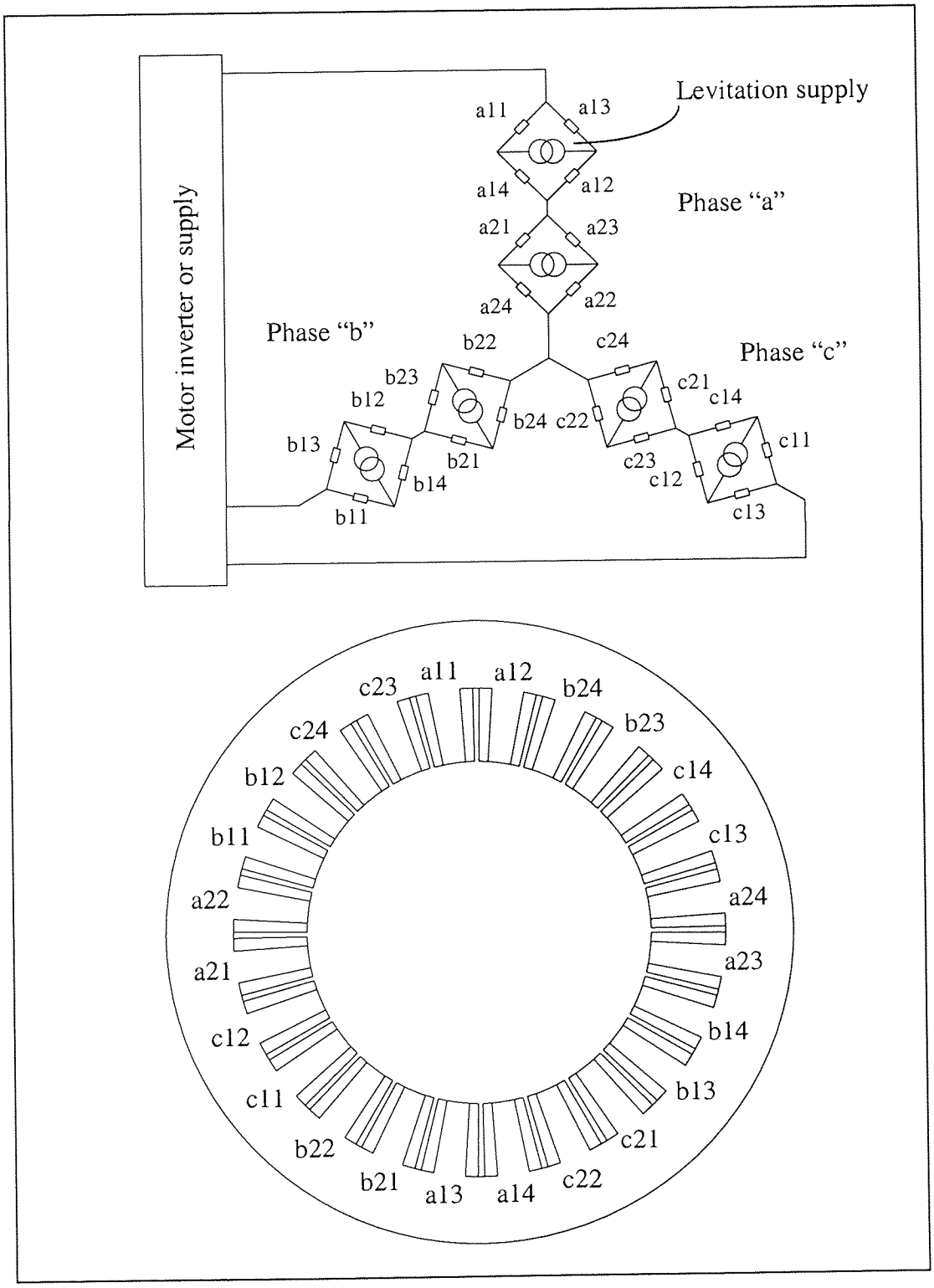

Figure 4.6: Winding arrangement of a three-phase self-bearing motor.

For the present arrangement coils-pairs "a11"-"a12" and "a13"-"a14" produce equal magnitude but opposite direction of bearing currents flow with respect to each other. The same current attributes also apply to coils-pairs "a21"-"a22" and "a23"-"a24" of the bottom bridge of phase "a". Since this is a 4-pole motor, a round trip along the periphery of the air gap interface yields four times of polarity change per phase. The imposed 2-pole levitation field, however, yields only twice polarity change per phase. This implies that coils-pairs "a11"-"a12" and "a21"-"a22" must be diametrically opposing coils-pairs "a13"-"a14" and "a23"-"a24" respectively according to the properties in table 4.1. Moreover, the coils in the respective top and bottom bridges of phase "a" must be orthogonal to each other. Similar arrangement also applies to phase "b" and phase "c" coils, and all phase coils are spaced 60° mechanical degrees apart around the slots of the machine as shown in figure 4.6.

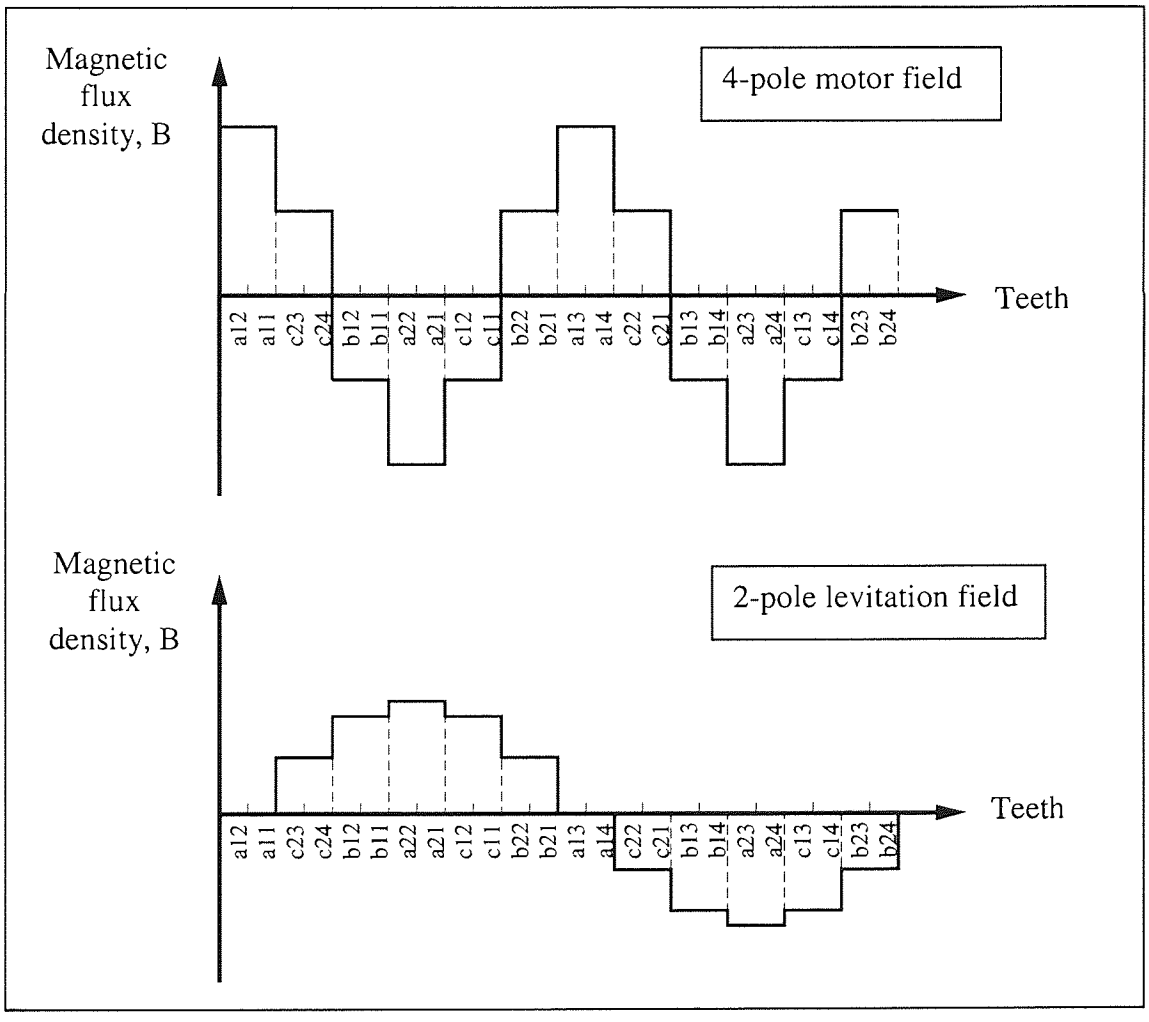

Figure 4.7: MMF distributions of a three-phase self-bearing motor with 24 stator slots.

When comparing to the single-phase self-bearing machine described earlier, the present three-phase machine has a better sinusoidal MMF distribution in the air gap. This is

attributable to the fact that the three-phase machine has more stator slots and offers more locations for the bearing currents to be injected. The increase in the number of locations for current injections means that the MMF distribution can be shaped to better approximate to a sinusoidal distribution as indicated in figure 4.7.

The bridge in Type I connection, however, is inherently unbalanced because of a phase shift in the back EMF generation. For example, coils "a11" and "a12" of a bridge are wound at adjacent stator teeth spaced at a certain angle. Because these coils are not wound coincidentally on the stator tooth there is bound to be a phase shift when back EMF is induced in the coils. As a result the machine torque may be slightly affected. As far as the injection of levitation current is concerned, the bridge is balanced naturally due to same potential drop on both parallel paths.

4.4.2 Concentrated winding (Type II)

The three-phase self-bearing motor with Type I concentrated windings described previously requires a total of 24 stator slots to accommodate all 24 phase coils. It can be seen in figure 4.7 that pairs of adjacent concentrated coils in the stator slots produce the same magnetic polarity regardless of whether the motor or levitation currents are flowing. Such a flux distribution in the air gap can be equally achieved by requiring only 12 stator slots, and, since the number of teeth has been reduced by half, more number of turns of copper can be accommodated in the slots.

Figure 4.8 illustrates how coil-pairs "a11"-"a12" and "a13"-"a14"of the top bridge in figure 4.6 can be arranged in a 12-tooth stator. Coils "a11" and "a12" are stacked up and aligned at the same axis of symmetry, thereby producing the same magnetic effect as having a single coil with twice number of turns. Likewise, coils "a13" and "a14" are wound at the diametrically opposite tooth and their terminals are connected to coils "a11" and "a12" to form a bridge. When coils in all bridges are connected in a similar manner, the resulting 12-tooth stator windings arrangement is shown in figure 4.9.

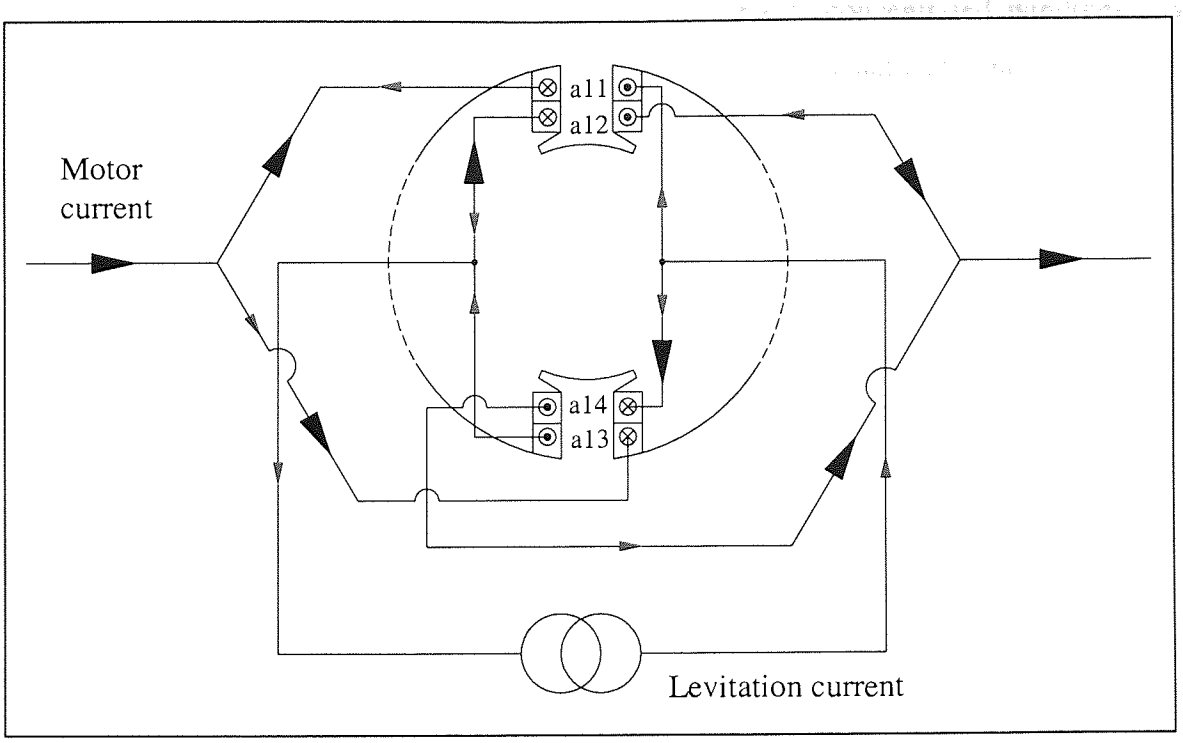

Figure 4.8: An alternative arrangement of the top bridge phase "a" coils.

Another way of describing this arrangement is that each coil wound around a single tooth is split into two smaller coils with equal number of turns. However, unlike early self-bearing motors that incorporate separate sets of windings for torque and lateral force production, the conductors in the present machine carry both motor and bearing currents simultaneously. This innovative arrangement essentially produces the same MMF pattern as that of Ohishi and Okada's bearingless machines but having advantages of needing only one motor inverter. Levitation forces are produced by employing six relatively low voltage and low current bearing inverters.

The issue of phase shift in back EMF generation, mentioned in the previous Type I connection, is not a concern for the present scheme. This is due to the fact that coil pairs in any bridge are wound coincidentally on the same stator tooth and so there is no space and time difference with respect to the rotor's rotation.

The method of winding the stator for the present self-bearing machines is perhaps most conveniently achieved by employing pre-wound coils where they can be placed and removed easily in the stator. The use of such coils, however, depends primarily on the physical geometry or shape of the stator tooth. Not every stator design or construction can

be used in conjunction with pre-wound coils. Nevertheless, concentrated windings have advantages such as shorter end winding and more dense and compact end winding.

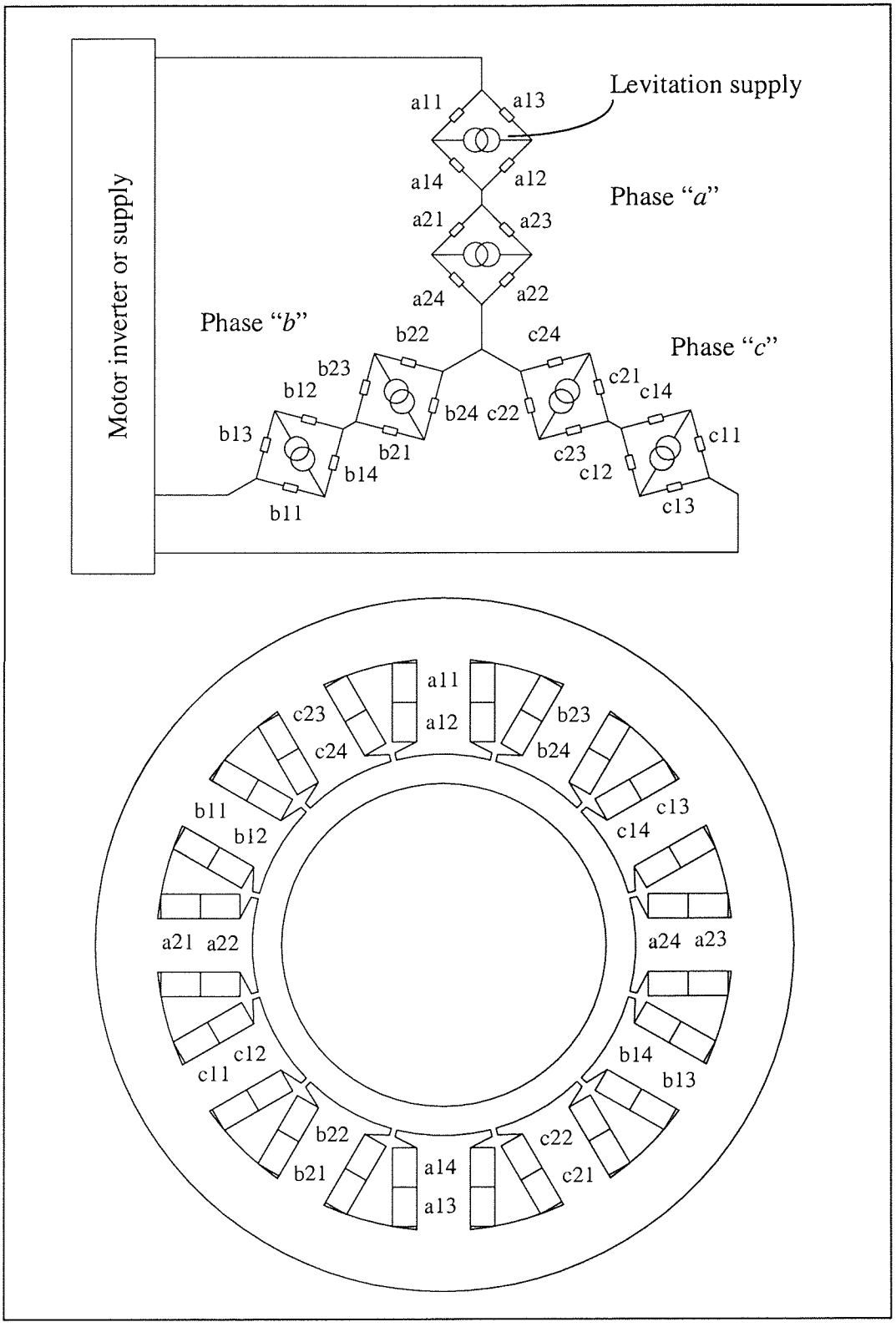

Figure 4.9: Stator coils of a three-phase self-bearing motor according to the method of connection shown in figure 4.8.

4.4.3 "Equivalent" distributed winding (Type I)

Concentrated windings are well suited to use in machines with a relatively low slot number. For the self-bearing motor with type II concentrated windings discussed earlier, the flux distribution around the air gap periphery as a result of current excitation is of a rectangular shape to some extent. It is natural, therefore, to suppose that with a higher number of stator teeth and more bridges per phase introduced, an improved sinusoidal flux distribution can be accomplished. For instance, a 24-tooth stator having type II concentrated winding would require twelve independent bearing inverters to give a better sinusoidal waveform. The drawback, however, is that the number of bearing supplies needed has been doubled and could be expensive and complicated to control.

The desire to minimise torque ripple reinforces the need to utilise distributed winding arrangement. Although distributed windings have longer end windings which increase the resistance, they are superior to concentrated windings in reducing the harmonic content and producing an MMF distribution closer to sinusoidal. Double layer distributed windings are commonly found in electrical machines where the windings are overlapped in the slots and *continuous from one phase to another*. These machines cannot be turned into self-bearing motors by simply injecting the appropriate magnitude and phase combinations of motor and bearing currents. Such windings can be retained in the machine if an additional set of windings is introduced for rotor position control. This idea, however, departs from our primary aim of utilising only a single set of windings and is therefore discarded.

There is a motivation to formulate alternative winding methods based on the bridge connection scheme to obtain a sinusoidal flux distribution with minimal additional power electronic devices. The properties listed in table 4.1 are used as basis to arrange the windings forming a magnetic flux distribution that is equivalent to that of conventional machines with double layer distributed windings. Consider a 4-pole self-bearing motor having a 24-tooth stator with double layer distributed winding arrangement. At this juncture we assume that the windings are so connected to produce the same 2D-magnetostatic flux distributions of in conventional machines.

Figures 4.10 and 4.11 respectively show the same set of double layer winding with distributed current densities in the stator slots producing a 4-pole motor and a 2-pole levitation fields at one instant. Without referring to how the coil sides are connected or

labelled, the current densities distribution resembles to that of a distributed fractional-pitch winding. Only a minimum number of flux lines is shown for clarity. As far as the 2D field with neglected end effects is concerned, the same motor or levitation MMF patterns can be produced so long as the same distributed current densities are applied as in figures 4.10 and 4.11. Consequently there are many ways in which the phase windings can be connected. Owing to the requirement that the same conductor must carry both motor and bearing currents, the manner in which the stator can be wound is restricted to a certain extent.

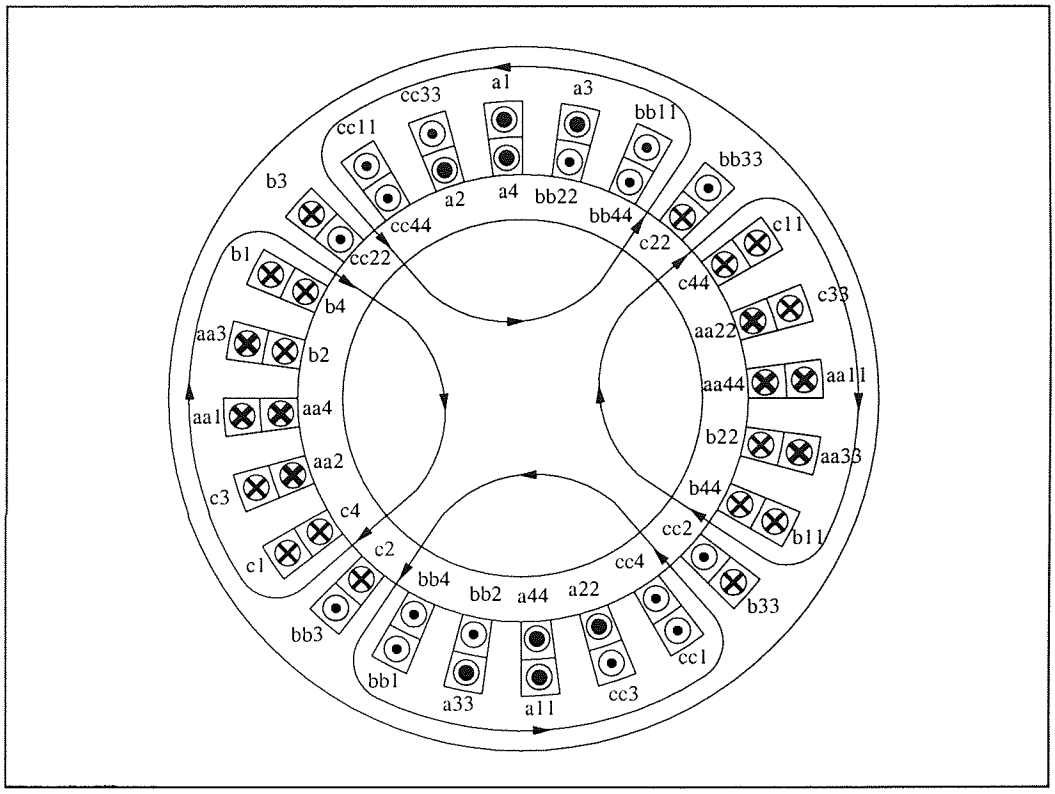

Figure 4.10: Distributed current densities in a 24-tooth stator producing a 4-pole motor field.

It is evident from figures 4.10 and 4.11 that some conductors carry the same magnitude and direction of current whereas some are of the same magnitude but opposite direction. The MMF patterns along the air gap periphery vary according to the attributes listed in table 4.1 and this suggests that it is possible to supply these conductors with only one common source. Using table 4.1 as a design aid, diametrically opposing conductors "a1" → "a4" and "a11" → "a44" must be linked together to form an independent bridge. Likewise, coils "aa1" → "aa4" and "aa11" → "aa44" must be associated to form another independent bridge. Therefore, the combination of two independent bridges constitutes phase "a" winding. In a similar fashion, phase "b" and "c" windings also provide two independent

bridges each and together with phase "a" winding, a total of six bearing inverters are needed.

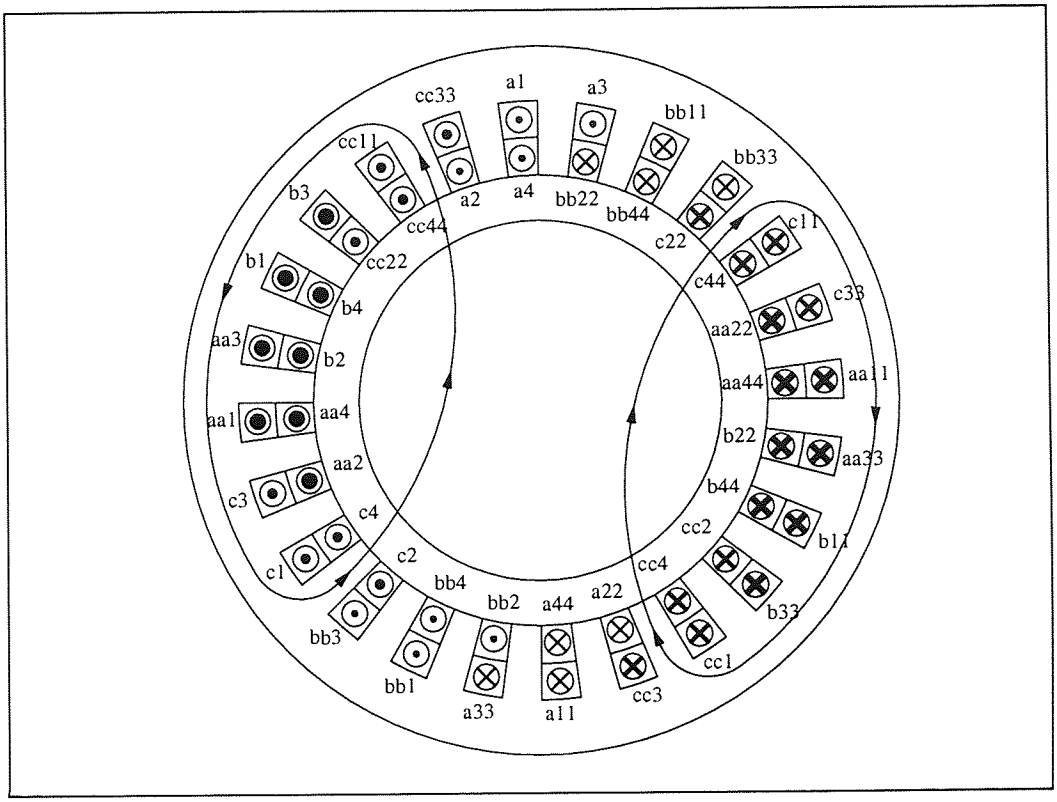

Figure 4.11: Distributed current densities in a 24-tooth stator producing a 2-pole levitation field.

It is required that a minimum of two levitation MMF axes must be present in order to obtain a resultant MMF axis that rotates in any arbitrary direction. This resultant MMF is dependent on the desired magnitude and direction of levitation force as well as the motor current and rotor angular displacement. In the present self-bearing motor, there are six possible 2-pole levitation MMF axes that can be generated so any two MMF axes can be selected. An example of a linear combination of two independent MMFs producing a resultant is shown in figure 4.12.

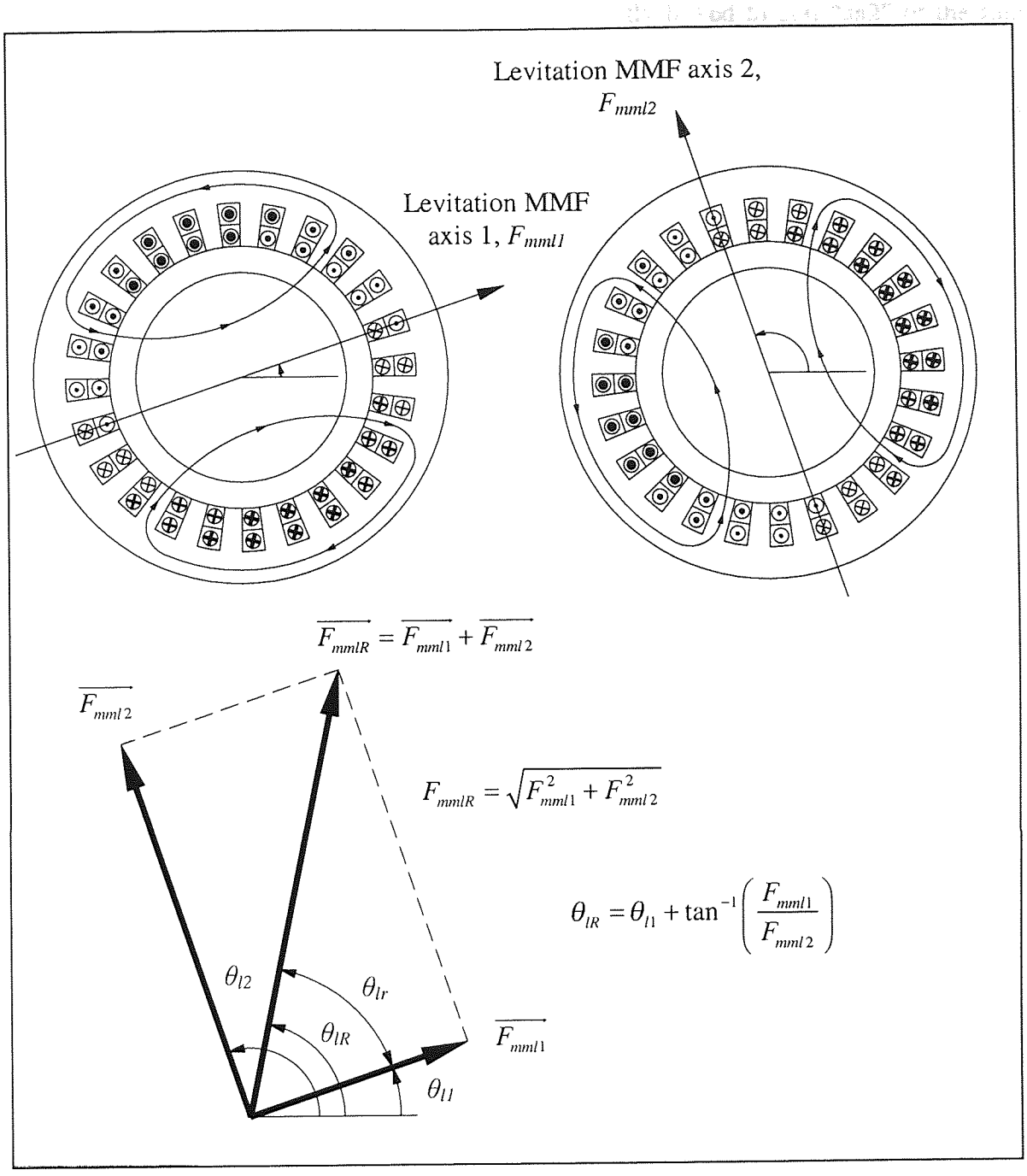

Figure 4.12: A resultant MMF in any arbitrary direction is produced when the vector of two independent MMFs are added.

In conventional distributed windings, any conductors in a "go" slot from the perspective of current flow must be accompanied by a "return" slot and vice versa. Figure 4.13 illustrates the motor and bearing currents flowing in all phases at one operating instant to produce the 4-pole motor and 2-pole levitation flux distributions as in figures 4.10 and 4.11 respectively. Note that only coil sides that produce the required motor and levitation fields are shown in the connection diagram. All other associated go or return paths are omitted for clarity

reasons. For example, coil "aa1" of a go path is directly linked to coil "aa2" of the same path without undergoing a return path explicitly.

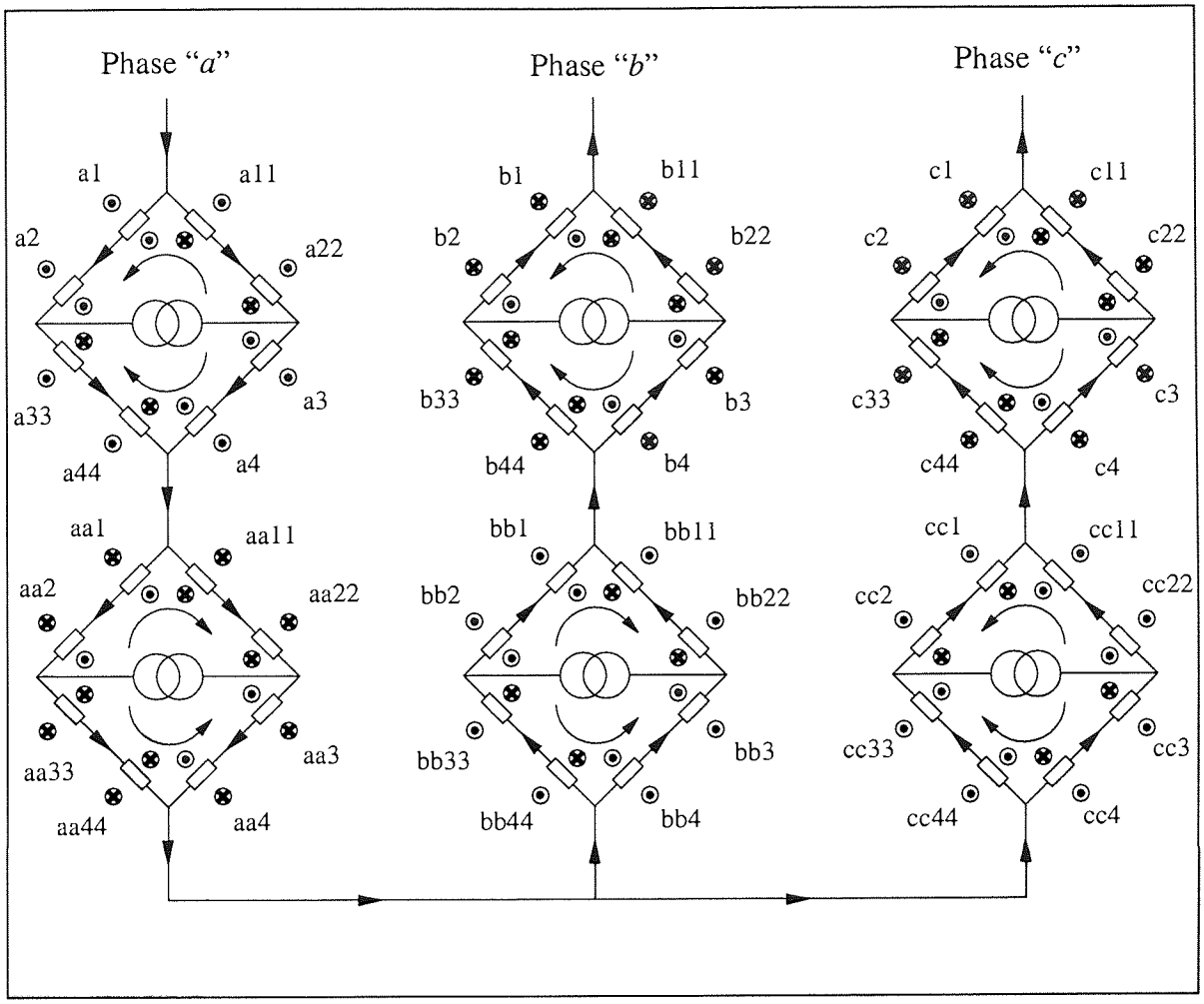

Figure 4.13: Instantaneous motor and bearing currents in all phase windings producing the flux distributions shown in figures 4.10 and 4.11 respectively.

Since diametrically opposing coil sides of each phase must form an independent bridge, there is a space constraint on where the respective go and return paths should be placed in the slots. These go and return paths produce their own magnetic fields and strictly speaking, they should not interfere with the required motor and levitation fields in the air gap. This requirement can be achieved by employing a toroidal or Gramme ring winding scheme where the omitted go and return paths described above are placed at the exterior of the stator, as depicted in figure 4.14. Because these coil sides are placed at the exterior, the flux distribution around the machine air gap will not be affected.

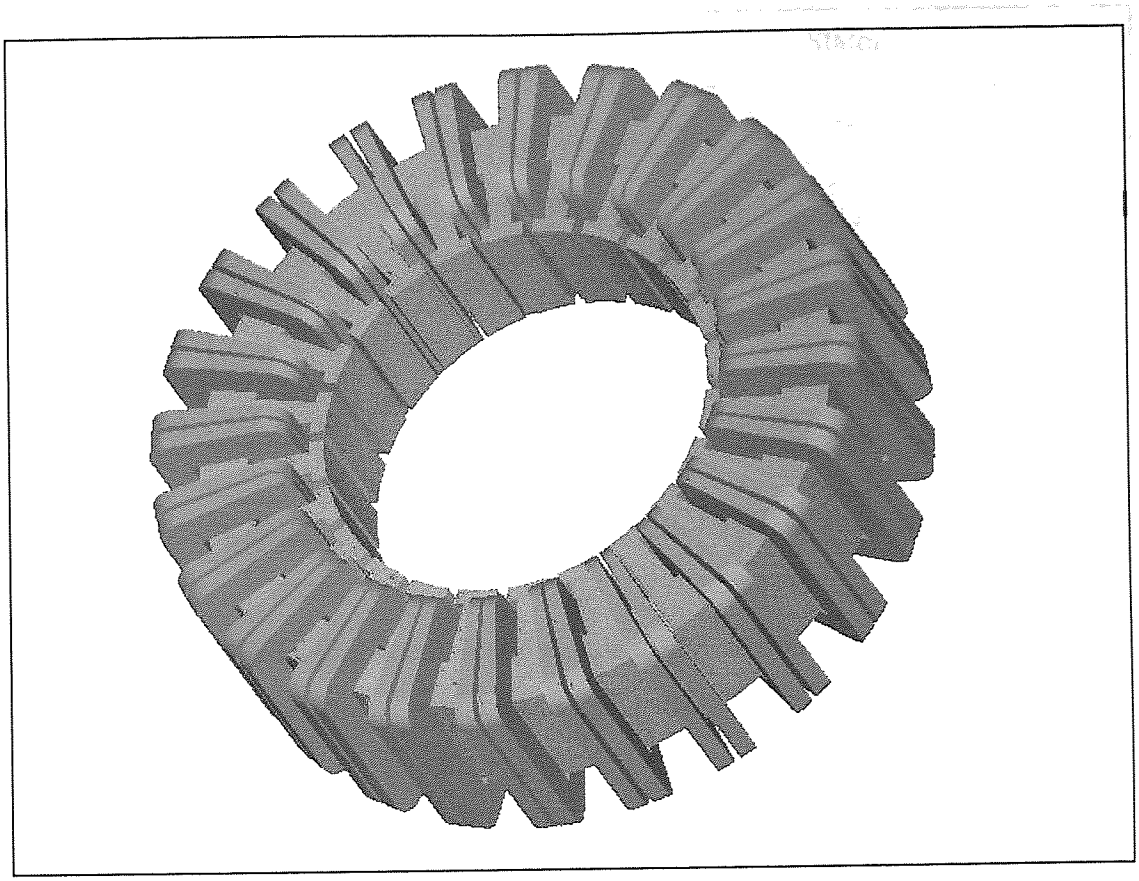

Figure 4.14: A self-bearing motor with a toroidal winding arrangement ("Equivalent" distributed winding - Type I).

In the conventional double layer winding, one coil side is placed on top of the other coil side in each stator slot. Unlike the conventional scheme, the present toroidal winding arrangement has two coils wound side by side around the back iron of the stator in each slot. The total current linked by a flux path is equal to the line integral of magnetic field intensity H over the path according to Ampere's law. The manner in which the conductors are arranged is trivial since the MMF concerned is dependent only on the total current enclosed by the flux path. This scenario is illustrated in figure 4.15.

In the toroidal winding scheme, if the coils in each slot were wound concentrically one on top of the other around the back iron, then this would result in an undesirable difference of end winding length. It is therefore important to wind the self-bearing motor as shown in figure 4.14 to keep the bridge balanced. The terminals of the coils are then connected externally according to the circuit schematic in figure 4.13.

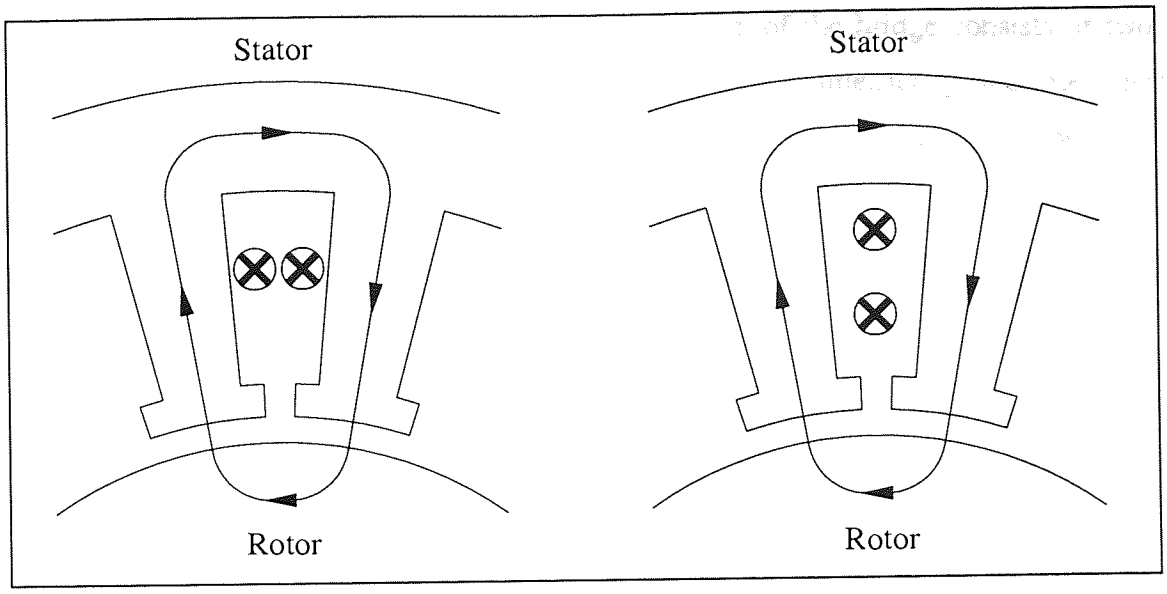

Figure 4.15: The MMFs produced are independent of how conductors are arranged in the enclosed flux path.

Toroidal windings can be widely found in many types of electrical machines [LF82], [FK83], [MBW99], [MO98], [GNW00]. Although toroidal windings are not as common as lap windings, they are used in many applications that require a savings of space. Typically, electrical machines with toroidal windings have a shorter axial length when compared to conventional lap windings. They are best used in stators with a short axial length and large diameter and thus, there is a reduction of end winding effect. However, a toroidal winding scheme may be unattractive because the coils wound around the back of the stator core can prevent heat from dissipating.

4.4.4 "Equivalent" distributed winding (Type II)

From our previous observations, if the diametrically opposite conductors have the same direction of motor current then the conductors at one slot must extend around the back of the stator core before making a connection to the conductors at the opposite slot. This is true for all motors with $4(1+n)$ pole number. On the other hand, motors with $2(1+2n)$ pole number have opposing direction of motor current flow at diametrically opposite slots, which implies that conductors at one slot can be directly connected to the opposite slot without needing to go round the back of the core. The fact that bearing currents are injected at the junction between the diametrically opposing conductors means that continuous winding from one slot to the other, as in lap windings, cannot be implemented.

However, if the coils are connected such that each arm of the bridge consists of two coil sides at 90° apart in the stator slots (as opposed to 180° diametrically opposite), then all conductors can be arranged within the stator slots. This removes the need for toroidally wound coils at the stator back core and thus moving towards a more conventional distributed winding arrangements. Consider an example of a 24 slots stator pictured in figures 4.16 and 4.17 with its connection scheme shown in figure 4.18. Slots "a1" and "a11" represent the sides of one coil where the copper conductor goes into slot "a1" and returns via slot "a11" making a number of turns. Any current injected in a coil side of that coil will result in an opposite direction of current flow in the other coil side. Another coil of the same direction of current flow linking slots "a3" and "a33" is connected at the opposite of the bridge since both coils have the same current reversing property. Two more coils linking slots "aa2"-"aa22" and "aa4"-"aa44" are then connected to coils "a1"-"a11" and "a3"-"a33" forming a bridge as depicted in figure 4.18. Therefore, a total of 8 coil sides or 4 separate coils constitutes a single bridge.

Since it is required that 16 coil sides to constitute a phase, each phase is extended to 2 series connected bridges. It can be seen that the circuit connection method and the number of power supplies are retained, i.e. one standard 3-phase motor supply and 6 bi-directional levitation current supplies. The circuit schematic in figure 4.18 shows the machine's instantaneous current flow producing a 4-pole motor field in figure 4.16 and a 2-pole levitation field in figure 4.17. As before, the directions of the motor and levitation currents are shown at the exterior and interior of the bridge respectively. Note that the resultant 4-pole motor field is of the same distribution as Type I toroidal winding arrangement would produce.

A net lateral force can be generated by appropriately exciting the phase levitation currents in any combination so long as the resultant field around the air gap is of either a 2-or 6-poles. It is important that at least two levitation MMF axes are generated so as to enable the control of force in any magnitude and arbitrary direction. The present scheme may not create a sinusoidal levitation field as perfectly as its predecessor because of the way it is connected. For example, when all phases are excited, the resulting levitation field will have a slight notch at its maximum peaks. Despite this minor imperfection the overall levitation field still resembles a sinusoidal waveform and a net lateral force can be accomplished.

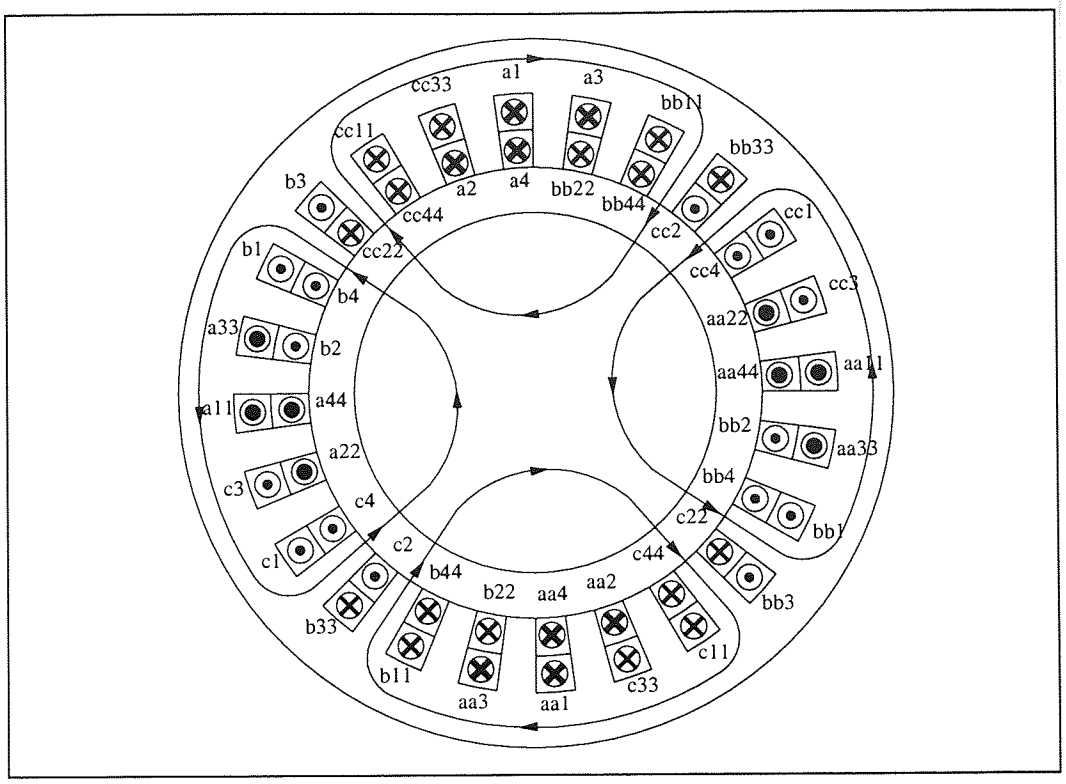

Figure 4.16: A self-bearing motor with "equivalent" distributed winding (Type II) producing a 4-pole motor field.

Since the active length of each coil is confined within two slots, the full arrangement of stator coils can be most conveniently achieved by employing pre-wound coils. Individual sets of pre-wound coil of the same length and number of turns can be slotted into the stator, and when held in place their terminals are connected according to the circuit schematic in figure 4.18. Unlike the previously described toroidal winding, the conductors in the present scheme are kept within the interior of the stator. Thus, type II "equivalent" distributed winding arrangement is more favourable in many applications in general when compared to type I toroidal winding.

Because some coils in each phase of figures 4.16 and 4.17 have the same magnitude and direction of current, it is possible to combine these coils such that only one bridge connection is formed in each phase. Such a variant connection is shown in figure 4.19 where two coils are connected in series in each branch of the bridge and so only three levitation supplies are required as opposed to six. As before, the directions of the motor current are shown at the exterior of the bridges whereas the levitation currents are shown at the interior. The resultant 4-pole motor field and 2-pole levitation field are equivalent to that of figures

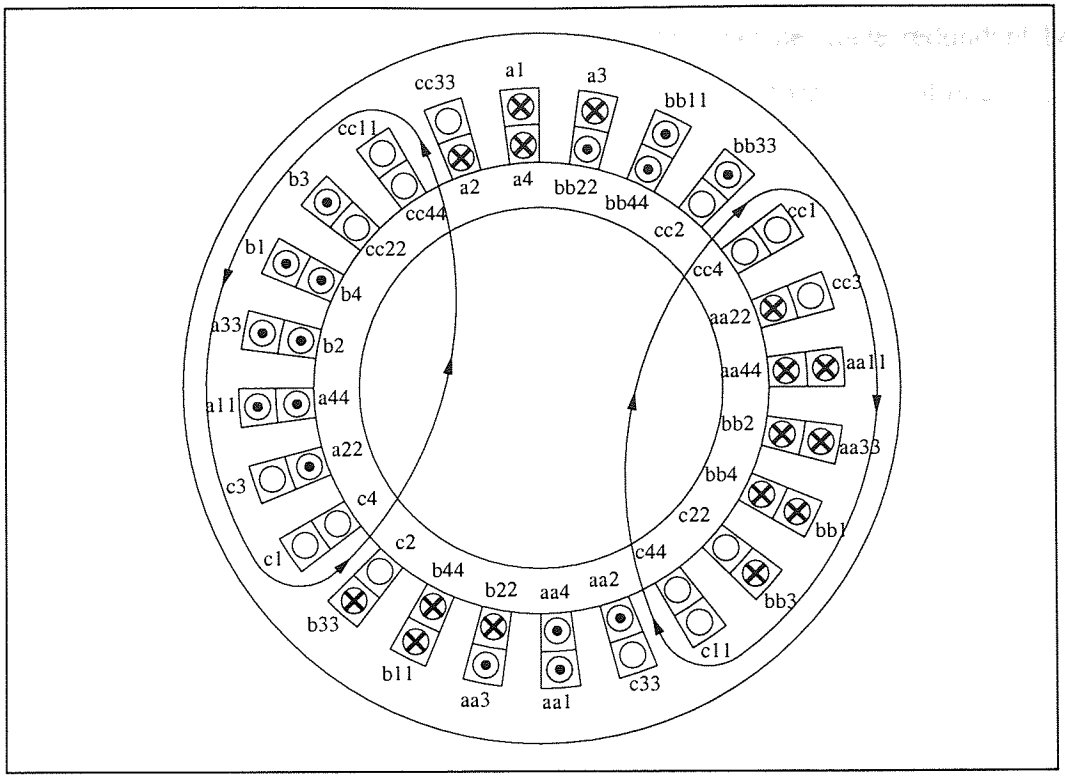

Figure 4.17: A self-bearing motor with "equivalent" distributed winding (Type II) producing a 2-pole levitation field.

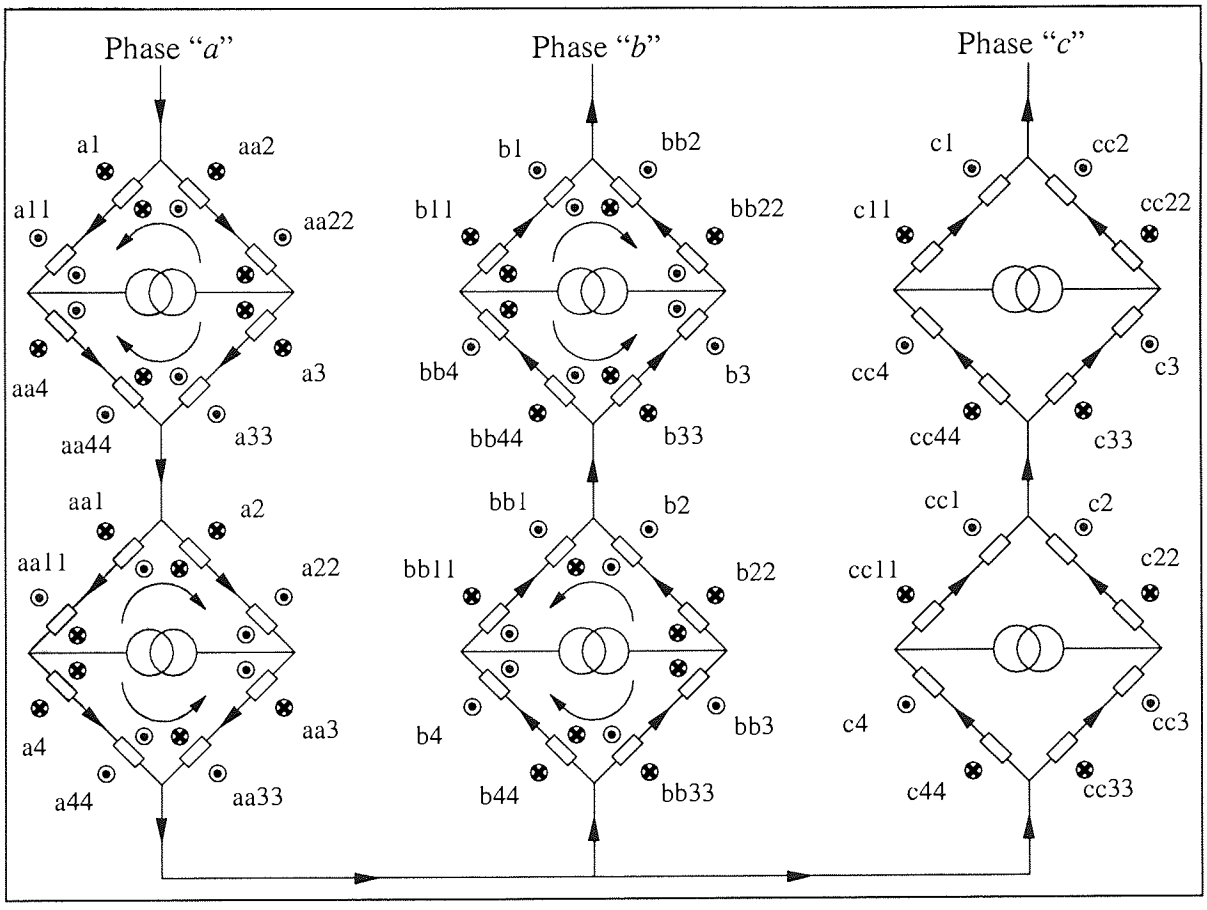

Figure 4.18: A schematic connection of the Type II "equivalent" distributed winding producing flux distributions in figures 4.16 and 4.17.

4.16 and 4.17 respectively. One of the bearing inverters can be made redundant because two levitation MMF axes are sufficient to provide a net lateral force control in any arbitrary direction.

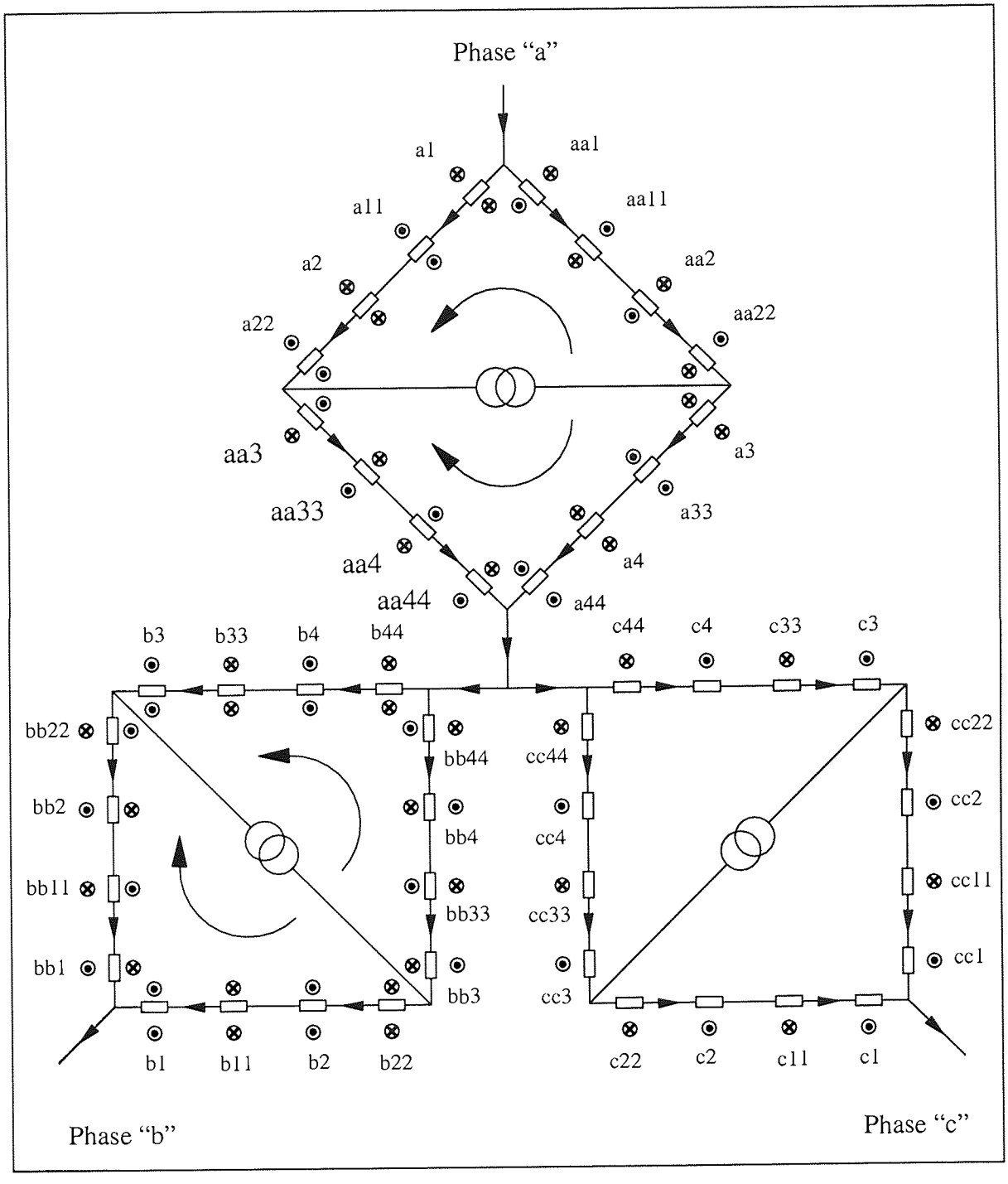

Figure 4.19: An alternative Type II "equivalent" distributed winding producing the same flux distributions as in figures 4.16 and 4.17.

4.4.5 Three-phase Star or Delta connections

The independent phase coils of all variants presented above are essentially star-connected circuits. Since the elementary bridge connection in figure 4.2 represents an independent single phase, windings can also be connected to form a delta circuit. This is illustrated in figure 4.20.

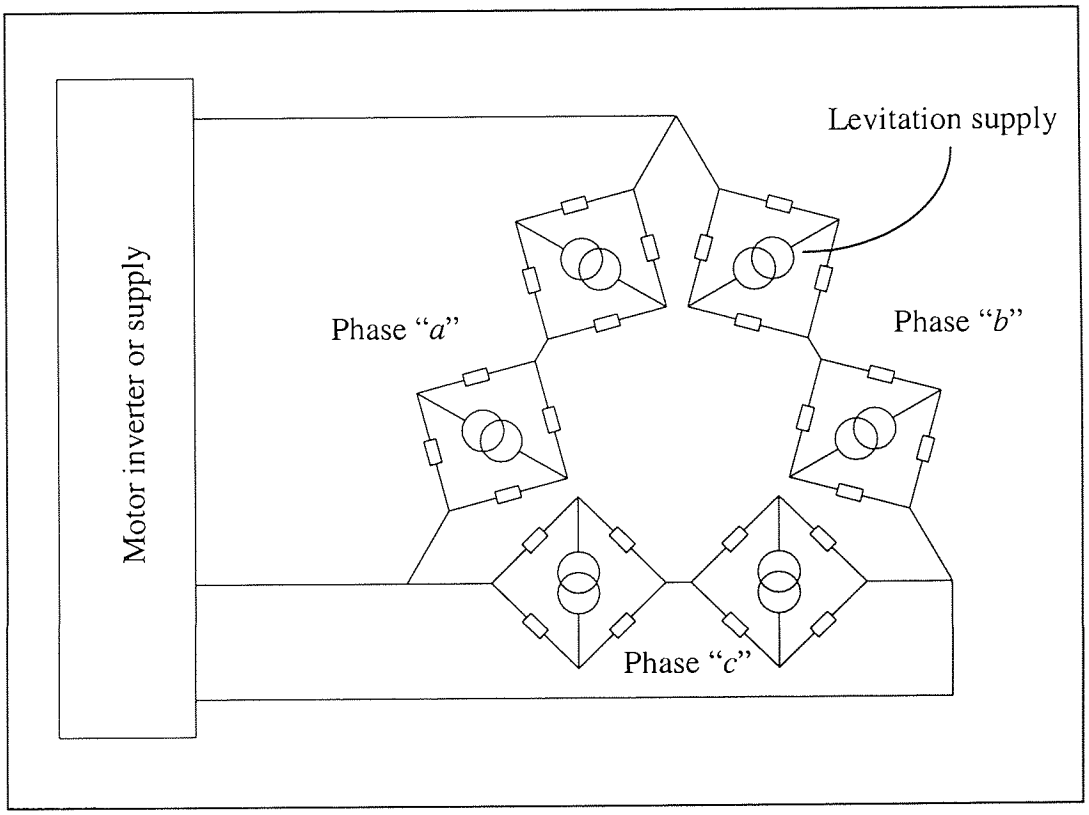

Figure 4.20: A delta-connected scheme.

4.4.6 Extension to higher phases independent

Three-phase connections are by far the most common of all polyphase machines. The extension of bridge connection to higher phases such as 5, 7 or 11 phase independent can be achieved by simply connecting the bridges to a single common point. The number of bridges in each phase can also be added as required and thus, it provides flexibility in the detail design.

4.5 Advantages of the bridge connection

The bridge connection is derived to eliminate the use of a second set of windings for the achievement of force production and to reduce the power needed for the levitation supplies. This is possible owing to the fact that the same set of conductors in the machine carries both force and torque-producing component of currents. In addition, the connection requires only one motor supply for torque production as in the case of a conventional motor control and drive system.

Lateral force is accomplished by incorporating additional small voltage and current ratings power supplies; each supply connects between the parallel paths of a bridge. In the presence of an appropriate rotor support, such as mechanical bearing, the levitation current supplies can be switched off and the machine can be operated with the motor inverter alone. This is a prominent advantage of the bridge connection.

Since the bridge connection has two parallel paths and with two ends, the bridge-like configuration essentially represents a distinct phase. Such a connection can be easily extended by adding yet more bridges in each phase and enables arbitrary combination of the number of poles and phases. The proposed scheme preserves the flexibility of having star- or delta-connections and simultaneously provides locations for injecting levitation currents with minimum coupling effects. This scheme also benefits from the feasibility of extending to higher independent phases such as four-, six- or twelve-phase machines for specialised applications. Moreover, the connection can be manipulated to obtain variants such as concentrated windings (Types I and II) and "equivalent" distributed windings (Types I and II).

Throughout the entire chapter the self-bearing motor is treated as a generic machine without explicitly referring it to any specific type of motor. In general any type of polyphase machines can be wound according to the proposed scheme. What is important is the mandatory requirement of producing both (N_{PPT}) pole motor and ($N_{PPL}\pm 1$) pole levitation fields. In addition, a set of windings must be present on at least one of the main components.

Further manipulation of the bridge connection by extending the bridges and combining series or parallel connections are possible although only several types of variant are

presented in this chapter. Consequently there are countless ways of winding a self-bearing motor based on the proposed scheme.

4.6 Some possible limitations of the bridge connection

The attributes of diametrically opposite teeth and conductors in table 4.1 are derived principally from integral slot stators where their windings are naturally regular and symmetrical. Perhaps a major limitation in the bridge connection is that it cannot be easily applied to fractional slot stators. Fractional slot stators have a non-integral number of slots per pole where the winding arrangement in the slots is not symmetrical. For example, a 4-pole motor with 15 slots gives a fraction number 3.75 slots/pole and there are no diametrically slots spanning 180° across. Thus, the attributes listed in table 4.1 do not apply for this unsymmetrical arrangement.

For the case of an 8-pole motor with 18 slots, however, the attributes listed in table 4.1 applies since the total number of slots is of an even number. Because its go and return coil sides are not regularly distributed as in the case of integral slot stators, the coil arrangement based on the bridge connection is more complicated to determine. This does not rule out completely the possibility of using the proposed scheme but a considerable ingenuity is required to arrange the winding. It is therefore preferable to use integral slot stators in conjunction with the bridge connection. Integral slot stators have a relatively high cogging effect in permanent magnet motors but such a negative effect can be reduced by employing skewed stator laminations or skewed permanent magnets.

4.7 Summary of principal matters

A novel winding scheme, referred to as the "bridge" connection is unveiled in this chapter. The principal feature of the connection is that the torque-producing component of current is divided into two parallel paths in each phase. A supply between mid points of each path in a bridge-like configuration provides the currents which will be responsible for the levitation forces. The concept can be extended by introducing yet more bridges between the parallel paths that carry the torque currents.

The main advantages of the bridge connection are:

- only a single set of windings are present, i.e. the same set of conductors carries both torque and levitation currents. This means that torque is not being compromised unlike conventional self-bearing motors with two sets of windings to carry different category of currents.
- only one power supply is required for the normal torque-producing function, unlike conventional self-bearing motors with a single set of windings that require more than one unit of independent power supply. This is of extreme importance because the proposed self-bearing motor resembles a conventional electrical machine in the absence of levitation currents, but when levitation currents are injected, a lateral force between the stator and rotor is produced.
- the achievement of lateral forces is provided by relatively small voltage and current ratings power supplies. The use of a number of independent supplies offers a redundancy for fault tolerant purposes.
- minimal dependence of the machine torque on the commanded lateral force.
- the connection preserves the flexibility of having star- or delta connections and easily extended to any polyphase self-bearing motors.
- Many variants of connection can be derived, such as concentrated and "equivalent" distributed windings.

There are limitations associated with the proposed connection, however. For fractional slot stators, in particular, the actual winding arrangement is difficult to determine because of the irregular and unsymmetrical nature. Consequently, it is preferable to use integral slot stators if wound according to the bridge connection. A disadvantage with integral slot stators is that they can produce relatively high cogging torque but this can be reduced by skewing the laminations or the rotor permanent magnets in a conventional way.

CHAPTER 5

FINITE ELEMENT MODELLING

The capability and potentials of the newly proposed bridge connection for a self-bearing machine are verified with 2D coupled-field finite element analyses. It is not the aim, however, to optimise the design or explore its performance limits. For the interest of simplicity, a 3-phase motor having a 12-tooth stator and a 4-pole surface mounted permanent magnet rotor is chosen as an illustrative example. Since the number of stator teeth is relatively small, a type II concentrated winding arrangement, as described in the previous chapter, is used. Analytical solutions of the magnetic fields and forces considering rotor eccentricity are derived at the beginning of the chapter. These analytical results are then compared with the results obtained from finite element modelling to validate the proposed connection scheme.

5.1 Analytical calculation of magnetic fields and forces

The presence of an appropriate combination of magnetic fields is necessary for the achievement of torque and lateral force between the stator and rotor. These components of field depend primarily on the type of machines considered. A switched reluctance self-bearing machine, for instance, has two distinct fields generated by the stator winding, i.e. torque and levitation-producing components. A permanent magnet self-bearing motor, however, has three separate component fields namely, motor current, permanent magnet and levitation current. This section provides a simple analytical approach based on Ampere's loop law and Maxwell's stress method to evaluate the field components in the air gap and the resultant lateral forces exerted on the rotor. In addition, the equations derived facilitate changing of the air gap size during rotor eccentricity. Thus, the negative stiffness of the self-bearing motor can be estimated.

5.1.1 Self-bearing motor specification

As an example a 3-phase 4-pole permanent magnet synchronous self-bearing motor having a 12-tooth stator is considered. The required number of pole-pair for levitation as per the $N_{PPL}=N_{PPT}\pm 1$ rule is chosen as 1 (2-pole levitation field). Any variants of the bridge

connection presented previously can be implemented. Since the stator has only 12 slots, both concentrated and distributed winding arrangements produce the same flux distribution around the air gap periphery. For this reason a type II concentrated winding of the bridge connection is chosen as the winding arrangement scheme. This particular connection and winding arrangement for a 12 slots stator are shown in figure 4.9.

The self-bearing motor has the following physical properties: permanent magnet remanence: 0.95 T; magnetic coercivity: 6.8E5 A/m; magnet thickness: 2 mm; air gap: 0.8 mm; rotor radius: 30 mm; stack length: 0.1m; number of turns per tooth: 120 (2 groups of 60 turns). More information with regard to its material and physical properties can be found in chapter 9.

5.1.2 Sign convention

The sign convention for all variables concerned is here defined and will be used throughout the whole thesis. Firstly, the direction of magnetic fluxes traversing from the stator to rotor or vice versa irrespective of the MMF sources is defined with an aid of an imaginary interface in the air gap. As shown in figure 5.1, flux radiating outwards and inwards of the imaginary interface surrounding the rotor are designated positive and negative respectively. At any operating instance the net total of fluxes entering and emerging from the imaginary interface must be zero according to the principle of conservation of flux.

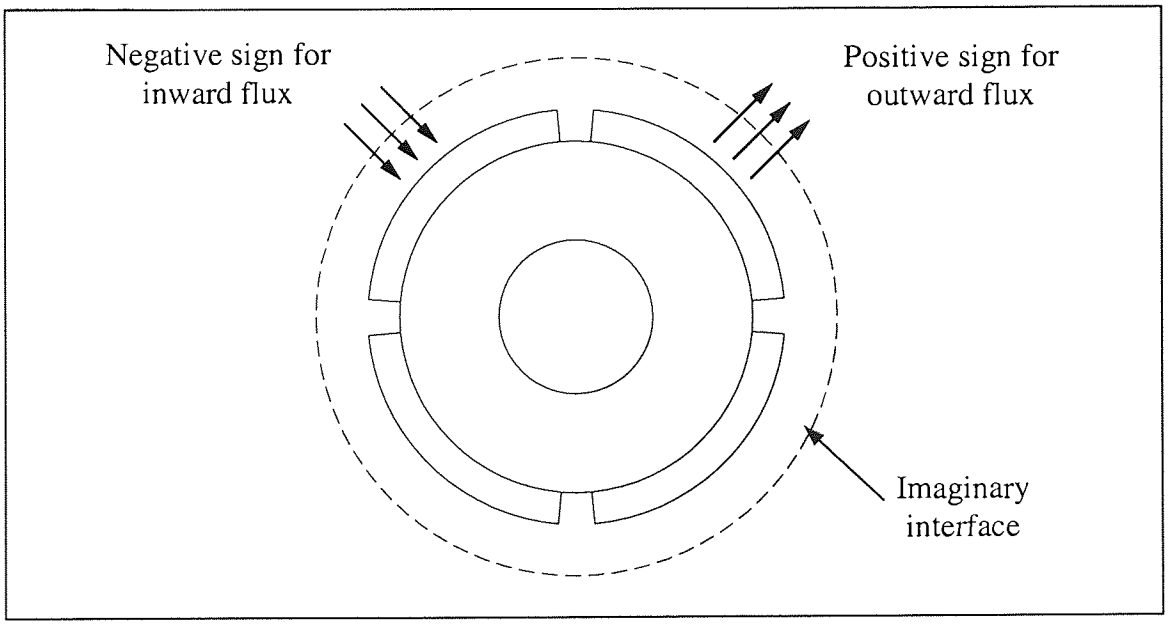

Figure 5.1: Convention for flux crossing the imaginary interface bounding the rotor.

Another convention used to describe the sign of the desired angle of lateral force γ, angular coordinate θ and frequency ωt is depicted in figure 5.2. A counter clockwise rotation from the horizontal axis is assumed to be positive. Also shown in the figure is the magnetisation of the surface mounted permanent magnets in the radial direction. The magnetic field created by permanent magnets is assumed to be sinusoidally distributed around the air gap periphery and this component of field is denoted by $B_{PM}(\theta,t)$.

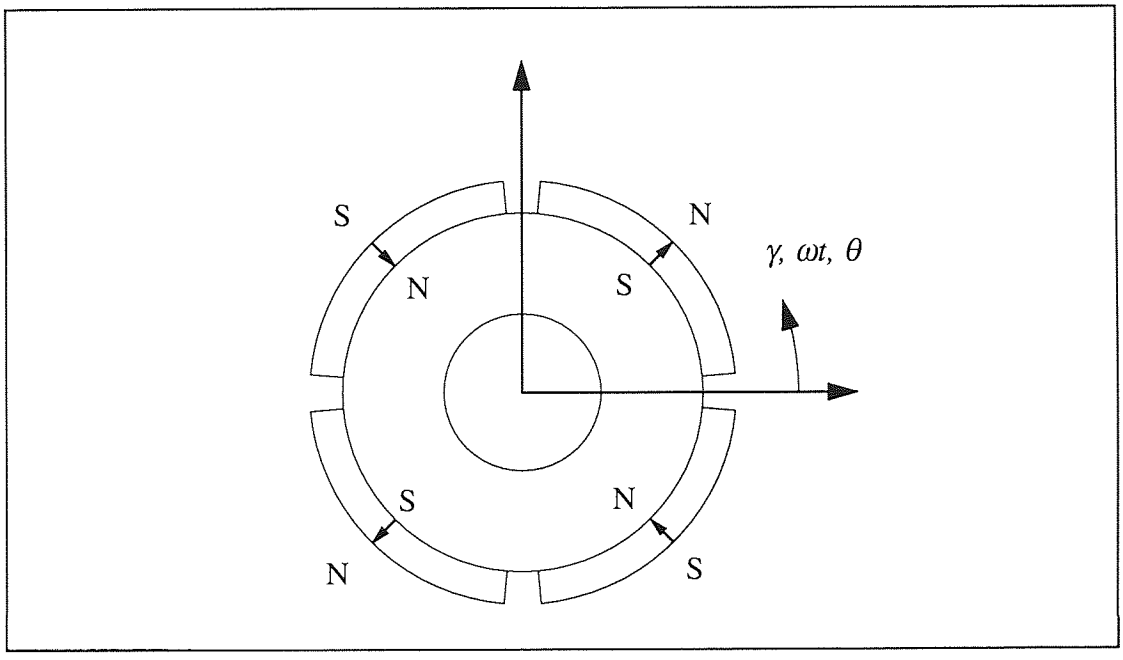

Figure 5.2: Sign convention of the desired angle of lateral force γ, angular coordinate θ and frequency ωt

5.1.3 Lateral force control

In any permanent magnet motor the net MMF causing torque is mostly contributed by the magnets. The excitation current usually generates a much lower MMF than the permanent magnets do, and for simplicity, this component of flux may be neglected. However, in the case where a high current excitation is required, the flux contributed by the coils can be substantial and increase torque. As far as a self-bearing motor is concerned, an increase of machine flux (MMFs generated by permanent magnets and stator coils excitation) in the air gap is beneficial where a lower levitation flux may now be used to generate the same force, according to expressions (3.11) and (3.12). However, the phase angle of the levitation currents must be adjusted appropriately to obtain a resultant force in the desired direction.

For analytical purposes, it is more realistic to include the motor current than to neglect it. This section derives how much phase compensation is required in the levitation flux so that the effect of increasing the motor current on the lateral force direction can be minimised.

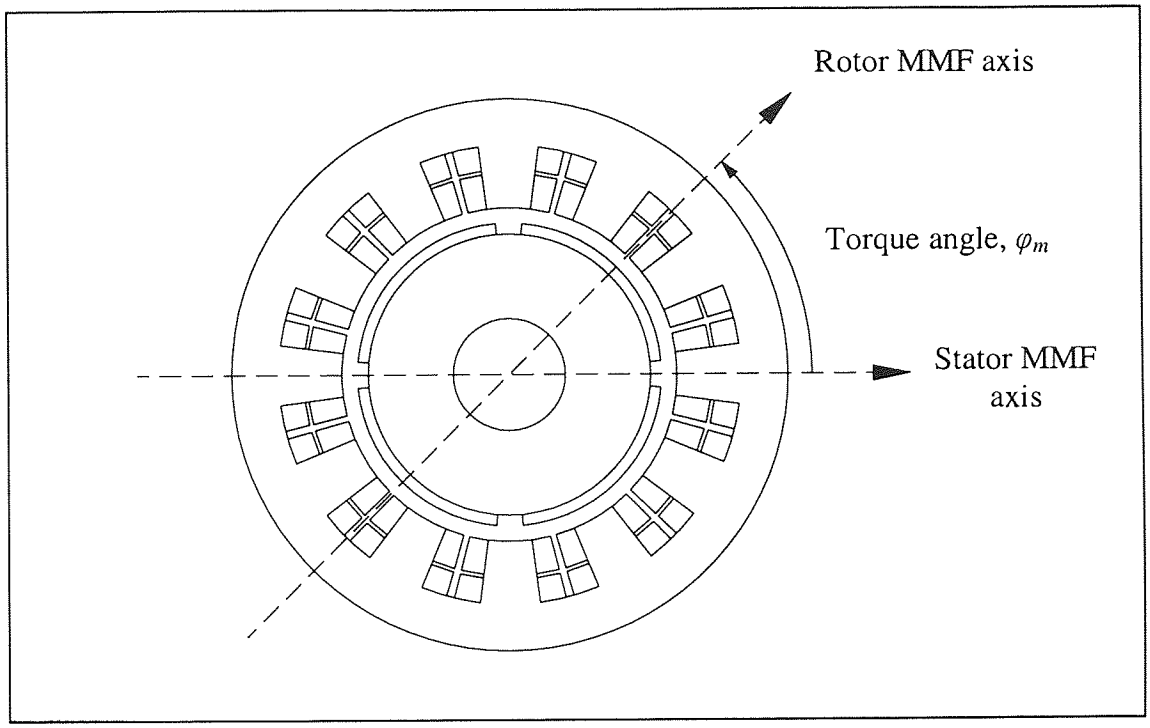

Figure 5.3: Mechanical torque angle φ_m between the stator and rotor MMF axes.

When the stator coils are excited another component of field, $B_{MC}(\theta,t)$, is generated and the interaction between $B_{MC}(\theta,t)$ and $B_{PM}(\theta,t)$ give rise to a machine torque. The magnitude and direction of torque is dictated by the torque angle φ_m, defined as the mechanical angle between the stator and rotor MMF axes. For the counter clockwise rotation that we assume, figure 5.3 shows a generator. For a motor the stator MMF must lead the rotor MMF. In a 4-pole machine, maximum torque occurs when the torque angle φ_m is at 45° or 135°, while higher pole number machines have maximum torque at:

$$\frac{90^\circ}{N_{PPT}} \text{ or } \frac{270^\circ}{N_{PPT}} \tag{5.1}$$

The electrical torque angle is denoted by φ_e and is related to the mechanical torque angle φ_m by:

$$\varphi_e = N_{PPT}\varphi_m \tag{5.2}$$

At any instant the flux densities in the air gap produced by the permanent magnets and motor current can now be written as follows:

$$B_{PM} = B_{PMMax} \sin(2\theta - \omega t) \tag{5.3}$$

$$B_{MC}(\theta) = B_{MCMax} \sin(2\theta - \omega t + \varphi_e) \tag{5.4}$$

The total flux density in the air gap is then the sum of expressions (5.3) and (5.4):

$$B_{AG} = B_{AGMax} \sin(2\theta - \omega t + \lambda) \tag{5.5}$$

where B_{AGMax} and λ are the maximum air gap flux density generated by both permanent magnet and motor current, and its phase angle respectively.

$$B_{AGMax} = \sqrt{\left[B_{PMMax} + B_{MCMax}\cos(\varphi_e)\right]^2 + \left[B_{MCMax}\sin(\varphi_e)\right]^2} \quad \text{and} \tag{5.6}$$

$$\lambda = \tan^{-1}\left[\frac{B_{MCMax}\sin(\varphi_e)}{B_{PMMax} + B_{MCMax}\cos(\varphi_e)}\right] \tag{5.7}$$

The levitation flux required to unbalance the total machine flux is similar to equation (3.5):

$$B_{LevMax}\sin(\theta - \omega t + \gamma) = B_{LevMax(X)}\sin(\theta - \omega t) + B_{LevMax(Y)}\cos(\theta - \omega t) \tag{5.8}$$

The angle γ is the desired direction of the net lateral force and is related to $B_{LevMax(X)}$ and $B_{LevMax(Y)}$ by the followings:

$$B_{LevMax(X)} = \frac{B_{LevMax}}{\sqrt{1+\tan^2\gamma}} \times SIGN\left[\cos(\gamma)\right] \tag{5.9}$$

$$B_{LevMax(Y)} = \sqrt{(B_{LevMax})^2 - (B_{LevMax(X)})^2} \times SIGN\left[\sin(\gamma)\right] \tag{5.10}$$

Referring back to equations (3.6)-(3.12), the components of levitation flux (5.8) are used in conjunction with the total machine flux (5.5) to produce lateral forces in *x*- and *y*-directions. The linear combination of such components dictates the resultant magnitude and direction

of the lateral force. Here B_{LevMax} and γ are adjusted appropriately to control the displacement of the rotor. The levitation field must take an additional phase angle λ into consideration in order to obtain the direction of force as specified by γ. Otherwise, the desired direction of the net lateral force is affected by the presence of the main motor currents and the overall force equations will carry an additional variable λ.

Mathematically the forces can be evaluated as:

$$F_X = \frac{1}{\mu_0} lr \int_0^{2\pi} B_{AGMax} \sin(2\theta - \omega t + \lambda).B_{LevMax(X)} \sin(\theta - \omega t + \lambda).\cos(\theta).d\theta$$
$$\therefore F_X = \frac{1}{2\mu_0} \pi lr B_{AGMax} B_{LevMax(X)} \tag{5.11}$$

$$F_Y = \frac{1}{\mu_0} lr \int_0^{2\pi} B_{AGMax} \sin(2\theta - \omega t + \lambda).B_{LevMax(Y)} \cos(\theta - \omega t + \lambda).\sin(\theta).d\theta$$
$$\therefore F_Y = \frac{1}{2\mu_0} \pi lr B_{AGMax} B_{LevMax(Y)} \tag{5.12}$$

Thus, the force expressions (5.11) and (5.12) have the same form as that of expressions (3.11) and (3.12). The levitation field expression in (5.8) and its corresponding current can now be rewritten as:

$$B_{LevMax} \sin(\theta - \omega t + \lambda + \gamma) = B_{LevMax(X)} \sin(\theta - \omega t + \lambda) + B_{LevMax(Y)} \cos(\theta - \omega t + \lambda) \tag{5.13}$$

$$I_{LevMax} \sin(\theta - \omega t + \lambda + \gamma) = I_{LevMax(X)} \sin(\theta - \omega t + \lambda) + I_{LevMax(Y)} \cos(\theta - \omega t + \lambda) \tag{5.14}$$

5.1.4 Assumptions made

Several assumptions are made to simplify the analysis:

- The stator and rotor iron have infinite permeability and so all energy is stored in the air gap. The MMF drops across the stator and rotor iron are negligible due to their high permeability nature. Furthermore, the material is isotropic and any change in

temperature as a result of high current excitation does not vary the characteristics of the B-H curve.

- The permanent magnet has a straight line B-H relationship in the second quadrant of the full hysteresis loop. This magnetisation characteristic is common for rare-earth magnet materials such as samarium cobalt and neodymium-iron-boron.
- Flux density is confined and uniform over the cross-sectional area of the stator pole and leakage is neglected. Therefore, a mean path is taken to represent collectively all fluxes that cross over the pole cross-sectional area. Harmonic flux components, eddy currents and back EMF are also ignored for simplicity.
- The slotting effect of the stator is assumed to be negligible.

5.2 Force expressions considering rotor eccentricity

From the force expressions (5.11) and (5.12), the parameter that dictates the magnitude and direction of lateral force is the magnetic flux density B. They are attractive in the sense that the resultant force can be computed easily if the maximum flux densities of the torque and levitation-producing component of fields are known. The force expressions do not include explicitly the variation of air gap size, but instead, any change to its air gap must be reflected in the magnetic field density B in order to calculate force.

Any rotor displacement will distort the magnetic field in the air gap periphery and so the force expressions (5.11) and (5.12) are no longer valid because they are derived based on sinusoidal distribution. If the force at each local stator tooth is known, then the overall force exerted on the eccentric rotor can be found by summing all these local forces around the rotor. This section presents an approximate method of evaluating the net lateral force due to rotor eccentricity.

Consider the components of lateral force around the air gap as a result of Maxwell stress:

$$F_X = \frac{lr}{2\mu_0}\int_0^{2\pi}\begin{pmatrix} {B_{AGMax}}^2 \sin(2\theta-\omega t+\lambda) \\ +2B_{AGMax}\sin(2\theta-\omega t+\lambda).B_{LevMax(X)}\sin\left(\theta-\omega t+\lambda\right) \\ +{B_{LevMax(Y)}}^2\sin\left(\theta-\omega t+\lambda\right)\end{pmatrix}.\cos\theta.d\theta \qquad (5.15)$$

$$F_Y = \frac{lr}{2\mu_0}\int_0^{2\pi}\begin{pmatrix} {B_{AGMax}}^2 \sin(2\theta - \omega t + \lambda) \\ +2B_{AGMax}\sin(2\theta - \omega t + \lambda).B_{LevMax(Y)}\cos(\theta - \omega t + \lambda) \\ +{B_{LevMax(Y)}}^2\cos(\theta - \omega t + \lambda) \end{pmatrix}.\sin\theta.d\theta \qquad (5.16)$$

As far as the concentric case is concerned, products $B_{AG}.B_{AG}$ and $B_{Lev}.B_{Lev}$ in the parentheses of expressions (5.15) and (5.16) above do not produce a net lateral force because any arbitrary diametrically opposite points on the rotor the flux densities are equal in magnitude and direction. This is no longer true when the rotor is displaced where these squared components of flux density are not equal at diametrical points of interest. As a consequence, a net lateral force is generated in the same direction as the displaced rotor.

At a local tooth the components of the force can be written similar to that of (5.15) and (5.16):

$$F_{(X)n} = \frac{A_p}{2\mu_0}\left[\left(\left(B_{PM(n)} + B_{MC(n)}\right)^2 + 2\left(B_{PM(n)} + B_{MC(n)}\right).B_{Lev(X)n} + {B_{Lev(X)n}}^2\right).\cos\theta_n\right] \qquad (5.17)$$

$$F_{(Y)n} = \frac{A_p}{2\mu_0}\left[\left(\left(B_{PM(n)} + B_{MC(n)}\right)^2 + 2\left(B_{PM(n)} + B_{MC(n)}\right).B_{Lev(Y)n} + {B_{Lev(Y)n}}^2\right).\sin\theta_n\right] \qquad (5.18)$$

where n denotes the tooth number and A_p is the tooth area. For a stator with N_s teeth, the overall components of force in the air gap is then the sum of local forces in equations (5.17) and (5.18):

$$F_{(X)n} = \frac{A_p}{2\mu_0}\sum_{n=1}^{N_S}\left[\left(\left(B_{PM(n)} + B_{MC(n)}\right)^2 + 2\left(B_{PM(n)} + B_{MC(n)}\right).B_{Lev(X)n} + {B_{Lev(X)n}}^2\right).\cos\theta_n\right] \qquad (5.19)$$

$$F_{(Y)n} = \frac{A_p}{2\mu_0}\sum_{n=1}^{N_S}\left[\left(\left(B_{PM(n)} + B_{MC(n)}\right)^2 + 2\left(B_{PM(n)} + B_{MC(n)}\right).B_{Lev(Y)n} + {B_{Lev(Y)n}}^2\right).\sin\theta_n\right] \qquad (5.20)$$

Here the required task is to establish relationships between each of the independent component of flux densities B_{PM}, B_{MC} and B_{Lev} and with the change of air gap. The subsequent sub-sections illustrate by examples how flux densities can be evaluated by using Ampere's loop law.

5.2.1 Calculation of magnetic field in the air gap: A horseshoe example

Consider an example of a simple unexcited horseshoe positioned nearby a permanent magnet rotor as illustrated in figure 5.4. Both surface mounted permanent magnets have opposite direction of magnetisation with respect to each other, and therefore creating a magnetic loop path as shown. A simple relationship between the flux density and the air gap separating the horseshoe and the rotor is derived as follows.

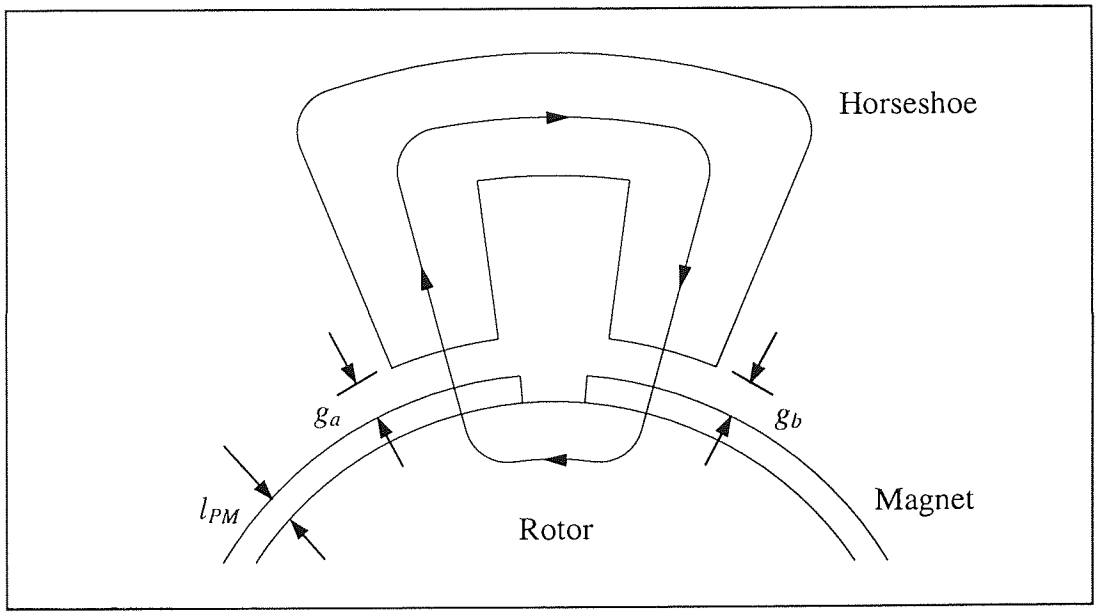

Figure 5.4: Magnetic loop path linking a horseshoe and a permanent magnet rotor.

According to the assumption made previously, the characteristic of the B-H curve for the magnet can be represented by:

$$B_{PM} = \mu_{PM} H_{PM} + B_0 \tag{5.21}$$

where μ_{PM} is the relative permeability, shown as the gradient of the B-H line in figure 5.5.

The flux density in the air gap can be estimated by applying the concept of magnetic circuit with the assumptions listed in section 5.1.4. The relationship between the MMF F_{mm} and the magnetic field intensity H, as derived from Ampere's law is:

$$F_{mm} = NI = \oint H.dl \tag{5.22}$$

where N = number of turns of a coil

I = coil current

l = mean path of the flux loop

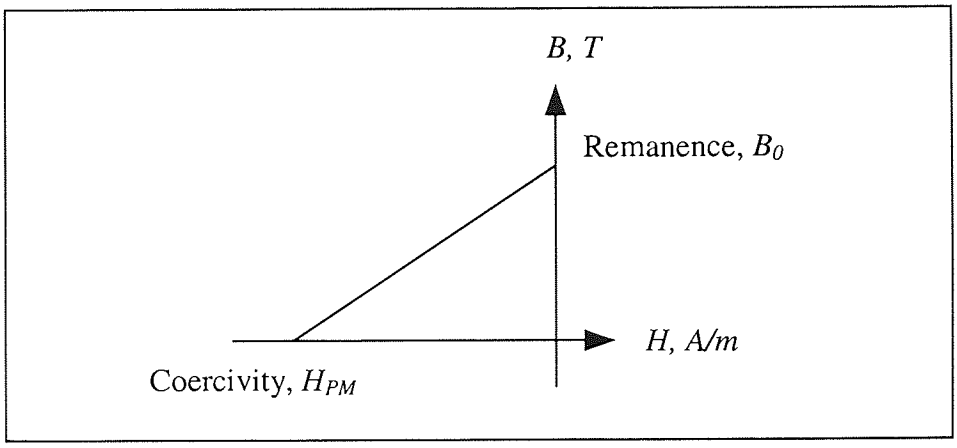

Figure 5.5: B-H characteristic for a rare-earth permanent magnet.

The B-H relationship in equation (5.21) can be manipulated to give an equivalent MMF form:

$$\frac{B - B_0}{\mu_{PM}} = H_{PM}$$

$$\frac{Bl_{PM} - B_0 l_{PM}}{\mu_{PM}} = H_{PM} l_{PM} \tag{5.23}$$

where l_{PM} is the radial thickness of the permanent magnet.

A mean loop path linking the stator teeth, air gaps, rotor and permanent magnets is then considered as shown in figure 5.4. Using equation (5.22) and assuming negligible MMF drops across the stator and rotor irons, only terms pertaining to air gaps and permanent magnets are retained.

$$H_a g_a + H_b g_b + H_{PM} l_{PM} + H_{PM} l_{PM} = 0 \tag{5.24}$$

where g_a and g_b are the air gap distance at teeth a and b respectively. Substituting equation (5.23) into (5.24) yields:

$$H_a g_a + H_b g_b + 2\left[\frac{Bl_{PM} - B_0 l_{PM}}{\mu_{PM}}\right] = 0 \tag{5.25}$$

The magnetic flux intensities at the air gaps g_a and g_b can be substituted to give magnetic flux densities B_{Gap} via the following relationship:

$$B_{Gap} = \mu_0 H_a = \mu_0 H_b \tag{5.26}$$

Equation (5.25) then becomes:

$$\frac{B_{Gap}}{\mu_0}(g_a + g_b) + \frac{2B_{Gap} l_{PM}}{\mu_{PM}} = \frac{2B_0 l_{PM}}{\mu_{PM}} \tag{5.27}$$

Further manipulation of equation (5.27) gives:

$$B_{Gap} = \frac{2B_0 l_{PM}}{\left[\frac{\mu_{PM}}{\mu_0}(g_a + g_b) + 2l_{PM}\right]} \tag{5.28}$$

Thus, the fundamental relationship between flux density and air gap variation is obtained. In this simple example only one magnetic loop path exists linking the horseshoe and rotor. However, when the horseshoe configuration is arrayed in a polar manner, forming a full stator, the resultant product is a multi-loop configuration. Having treated this simple horseshoe example, attention is given next to the main problem, i.e. a self-bearing motor.

5.2.2 Calculation of magnetic field in the air gap: A self-bearing motor example

There are essentially three components of magnetic flux density exists in the present self-bearing motor namely, B_{PM}, B_{MC} and B_{Lev}. By applying Ampere's law, the MMFs originated from the stator coils can be straightforwardly calculated as the product of current and the number of coil turns (an MMF drop). The MMF generated by permanent magnets can be

represented by an equivalent current source with an appropriate air gap thickness. Each component of flux densities will be considered independently as follows.

5.2.2.1 Flux densities due to permanent magnets, B_{PM}

Flux densities due to permanent magnets are first considered. For a multi-loop configuration, such as this example, flux density in the air gap under a particular stator tooth is dependent on the air gap variation at other stator teeth (linked together by the loops). In general, the MMF can be calculated by taking any arbitrary loop paths in the stator. However, it is more convenient to choose loops that are associated with the equal magnitude of equivalent current sources but in the opposite direction. One example is illustrated in figure 5.6 where the permanent magnets form a 4-pole field around the air gap periphery. The mean flux loops are chosen to enclose the same magnitude of equivalent current sources namely, at teeth no. 1, 4, 7 and 10. This means that for a stator with 12 slots and a 4-pole field, flux density in the air gap under stator tooth no. n is dependent on the variation of air gap at stator tooth no. *(n-3) anticlockwise* and *(n+3) clockwise*. Such circular linked flux densities around the air gap can be conveniently solved by using matrices.

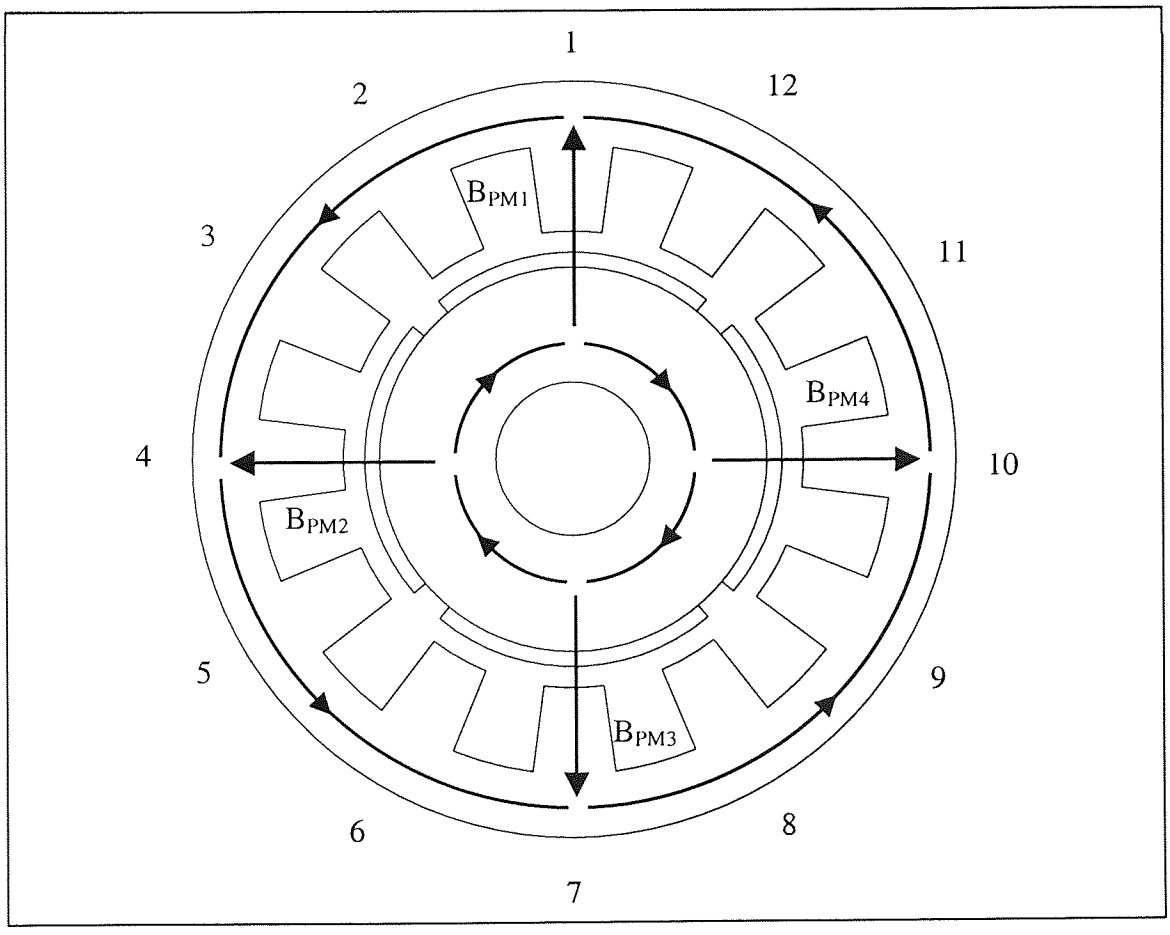

Figure 5.6: Sign convention of the chosen 4-pole flux loops.

Applying Ampere's law results in 3 equations:

$$
\begin{aligned}
B_{PM1}\left(\frac{g_1}{\mu_0}+\frac{l_{PM}}{\mu_{PM}}\right)-B_{PM4}\left(\frac{g_4}{\mu_0}+\frac{l_{PM}}{\mu_{PM}}\right)&=\frac{B_0 l_{PM}}{\mu_{PM}}\sin\left(2\left(\frac{\pi}{2}\right)-\omega t\right)-\frac{B_0 l_{PM}}{\mu_{PM}}\sin\left(2(\pi)-\omega t\right)\\
B_{PM4}\left(\frac{g_4}{\mu_0}+\frac{l_{PM}}{\mu_{PM}}\right)-B_{PM7}\left(\frac{g_7}{\mu_0}+\frac{l_{PM}}{\mu_{PM}}\right)&=\frac{B_0 l_{PM}}{\mu_{PM}}\sin\left(2(\pi)-\omega t\right)-\frac{B_0 l_{PM}}{\mu_{PM}}\sin\left(2\left(\frac{3\pi}{2}\right)-\omega t\right)\\
B_{PM7}\left(\frac{g_7}{\mu_0}+\frac{l_{PM}}{\mu_{PM}}\right)-B_{PM10}\left(\frac{g_{10}}{\mu_0}+\frac{l_{PM}}{\mu_{PM}}\right)&=\frac{B_0 l_{PM}}{\mu_{PM}}\sin\left(2\left(\frac{3\pi}{2}\right)-\omega t\right)-\frac{B_0 l_{PM}}{\mu_{PM}}\sin\left(2(2\pi)-\omega t\right)
\end{aligned}
\tag{5.29}
$$

where g_n, l_{PM} and μ_{PM} are the air gap at stator tooth n, magnet thickness and permeability of the magnet respectively. Another equation required for solving the flux densities is the conservation of flux:

$$B_{PM1}A_p + B_{PM4}A_p + B_{PM7}A_p + B_{PM10}A_p = 0 \tag{5.30}$$

Equations (5.29) and (5.30) can be arranged in a matrix form:

$$
\begin{bmatrix}
\frac{g_1}{\mu_0}+\frac{l_{PM}}{\mu_{PM}} & -\frac{g_4}{\mu_0}-\frac{l_{PM}}{\mu_{PM}} & 0 & 0\\
0 & \frac{g_4}{\mu_0}+\frac{l_{PM}}{\mu_{PM}} & -\frac{g_7}{\mu_0}-\frac{l_{PM}}{\mu_{PM}} & 0\\
0 & 0 & \frac{g_7}{\mu_0}+\frac{l_{PM}}{\mu_{PM}} & -\frac{g_{10}}{\mu_0}-\frac{l_{PM}}{\mu_{PM}}\\
1 & 1 & 1 & 1
\end{bmatrix}
\begin{Bmatrix} B_{PM1}\\ B_{PM4}\\ B_{PM7}\\ B_{PM10}\end{Bmatrix}
$$

$$
=\frac{B_0 l_{PM}}{\mu_{PM}}\begin{Bmatrix}
\sin\left(2\left(\frac{\pi}{2}\right)-\omega t\right)-\sin\left(2(\pi)-\omega t\right)\\
\sin\left(2(\pi)-\omega t\right)-\sin\left(2\left(\frac{3\pi}{2}\right)-\omega t\right)\\
\sin\left(2\left(\frac{3\pi}{2}\right)-\omega t\right)-\sin\left(2(2\pi)-\omega t\right)\\
0
\end{Bmatrix}
\tag{5.31}
$$

Matrix (5.31) can be written succinctly as:

$$\{B_{PM}\}[R_{PM}]=\{M_{PM}\} \tag{5.32}$$

The flux densities (due to permanent magnets) in the air gap at stator teeth no. 1, 4, 7 and 10 can then be solved:

$$\{B_{PM}\}=[R_{PM}]^{-1}\{M_{PM}\} \tag{5.33}$$

Two other sets of stator teeth 2, 5, 8, 11 and 3, 6, 9, 12 also form similar loop paths and matrices as in (5.31). Denoting these separate sets of stator teeth as subscript *a*, *c* and *b* respectively, the whole collective matrix can be organised as:

$$\begin{Bmatrix} B_{PMa} \\ B_{PMc} \\ B_{PMb} \end{Bmatrix} = \begin{bmatrix} R_{PMa} & 0 & 0 \\ 0 & R_{PMc} & 0 \\ 0 & 0 & R_{PMb} \end{bmatrix}^{-1} \begin{Bmatrix} M_{PMa} \\ M_{PMc} \\ M_{PMb} \end{Bmatrix} \tag{5.34}$$

5.2.2.2 Flux densities due to motor currents, B_{MC}

Because the torque-producing motor currents have the same pole number as the magnets, the flux loops in figure 5.6 can also be used to derive the corresponding flux densities:

$$\begin{bmatrix} \frac{g_1+l_{PM}}{\mu_0} & \frac{-g_4-l_{PM}}{\mu_0} & 0 & 0 \\ 0 & \frac{g_4+l_{PM}}{\mu_0} & \frac{-g_7-l_{PM}}{\mu_0} & 0 \\ 0 & 0 & \frac{g_7+l_{PM}}{\mu_0} & \frac{-g_{10}-l_{PM}}{\mu_0} \\ 1 & 1 & 1 & 1 \end{bmatrix} \begin{Bmatrix} B_{MC1} \\ B_{MC4} \\ B_{MC7} \\ B_{MC10} \end{Bmatrix}$$

$$= 2NI_{MCMax}\begin{Bmatrix} \sin\left(2\left(\frac{\pi}{2}\right)-\omega t+\varphi_e\right)-\sin\left(2(\pi)-\omega t+\varphi_e\right) \\ \sin\left(2(\pi)-\omega t+\varphi_e\right)-\sin\left(2\left(\frac{3\pi}{2}\right)-\omega t+\varphi_e\right) \\ \sin\left(2\left(\frac{3\pi}{2}\right)-\omega t+\varphi_e\right)-\sin\left(2(2\pi)-\omega t+\varphi_e\right) \\ 0 \end{Bmatrix} \quad (5.35)$$

where N is the number of turns and I_{MCMax} is the motor current in the parallel path . Note that there are 2 coils at each stator tooth with reference to figure 4.9. Using the same denotation for the sets of stator teeth as before, the overall flux densities due to motor currents can be written as:

$$\begin{Bmatrix} B_{MCa} \\ B_{MCc} \\ B_{MCb} \end{Bmatrix} = \begin{bmatrix} R_{MCa} & 0 & 0 \\ 0 & R_{MCc} & 0 \\ 0 & 0 & R_{MCb} \end{bmatrix}^{-1} \begin{Bmatrix} M_{MCa} \\ M_{MCc} \\ M_{MCb} \end{Bmatrix} \quad (5.36)$$

5.2.2.3 Flux densities due to levitation currents, B_{Lev}

For the levitation current, a convenient flux loop can be formed at diametrically opposite stator teeth because of its 2-pole configuration as depicted in figure 5.7. In this case flux loops are formed at sets of teeth: 1 & 7; 2 & 8; 3 & 9; 4 & 10; 5 & 11; and 6 & 12:

$$\begin{bmatrix} \frac{g_1+l_{PM}}{\mu_0} & \frac{-g_7-l_{PM}}{\mu_0} \\ 1 & 1 \end{bmatrix} \begin{Bmatrix} B_{Lev(X)1} \\ B_{Lev(X)7} \end{Bmatrix} = 2NI_{LevMax(X)} \begin{Bmatrix} \sin\left(\left(\frac{\pi}{2}\right)-\omega t+\varphi_e\right)-\sin\left(\left(\frac{3\pi}{2}\right)-\omega t+\varphi_e\right) \\ 0 \end{Bmatrix}$$

(5.37)

Sets of stator teeth 1 & 7; 2 & 8; 3 & 9; 4 & 10; 5 & 11; and 6 & 12 are denoted as subscript a1, c2, b1, a2, c1 and b2 respectively for reference. Arranging these sets of flux densities in a matrix form:

$$\begin{Bmatrix} B_{Lev(X)a1} \\ B_{Lev(X)c2} \\ B_{Lev(X)b1} \\ B_{Lev(X)a2} \\ B_{Lev(X)c1} \\ B_{Lev(X)b2} \end{Bmatrix} = \begin{bmatrix} R_{Leva1} & 0 & & \cdots & & 0 \\ 0 & R_{Levc2} & & & & \\ & & R_{Levb1} & \ddots & & \vdots \\ \vdots & & \ddots & R_{Leva2} & & \\ & & & & R_{Levc1} & 0 \\ 0 & & \cdots & & 0 & R_{Levb2} \end{bmatrix}^{-1} \begin{Bmatrix} M_{Lev(X)a1} \\ M_{Lev(X)c2} \\ M_{Lev(X)b1} \\ M_{Lev(X)a2} \\ M_{Lev(X)c1} \\ M_{Lev(X)b2} \end{Bmatrix} \tag{5.38}$$

Similarly the y-direction levitation component of flux densities can be written as:

$$\begin{Bmatrix} B_{Lev(Y)a1} \\ B_{Lev(Y)c2} \\ B_{Lev(Y)b1} \\ B_{Lev(Y)a2} \\ B_{Lev(Y)c1} \\ B_{Lev(Y)b2} \end{Bmatrix} = \begin{bmatrix} R_{Leva1} & 0 & & \cdots & & 0 \\ 0 & R_{Levc2} & & & & \\ & & R_{Levb1} & \ddots & & \vdots \\ \vdots & & \ddots & R_{Leva2} & & \\ & & & & R_{Levc1} & 0 \\ 0 & & \cdots & & 0 & R_{Levb2} \end{bmatrix}^{-1} \begin{Bmatrix} M_{Lev(Y)a1} \\ M_{Lev(Y)c2} \\ M_{Lev(Y)b1} \\ M_{Lev(Y)a2} \\ M_{Lev(Y)c1} \\ M_{Lev(Y)b2} \end{Bmatrix} \tag{5.39}$$

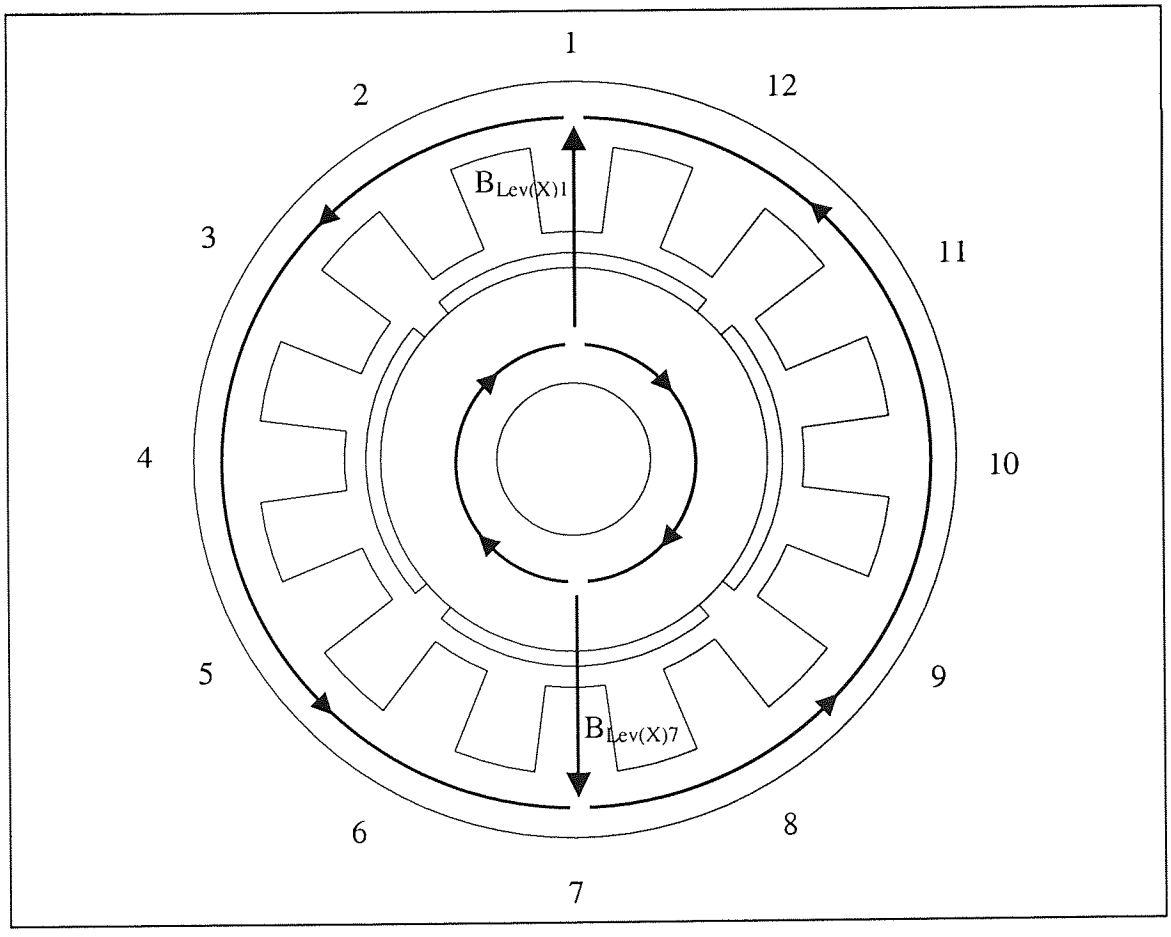

Figure 5.7: Sign convention of the chosen 2-pole flux loops.

With all the necessary flux components computed from matrices (5.34), (5.36), (5.38) and (5.39), they are substituted into equations (5.19) and (5.20) to give lateral forces $F_{(X)}$ and $F_{(Y)}$. A sample program listing of lateral force calculation can be found in appendix E.

5.3 Finite element analysis of a self-bearing motor

Finite element analysis (FEA) is a powerful tool used to predict the performance and characteristics of any electromagnetic structures. Rather than being inundated with the overly complex magnetic equations introduced by the non-trivial geometries in analytical techniques, commercial FEA packages can be used to expedite the design and validation processes during prototyping. Any physical dimensions or material properties can be varied with ease. Thus, the model can be optimised rapidly and can significantly reduce the testing and prototyping time.

A commercial FEA software called ANSYS was used to simulate the permanent magnet self-bearing motor. The aims of this chapter are to validate and verify that a machine with the proposed bridge connection is capable of producing torque and lateral forces, as in conventional self-bearing motors. In particular, 2D magneto-static coupled-field simulations are performed for both linear and non-linear models, and these include cases where the rotor is concentric and eccentric with respect to the stator.

The strength of a coupled-field analysis lies in its ability to simulate multi-physics simultaneously. In this thesis the finite element model is coupled to an external circuits representing its actual winding connection. Without any circuit coupling the excitations are applied on the basis of current density and therefore, any current excitations must be computed before being applied to the coil areas of the finite element model. The main advantage of using a coupled field is that external current sources can be varied at ease without needing to calculate the resultant current density. This is especially useful in circumstances where there are more than one current sources or other circuit components involved in exciting a network of coils.

More description with regard to ANSYS and FEA modelling techniques can be found in appendix D.

5.3.1 Material properties

Silicon iron is used as the stator and rotor lamination material. Such a ferromagnetic material has a B-H curve shown in figure 5.8 below where it starts to saturate at about 1.3 T. This particular B-H curve is assigned to the stator and rotor 2D model areas in order to set up a non-linear simulation. The linear portion of the curve yields a relative permeability of approximately 8000 and this value is assigned to the stator and rotor components for all linear analyses. In practice any increase in temperature will invariably cause degradation in properties of the machine's performance. For simplicity in modelling, however, we assume that the ferromagnetic material is remain fixed within the excitation range of interest.

A type of rare earth magnet known as samarium cobalt which has a magnetisation characteristic shown in figure 5.5 is used. Since the magnet has a straight line B-H relationship in the second quadrant, a list of B-H data is not required, but can be assumed to be linear by defining its isotropic relative permeability and a vector quantity coercive force. Given that the magnet has a remanence and coercive force of 0.95T and 6.8E5 A/m respectively, its relative permeability can be calculated as 1.11. The electrical resistivity of the copper coils is 3E-8 Ωm. More material and physical properties of the FEA model are detailed in chapter 9.

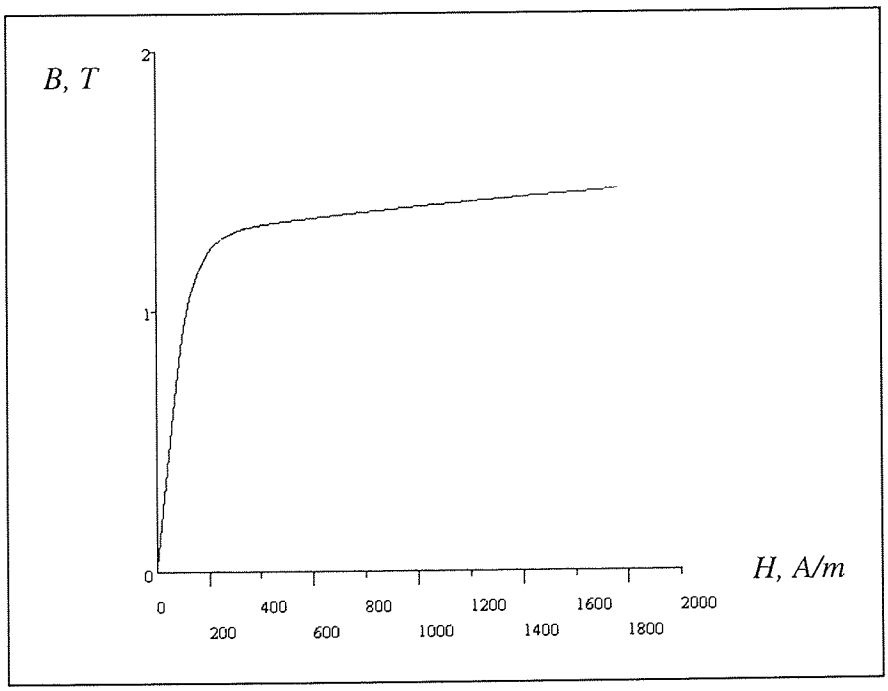

Figure 5.8: B-H curve of Silicon iron.

5.3.2 FEA loads and boundary conditions

The usual practice in FEA is to apply loads and boundary conditions to the meshed model before invoking the solution. The loads in the analysis are motor and levitation currents, and they are applied through a coupled external circuit as connected in figure 4.9. Thus, we can observe the characteristic of the machine by merely varying the applied current of the circuit elements. Section 5.4 below details the simulated forces and torques as a result of varying the applied currents.

There are a few essential boundary conditions required in the analyses. Firstly, the flux is forced to travel parallel to the exterior nodes of the stator core, and thus no leakage occurs at this boundary. For the sake of convenient in rotating the rotor, the stator and rotor components are created and meshed independently. This led to a dissimilar mesh between the components at the mid radius of the air gap where they are not physically connected. As a consequence, there are discontinuities of flux traversing across the air gap boundary. Here the second boundary condition required is to join the nodes of dissimilar component elements around the air gap by issuing the constraint equation generator. The final boundary condition needed is to set flags to the rotor so as to enable computation of force and torque.

The sign convention of flux flow and angles defined in section 5.1.2 also applies to the finite element simulations.

5.4 Simulation tasks

Note that it is not the aim of this thesis to optimise the overall machine designs, but to verify that the bridge connection can be used as a potential alternative to conventional self-bearing motor winding arrangements. FEA's post-processing results are computed by the virtual work and Maxwell's stress tensor methods. All simulations undertaken are crosschecked with the analytical results obtained from section 5.2 above. The breakdown of the FEA tasks is as follows:

- Verification of flux densities B_{PM}, B_{MC} and B_{Lev}. As a precursor to the principal simulation tasks, the components of flux density due to permanent magnets, motor excitation and levitation currents are independently verified. It is essential that these

components around the air gap vary according to equations (5.3), (5.4) and (5.8) respectively (approximately).

- Verification of torque production. The main purpose is to ensure the proposed self-bearing motor is capable of producing torque at different levels of excitation. No levitation current is supplied at this stage. The torque constant will be derived from a plot of torque versus motor current.
- Verification of lateral force production. This section verifies that the machine has magnetic bearing capability and that force can be controlled according to the method presented in section 5.1.3. The actuator gain, which relates lateral force to the applied levitation current, will be derived. Further, the effect of increasing motor current to the lateral force production will be observed.
- Estimation of negative stiffness. Without any excitations, the rotor is displaced in a gradual manner with respect to its centred position and the resultant attractive force due to permanent magnets is estimated. The gradient of the plot of force versus displacement gives the negative stiffness of the machine.

Other simulation results such as force and torque ripple due to a rotating rotor are included in appendix C.

5.4.1 Verification of flux densities B_{PM}, B_{MC} and B_{Lev}

Prior to simulating the principal problems, it is important to verify that the machine is capable of producing flux densities B_{PM}, B_{MC} and B_{Lev} in accordance to their corresponding means of excitation. This is to ensure that any magnitude or direction errors introduced by these components will not be propagated to the subsequent simulations. Each component is independently verified from the other. Both flux densities B_{PM} and B_{MC} are 4-pole fields responsible for torque production whereas the levitation flux is of a 2-pole field.

Without supplying any currents to the coils, the flux density due to permanent magnet B_{PM} is first investigated. The resulting 2D flux plot as well as a graph of how flux density varies around the air gap periphery are shown in figure 5.9(a). As revealed in the graph, the permanent magnets give rise to a square waveform of flux density distribution in the air gap around the rotor. Such a result is not surprising since the surface mounted magnets are magnetised equally in the radial direction across their thickness. The flat portions of the flux density correspond to the angle subtended by each permanent magnet on the rotor.

A better sinusoidal flux distribution can be obtained if the magnets are shaped to vary their thickness. Ideally the flux distribution should be made equal to the distribution described by equation (5.3). Since it not the aim of the thesis to embrace any design optimisation, the square waveform shown in figure 5.9(a) is accepted as an approximation to a sinusoidal distribution. What is more important in this circumstance is that there are four pole changes around the air gap periphery.

The analytical solution presented in 5.2.2.1 is about 86.3% - 98.8% of the FEA solution depending on the frequency ωt or angle of rotation. This is because only 12 fixed positions under the pole face or mean paths are selected for analytical computation and so a smooth sinusoidal curve is virtually impossible to be plotted. Thus, the analytical calculation is not expected to generate an accurate answer but to provide a quick but approximate solution. It will be seen later that the forces derived from the analytical method are quite satisfactory compared to those from the FEA.

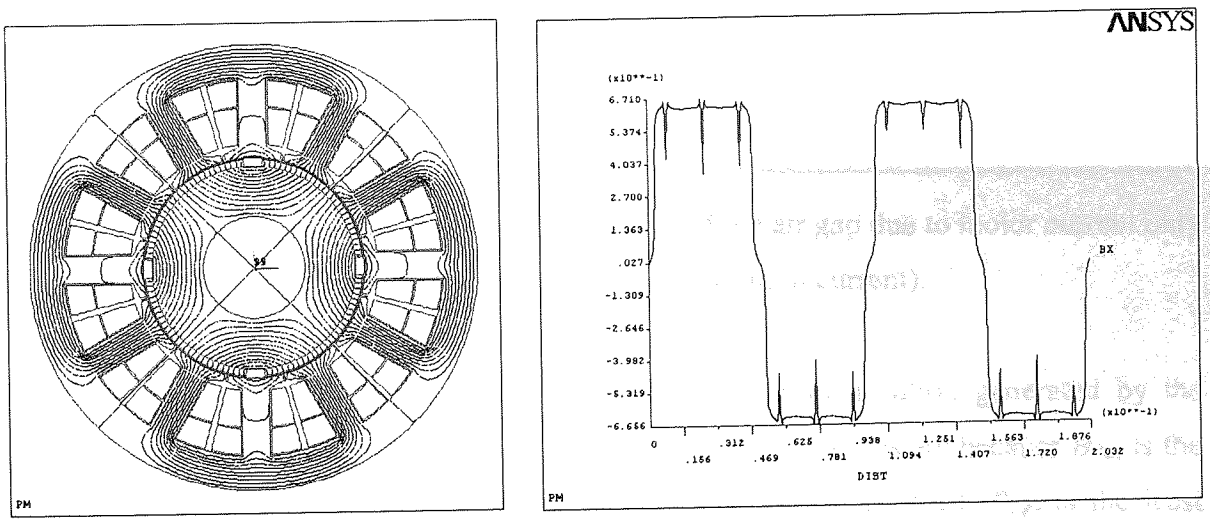

Figure 5.9(a): 2D flux plot and flux distribution around the air gap due to permanent magnets (without any coil excitation).

The magnetic field due to the applied three-phase motor current is determined next. Before the FEA is solved the magnetisation of the permanent magnets are removed. A permanent magnet is essentially equivalent to the air gap because its relative permeability approximates to unity. With the magnetisation removed, the flux distribution due to motor excitation alone can be observed.

Figure 5.9(b) shows the flux plots for a maximum motor current excitation of 6A. At that operating instant the FEA solution gives a maximum B_{MC} of 0.1633 T whereas the analytical calculation gives 0.1616 T, which might be judged as close. The "steps" in the waveform is due to the small number of stator teeth and that each tooth is excited via a concentrated winding. It is common to skew the stator laminations in practice in order minimise the steps in the overall flux distribution waveform. However, the skewed model is not simulated as this would need a 3D model which is computationally expensive. Nevertheless, 2D models are sufficient for our verification purposes.

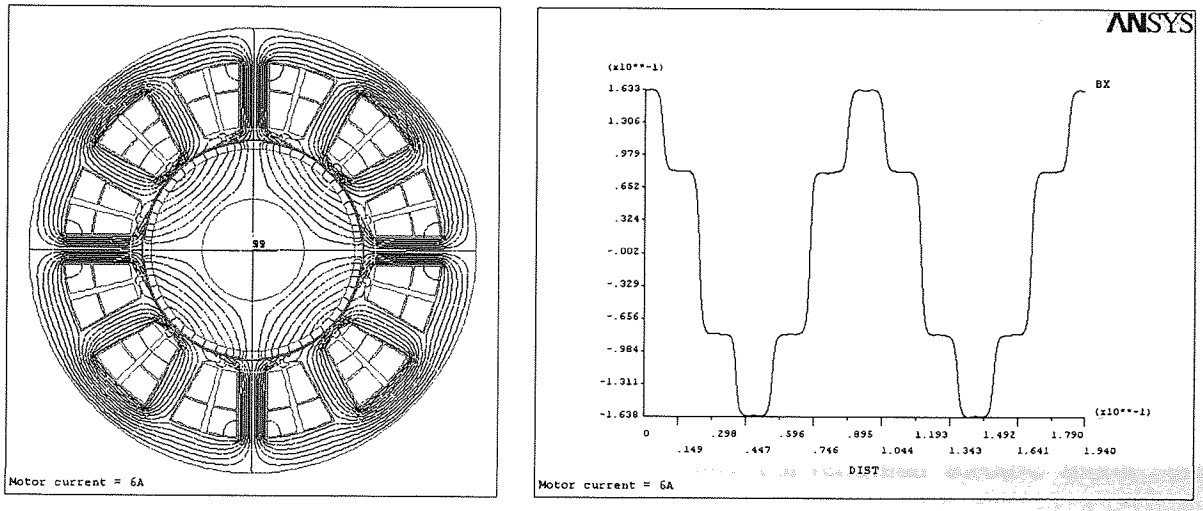

Figure 5.9(b): 2D flux plot and flux distribution around the air gap due to motor current only (without permanent magnets or levitation current).

The same procedure also applies when verifying the flux distribution generated by the levitation current B_{Lev}. The removal of permanent magnets is a necessity because B_{PM} is the most prominent among all components of flux density, and in contrast, B_{Lev} is the least significant. Without removing the magnet, the change of flux due to levitation current is extremely difficult to detect. Figure 5.9(c) depicts the flux distribution generated by the levitation current sources (maximum current of 0.3A). In comparison to B_{PM} and B_{MC} , B_{Lev} has a smoother transition of flux distribution because it has a smaller number of pole-pairs and higher number of independent excitation coils. Because of this the flux distribution of the analytical solution fits well to the FEA plot.

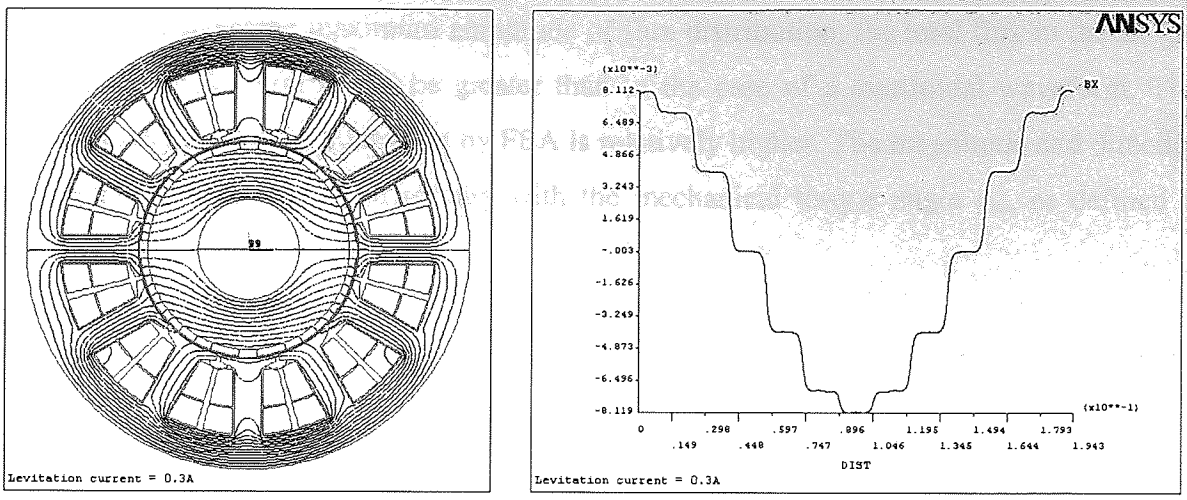

Figure 5.9(c): 2D flux plot and flux distribution around the air gap due to levitation current only (without permanent magnets or motor current).

5.4.2 Verification of torque production

Torque production is the most important function for any electric motor. Thus, for a self-bearing motor to be accepted in an array of applications, its torque production must not be compromised. We confirm that the so connected machine is capable of producing torque before pursuing its levitation potential. As with any conventional electric motor, the proposed self-bearing motor must generate a torque proportional to the applied current, where the relationship is essentially linear over a certain range of excitation before the magnetic material saturates.

The self-bearing motor is excited with a range of three-phase supply currents while keeping the electrical torque angle φ_e constant at 90°. Figure 5.10 shows that the machine torque is indeed proportional to the increasing applied motor current over the selected range of excitation. The torque computed by virtual work (VW) method is quite close that of Maxwell's stress tensor and this indicates that mesh used is adequately fine for our verification purposes.

The analytical torque is calculated using expression (3.15). In comparison to the FEA results the analytical method produces a lower magnitude of torque although its relationship with increasing currents is linear. This is attributable to the fact that expression (3.15) is derived based on sinusoidal air gap MMFs whereas the flux density produced by the permanent magnets is of a square waveform (figure 5.9(a)). It is evident from the area under the flux

plots that for the same maximum amplitude of flux distribution, the total flux in the air gap for the square waveform will be greater than in the case of a sinusoidal waveform. This explains why the torque computed by FEA is relatively higher. The magnitude and direction of torque are also confirmed to vary with the mechanical torque angle φ_m, as defined in equation (3.15).

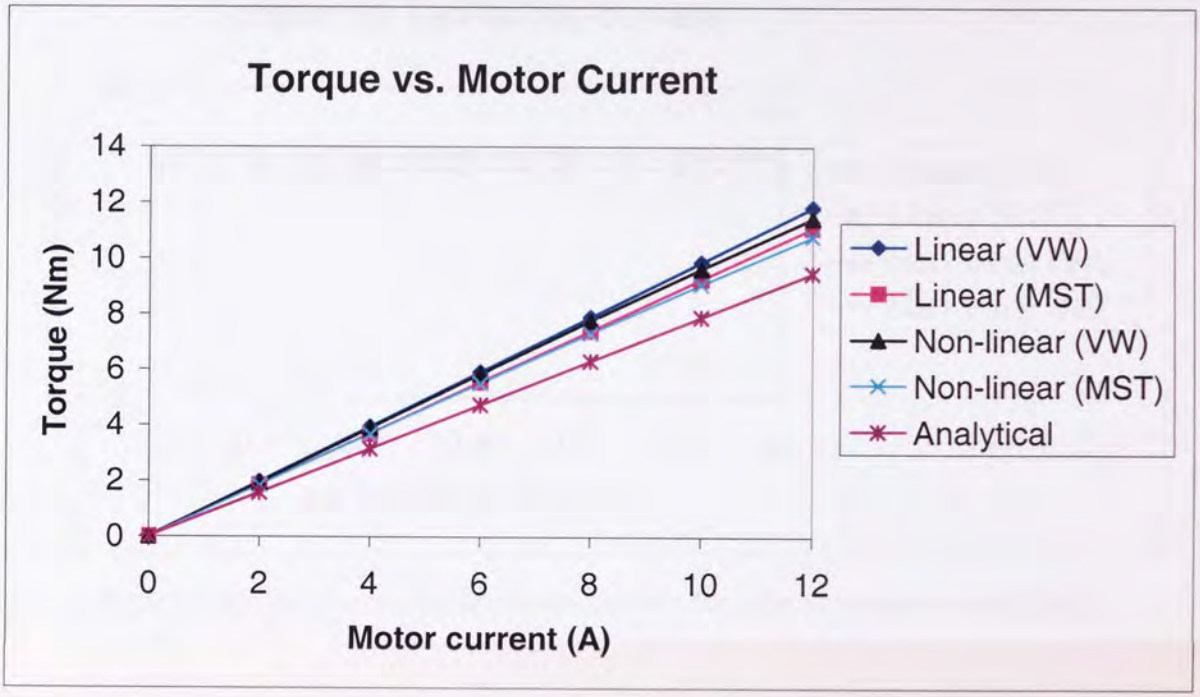

Figure 5.10: Torque characteristic of the proposed self-bearing motor (without excitation of levitation current).

The gradient of the plot shown in figure 5.10 is the torque constant K_T where:

$$T = K_T I_{MC} \tag{5.40}$$

Evaluating the torque constant K_T from the non-linear plot gives a value of approximately 0.933 Nm/A. This value is higher than in practice because the effect of eddy current and back EMF are ignored in static analysis.

Secondary to the torque production verification is the concern of whether any injection of levitation current will affect the magnitude or direction of the machine torque. It can be appreciated from figure 5.11 that varying the levitation does not affect the motor torque. Two factors account for this observation, namely:(1) the fact that the levitation current has

an N_{PPL} pole-pair field means it does not interact with the N_{PPT} pole-pair of the permanent magnets; and (2) the magnitude of the levitation flux is much smaller than that of the motor flux to cause any distortion of flux distribution in the air gap and for this reason torque production is not affected.

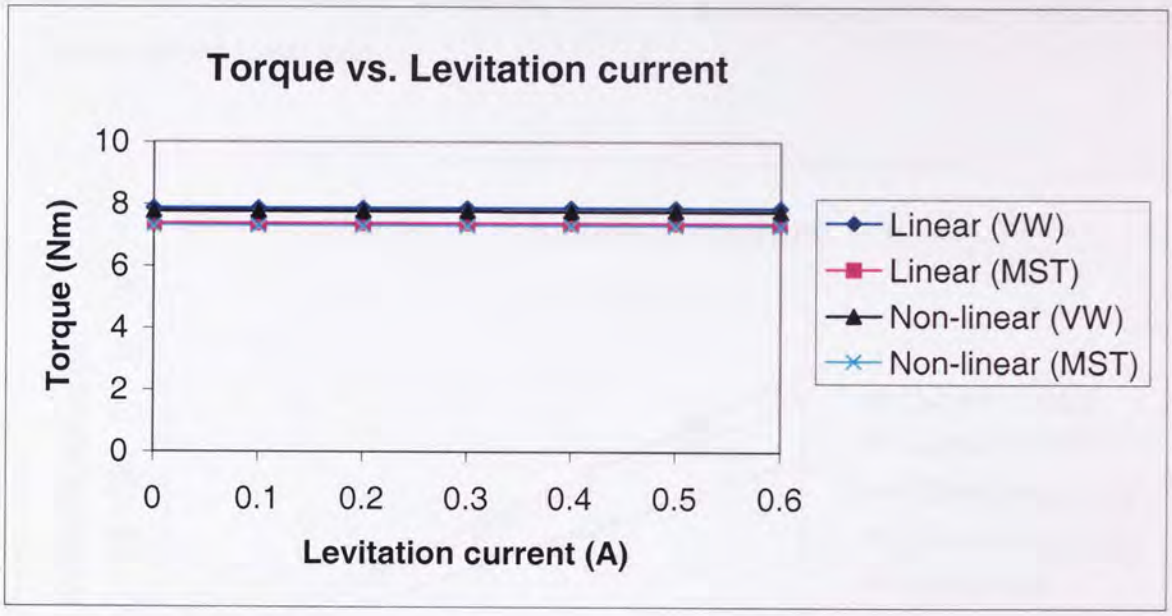

Figure 5.11: Torque versus levitation current for a fixed motor current (8A).

While the linear finite element simulations display a linear relationship between torque and applied motor current, this is not so for non-linear simulations because of saturation of the ferromagnetic material. This inevitably limits the performance of any electrical machines in general. It is not of the present interest to determine the machine's performance in relation to its degree of saturation; neither do we intend to push its performance limits. As far as its primary function is concerned, the proposed self-bearing motor exhibits the torque characteristic of a conventional motor even in the presence of additional levitation currents. However, this is not quite true for induction motors where the injected levitation currents may have an adverse effect on their torque production. The reader is invited to consult chapter 8 for more information with regard to this matter.

5.4.3 Verification of lateral force production

The self-bearing motor is next tested for its magnetic bearing capability where the coils are excited with a fixed motor current and increasing levitation current. The injection of levitation currents follows equation (5.14) with the appropriate phase compensation

calculated from equation (5.7) to ensure that the net lateral force produced is in the vertical direction. With reference to figure 5.12, the levitation force is found to increase proportionally with increasing current for all linear and non-linear simulations. The slight discrepancy between the analytical calculation and linear simulation is due to the assumptions made in the equations and also the square waveform of the permanent magnet flux density. The non-linear simulation, however, exhibits a lower force production when compared to the linear case.

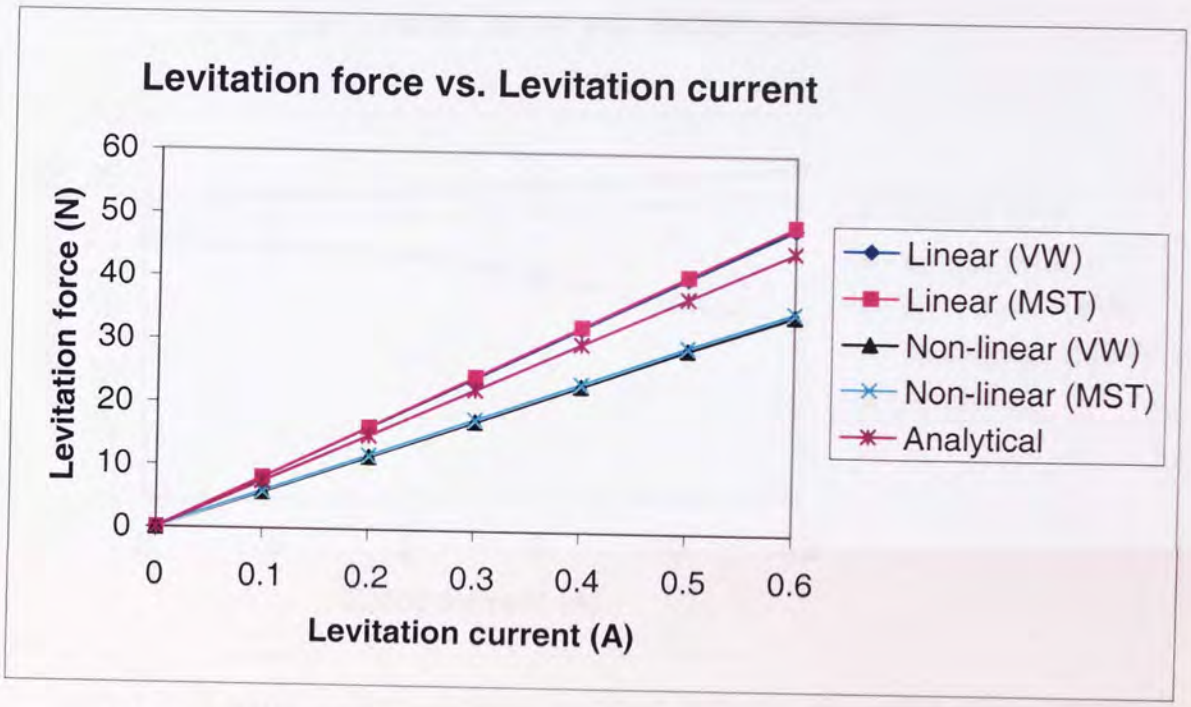

Figure 5.12: Force versus levitation current for a fixed motor current (8A).

From equation (3.3), assuming that the rotor is centred, the lateral force produced as a result of injection of levitation current is simply:

$$F = K_I I_{Lev} \tag{5.41}$$

The actuator gain K_I is evaluated as from the gradient from the non-linear plot since it represents a more realistic example. This yields a value of 58 N/A.

It can be easily appreciated that the excited levitation current can be relatively small when compared to the motor current. For this particular example, a maximum levitation current of 0.3A is sufficient to levitate a rotor of 22 N under a 0.657 T of air gap flux (4-pole) in the linear analysis. Naturally one would suppose that the required levitation current can be

further reduced if the flux density in the air gap is higher according to force expressions (5.11) and (5.12). This is true as far as the linear analysis is concerned, as plotted in figure 5.13. The non-linear simulation, however, shows a contradiction in which the levitation force drops with increasing motor current. Thus, in real practical applications, the levitation current must be increased slightly to counter the drop of force when increasing the motor currents.

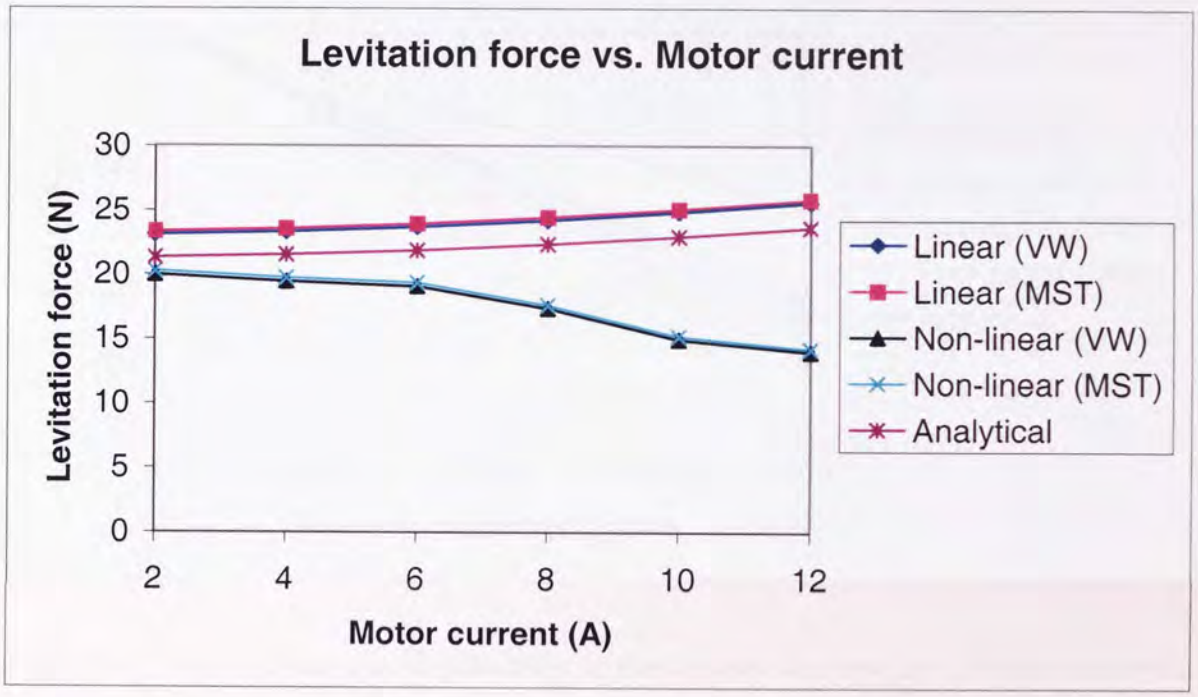

Figure 5.13: Levitation force (constant levitation current 0.3A) versus motor current.

5.4.4 Estimation of negative stiffness or open-loop stiffness

The negative stiffness or open-loop stiffness, as commonly found in magnetic bearing applications, is the magnetic attraction between the stator and rotor per unit displacement of rotor. Such a force is due to the natural tendency of permanent magnets to attract ferromagnetic materials and it occurs when there is rotor eccentricity with respect to the stator. For the present type of self-bearing motor, the attractive force is dominated by the permanent magnets and thereby causes instability of rotor displacement control. This is one of the critical problems plaguing rotating machine designers.

The relationship between the attractive force and rotor eccentricity is essential non-linear if a full excursion of rotor is taken within the air gap. However, it is impractical to allow a maximum rotor deflection because of the associated high currents needed to pull the rotor

back to its concentric position. Usually backup bearings are employed to prevent a direct physical contact between the rotor and stator in the event of control failure and also serve to support the rotor at rest. These mechanical bearings have a smaller clearance than the air gaps of the self-bearing motor or magnetic bearing.

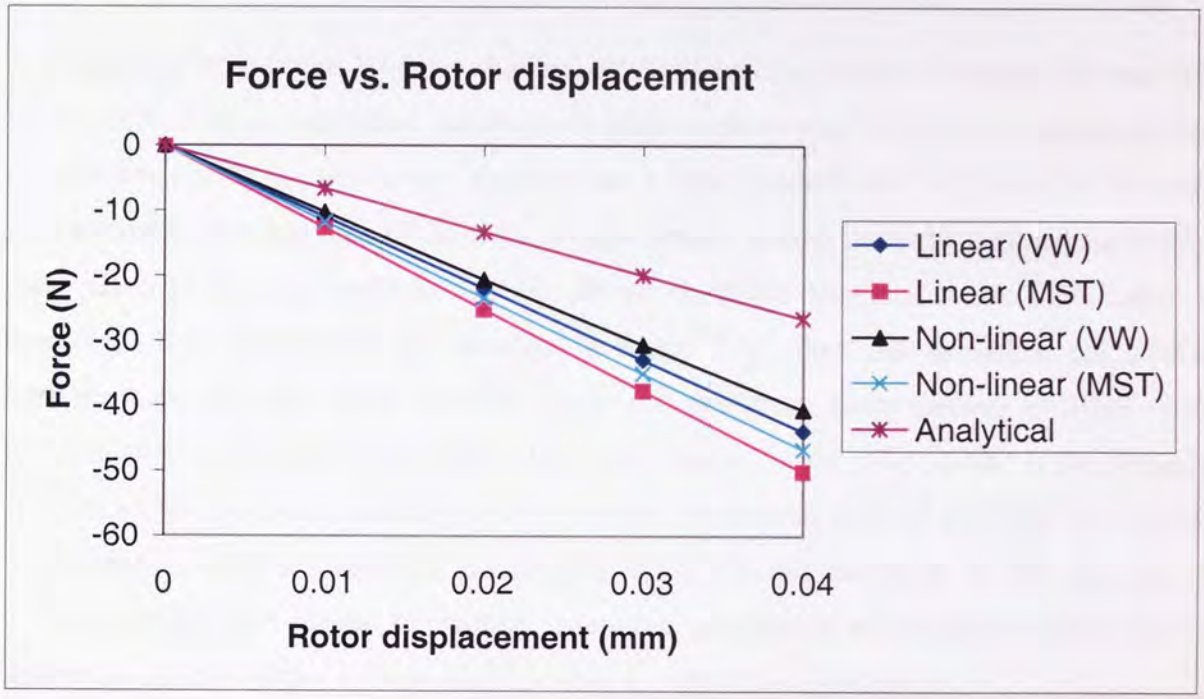

Figure 5.14: Force versus rotor displacement in the absence of motor and levitation currents.

Although the relationship between force and eccentricity is inherently non-linear, a linearised negative stiffness can be obtained by perturbing the rotor displacement about its concentric position (usually less than 10% of full air gap size). Figure 5.14 depicts a plot of attractive force with increasing rotor displacement over a perturbation of up to 5% of the air gap. On contrary to the simulated concentric cases, the forces computed via virtual work and Maxwell's stress tensor for rotor eccentricity show a relatively noticeable discrepancy for both linear and non-linear plots. This suggests that the meshing of rotor eccentricities could be inadequate and that further refining of mesh is required. However, no further attempt is made to obtain a more accurate result at this juncture since this is largely detail work.

Taking equation (3.3) and substituting a zero for the levitation current, the force due to permanent magnets in relation to the rotor displacement is:

$$F = K_x x \tag{5.42}$$

The negative stiffness or open-loop stiffness can be estimated by taking the gradient of the plot in figure 5.14. As an example the non-linear plot yields an averaged value of -1.09E6 N/m.

It is apparent from figure 5.14 that the analytical calculation of force is much less than that of the FEA. Such a significant difference is attributable to the fact that the simulated flux distribution due to the permanent magnets has a square waveform, and therefore the total flux around the surface area of the rotor is considerably greater than the assumed sinusoidal distribution in the analytical calculation. However, if the magnets in the FEA create a sinusoidal flux distribution, as depicted in figure 5.15, then the analytical calculation approximates very well to the resultant linear and non-linear finite element analyses. This result is shown in figure 5.16 below. Here each magnet in the FEA model is deliberately split into a few segments radially and the material property is defined such that the overall magnetisation is of a sinusoidal distribution. Note that the thickness of the magnets is unaltered in the FEA model. In practice, it is more economical to vary the thickness of the magnet in order to obtain a sinusoidal flux than to vary the magnetisation.

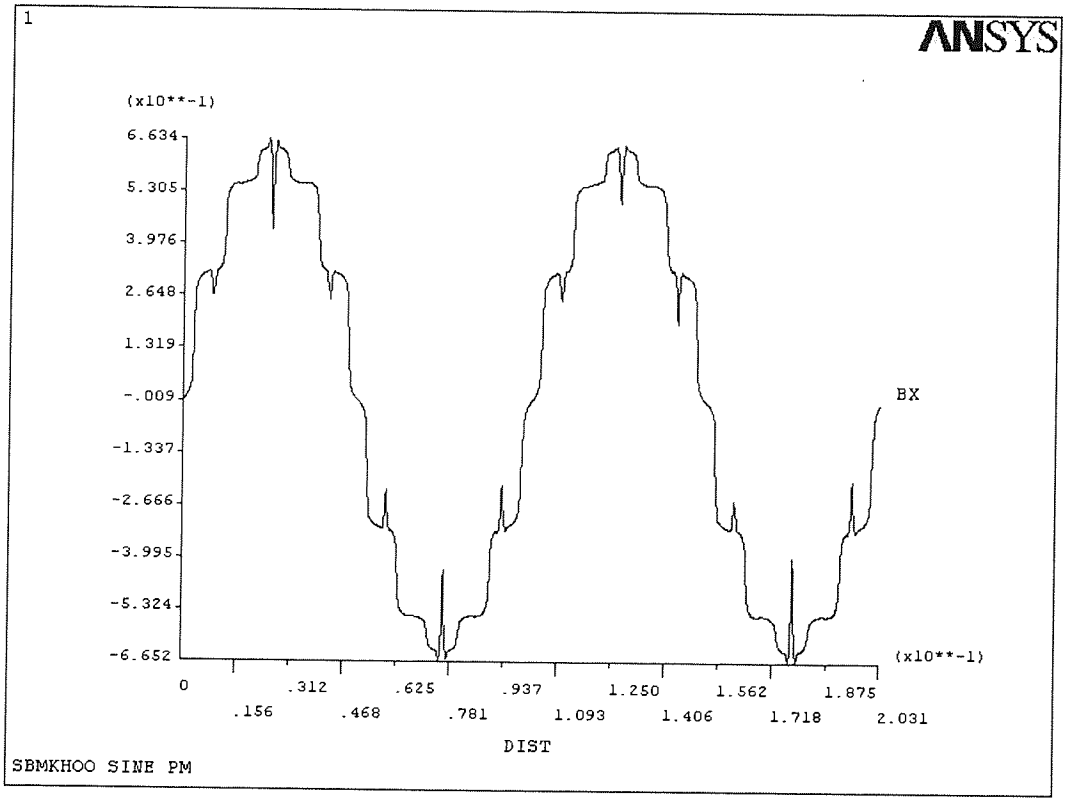

Figure 5.15: A sinusoidal flux distribution around the air gap created by appropriate remodelling of permanent magnets.

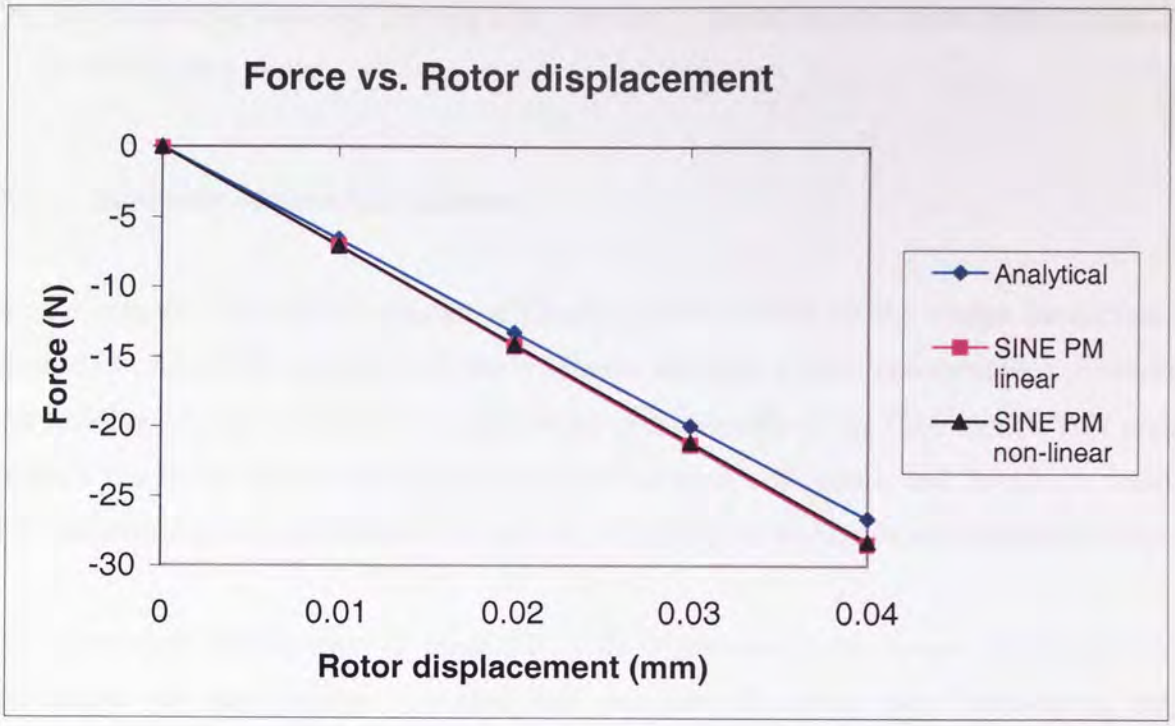

Figure 5.16: Force versus rotor displacement in the absence of motor and levitation currents (with a sinusoidal permanent magnet flux distribution in the air gap).

5.4.5 Finite element simulations of a rotating rotor

Previously performed analyses are all based on a non-rotating rotor. This section supplements the main FEA results in which the torque ripple, cogging torque and force ripple due to a rotating rotor will be observed. Since the stator has 12 poles or teeth spacing at 30° apart, any torque or force variation observed within a particular 30° interval will be repeated 11 times throughout the full circumference of the stator. Full FEA results are shown in appendix C. Accordingly the main observations can be summarised as follows:

Torque ripple = 13.5 %; Cogging torque = 0.186 Nm; Force ripple = 5.37 %

It is evident that the force ripple experienced by the machine is low and seems acceptable. These ripple effects can be further smoothed by minimising the slot openings or by appropriately compensating the levitation currents. The torque ripple and cogging torque of the simulated machine, however, are relatively high due to its low number of stator slots and poles. There are many ways to reduce these negative effects such as skewing the laminations or permanent magnets, using a larger number of slots/pole, improving the geometric design, etc. These improvements will not be explored in this thesis but will be left

for future attempts since our primary aim is to verify the torque and lateral force production of the self-bearing motor.

5.5 Summary of principal matters

In this chapter a permanent magnet self-bearing motor based on the bridge connection is simulated using a 2D coupled-field finite element analysis. Circuit connections representing the winding scheme are directly coupled to the coil elements in the FEA model. This multi-physics simulation feature allows easy superposition of both motor and levitation current, without requiring the user to sum the currents and apply the excitation as a current density.

An appropriate combination of magnetic fields is mandatory for torque and lateral force production in the machine. An analytical solution of lateral force considering rotor eccentricity is presented where the components of magnetic field generated by motor current, permanent magnet and levitation current are independently evaluated using Ampere's loop law before the force is computed via Maxwell's stress method. It is essentially a linear analysis intended to provide an approximate and rapid solution.

Simulations of all components of magnetic field, torque and force productions are systematically performed and compared with the analytical solutions. Parameters such as the torque constant, actuator gain and negative stiffness are also estimated. Both analytical and FEA results show good agreement in general. The main source of error arises from the fact that the analytical solution assumes a sinusoidal permanent magnet flux distribution whereas the FEA model has a square wave distribution. There are some noticeable differences between linear and non-linear analyses: the computed forces are lower in the latter case. Cogging and ripple effects are observed in the simulation as the rotor is rotated. These undesirable effects can be reduced by adopting appropriate design methods, but are not attempted here since these details depart from our scope of research.

Overall, the self-bearing motor with the proposed bridge connection exhibits the characteristics of a conventional self-bearing motor. Having verified that the self-bearing is capable of producing torque and lateral forces, the next chapter compares the bridge connection with other conventional winding schemes and to establish relative merits between them.

CHAPTER 6

COMPARISON WITH CONVENTIONAL SELF-BEARING MOTORS

A novel single set of windings for AC polyphase self-bearing motors known as the bridge connection has been proposed in chapter 4. Besides merely verifying its capability of producing lateral forces and torque, it is essential to compare the newly proposed winding scheme with that of conventional self-bearing machines so that their relative merits of the connections can be deduced. A quantitative comparison is made in this chapter in terms of power loss for a given machine performance. Power loss or copper loss of the machines is computed by using a 2D harmonic finite element analysis and verified analytically. Other aspects such as cost, design and implementation are compared qualitatively to reinforce the feasibleness of the proposed connection as a potential alternative to currently available schemes.

6.1 Conventional self-bearing motors

Two conventionally implemented winding schemes are considered for the purpose of comparison: (1) single set of windings; and (2) dual set of windings configurations. Both machines have the same physical dimensions and properties as that of the newly proposed self-bearing motor so as to refrain from indicating any bias or favouritism to a particular machine before the comparison is made. All machines have concentrated coils wound around a 12-slot stator and with a maximum of 120 turns per tooth. The only essential difference between them is the way the coils are connected. More details of the conventional machines are furnished below.

6.1.1 A conventional self-bearing motor with a single set of windings

The selected machine is a four-pole permanent magnet self-bearing motor, similar to the class of machine analysed in the previous chapter. Each coil of this machine is excited by separate bi-directional power supplies to carry both torque and levitation-producing component of currents, as shown in figure 6.1. Thus, the self-bearing motor has a total of 12 power supplies where each of the four supplies constitute a single phase.

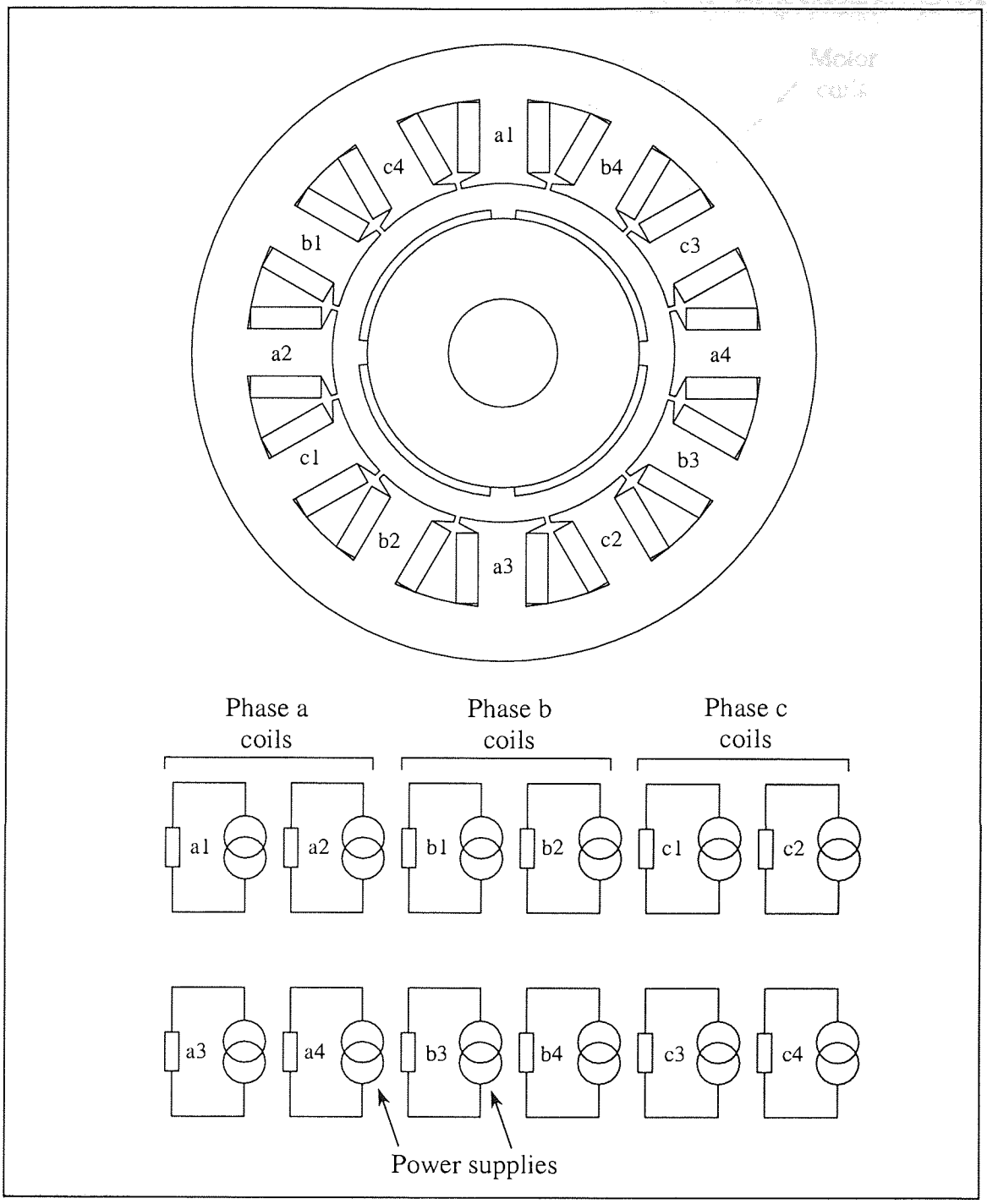

Figure 6.1: A conventional self-bearing motor with a single set of coils excited by 12 independent power supplies.

6.1.2 A conventional self-bearing motor with a dual set of windings

For the configuration with two sets of windings, shown in figure 6.2, the primary set forms a three-phase star connection whereas the secondary set are connected to six independent bi-directional supplies. The number of copper conductors used per slot is the same as in the other machines where the winding ratio between the former and latter sets is 9:1.

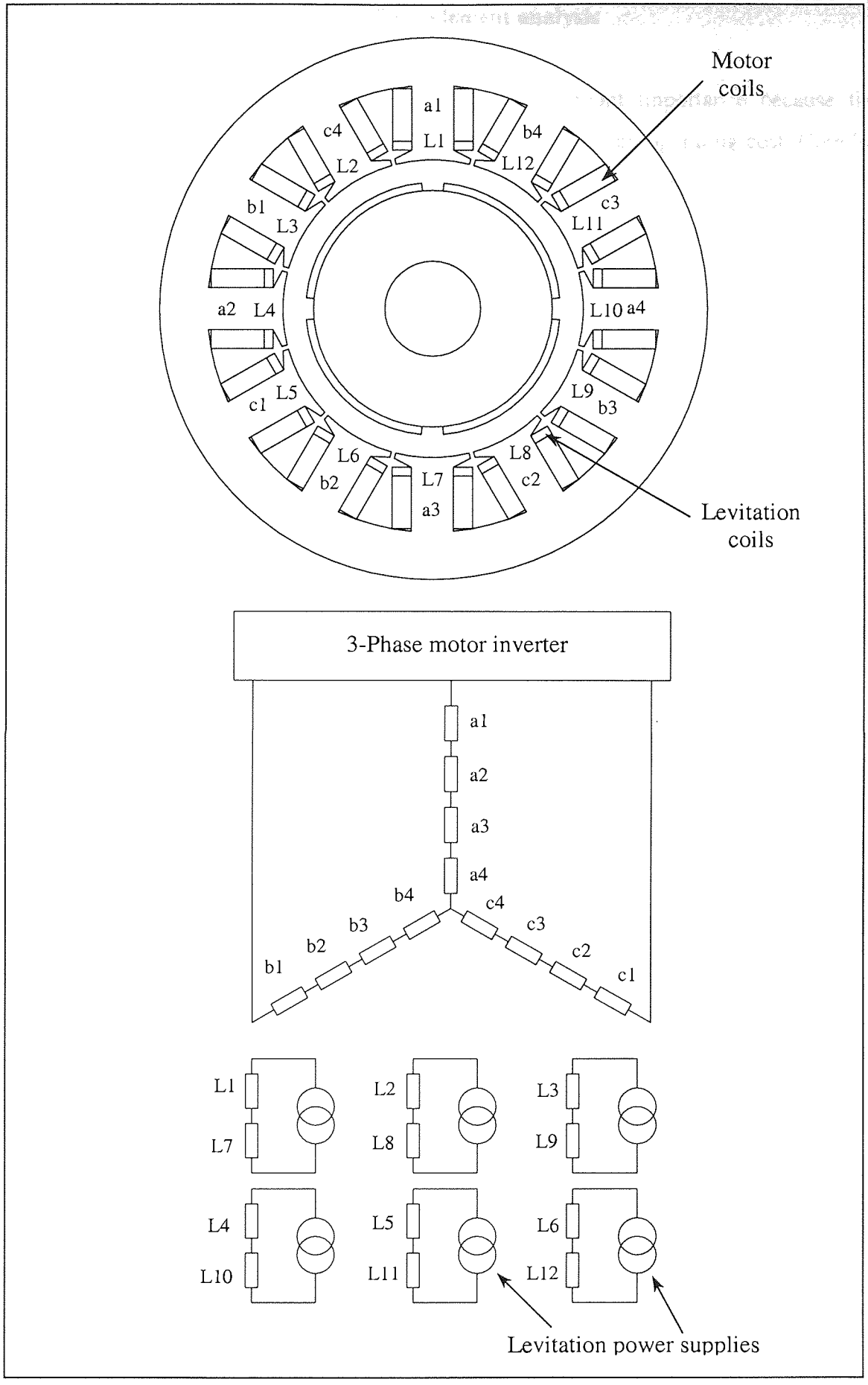

Figure 6.2: A conventional self-bearing motor with two sets of coils.

6.2 Comparison of power loss by finite element analysis

Within the assembly of the motor, losses are of paramount importance because they determine the efficiency of the machine and ultimately the overall operating cost. Core loss is due to the changing of flux densities in the ferromagnetic material and can be sub-divided into two groups, i.e. hysteresis and eddy current losses. This category of losses depends primarily on the characteristics of the iron used and usually the iron is laminated between thin layers of insulation to reduce the eddy current effect. Fortunately, mechanical losses as a result of bearings and brush-contact friction are completely eliminated in self-bearing machines because of their non-contacting technology. Stray loss arising from leakage flux pulsation near the end windings is also present, but as far as our interest of comparing the self-bearing motors is concerned, the aforementioned losses more or less equal for the same dimension and material used. Moreover core and stray losses are less significant when compared with copper loss and can be neglected under normal circumstances. Thus, the performance and copper loss parameters are chosen as a basis for comparing the respective self-bearing motors.

Since we have specified that the number of conductor turns must be the same for all candidates of self-bearing motor, one would intuitively think that the associated copper losses must be equal for the same machine performance. However, self-bearing motors are different from conventional motors in the sense that a secondary component of current must be present for levitation purposes. This calls for a superposition of the levitation-producing component of current in the air gap, either by using the same or separate set of windings. It is the aim of this chapter to compare the power loss between the motors when operating to give the equal torque and net lateral force production.

6.2.1 Finite element analysis of power loss

A couple-field FEA is performed for the connections shown in figures 4.9, 6.1 and 6.2 and each is excited accordingly to generate the same magnitude and direction of torque and lateral force. The power loss is then computed via a harmonic analysis in the post processing section. It is evident from figure 6.3 that for a given performance requirement the power loss for the dual set of windings scheme (denoted "DS") is found to be highest among the compared self-bearing motors. This is attributable to the fact that the number of turns allocated for motoring torque has been reduced in order to accommodate the

secondary set of windings. On the contrary, the presently proposed connection (denoted "Bridge") allows both motor and levitation currents to flow in the same set of windings thereby taking the full advantage of the available number of turns. Thus both the bridge connection and the conventional single set of windings scheme (denoted "SS") produce exactly the same copper losses in each motor.

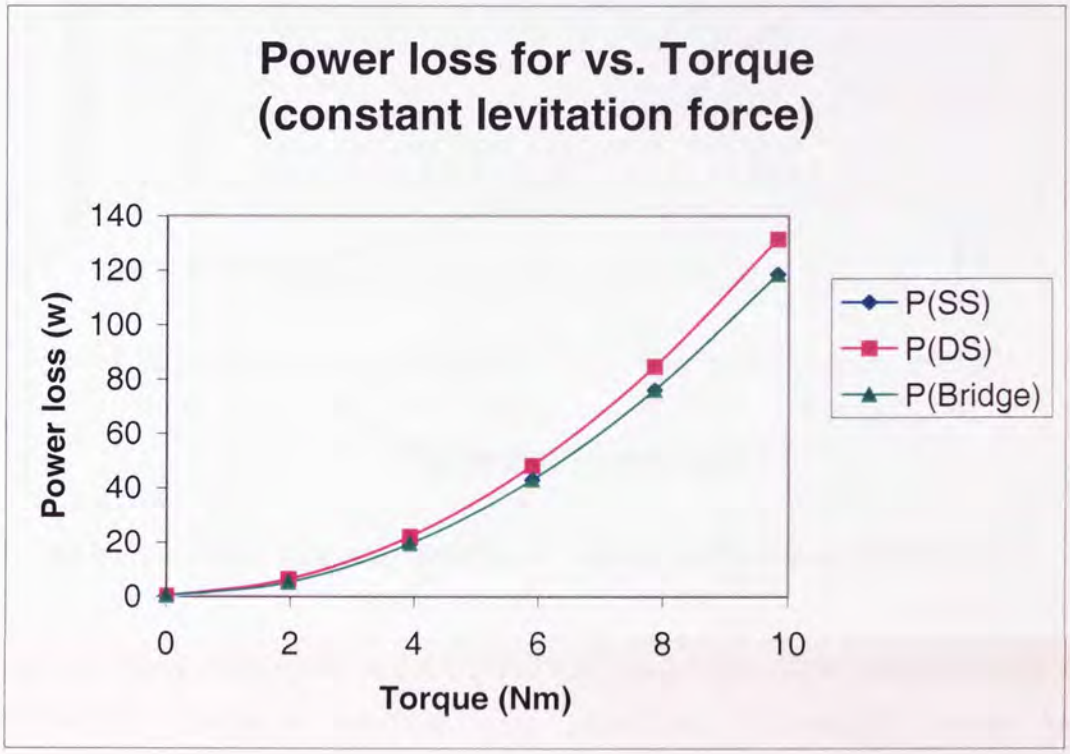

Figure 6.3: Power loss for a given machine performance (same force and torque).

Another interesting plot of how the power loss ratio of the dual set of windings scheme (DS) to the single set of windings scheme (SS) varies as the per unit (p.u.) ratio of force to torque increases is shown in figure 6.4. The bridge connection scheme is omitted because it produces the same losses as the single set of windings scheme, as verified from figure 6.3. It can be observed that the "DS" scheme has at least 10% more power loss than the "SS" scheme, and the difference in losses is more pronounced as the p.u. ratio of force to torque increases. This undesirable characteristic is expected because higher currents are required to produce the same magnitude of force and torque in the DS scheme. An increase in the number of conductor turns for torque production is at the expense of the levitation force production and vice versa. Thus the specific power rating of this particular machine is relatively low.

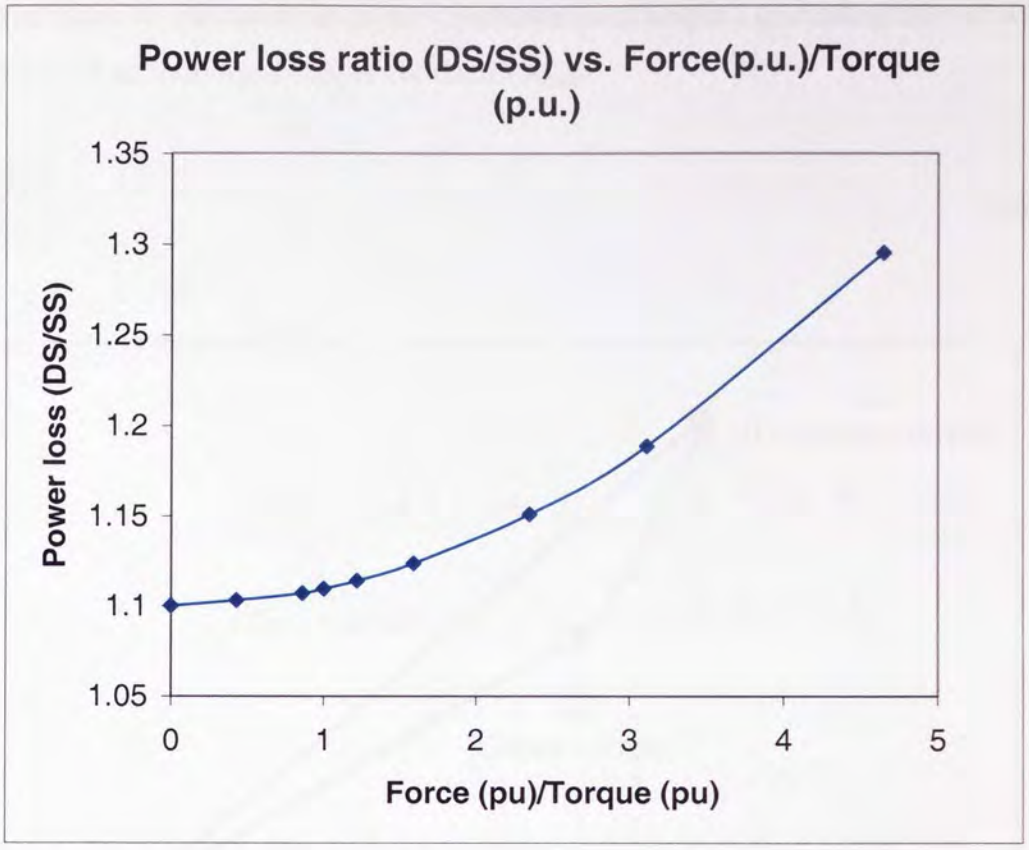

Figure 6.4: Power loss ratio (DS/SS) for a given performance (force/torque).

Although the above comparison is confined to just concentrated coils, similar results would be obtained if distributed windings were considered. Accordingly, power loss is proportional to the square of the currents and so the use of a secondary set of windings has inevitably led to a higher power loss for a given machine size and performance.

6.2.2 Analytical calculation of power loss

The copper losses are computed from the effective DC resistance R_K of the winding namely:

$$\begin{aligned} P_{loss} &= \left({I_{RMS}}^2 R_K \right) N_{coilside} \\ &= \left(\frac{I_K}{\sqrt{2}} \right)^2 R_K N_{coilside} \\ &= \left(\frac{{I_K}^2}{2} \right) R_K N_{coilside} \end{aligned} \tag{6.1}$$

where I_{RMS} and $N_{coilside}$ are the root mean square (RMS) current and number of coil sides per tooth respectively. The DC resistance of the copper (per coil side) is calculated from the

number of turns N, the resistivity ρ, the conductor axial length l (including the end winding) and the area of an individual copper conductor A_{cond}:

$$R_K = \frac{N\rho l}{A_{cond}} \tag{6.2}$$

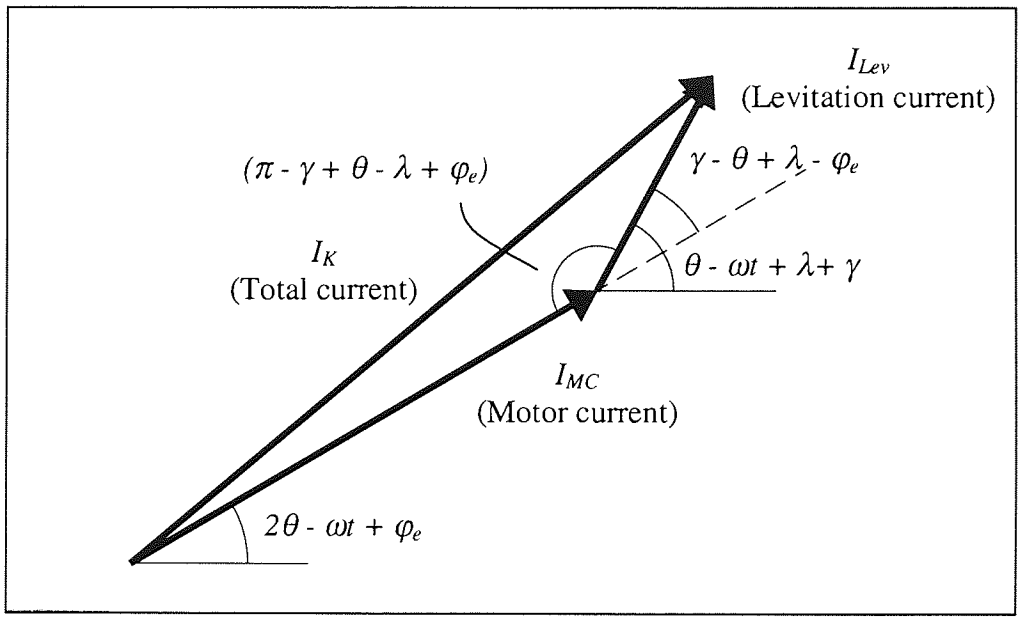

Figure 6.5: Vector sum of the torque and levitation-producing component of currents.

The current I_K is the vector sum of motor current I_{MC} and levitation current I_{Lev} in the copper conductors as given in figure 6.5 above. Here I_{MC} and I_{Lev} vary in space and time according to:

$$I_{MC} = I_{MCMax} \sin\left(2\theta - \omega t + \varphi_e\right) \tag{6.3}$$

$$I_{Lev} = I_{LevMax} \sin\left(\theta - \omega t + \lambda + \gamma\right) \tag{6.4}$$

In terms of tooth number n, both former and latter currents can be rewritten as:

$$I_{MC(n)} = I_{MCMax} \sin\left(\frac{\pi}{3}(n+2) - \omega t + \varphi_e\right) \tag{6.5}$$

$$I_{Lev(n)} = I_{LevMax} \sin\left(\frac{\pi}{6}(n+2) - \omega t + \lambda + \gamma\right) \tag{6.6}$$

$$\therefore I_K^{\,2} = I_{MC}^{\,2} + I_{Lev}^{\,2} + 2I_{MC}I_{Lev}\cos\left(\pi - \gamma + \theta - \lambda + \varphi_e\right) \tag{6.7}$$

Substituting equation (6.7) into (6.1) and summing the losses for all stator teeth yield:

$$P_{loss} = \sum_{n=1}^{N_s} \left[I_{MC(n)}{}^2 + I_{Lev(n)}{}^2 + 2 I_{MC(n)} I_{Lev(n)} \cos\left(\pi - \gamma + \theta - \lambda + \varphi_e\right) \right] \frac{R_K N_{coilside}}{2} \qquad (6.8)$$

where $N_{coilside}$ is 4 for the bridge connection. A comparison of power loss with the FEA reveals that the analytically method provides a very good agreement, as plotted in figure 6.6.

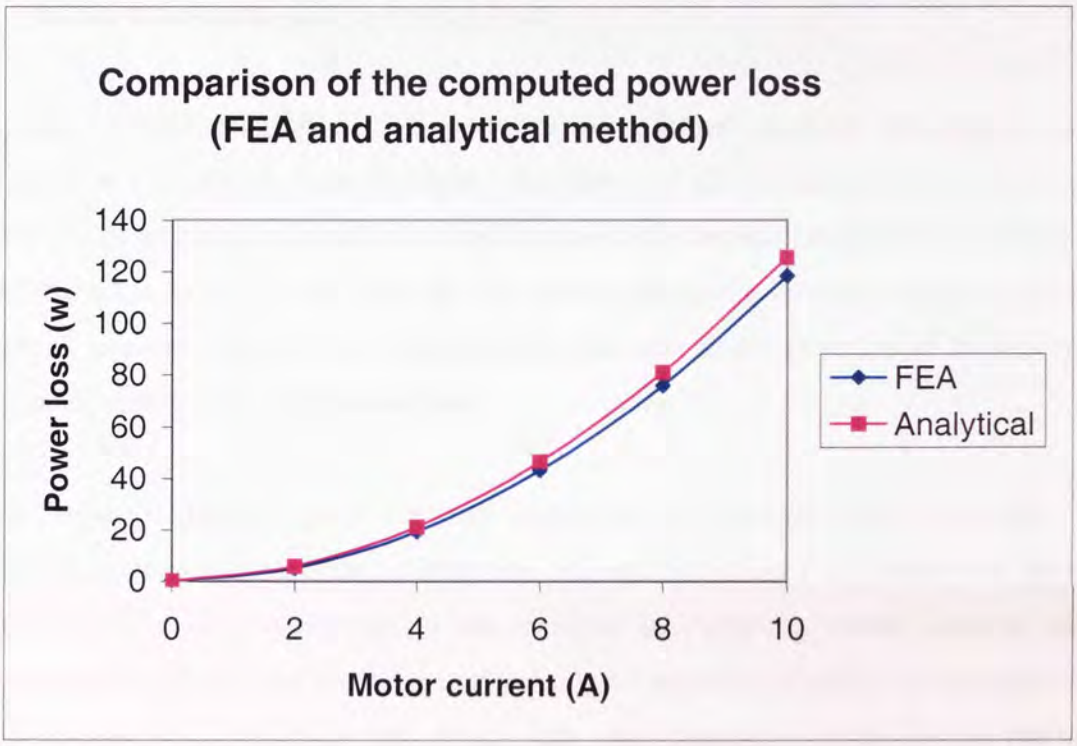

Figure 6.6: Comparison of the computed power loss by FEA and analytical method.

Since both bridge and SS winding schemes employ the same set of windings for force and torque production, equation (6.8) can also be used to calculate power loss for the SS scheme by simply substituting $N_{coilside}$=2, i.e. two coil sides per tooth and N=120. For the case of DS winding scheme, equation (6.8) must be modified where the components of current are now segregated between two sets of coils, i.e.:

$$P_{loss} = \sum_{n=1}^{N_s} \left[I_{MC(n)}{}^2 N_{MC} + I_{Lev(n)}{}^2 N_{Lev} \right] \frac{\rho l N_{coilside}}{2\pi r_{cond}{}^2} \qquad (6.9)$$

where $N_{coilside}$ is 2 and N_{MC} and N_{Lev} refer to the number of turns of motor and levitation windings respectively. A sample program listing for computing the power loss is given in appendix E.

6.3 Qualitative comparisons

While the single set of windings schemes (both bridge and SS) produce a lower power loss for a given performance, other aspects such as cost and feasibility of design and implementation must be contemplated in each area of application. This section aims to provide a brief qualitative comparison between the aforesaid self-bearing motors.

6.3.1 Initial investment and operating costs

In general, a high efficiency, high performance machine coupled with relatively low investment and operating costs is highly desirable. Of all the associated costs, one that directly relates to electrical machinery and is a key criterion to distinguish one self-bearing motor from the other is the cost of the power electronic drivers. Motor drivers are ubiquitous in every variable speed motor application and so the selection of these drivers is important to justify the overall investment.

Conventional self-bearing machines with single set of windings have a number of bi-directional power supplies, each exciting one coil and switching both motor and levitation currents. Because all power supplies are involved in switching motor currents, the SS configuration is perhaps the most expensive from the aspect of drivers. On the other hand, the DS scheme has a relatively high power loss when compared to the SS and the bridge connection scheme, which suggests that the DS scheme is slightly more expensive to operate. The proposed bridge connection isolates the motor and levitation control while permitting both categories of current to flow simultaneously in the coils. Thus, only a high rating motor inverter is required for the normal torque-producing function and the levitation control is achieved by employing much smaller rating power supplies. As a result, the bridge connection could be a potential cost-saving solution for any polyphase self-bearing machines.

It is clear that for the same design parameters and torque requirement, self-bearing motors inevitably have higher power losses than conventional electric motors because of the additional levitation currents needed. However, because self-bearing motors make use of the machines' fluxes, they are expected to suffer less power loss than conventional motor-magnetic bearing systems. This is one of the distinct advantages of self-bearing motors over motor-magnetic bearing systems.

6.3.2 Feasibility of design and implementation

The feasibility of design and implementation of self-bearing machines and in particular aspects related to methods of winding and control are briefly discussed in this section.

Conventional SS scheme uses a dual terminal output power supply to excite each stator coil where the number of units needed is dependent on the total number of coils. Usually concentrated coils are wound around the stator teeth for convenience though a toroidal winding is an alternative. This scheme is typically found in stators with a small number of teeth count. For applications which demand a smooth torque, the SS winding scheme may not be economically feasible to implement with a stator with many teeth because of the high number of power supplies required. This is one of the limitations of the conventional SS scheme. On the contrary, conventional DS scheme can be wound in a concentrated or distributed fashion irrespective of the number of stator teeth, as in conventional electric machines. Thus, the DS scheme is preferable than its SS counterpart from the aspect of winding arrangement but the DS scheme is expected to have a higher power loss according to the FEA results in section 6.2.

The bridge connection is comparable to the conventional SS scheme in terms of power loss, as verified in the previous section. In addition to its single set of windings feature, the proposed connection offers more flexibility in the winding arrangements such as concentrated or equivalent distributed windings, and many other variants can also be derived. This means that the bridge connection can be extended far more easily with a minimum addition of small rating power supplies than the conventional SS scheme. Only a single motor driver is required for any extension of windings. Furthermore, pre-wound coils could be conveniently arranged, depending on the physical geometry of the stator, and all that is required is to link the coils' terminals to form independent bridges as in figure 4.9.

Another important aspect, although not an absolute necessity, is to preserve the conventional method of motor drive or control. Self-bearing motors with a DS winding connection are indeed driven like conventional electrical machines because of their so connected motor windings. Thus, in the presence of an appropriate rotor support or coupling to external mechanisms, self-bearing motors with DS winding scheme can be satisfactorily driven with a standard power supply (for example, a 3-phase motor inverter). The bridge connection has a similar feature that, if only the torque-producing function is required, then

the levitation supplies can be switched off leaving the motor inverter driving the self-bearing motor. It is rather unconventional to drive a self-bearing motor having the SS connection with a number of dual output terminals power supplies for torque production. Here the power supplies must be properly controlled so that the overall outcome is to produce a rotating magnetic field in the air gap. The conventional split winding scheme as described in section 2.1.2 (figure 2.1(c)) is also unconventional.

Although self-bearing motors with SS scheme require a high number of power supplies, they are advantageous in offering fault tolerance by redundancy in both motor and levitation controls. For fault tolerant control, a failure in one of the power supplies or coils does not significantly impair the overall operation of the self-bearing motor. Fault tolerance for the conventional DS scheme and bridge connection is limited to the levitation control only because both schemes utilise a single motor inverter. Unless a backup inverter is incorporated in conjunction with the main inverter, the former and latter schemes do not have fault tolerant capability in motor control.

6.4 Summary of principal matters

Central to this chapter is the FEA comparison of power loss for a given machine performance between conventional SS and DS schemes and the newly proposed bridge connection. The comparison is made based on the same physical size of stator and with the same number of turns per tooth. It is shown that the power loss is higher in the DS scheme than for both SS scheme and the bridge connection. This is attributable to the fact that the incorporation of a secondary set of windings for levitation control is at the expense of torque production, and has ineluctably led to relatively high currents needed to give the equivalent performance as produced by self-bearing machines with a single set of windings.

The proposed bridge connection has the advantages of both conventional SS and DS schemes in terms of cost and implementation. Motor and levitation controls are isolated by employing separate power electronics where in the presence of a suitable rotor support, the levitation power supplies are switched off and the self-bearing motor can then be driven conventionally by using the motor inverter. The use of separate small rating levitation power supplies is a potential cost-saving solution because only a small amount of current is required to create an unbalance flux distribution in the air gap. The number of levitation

supplies could be reduced by appropriately combining some coils to form a bridge connection. Furthermore, the bridge-like configuration can be easily extended to form other polyphase connections including spread windings. The latter maybe useful in achieving low torque fluctuations in come circumstances.

To summarise, some of the attractive features of the bridge connection are: (1) all conductors carry both torque and levitation currents; (2) levitation control can be achieved by employing power supplies that are relatively small current and voltage rating; (3) only one motor inverter is required for the normal torque-producing function; (4) can be easily extended to other polyphase machines; and (5) many variants of connections are possible.

CHAPTER 7

LEVITATION AND TORQUE CONTROL SYSTEM

The mechanisms of lateral force production in self-bearing rotating machines have been described in the foregoing chapters where the required magnitude and direction of forces are frequently mentioned in relation to the flux densities or excited currents. Thus far, the manner in which the force is controlled in conjunction with torque production has not been elaborated. This chapter aims to bridge this gap by outlining the implementation of a general feedback control system which may be divided into two parts, namely motor control and levitation control.

7.1 Motor control

The proposed bridge connection retains its form of having 3 terminal wires so that the self-bearing motor can be controlled in a conventional way via a 3-phase motor inverter. There are three modes of operation commonly found in electric motor applications, i.e. torque, velocity and position control modes.

Figure 7.1 shows a general control system for a self-bearing motor where the top half is a conventional motor control loop. Prior to amplifying the phase currents for rotation, the resting rotor must be first levitated by means of injection of levitation currents into the coils. An initialisation procedure must be performed to locate the magnetic field vector of the permanent magnet rotor so that appropriate levitation currents can be supplied. This information is provided by shaft position transducers, either by a resolver or Hall-effect sensors, as typically found in brushless motor applications. For motor commutation purposes, either a resolver or a combination of optical incremental encoder and Hall-effect sensors may be incorporated in the assembly.

When the rotor is lifted a rotation may be initiated by supplying phase currents to the self-bearing motor. As shown in figure 7.1, the standard 3-phase motor inverter or drive consists of position, speed and current regulators and their functions are co-ordinated by a controller or a digital signal processing (DSP) computer host. Controller parameters such as a PID (proportional, integral and derivative) controller can be tuned according to a specific application requirement. Speed and position reference signals are compared with that of the

error signals provided by the rotary transducers and the resultant difference signals are input into the controller which calculates the required frequency and amount of current to be supplied to the motor. The corresponding request signal is then sent to the current regulator to generate a voltage command for switching pulse width modulation (PWM). This PWM signal turns on and off the power amplifier in each phase at a certain time and thereby creating a 3 phase currents to operate the motor.

7.2 Levitation control

Levitation control is implemented as a separate unit from the motor control hardware as depicted in figure 7.1. This allows torque production of the self-bearing motor to be controlled independently from its levitation control, as in a conventional standalone motor. While magnetic bearings are controlled independently from the motor, this is not true for the case of self-bearing motors because of their utilisation of motor field in producing a net levitation force. As stated in chapter 3, the motor and levitation fields must be of a pole-pair difference so that any injection of levitation currents will not affect the machine's torque.

Two discrete proximity sensors such as inductive or eddy current sensors are employed to detect the displacement of the rotor. They are preferably mounted on the stator and located at orthogonal positions with respect to each other. There must be a small clearance between the sensor probe and rotor. Precautions must be taken to avoid damage to probes caused by excessive rotor displacement during failure o transient. One way of circumventing this problem is to use back up bearings that have a smaller clearance than the motor air gap.

Signals provided by the proximity sensors are input into an electronic filter to eliminate high frequency noise before being processed by the controller. As described in equations (5.5)-(5.14) of chapter 5, the levitation field produced is of the same rotating frequency as the rotating motor field. Factors affecting the computation of the amount of levitation currents required are:

- motor current, I_{MC} or motor flux density, B_{MC}
- permanent magnet flux density, B_{PM}
- torque angle, φ_e
- frequency, ωt
- angle of desired force, γ

- rotor displacement in x- and y-direction

From the detected rotor displacement, the controller calculates the required magnitude and direction of levitation force to overcome the rotor's weight and negative stiffness according to expression (3.3), so that there is a net force pulling the rotor back to its concentric position. Subsequently, the controller sends request signals to the bi-directional levitation supplies, which in turn inject levitation currents into the phase coils. These currents are adjusted appropriately to superimpose on the motor currents in the same coils to provide a magnetic bearing capability via unbalancing the air gap field.

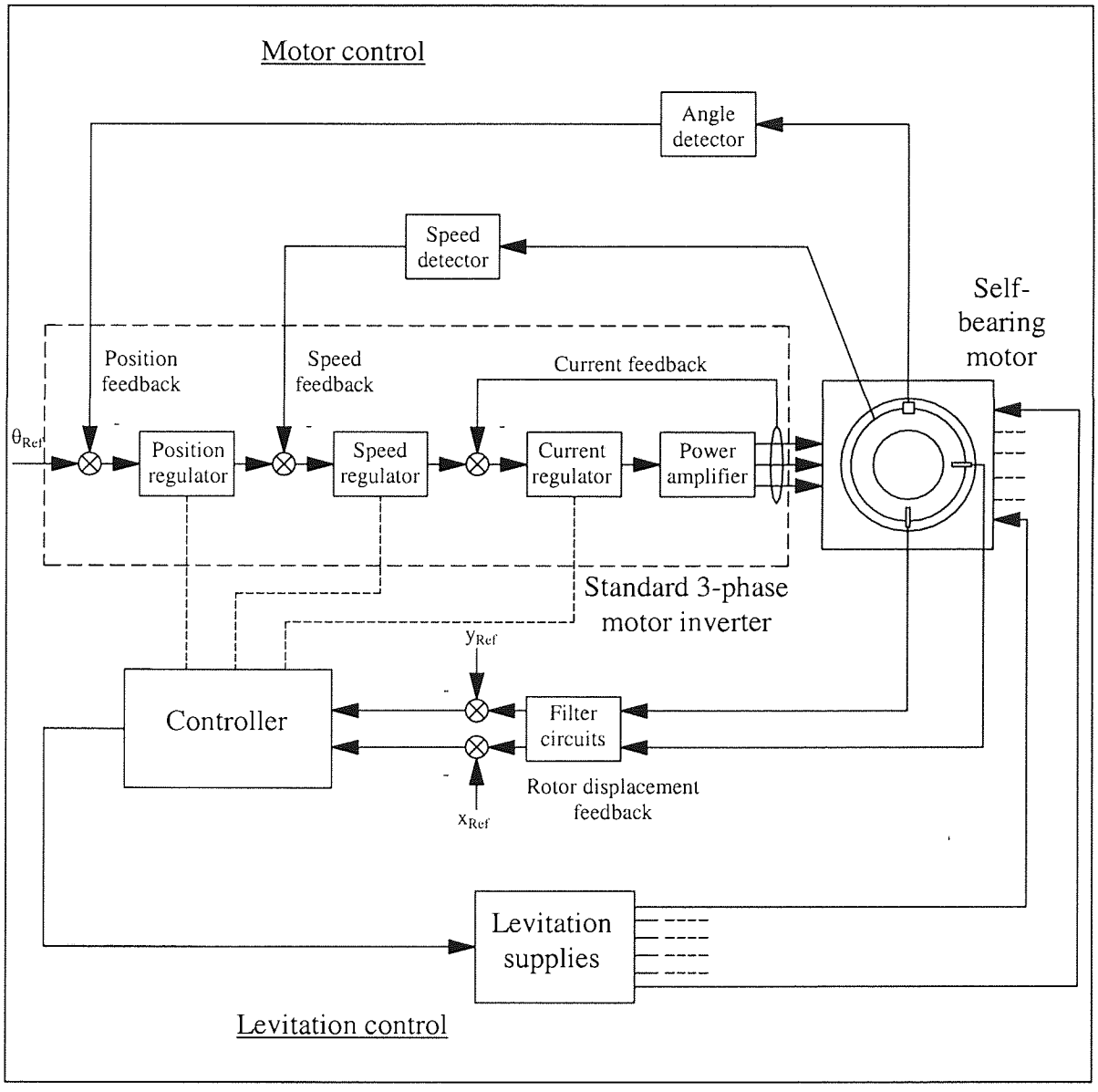

Figure 7.1: A general self-bearing motor control system.

7.3 Summary of principal matters

The control system for a self-bearing motor can generally be segregated into two parts namely, motor control and levitation control. Torque production is controlled conventionally with standard controllers, a motor drive and rotor position and speed transducers. Proximity sensors are employed to sense the rotor displacement. Information concerning motor current, rotor angular position and speed and rotor displacement are provided to the levitation controller so that the amount of current required to cause a net lateral force exerted on the rotating rotor can be synthesised. These levitation currents are supplied to the phase coils via a number of standard small rating bi-directional power supplies. A pole-pair difference of 1 between the motor and levitation fields must be complied so that any injection of levitation currents will not affect torque production.

CHAPTER 8

GENERAL APPLICATIONS

Throughout the preceding chapters, permanent magnet self-bearing motors are considered as an illustrative example of application of the newly proposed connection. Since all electric machines must have a field of their own in the air gap to order to rotate or produce torque, they are potentially self-bearing machines. Additional currents may be introduced to unbalance the existing flux distribution around the air gap so that a net lateral force is exerted on the rotor. This is the principle of lateral force production in self-bearing motors. This chapter aims to extend the application of the bridge connection to other types of machine and also other uses such as magnetic bearing applications.

8.1 Application to other AC polyphase machines

In permanent magnet self-bearing machines, as described pervasively in this thesis, the magnets on the rotor contribute substantially to the net MMF in the air gap for torque production. The corresponding flux distribution is known as the main or motor field. With appropriate injections of small currents via the same set of windings, a net lateral force exerting on the rotor is created. An important observation here is that the presence of the main or motor field is a necessity for creating a differential circumferential flux distribution around the air gap. Otherwise the electromagnetic action of lifting the rotor will be similar to that of magnetic bearings.

Another crucial observation is that a single set of windings must be present on at least one main component so that levitation can be controlled stably. This is in accordance to a corollary of Earnshaw's theorem [Ear1842] developed by Braunbeck [Bra39] showing that a levitation system using permanent magnets or electromagnets with constant current is inherently unstable. Thus, to achieve stable levitation of a rotor against gravity, the system must be provided with a current regulation control together with its position feedback. With these general observations, the possibility of applying the newly proposed scheme to other types of electric machinery can then be contemplated. The following discussions make use of the understanding of MMF contributions in any machines as described in chapter 3.

8.1.1 Switched variable reluctance motor

Torque production in switched variable reluctance motors is based on the natural tendency of their rotor to align with the stator poles where the flux linkages or inductance of the excited coil is maximised. Switched reluctance machines require power electronic switching to sequentially energise their phase coils in relation to the rotor position so that a continuous rotation or torque can be generated. This class of machine can be categorised into two groups: singly salient and doubly salient. A major difference between this machine and permanent magnet motors is that the rotor in the former does not contribute any MMF. This means that there is no interaction between the stator and rotor MMFs to produce the so-called cylindrical torque, but a reluctance torque results from the stator excitation alone.

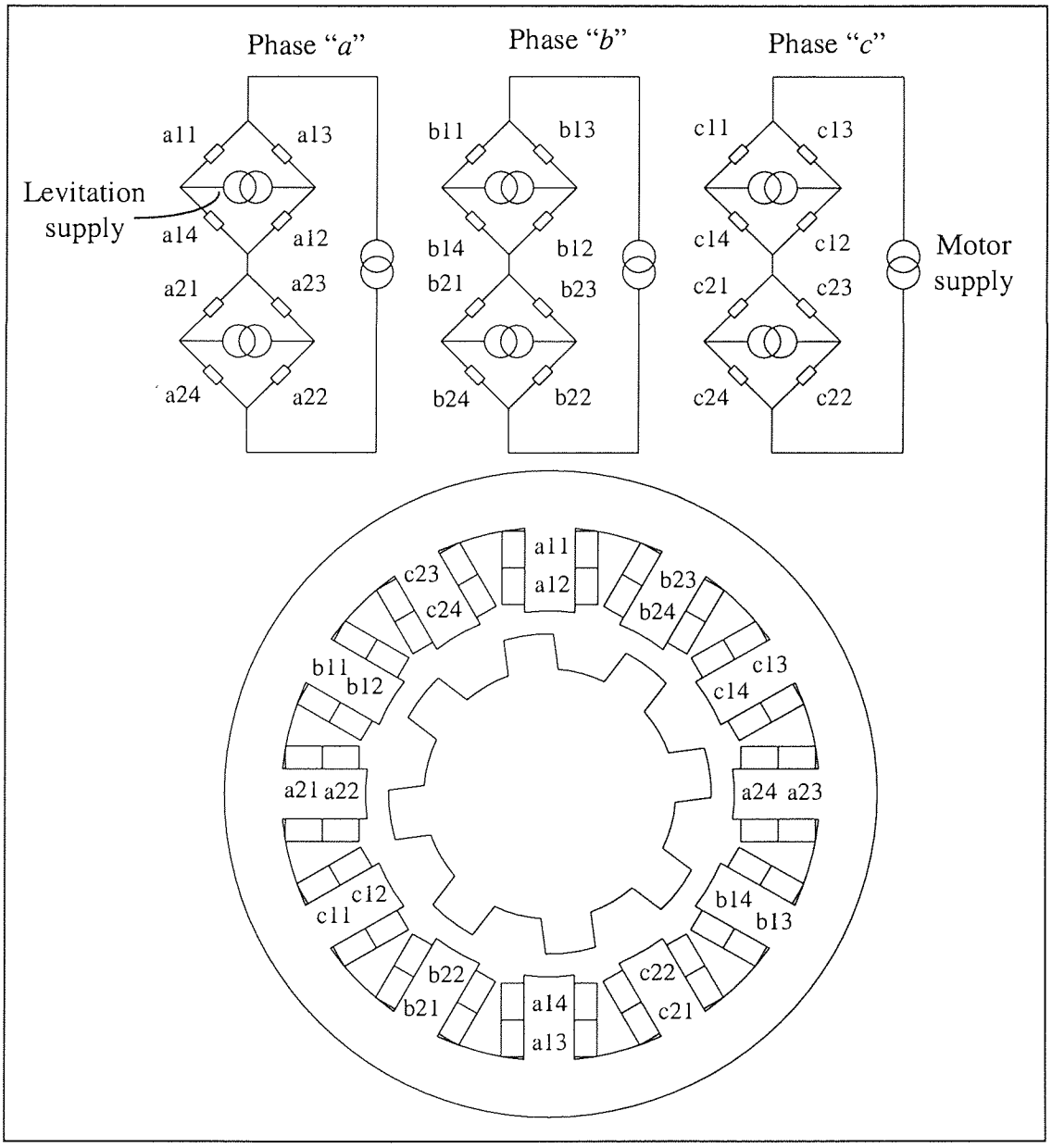

Figure 8.1: A switch reluctance motor with the bridge connection scheme.

For a switched reluctance machine to incorporate magnetic bearing capability, the stator coils must carry an additional component of currents to create a field of a pole-pair difference from the main motor field. Some examples of conventional switched reluctance motors with two sets of coils are reported by Chiba et al. [CCF90], [CRF91]. Single sets of windings machines with both main and levitation currents superimposed have also been proposed [PLRC94]. The bridge connection can be implemented as an alternative scheme to the conventional machines. Coils from each phase are grouped to form bridges and connected to a single motor supply. Small rating supplies can then be used to supply levitation currents in between the respective bridges. For instance, a three-phase reluctance motor with a 12-tooth stator would require 3 main power supplies and 6 levitation supplies as illustrated in figure 8.1. Because of a large difference in air gap permeance (due to salient components), the torque and levitation force produced by switched variable reluctance motors are somewhat rippled. This calls for a controller to compensate or minimise the ripples.

8.1.2 Polyphase synchronous motor

Polyphase synchronous motors are doubly excited machines where both stator and rotor contribute to the net MMFs in the machine. The field MMF is stationary with respect to the winding of origin. A steady state torque is produced based on the principle that the rotor MMF will tend to line up with the rotating stator MMF around the air gap, and both MMFs must rotate at a synchronous speed determined by the system frequency. If both rotate asynchronously the torque will vary with instantaneous rotor position and ultimately lead to an average of zero torque, unless the induced currents in the rotor body become significant.

The synchronous motor is somewhat similar to the permanent magnet motor where the magnets are simply replaced by a DC current excitation. This is to fulfil the condition set by equation (3.1). Current sources must present on both sides of the uniform air gap so that there exists a tangential stress for torque to be developed. For the reason of similarity in its principle of torque production, a permanent magnet motor can also be called a synchronous permanent magnet motor. Since both stator and rotor MMFs constitute the main motor field, synchronous motors can be suitably converted into a self-bearing motor by appropriately injecting some additional currents to unbalance its main field.

The proposed connection schemes in chapter 4, i.e. concentrated winding (Type I), equivalent distributed winding (Type I - toroidal winding) and equivalent distributed winding (Type II) can be incorporated in the synchronous motors. Because the field currents may affect the direction of the levitation force, depending on its magnitude, the phase of the injected levitation current many need to be compensated as outlined in section 5.1.3.

8.1.3 Induction motor

An induction motor has the same stator construction as the synchronous motor but requires no DC field current for its rotor. The motor relies on the induced eddy current on its special rotor to produce a rotating MMF. Most commonly used is the squirrel cage rotor that consists of a series of electrically shorted conducting bars although wound rotor types are used. When the stator winding is excited to produce a rotating MMF, eddy currents are induced in the rotor bars which in turn create an MMF. In effect the induced rotor MMF rotates at synchronous speed in the same direction as the rotating stator MMF while the rotor itself rotates at a slower speed. The fact that the rotor can never rotate as fast as the synchronous speed means there is always a slip between the rotating stator MMF and the rotor which generates low frequency currents in the rotor.

As before, the proposed winding schemes in chapter 4 can be employed in induction motors to produce the required rotating stator MMF. Problems that plague self-bearing induction motors irrespective of the types of connection used are the mutual interference between x- and y-directions of lateral force control and the disturbance of torque by lateral force control [ODO95], [CFA+97], [OMS00]. Mutual coupling between the orthogonal directions of lateral force control is due to the interaction of levitation field and motor field, a similar case observed in permanent magnet motors. For induction motors the excitation of levitation currents in the stator will cause another set of revolving MMF to be created as a result of voltage induction. This secondary rotor MMF will interact with the stator levitation MMF, thereby producing its own torque. As a consequence the intended torque generated by the motor will be affected by the presence of levitation currents. It is almost inevitable that a decoupling control scheme must be implemented to circumvent the problem.

8.1.4 Other motor topologies

Because the bridge connection does not require special electromagnetic structures to house the windings, the proposed scheme can be implemented in many types of motor topology just as conventional windings would. The afore-mentioned motors are most commonly found in practical applications. Other possible applications include slotless motors, ironless motors, axial field air gap motors, etc.

8.2 Magnetic bearing

A common ferromagnetic stator can be used as a motor, magnetic bearing or self-bearing motor depending on its winding scheme, type of rotor and how the MMF is controlled. It is known that if the levitation current were utilised in conjunction with the motor field then the amount of levitation current required to lift the rotor would be small. Such a principle could be exploited in magnetic bearings where the journal of a shaft is mounted with permanent magnets and the levitation is controlled as if it is a self-bearing motor. The only difference here is that no motor component of current is provided and thus coupling of force control is precluded. Many connection schemes can be used of course. Although not necessary, if there is a demand of one winding arrangement for all functions, then perhaps the bridge connection could be an attractive choice.

8.3 Summary of principal matters

Much has been described previously with respect to permanent magnet self-bearing motors. This chapter outlines the potential application of the newly proposed connection to other AC polyphase electrical machines such as switched variable reluctance motor, synchronous motor, induction motor, etc and also in magnetic bearing. The absolute requirement for any self-bearing motor to be implemented is that a single set of windings must be present in either the stator or rotor to produce the necessary motor and levitation MMF.

CHAPTER 9

A DESIGN STUDY OF A MOTOR TO DRIVE A VACUUM PUMP

An application of self-bearing motors is outlined as an example in this chapter. A vacuum pump suitable for the use in industry or laboratory chambers is described and its specifications are derived based on the self-bearing motor simulated in the preceding chapters. The ratings of the levitation power supplies are of particular interest, and are estimated from the required force slew rate and dynamics of the system. This chapter ends with a brief description of the levitation control system.

9.1 Problem definition

Several identical vacuum pumps are required to evacuate dry air from a chamber and maintain its vacuum cleanliness for a certain sensitive process to be undertaken. Lubricating fluids must not be exposed directly to the vacuum in the pumping chamber. One of the most common failures in vacuum pumps is due to mechanical bearings and the reliability of the pump must be further improved to avoid high maintenance costs. Power loss should also be minimal throughout the operation.

9.2 A vacuum pump having self-bearing motors

From a cursory glance, a conventional vacuum pump seems to be appropriate for the required job. However, the requirements of high reliability and no contamination from lubricants have singled out the use of a magnetically supported rotor as a potential candidate. It is apparent that magnetic bearings and self-bearing motors fall in the same non-contact lubricant-free category and so both configurations are expected to work satisfactorily. As mentioned in chapter one, a self-bearing motor is more compact due to a reduction in the component count. A longer shaft, such as in the case of a magnetic bearing configuration, tends to be more flexible and is more difficult to control. In addition, self-bearing motors require only a small amount of current to exert a net lateral force on the rotor and so they can have lower power losses when compared to magnetic bearings. Thus, self-bearing motors are a preferred solution.

The configuration of a vacuum pump is described in the next section and subsequently the specifications of the motor and levitation supplies are derived according to the performance requirements. The self-bearing motors provided for the vacuum pump are exactly same machine simulated in chapters 5 and 6.

9.3 Configuration of a self-bearing vacuum pump

Figure 9.1 illustrates a schematic of a vacuum pump with an overhung rotor configuration. The role of the impeller is to create a pressure difference between the inlet and outlet ports so that a continuous stream of air can be evacuated from the chamber through the inlet port and discharged at the outlet port. Due to the existence of pressure differences during operation, the vacuum pump exerts forces on both stator and rotor but the latter is of a concern which leads to an unbalanced rotating shaft.

By convention, components closest to the impeller are known as inboard components whereas those farther away are outboard components [KM98]. Both inboard and outboard self-bearing motors produce lateral forces to support and counter the rotor unbalance in four degrees of freedom. Although some axial forces may be balanced by appropriate impeller and casing designs, an axial active magnetic bearing (AMB) must be employed to compensate for this axial unbalance. The axial AMB may be placed anywhere along the axial length of the shaft but the location at the opposite end of the impeller is preferable primarily to better balance the overall self-bearing loads.

The rotor displacement is detected by inboard, outboard and axial proximity sensors and currents in the self-bearing motors are controlled on the basis of the sensors' output so that the rotor can be retained in at the centre position. A means of detecting the rotor speed and orientation is also incorporated in the vacuum pump assembly. Inboard and outboard backup bearings are provided for preventing the collision of the stator and rotor during catastrophic failure and also for supporting the rotor at rest. These backup bearings have a smaller air gap size (0.4 mm) than that of the self-bearing motors and are not lubricated to eliminate contamination.

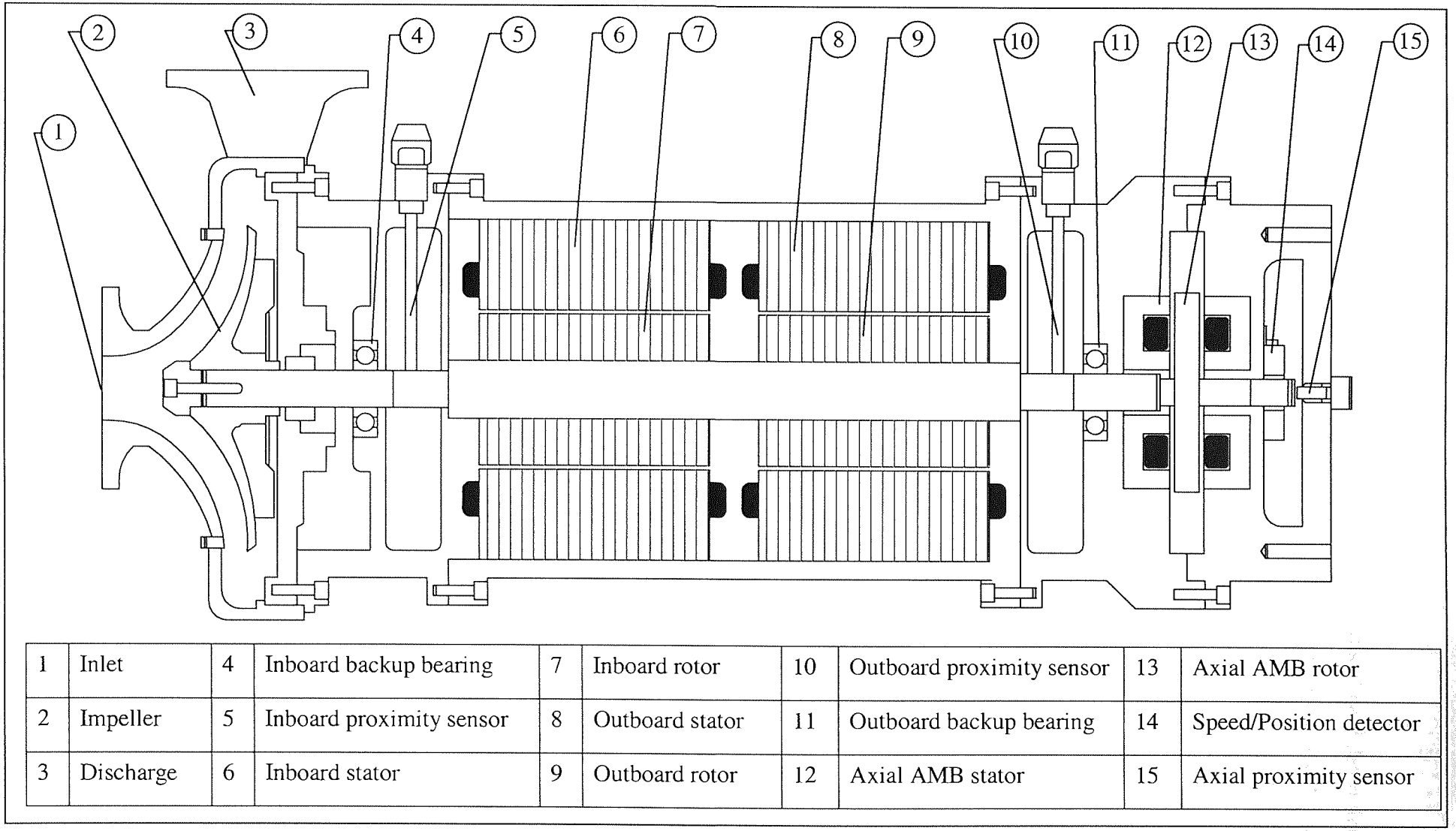

1	Inlet	4	Inboard backup bearing	7	Inboard rotor	10	Outboard proximity sensor	13	Axial AMB rotor
2	Impeller	5	Inboard proximity sensor	8	Outboard stator	11	Outboard backup bearing	14	Speed/Position detector
3	Discharge	6	Inboard stator	9	Outboard rotor	12	Axial AMB stator	15	Axial proximity sensor

Figure 9.1: A vacuum pump with self-bearing motors

9.4 Motor specifications

The rate of evacuation and the ultimate pressure to be achieved and held determine the size and number of pumps required. For simplicity, these parameters are not defined but any application requirement is achievable by employing a multiple array of pumps to give an equivalent performance. It is assumed that the impeller requires a low torque for pumping air. Table 9.1 below summarises the normal operating condition for the motors. More information about the motor operating voltage and current can be found in section 9.7.

Power (P)	1.2 kW
Speed (ω_s)	3000 rpm

Table 9.1: Motor normal operating condition.

9.5 Finite element model and material properties

With reference to figure 4.9, there are 2 coils wound around each stator tooth which gives a total of 4 coil sides per stator slot. The permanent magnet used is Samarium-Cobalt. Tables 9.2 and 9.3 below show the data used to construct the finite element models in the thesis.

9.5.1 Model geometry and physical properties

Stator outer radius (r_{sta_o})	66 mm
Stator inner radius (r_{sta_i})	32.8 mm
Rotor radius (r)	30 mm
Permanent magnet radial thickness (l_{PM})	2 mm
Air gap size (g_0)	0.8 mm
Length of motor (l)	100 mm
Number of stator teeth (N_s)	12
Slot area (A_{slot})	2.485E-4 m^2
Number of conductor per slot (N_{slot})	240
Radius of a copper conductor (r_{cond})	4E-4 m
Approximate length of one turn of coil (l_{coil})	0.22 m

Approximate pole area (A_p)	1.676E-3 m^2
Coil side area ($A_{coilside}$)	6.213E-5 m^2
Number of turns of a coil (N)	60
Coil axial length (l) (Note: adjusted to take into account of the end windings)	0.1133 m
Coil fill factor (C_f) (see calculation below)	0.5

Table 9.2: Model geometry and physical properties.

9.5.2 Material properties

Permanent magnet remanence (B_0)	0.95 T
Magnetic coercivity (H_{PM})	6.8E5 A/m
Coils resistivity (ρ)	3E-8 Ωm
Relative permeability of stator (μ_{sta}) (see figure 5.8 for non-linear BH curve)	8000 (linear)
Relative permeability of rotor (μ_{rot}) (see figure 5.8 for non-linear BH curve)	8000 (linear)

Table 9.3: Material properties.

9.6 Coil impedance calculation

The coil resistance is calculated simply from the geometry and properties defined in tables 9.2 and 9.3 above whereas the coil inductance is calculated from the flux density obtained from running the Matlab script in appendix E.

9.6.1 Coil resistance

Total resistance of a single coil, $R_{coil} = \frac{N \rho l_{coil}}{A_{cond}}$ (9.1)

$$R_{coil} = \frac{(60)(3E-8)(0.22)}{\pi(4E-4)^2}$$

$$= 0.7878\ \Omega$$

$$\text{Coil fill factor, } C_f = \frac{N^2 \rho l}{\frac{R_{coil}}{2}(A_{coilside})} \tag{9.2}$$

$$C_f = \frac{(60)^2(3E-8)(0.1133)}{\left(\frac{0.7878}{2}\right)(6.213E-5)}$$

$$= 0.5$$

Resistance for a single bridge, $R_{Bridge} = R_{coil} = 0.7878\ \Omega$

Resistance for a single phase, $R_{Mtrphase} = 2 \times R_{coil} = 1.5756\ \Omega$

9.6.2 Coil inductance

The inductance of each phase connection can be estimated from its flux linkage due to load currents. The stator current is first evaluated from the power and torque equations:

$$P = T\omega_s \tag{9.3}$$

$$1200 = T \times 3000 \times \left(\frac{2\pi}{60}\right)$$

$$T = 3.82\ \text{Nm}$$

Thus, from the torque and current relationship in equation (5.40), the stator current is:

$$T = K_T I_{MC}$$

where K_T is the torque constant.

$$I_{MC} = \frac{3.82}{0.933}$$

$$= 4.09\ \text{A}$$

The corresponding maximum flux density can then be approximated using the program listing in appendix E where:

$$B_{MC} = 0.11 \text{ T}$$

The total flux linkage due to the stator currents in a single coil is:

$$\Psi = NBA_p \tag{9.4}$$
$$= 60 \times 0.11 \times 1.676\text{E}-3$$
$$= 0.0112 \text{ Wb}$$

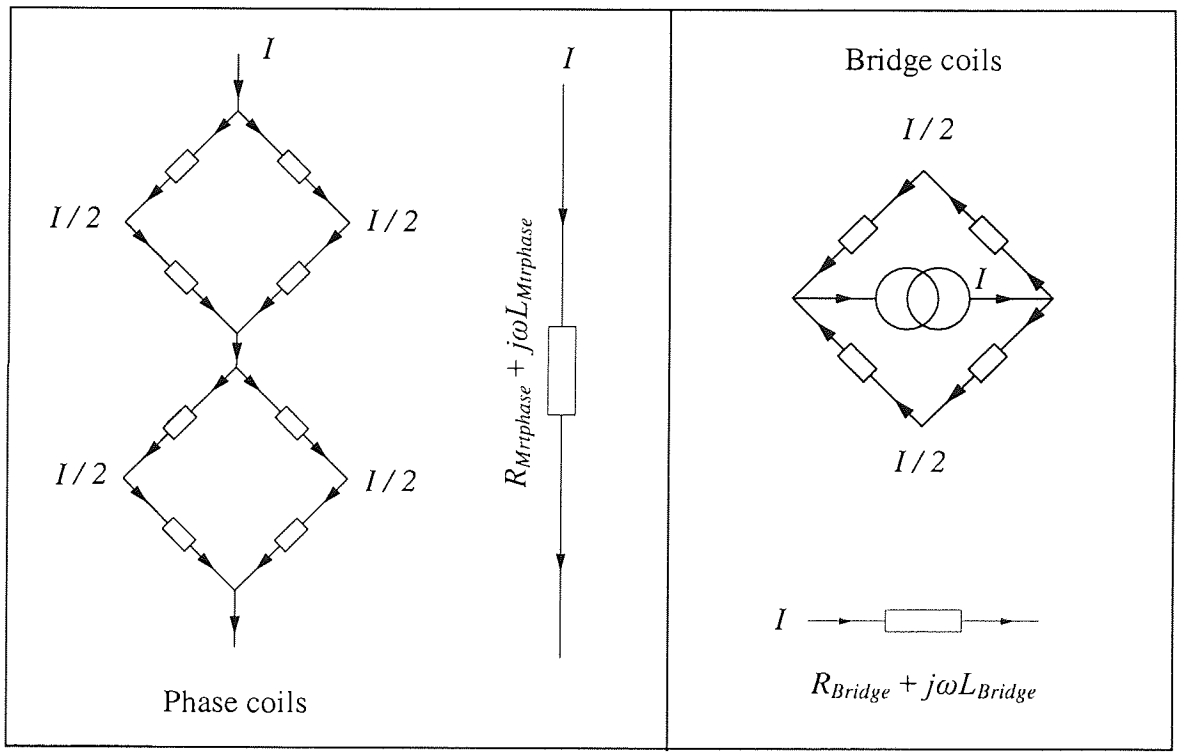

Figure 9.2: Effective impedance of phase coils and bridge coils.

For 4 coils in series as shown in figure 9.2, the total flux linkage is:

$$\Psi_T = 4 \times \Psi = 0.0448 \text{ Wb} \tag{9.5}$$

The inductance for 4 coils in series is:

$$L = \frac{\Psi}{\frac{I_{MC}}{2}} \tag{9.6}$$

$$\therefore L = \frac{0.0448}{\frac{4.09}{2}} = 0.022 \text{ H}$$

Since there 2 parallel paths in each phase connection, the effective inductance of a phase is:

$$L_{Mtrphase} = 0.5 \times L \tag{9.7}$$

$$\therefore L_{Mtrphase} = 0.011 \text{ H}$$

The effective inductance of the bridge levitation circuits can be calculated in a similar manner.

$$L_{Bridge} = 0.0055 \text{ H}$$

9.7 Motor ratings

The following calculations give approximate information about ratings and operational requirements of the motors.

9.7.1 Phasor diagram

The maximum generated voltage can be found from the flux waveform and the speed. The waveform of the generated voltage contains harmonics but the fundamental has, by this calculation, an RMS value of 107 V. Figure 9.3 shows the phasor diagram of the motor. The motor will be operated with the load angle, δ equal to the power factor angle, θ, so that the torque angle, φ_e, is 90°.

$$\text{Power} = \frac{3E_{\phi-n}V_{\phi-n}}{X}\sin\delta = 3E_{\phi-n}I_{MC} \qquad \text{if } \delta=\theta$$

where X, $E_{\phi-n}$ and $V_{\phi-n}$ are phase reactance, phase to neutral generated voltage and phase to neutral supply voltage respectively. Given the power P and current I_{MC}, $E_{\phi-n}$ can be evaluated as 97 V. This does not exactly match the generated voltage previously found. The discrepancy is likely to lie in the non-sinusoidal character of the waveform.

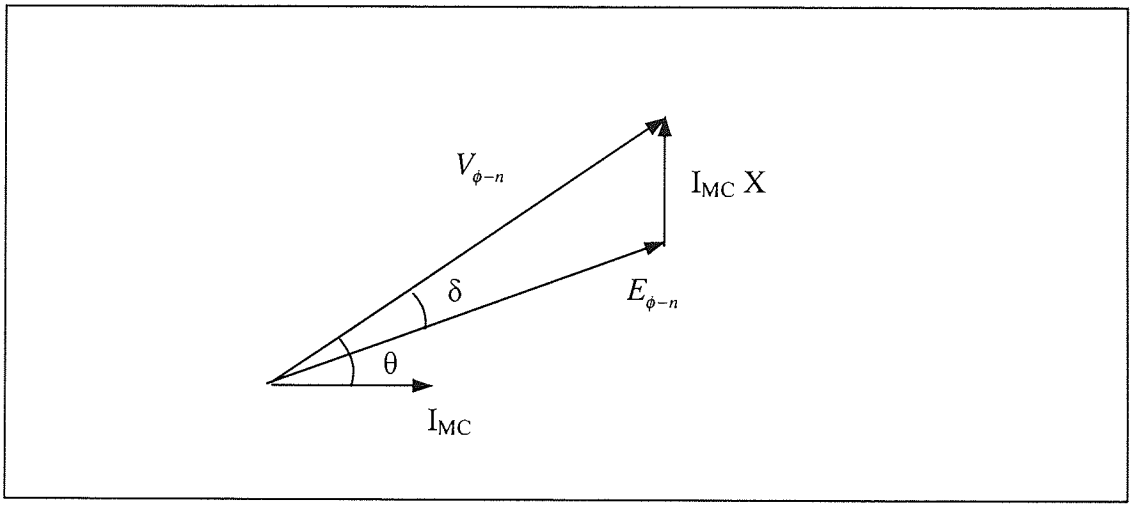

Figure 9.3: Phasor diagram of the motor.

9.7.2 Power supply for rotational drive

The required current, I_{MC}, is 4.09 A and the supply voltage we have estimated at 100 V ± 5 V phase to neutral. Thus, allowing for errors in the design calculation a power electronic drive for 5 A and 200 V phase to phase will meet the requirements.

9.8 Dynamics and slew rate requirements for levitation robustness

As common with magnetic bearings, the dynamics and slew rate of the self-bearing motors must be estimated to give information with regard to the ratings of the levitation supplies. The allowable displacement of the rotor is restricted for several reasons. Firstly, a small perturbation displacement around the equilibrium or centre position gives good linear mathematical relationships which simplifies the control. Secondly, because large displacement demands a higher levitation current to oppose the negative stiffness due to unbalanced magnetic pull (UMP), it is always economical to utilise smaller currents. The following calculations estimate the minimum voltage rating of the levitation supplies to

provide the required slew rate in response to two categories of perturbation, namely impulse input and step input.

9.8.1 Impulse input

For simplicity the system is represented by a rigid body with mass m suspended by a levitation force. The effect of the impulse force is taken into account by supplying an initial velocity to the disturbed rotor.

$$F = ft \tag{9.8}$$

where f is the slew rate and t is the time. The system's equation of motion is:

$$m\ddot{x} = -ft + K_x x \tag{9.9}$$

where K_x is the negative stiffness of the self-bearing motor, x is the rotor displacement and t is time. Rearranging equation (9.9) and taking Laplace tranform with initial conditions $t=0$, $x=0$ and $\dot{x} = v_0$ yields:

$$X\left(ms^2 - K_x\right) = -\frac{f}{s^2} + mv_0$$

$$X = -\frac{f}{s^2\left(ms^2 - K\right)} + \frac{mv_0}{ms^2 - K} \qquad \text{which can be expanded to}$$

$$X = \frac{f}{K_x s^2} - \frac{mf}{K_x\left(ms^2 - K_x\right)} + \frac{mv_0}{\left(ms^2 - K_x\right)} \tag{9.10}$$

Taking the inverse Laplace transform of equation (9.10) the response in time domain:

$$\begin{aligned} x &= \frac{f}{K_x}t - \frac{f\sqrt{m}}{K_x^{3/2}}\sinh\left(\sqrt{\frac{K_x}{m}}t\right) + \frac{v_0\sqrt{m}}{\sqrt{K_x}}\sinh\left(\sqrt{\frac{K_x}{m}}t\right) \\ &= \frac{f}{K_x}t + \left(\frac{v_0\sqrt{m}}{\sqrt{K_x}} - \frac{f\sqrt{m}}{K_x^{3/2}}\right)\sinh\left(\sqrt{\frac{K_x}{m}}t\right) \end{aligned} \tag{9.11}$$

which can be expanded into:

$$x = \frac{f}{K_x}t + \left(\frac{v_0\sqrt{m}}{\sqrt{K_x}} - \frac{f\sqrt{m}}{K_x^{3/2}}\right)\left[\sqrt{\frac{K_x}{m}}t + \frac{1}{6}\left(\sqrt{\frac{K_x}{m}}t\right)^3 + \ldots\right] \tag{9.12}$$

Neglecting the third and higher order of expansion equation (9.12) can be written as:

$$x = -\frac{ft^3}{6m} + v_0 t + \frac{v_0 K_x t^3}{6m} \tag{9.13}$$

Differentiating equation (9.13) with respect to time to obtain the velocity:

$$\dot{x} = -\frac{ft^2}{2m} + v_0 + \frac{v_0 K_x t^2}{2m} \tag{9.14}$$

The rotor velocity ($\dot{x}$) is zero at the maximum allowable displacement (x_0), i.e. the boundary conditions are $\dot{x} = 0$ and $x = x_0$. Substituting these boundary conditions into equations (9.13) and (9.14) and solving for t and f yield:

$$t = \frac{3x_0}{2v_0} \tag{9.15}$$

$$f = \frac{8mv_0^3}{9x_0^2} + v_0 K_x \tag{9.16}$$

Specifying that the system must be capable of withstanding an impulse of 0.1 Ns and that the rotor mass supported by each self-bearing motor is 2.5kg, the initial velocity v_o can be calculated.

$$\text{Impulse} = mv_0 = 0.1 \tag{9.17}$$

$$v_0 = \frac{0.1}{2.5}$$

$$= 0.04\text{m/s}$$

Further, if the maximum permissible displacement is 0.04mm or 5% of the full air gap and the negative stiffness K_x is 1.09E6 N/m (from chapter 5), the force slew rate f is:

$$f = \frac{8(2.5)(0.04)^3}{9(0.04\text{E}-3)^2} + (0.04)(1.09\text{E}6)$$

$$= 1.33\text{E}5 \text{ N/s}$$

From equation (5.41) the force produced by the self-bearing motor as a result of injection of levitation current is:

$$F = K_I I_{Lev}$$

where K_I is the actuator gain. Therefore, the force slew rate is simply:

$$f = \frac{dF}{dt} = K_I \frac{dI_{Lev}}{dt} \tag{9.18}$$

The voltage across the bridge connection is given by:

$$V_{Bridge} = I_{Lev} R_{Bridge} + L_{Bridge} \frac{dI_{Lev}}{dt} \tag{9.19}$$

$$\therefore \frac{dI_{Lev}}{dt} = \left(\frac{V_{Bridge} - I_{Lev} R_{Bridge}}{L_{Bridge}} \right)$$

which may be approximated to:

$$\frac{dI_{Lev}}{dt} \simeq \frac{V_{Bridge}}{L_{Bridge}} \tag{9.20}$$

Substituting equation (9.18) into (9.20) gives the relationship between the force slew rate and levitation supply voltage.

$$f = \frac{dF}{dt} = K_I \left(\frac{V_{Bridge}}{L_{Bridge}} \right) \tag{9.21}$$

It is apparent from equation (9.21) that for a fixed actuator gain and coil inductance, increasing the levitation supply voltage will lead to a higher force slew rate. Information about slew rate in magnetic bearings can be found in appendix A.

For a force slew rate of 1.33E5 N/s, the required levitation supply voltage is:

$$1.33\text{E}5 = 58\left(\frac{V_{Bridge}}{0.0055}\right)$$

$$V_{Bridge} = 13 \text{ V}$$

Thus, the levitation voltage supply required is much lower than the motor phase to phase voltage of 200 V. The time taken for the rotor to displace from its concentric position to the maximum permissible distance of 0.04mm is (from equation (9.15)):

$$t = \frac{3(0.04\text{E-}3)}{2(0.04)}$$

$$= 1.5 \text{ ms}$$

It is essential that the levitation inverter must have a higher PWM switching frequency so that current can be stepped up rapidly to maintain the rotor excursion within the allowable limits. A PWM frequency of 2kHz where its switching period is 5E-4s would be appropriate for the present requirement. Figure 9.4 below illustrates an example of how levitation currents are stepped up to counter perturbations.

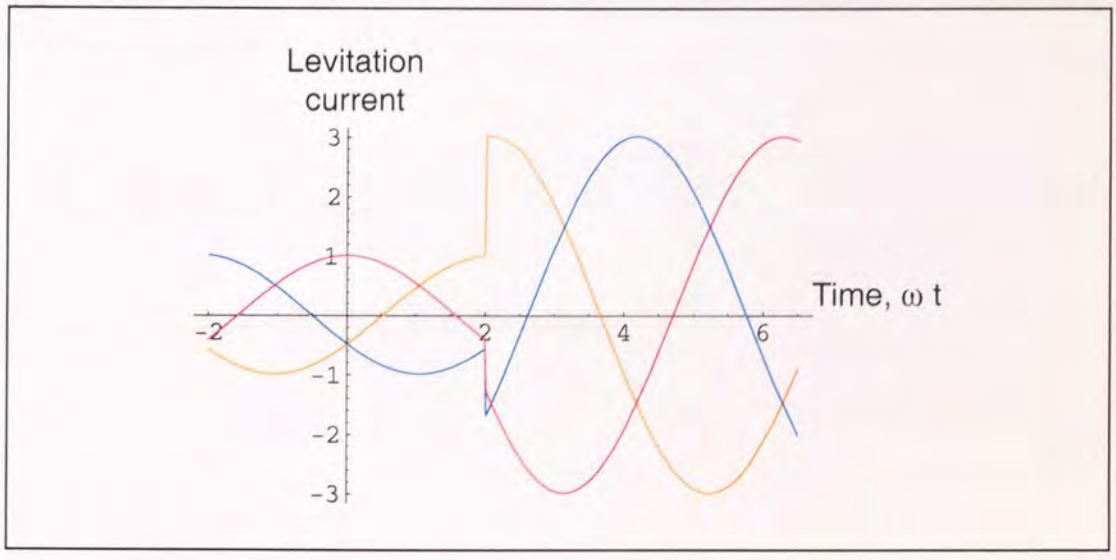

Figure 9.4: Stepped levitation currents.

9.8.2 Step input

The system's equation of motion under a step input F_s is:

$$m\ddot{x} = -ft + F_s + K_x x \tag{9.22}$$

Rearranging equation (9.22) and taking Laplace transform with initial conditions $t=0$, $x=0$ and $\dot{x} = 0$ gives:

$$X\left(ms^2 - K_x\right) = -\frac{f}{s^2} + \frac{F_s}{s}$$

$$X = -\frac{f}{s^2\left(ms^2 - K_x\right)} + \frac{F_s}{s\left(ms^2 - K_x\right)}$$ which can be expanded to

$$X = \frac{f}{K_x s^2} - \frac{mf}{K_x\left(ms^2 - K_x\right)} - \frac{F_s}{K_x s} + \frac{F_s ms}{K_x\left(ms^2 - K_x\right)} \tag{9.23}$$

Taking the inverse Laplace transform of equation (9.23):

$$x = \frac{f}{K_x}t - \frac{f\sqrt{m}}{K_x^{3/2}}\sinh\left(\sqrt{\frac{K_x}{m}}t\right) - \frac{F_s}{K_x} + \frac{F_s}{K_x}\cosh\left(\sqrt{\frac{K_x}{m}}t\right) \tag{9.24}$$

Expanding the sinh and cosh terms in equation (9.24) and neglecting the third and higher order expansion yields:

$$x = -\frac{ft^3}{6m} + \frac{F_s t^2}{2m} + \frac{F_s K_x t^4}{24m^2} \tag{9.25}$$

Differentiating equation (9.25) to give the velocity:

$$\dot{x} = -\frac{ft^2}{2m} + \frac{F_s t}{m} + \frac{F_s K_x t^3}{6m^2} \tag{9.26}$$

With the boundary conditions $x = 0$ and $x = x_0$, the force slew rate f can be found from equation (9.26):

$$f = \frac{2F_s}{t} + \frac{F_s K_x t}{3m} \tag{9.27}$$

Assuming a step input F_s=100 N, t can be solved from equation (9.25) and (9.27):

$$\left(\frac{F_s K_x}{72m^2}\right)t^4 - \left(\frac{F_s}{6m}\right)t^2 + x_0 = 0 \qquad \text{in which}$$

t = 4.33ms, 2.97ms and the corresponding force slew rate:

f = 1.09E5 N/s, 1.11E5 N/s

Comparing the force slew rate f in both impulse and step inputs, we can conclude that a levitation supply of 13 V is sufficient to produce the required slew rate for the step load as well because its slew rate is less than that of the impulse input.

9.9 Initial control system design

This section outlines an initial attempt to the design of a controller for levitating the rotor shaft of the vacuum pump. A PID control is given as an example and the system response to step and impulse inputs are investigated. Figure 9.5 illustrates the block diagram of the levitation control system.

The primary objective of the control system is to retain the rotor at its concentric position with respect to the stator in the presence of an external disturbance force, F_D and unbalanced magnetic pull. If the rotor is concentric then no control action is provided at that instant since a zero in displacement Δx gives rise to a zero actuation force.

The overall transfer function with the disturbance force F_D taken as the input is:

$$\frac{\Delta x}{F_D} = \frac{\dfrac{1}{ms^2}}{1-\left[\dfrac{K_x}{ms^2} - \dfrac{\left(K_p K_I G_s + \dfrac{K_p K_I G_s}{T_i s} + K_p K_I G_s T_d s\right)}{ms^2(R+Ls)}\right]}$$

$$\therefore \frac{\Delta x}{F_D} = \frac{LT_i s^2 + T_i R s}{(mLT_i)s^4 + (mT_i R)s^3 + (T_i K_p K_I G_s T_d - K_x L T_i)s^2 + (T_i K_p K_I G_s - K_x R T_i)s + K_p K_I G_s} \qquad (9.28)$$

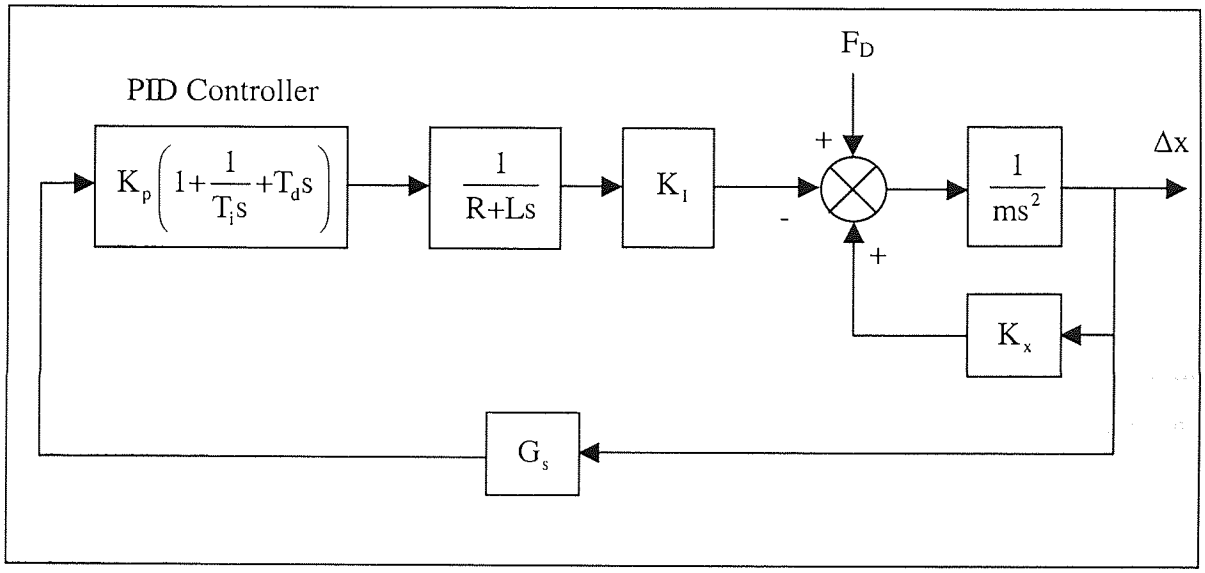

Figure 9.5: Levitation control system.

To achieve stability, all closed loop poles of the system must be negative or lie on the left-hand side of the s-plane. Therefore, the PID control variables K_p, T_i and T_d must be chosen such that the coefficients of the transfer function in (9.28) are all positive. Substituting the parameters of table 9.4 into transfer function (9.28) yields:

$$\frac{\Delta x}{F_D} = \frac{4.95\text{E-}4s^2 + 7.09\text{E} - 2s}{1.238\text{E-}3s^4 + 0.177s^3 + 5.22\text{E}6s^2 + 5.212\text{E}7s + 5.8\text{E}8} \qquad (9.29)$$

Proportional controller (K_p)	50
Integral controller (T_i)	0.09
Derivative controller (T_d)	0.1
Coil resistance (R)	0.7878
Coil inductance (L)	5.5E-3
Actuator gain (K_I)	58
Rotor mass (m)	2.5
Negative stiffness (K_x)	1.09E6
Sensor gain (G_s)	2E5

Table 9.4: Control system parameters.

To investigate stability, the system is subjected to a step input and an impulse input and the resultant plots are shown in figures 9.6 and 9.7 respectively. It is evident that the system is stable because the amplitude of the oscillations has been reduced to approximately zero steady state value. Furthermore, the rotor displacement under both step and impulse inputs is well below the maximum permissible displacement of 0.04 mm. The effect of step disturbance can be further reduced by incorporating a higher value of the proportional component, K_p. However, increasing the value of the derivative component T_d results in a more oscillatory response. The integral component T_i affects the steady state error of the response.

We can conclude that the PID variables suggested in table 9.4 meets the requirement of the present design study although the response could be further optimised. Further investigation of the control algorithm design may be undertaken with a view of improving the time taken to suppress the disturbance.

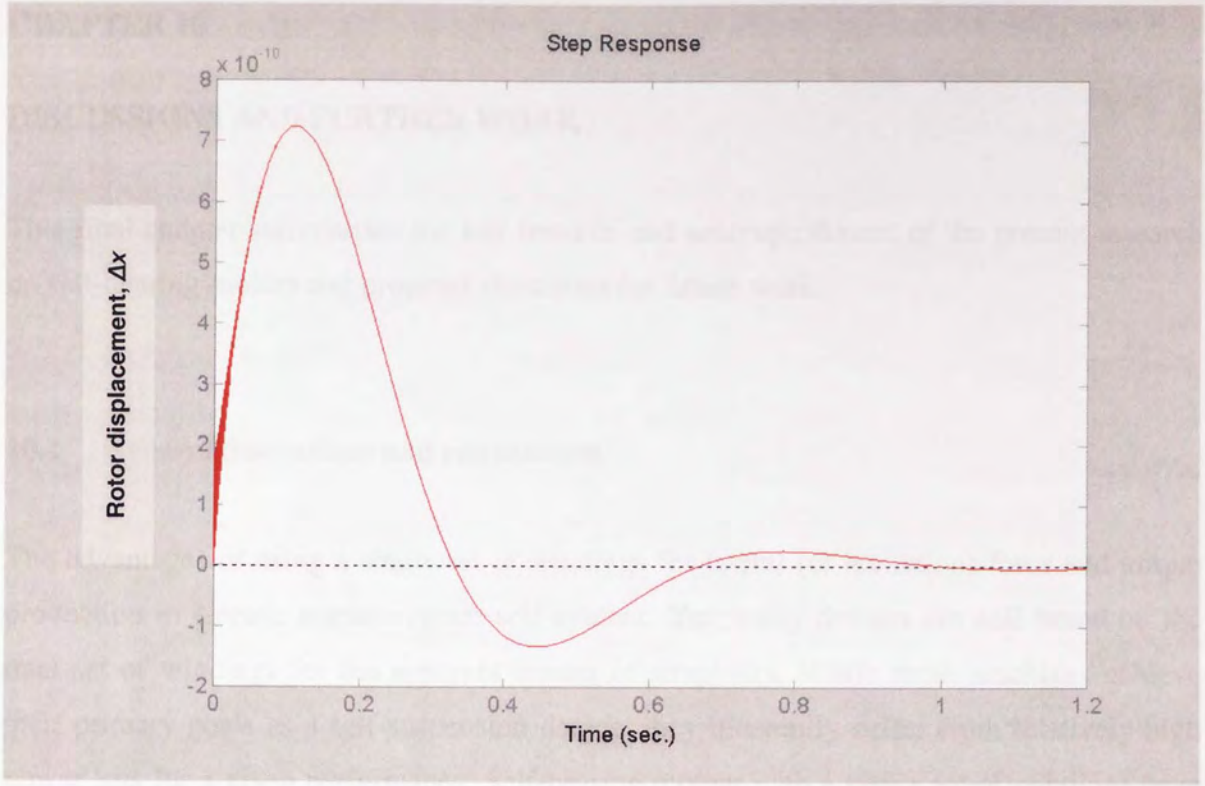

Figure 9.6: Step response of the levitation control system.

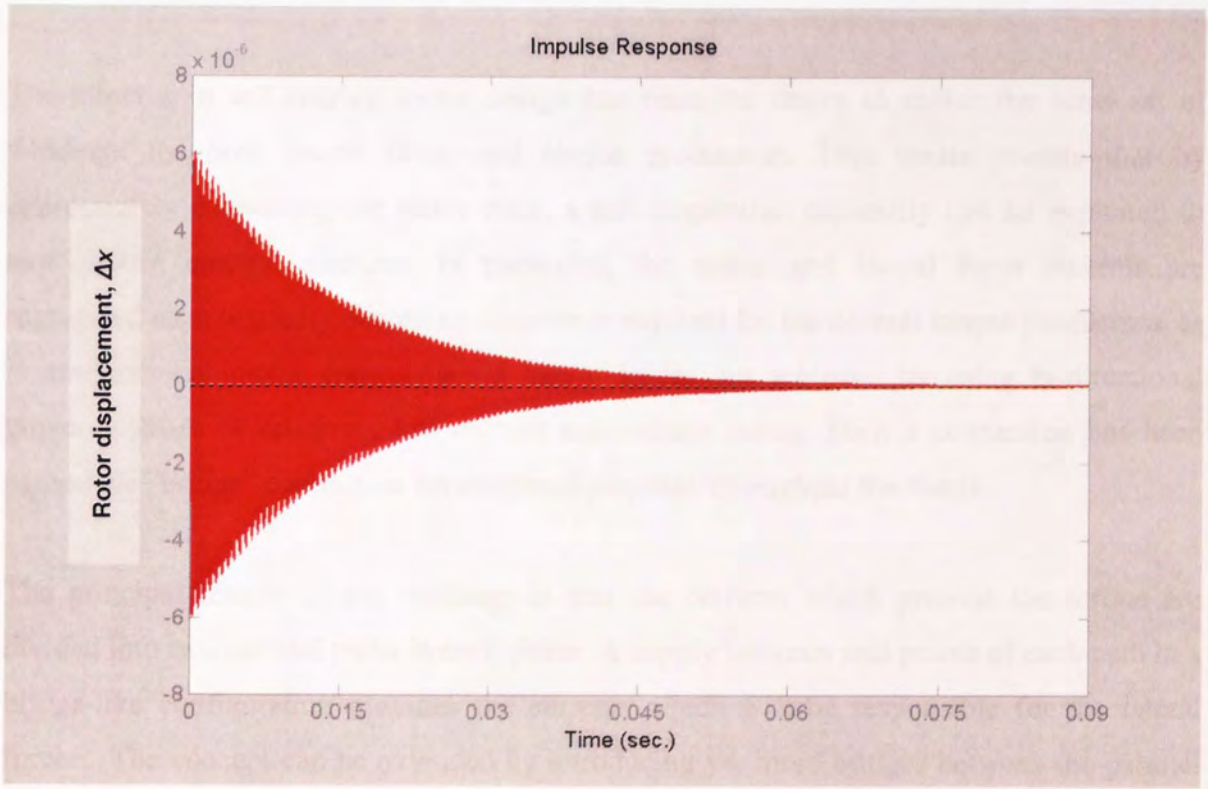

Figure 9.7: Impulse response of the levitation control system.

CHAPTER 10

DISCUSSIONS AND FURTHER WORK

This final chapter summarises the key features and accomplishment of the present research on self-bearing motors and proposes directions for future work.

10.1 General discussions and conclusions

The advantages of using a single set of windings for lateral (or levitation) force and torque production in electric machinery are self-evident. Yet, many designs are still based on the dual set of windings for the apparent reason of simplicity. While these machines achieve their primary goals as a self-suspension device, they inherently suffer from relatively high power loss for a given performance. Self-bearing motors with a single set of windings have also been developed. However, these self-bearing motors require a high number of inverter of high current and voltage ratings and the manner they are controlled as a motor is somewhat unconventional.

The impetus in self-bearing motor design has been the desire to utilise the same set of windings for both lateral force and torque production. This thesis reveals that by appropriately connecting the stator coils, a self-suspension capability can be exploited in any general electric machine. In particular, the motor and lateral force controls are segregated such that only one motor inverter is required for the normal torque production, as in conventional motor control, while lateral forces are achieved by using bi-directional power supplies of relatively low current and voltage rating. Such a connection has been named the "bridge" connection for reference purposes throughout the thesis.

The principal feature of the windings is that the currents which provide the torque are divided into two parallel paths in each phase. A supply between mid points of each path in a bridge-like configuration provides the currents which will be responsible for the lateral forces. The concept can be extended by introducing yet more bridges between the parallel paths that carry the torque currents: this provides flexibility in the detail design. Coils are wound in the stator such that when both motor and levitation currents are provided, two

rotating fields of a pole-pair difference are generated in the machine. This is an essential requirement for any self-bearing motor to produce a substantial amount of lateral force.

The proposed bridge connection scheme has the following advantages:

- Low power loss for a given machine size and performance when compared to conventional dual set of windings scheme.
- Only one motor power supply such as a three-phase inverter is required for driving the motor producing torque. Therefore the conventional way of motor control is preserved unlike the presently available self-bearing motors with a single set of windings.
- Lateral or levitation forces are supplied by independently controlled low current and low voltage bi-directional power supplies. This is a potential cost-saving solution because only a small amount of current is required to create an asymmetrical flux distribution in the air gap.
- The use of a number of small power supplies means the system has a degree of fault tolerance.
- Can be easily extended by adding more bridges in each phase to enable any arbitrary combinations of poles and phases in star- or delta-connections.
- Feasible of extending to higher phases number such as 5, 7 or 11 phase machines.
- Can be manipulated to obtain variants such as concentrated or distributed windings.
- Applicable to various types of motor or topologies such as switched reluctance, induction, permanent magnet and synchronous motors.

In common with conventional self-bearing motors, the present proposal also takes the advantage of the motor MMF so that the superimposed levitation MMF can be kept small producing a net lateral force. The sources that contribute to this net motor MMF are dependent on the types of machine concerned. In surface mounted permanent magnet machines, the net MMF is contributed mostly by the permanent magnets on the rotor, unless the stator is excited with a very high current. For an induction motor, the net MMF is contributed partly by the induced rotor currents and partly by the motor currents. In contrast to permanent magnet and induction motors, the rotor of the switched reluctance machines is not excited by any means and so the stator alone contributes the net MMF.

The proposed bridge connection has been verified to exhibit the characteristics of a self-bearing motor via coupled-field finite element analysis. Results obtained from finite element analyses are crosschecked with the analytical methods for validation purposes. A comparison of power loss for a given machine performance has also been conducted between the proposed connection scheme with that of conventional self-bearing motors. The FEA result indicates that a motor with a single set of windings has at least 10% lower power loss than its dual set of windings counterpart. Overall, the proposed design is also advantageous in terms of cost and implementation.

10.2 Directions of further research

This thesis aims to present a general framework of how the bridge connection can be realised without being inundated with the complexity of optimal design. Perhaps the most immediate work required is to build a prototype of the proposed self-bearing motor by retrofitting the windings of a conventional motor. Most commercial electric motors have been optimised in their designs and so we can emphasize aspects related to levitation and motor control. Suggestions for experimental work are given in appendix B. Other possible areas of improvement are discussed below.

10.2.1 Optimisation of winding designs

In general, there are many ways in which the proposed connection can be wound in a motor stator. Some arrangements may be better than the others in terms of reducing the size of the end windings depending on the physical geometry of the stator and the number of poles required. For instance, a toroidal or Gramme ring winding scheme may be implemented for a short span with large diameter stator to reduce the end winding effects. Alternatively a distributed winding scheme with a larger pole number can also be employed. The relative merits of these variants can be investigated. Furthermore, the number of bridges may be reduced or extended depending on the number of poles and phases of the self-bearing motor and special attention should also be given to harmonics.

There is the question of whether more coils should be connected to form a single bridge or whether coils should be connected to form several smaller bridges. Another area that has not

been explored is the use of fractional slot stators. This thesis did not focus on optimisation of winding designs and the subject is worth investigating in the future.

10.2.2 Optimisation of current switching

Closely related to the winding design is the current switching sequence. It is known that a small asymmetry in the air gap flux distribution is sufficient to cause substantial UMP on the rotor. Levitation power supplies between the bridges are controlled to collectively produce a necessary field for unbalancing the main motor field. If the relationship between levitation current injections and magnitude and direction of force is known, then the net lateral force can be controlled as desired. A corollary of this observation is that there exists many choices of levitation current switching to obtain the same magnitude and direction of force. Different strategies of levitation current switching will give rise to different levels of efficiency. One optimisation target is the set of levitation currents that minimise the power loss.

10.2.3 Advance control methods

The control methodology of magnetic bearings has shifted over the past two decades from classical control techniques (PI and PID controllers) to modern robust control techniques (μ-synthesis, H_∞, mixed H_2/H_∞ controllers). These modern controllers achieve stability and accuracy requirements and their performance is insensitive to plant uncertainty, parameter variation, and external disturbances. However, advanced multivariable control of self-bearing motors has not been reported yet. It is to be expected that the control methods of self-bearing motors will follow the same trend as that of magnetic bearings and therefore it lead to new areas of research.

10.2.4 Finite element analysis (FEA)

Whereas some improvements may be gained by capitalising on the appropriate design methodologies, the subject requires more study via finite element optimisation. This area of research is essentially a subset of motor design where factors concerning stator and rotor design should be resolved. Experimental work on other machines such as induction and switched reluctance motors should also be pursued and compared with the finite element results.

10.3 Final remark

The general trend of engineering achievements is these days towards the concept of integrated devices. While active magnetic bearings have recently found more applications, self-bearing motors maybe the ultimate integrated solution. Current development of self-bearing motors is very much driven by the demand of specific applications. Self-bearing motors have the same capability as magnetic bearings but with an added advantage of being compact. Thus, self-bearing motors maybe expected to supersede magnetic bearings in the role of active suspension in the future. However, the prospect of self-bearing motors is highly dependent on the success of active magnetic bearings. If magnetic bearings were perceived as a failure in too many engineering applications then the future of self-bearing motors would be inevitably dimmed. Thankfully the outlook for active magnetic bearings is positive primarily because of the 'electric' movement such as the 'more electric' aircraft and 'more electric' ship. It will be exciting to witness these major changes in military or commercial vehicles in the coming future, particularly the transition of active magnetic bearings to self-bearing motors.

REFERENCES

[ABB97] Kelly W.S., (19 Dec. 1997) "U.S. Unit of ABB Installs World's Largest Drive At NASA's National Transonic Facility Wind Tunnel", ABB, (http://www.abb.com/usa).

[Ans23] Anschutz-Kaempfe H., "Gyroscopic Apparatus", *United States Patent*, No. 1589039, 1923.

[AP01] International (1 Mar 2001), "China Starts Building Levitating Train", Associated Press, http://wire.ap.org/APnews/?SITE=CACDE&FRONTID=HOME).

[AS98] Amrhein W. and Silber S., "Bearingless single-phase motor with concentrated full pitch windings in interior rotor design", *Proceedings of the Sixth International Symposium on Magnetic Bearings*, pp.486-496, MIT, USA, Aug. 1998.

[BD73] Binns K.J. and Dye M., "Identification of principal factors causing unbalanced magnetic pull in cage induction motors", *IEE Proc.*, vol. 120, no. 3, pp. 349-354, Mar. 1973.

[Bea37] Beams J.W., "High Rotation Speeds", *Journal of Applied Physics*, Vol. 8, No. 12, pp. 795-806, 1937.

[Bos88] Bosch R., "Development of a bearingless electric motor", *Proceedings of the International Conference on Electric Machines (ICEM)*, Vol. 3, pp. 373-375, 1988.

[Bra39] Braunbeck W., "Free suspension of bodies in electric and magnetic fields." *Zeitchrift fur Physik*, vol. 112, no. 11, pp.753-63, 1939.

[Bri99a] "Effects of varying magnetic fields", *Encyclopaedia Britannica DVD 2000*, 23 Nov. 1999.

[Bri99b] "Nikola Tesla", *Encyclopeadia Britannica DVD 2000*, 23 Nov. 1999.

[BWR99] Benhama A., Williamson A.C. and Reece A.B.J., "Force and torque computation from 2-D and 3-D finite element field solutions", *IEE Proc.-Electrical Power Applications*, vol. 146, no. 1, pp. 25-31, Jan. 1999.

[BYM46] Beams J.W., Young J.L. and Moore J.W., "The Production of High Centrifugal Fields", *Journal of Applied Physics*, Vol. 17, pp. 886-890, 1946.

[CCF90] Chiba A., Chida K. and Fukao T., "Principles and characteristics of a reluctance motor with windings of magnetic bearings", *Proceedings of the International Power Electronics Conference (IPEC)*, Tokyo, pp. 919-926, Apr. 1990.

[CDFR94] Chiba A., Deido T., Fukao T. and Rahman M.A., "An analysis of bearingless AC motors" *IEEE Trans. Energy Conversion*, vol. 9, no. 1, pp. 61-67, Mar.1994.

[CFA+97] Chiba A., Furuichi R., Aikawa Y., Shimada K., Takamoto Y. and Fukao T., "Stable operation of induction-type bearingless motors under loaded conditions", *IEEE Trans. Industrial Applications*, pp. 919-924, vol.33, no. 4, pp. 919-924, July/Aug. 1997.

[CFM96] Chiba A., Fukao T and Maejima Y., Seiko Instruments Inc., "Electromagnetic rotary machine having magnetic bearing", *United States Patent*, No. 5955811, Filed 8 Feb. 1996.

[Cou83] Coulomb J.L., "A methodology for the determination of global electromechanical quantities from a finite element analysis and its application to the evaluation of magnetic forces, torques and stiffness", *IEEE Trans. Magnetics*, vol. 19, no. 6, pp.2514-2519, Nov. 1983.

[Cra31] Cramp W., "The year 1800", *Michael Faraday and Some of His Contemporaries*, London: Sir Isaac Pitman, pp. 10, 1931.

[CRF91] Chiba A., Rahman M.A. and Fukao T., "Radial force in a bearingless reluctance motor" *IEEE Trans. Magnetics*, vol. 27, no.2, pp. 786-790, Mar. 1991.

[CS99] Casemore M.A. and Stephens L.S., "Actuator gains for a toothless permanent-magnet self-bearing motor", *IEEE Trans. Magnetics*, vol. 35, no. 6, pp. 4482-4489, Nov. 1999.

[Dor99] Dorrell, D.G., "Experimental behaviour of unbalanced magnetic pull in 3-phase induction motors with eccentric rotors and the relationship with tooth saturation", *IEEE Trans. Energy Conversion*, vol. 14, no. 3, pp. 304-309, Sept. 1999.

[DRM98] De Medeiros L.H., Reyne G. and Meunier G, "Comparison of global force calculations on permanent magnets", *IEEE Trans. Magnetics*, vol. 34, no. 5, pp. 3560-3563, Sept. 1998.

[Ear1842] Earnshaw S., "On the nature of the molecular forces which regulate the constitution of the luminferous ether", *Trans. Cambridge Philos. Soc.*, vol. 7, pp. 97-112, 1842

[Eve1900] Evershed S., "A Frictionless Motor Meter", *Journal IEE*, Vol. 29, pp. 743-794, 1900.

[Eve75] Everitt C.W.F., "Electromagnetism: Foundations of Maxwell's Theory", *James Clerk Maxwell – Physicist and Natural Philosopher*, Charles Scribner's Sons: New York, pp. 80-110, 1975.

[Fau39] Faus H.T., General Electric Company, "Magnetic suspension", *United States Patent*, No. 2315408, Filed 12 Oct. 1939.

[FCM96a] Fukao T., Chiba A. and Michioka C., Ebara Corp., Nikkiso Co. Ltd and Seiko Co. Ltd, "Variable speed dynamotor", *United States Patent*, No. 5880550, Filed 26 Mar. 1996.

[FCM96b] Fukao T., Chiba A. and Michioka C., Ebara Corp., Nikkiso Co. Ltd and Seiko Co. Ltd, "Electromagnetic rotating machine", *United States Patent*, No. 5936370, Filed 19 Apr. 1996.

[FK83] Fukasawa I. and Kumagai Y., Hitachi Ltd., "Electric rotary machine with toroidal windings on an annular stator core", *United States Patent*, No. 4563606, Filed 13 Jul. 1983.

[FK92] Fukata S. and Kouya Y., "Dynamics of active magnetic bearings with magnet cores in the shaped of a cone", *Proceedings of the Third International Symposium on Magnetic Bearings*, pp.339-348, Alexandria, Virginia, Jul. 1992.

[FKU92] Fitzgerald A.E., Kingsley Jr. C. and Umans, S.D., "Power-angle characteristics of salient-pole machines", *Electric machinery*, 5th ed., Singapore, McGraw-Hill Book Co., pp. 252-254, 1992.

[Gem96] Gempp T., "Design of a bearingless canned motor pump", *Proceedings of the Fifth International Symposium on Magnetic Bearings*, Kanazawa, Japan, pp. 333-338, Aug. 1996.

[GNW00] Garvey S.D., Norris W.T. and Wright M.T., "The role of integrated passive components in protecting motor windings", *IEE Proc.-Electrical Power Applications*, vol. 147, no. 5, 5 Sept. 2000.

[Goo99] Goodall R., "Maglev – Concepts and Applications", *IEE Midlands Power Group Lecture*, Birmingham, 2 Nov., 1999.

[Gra11] Graeminger B., "Electromagnetic Suspension Devices", *British Patent*, Nos 24499, 1912 and 24541, 1912.

[Gra89a] Gray C.B., "The tangential magnetic field of armature windings", *Electrical machines and drive systems*, Singapore, Longman Scientific & Technical, pp. 151-158, 1989.

[Gra89b] Gray C.B., "Power/load angle relationships for the salient-pole synchronous machine on constant-voltage, constant-frequency busbars", *Electrical machines and drive systems*, Singapore, Longman Scientific & Technical, pp. 316-317, 1989.

[Har96] Hart R.M., Abiomed Inc. & Danvers Inc., "Bearingless blood pump and electronic drive system", *United States Patent*, No. 6071093, Filed 18 Oct. 1996.

[Haw73] Hawes M.A., "Salient-pole machines", *Electromagnetic machines: The field centred approach for students*, vol. 2, Great Britain, Collins, pp. 132-136, 1973.

[HE99] Hultman A. and Eriksson M.L., "The Attraction of Magnetic Bearings", *Evolution: Business and technology magazine from SKF*, Jan. 1999.

[Her73] Hermann P.K., "A radial active magnetic bearing", *British Patent*, No. 1478868, Filed 20 Nov. 1973.

[Her74] Hermann P.K., "A radial active magnetic bearing having a rotating drive", *British Patent*, No. 1500809, Filed 9 Feb. 1974.

[Hig86] Higuchi T., Nippon Seiko Kabushiki Kaisha, "Magnetically floating actuator having positioning function", *United States Patent*, No. 4683391, Filed 18 Mar. 1986.

[HL79] Habermann H., and Liard G.L., "Practical Magnetic Bearings", *IEEE Spectrum*, Sept., pp. 26-30, 1979.

[Jay81] Jayawant B.V., "Suspension using controlled DC electromagnets", *Electromagnetic Levitation and Suspension Techniques*, Thomson Litho: GB, pp.12-16, 1981.

[JKL94] Jeong H.-S., Kim C.-S. and Lee C.-W., "Modelling and control of cone-shaped active magnetic bearing system", *Proceedings of the Fourth International Symposium on Magnetic Bearings*, pp.23-28, ETH Zurich, Aug. 1994.

[KC96] Knospe C.R. and Collins E.G., "Introduction to the special issue on magnetic bearing control", *IEEE Trans. Control System Technology*, vol. 4, no. 5, pp. 481-483, Sept. 1996.

[Kem37] Kemper H., "Overhead Suspension Railway with Wheelless Vehicles Employing Magnetic Suspension From Iron Rails (Schwebebahn mit raderlosen Fahrzeugen die an eisernen Fahrschienen mittels magnetischer Felder schwebend entlang gefuhrt werden) ", *German Patent*, Nos 643316, 1937 and 644302, 1937.

[KM98] Karassik I.J and McGuire T., "Bearings", *Centrifugal pumps*, 2nd ed., USA, Chapman & Hall, pp. 212, 1998.

[KO00] Kanebako H. and Okada Y., "Development of hybrid type self-bearing motor without extra bias permanent magnets", *Seventh International Symposium on Magnetic Bearings*", pp. 347-352, ETH Zurich, Aug. 2000.

[KSKO00] Kim S., Shimonishi T., Kanebako H. and Okada Y., "Design of a hybrid-type short span self-bearing motor", *Proceedings of the Seventh International Symposium on Magnetic Bearings*", pp. 359-364, ETH Zurich, Aug. 2000.

[LF82] Langley L.W. and Fisher R.L., Kollmorgen Technologies Corp., "Toroidally wound brushless DC motor", *United States Patent*, No. 4547713, Filed 5 Nov. 1982.

[LJ96] Lee C.-W. and Jeong H.-S., "Dynamic modelling and optimal control of cone-shaped active magnetic bearings systems", *Control Engineering Practice*, vol. 4, No. 10, pp. 1393-1403, 1996.

[LL98] Lahteenmaki J.K. and Lantto E.J., "Optimisation of the conical angle of cone-shaped active magnetic bearings", *Proceedings of the Sixth International Symposium on Magnetic Bearings*, pp.224-233, MIT, USA, Aug. 1998.

[MBW99] Muljadi E., Butterfield C.P. and Wan Y.H., "Axial flux, modular, permanent-magnet generator with a toroidal winding for wind turbine applications", *IEEE Trans. Industry Applications*, vol. 35, no. 4, pp. 831-836, Jul.-Aug. 1999.

[MF74] Meinke P. and Flachenecker G., Maschinenfabrik Augsburg-Nurnberg AG, "Electromagnetic drive assembly for rotary bodies using a magnetically mounted rotor", *United States Patent*, No. 3988658, Filed 29 Jul. 1974.

[MHSH89] Maslen H., Hermann P., Scott M. and Humphris R.R., "Practical limits to the performance of magnetic bearings: Peak force, slew rate, and displacement sensitivity", *Trans. ASME Journal of Tribology*, vol. 111, pp. 331-336, April 1989.

[MMN96] Meeker D.C., Maslen E.H. and Noh M.D., "An augmented circuit model for magnetic bearings including eddy currents, fringing and leakage", *IEEE Trans. Magnetics*, vol. 32, no. 4, pp. 3219-3227, Jul. 1996.

[MO98] Miller J.M. and Ostovic V., Ford Global Technologies, "Poly-phase modulated toroidal winding for an induction machine", *United States Patent*, No. 5977679, Filed 5 Mar. 1998.

[MOFN97] Matsumura F., Okada Y., Fujita M. and Namerikawa T., "State of the Art of Magnetic Bearings", *JSME International Journal*, Series C, vol. 40, no. 4, pp. 553-560, 1997.

[MT98] Maurio J.M. and Thaxton E.S., Electric Boat Corp., "Permanent magnet synchronous machine with integrated magnetic bearings", *United States Patent*, No. 6020665, Filed 25 Feb. 1998.

[MTZ96] Mishkevich V.G., Terpay G.W. and Zipfel G.G.J, General Dynamics Advanced Technology Systems Inc., "Unbalanced force generation in motors", *United States Patent*, No. 5949162, Filed 13 Dec. 1996.

[NAS00] Nenninger K., Amrhein W. and Silber S., "Bearingless single-phase motor with fractional pitch windings", *Proceedings of the Seventh International Symposium on Magnetic Bearings*", pp. 371-375, ETH Zurich, Aug. 2000.

[NJL+98] Nichols S.B., Jagannathan S., Leary K., Eisenhaure D., Stanton W., Hockney R., Downer J. and Gondhalekar V., Satcon Technology Corp., "Integrated magnetic levitation and rotation system", *United States Patent*, No. 6049148, Filed 2 Oct. 1998.

[OCFR96] Ooshima M., Chiba A., Fukao T. and Rahman M.A., "Design and analysis of permanent magnet-type bearingless motor" *IEEE Trans. Industrial Electronics*, vol. 43, no. 2, pp. 292-299, Apr. 1996.

[ODO95] Okada Y., Dejima K. and Ohishi T., "Analysis and comparison of PM synchronous motor and induction motor type magnetic bearings", *IEEE Trans. Industrial Applications*, vol. 31, no. 5, pp. 1047-1053, Sept./Oct. 1995.

[OGS98] Osama M., Garrigan N.R. and Soong W.L., General Electric Company, "Compact bearingless machine drive system", *United States Patent*, No. 6034456, Filed 21 Oct. 1998.

[Ohi92] Ohishi T., Shinko Electric Co. Ltd, "Magnetic bearing device with a rotating magnetic field", *United States Patent*, No. 5237229, Filed 16 Apr. 1992.

[OMD+96] Ooshima M., Miyazawa S., Deido T., Chiba A., Nakamura F. and Fukao T., "Characteristics of a permanent magnet type bearingless motor" *IEEE Trans. Industrial Applications*, vol. 32, no. 2, pp. 363-370, Mar./Apr. 1996.

[OMO96] Okada Y., Miyamoto S. and Ohishi T., "Levitation and torque control of internal permanent magnet type bearingless motor", *IEEE Trans. Control Systems Technology*, vol. 4, no.5, pp. 565-571, Sept. 1996.

[OMS+98] Ooshima M., Miyazawa S., Shima Y., Chiba A., Nakamura F. and Fukao T., "Increase in radial forces of a bearingless motor with buried permanent-magnet type rotor", paper read to the *Fourth International Conference on Motion and Vibration Control*, ETH Zurich, Switzerland, Aug. 25, 1998.

[OMS00] Ohsawa M., Mori S. and Satoh T., "Study of the induction type bearingless motor", *Proceedings of the Seventh International Symposium on Magnetic Bearings*", pp. 389-394, ETH Zurich, Aug. 2000.

[OSUO98] Okada Y., Shinohara K., Ueno S. and Ohishi T., "Hybrid AMB type selfbearing motor", *Proceedings of the Sixth International Symposium on Magnetic Bearings*, pp. 497-506, MIT, USA, Aug. 1998.

[PLRC94] Preston M.A., Lyons J.P.F., Richter E. and Chung K., General Electric Company, "Integrated magnetic bearing/switched reluctance machine", *United States Patent*, No. 5424595, Filed 22 Dec. 1994.

[SA98] Silber S. and Amrhein W., "Bearingless single-phase motor with concentrated full pitch windings in exterior rotor design", *Proceedings of the Sixth International Symposium on Magnetic Bearings*, pp. 476-485, MIT, USA, Aug. 1998.

[SB97] Schoeb R. and Barletta N., "Principle of a bearingless slice motor", *JSME International Journal*, Series C, vol. 40, no. 4, pp. 593-598, 1997.

[SBF+00] Schoeb R., Barletta N., Fleischli A., Foiera G., Gempp T., Poirier V.L., Gernes D.B., Bourque K., Loree H.M. and Richardson J.S, "A Bearingless Motor For a Left Ventricular Assist Device (LVAD)", *Proceedings of the Seventh International Symposium on Magnetic Bearings*, pp. 383-388, ETH Zurich, Switzerland, Aug. 2000.

[SBWR98] Schoeb R., Barletta N., Weber M. and Rohr R.V., "Design of a bearingless bubble bed reactor", *Proceedings of the Sixth International Symposium on Magnetic Bearings*, pp. 507-516, MIT, USA, Aug. 1998.

[Seg01] Segway HT, (2001), "How It Works", Segway, (http://www.segway.com/segway/how_it_works.html)

[Sin87] Sinha P.K., "Ferromagnetic suspension", *Electromagnetic Suspension: Dynamics and Control*, IEE, pp.27-51, 1987.

[SOM98] Satoh T., Ohsawa M. and Mori S., Ebara Corp., "Bearingless rotary machine", *United States Patent*, No. 6078119, Filed 25 Nov. 1998.

[SR99] Santisteban J.A. and Stephan R.M., "Analysis and control of a loaded bearingless motor", *IEEE Trans. Magnetics*, vol.35, no. 5, pp. 3998-4000, Sept. 1999.

[SSSD96] Santisteban J.A., Salazar A.O., Stephan R.M. and Dunford W.G., "A bearingless machine – An alternative approach", *Proceedings of the Fifth International Symposium on Magnetic Bearings*, pp.345-349, Kanazawa, Japan, Aug. 1996.

[Tay96] Taylor, L.S. (1996), "Gallery of Electromagnetic Personalities", Professor Taylor's Ohm Page, Dept. of Electrical and Computer Engineering, University of Maryland, http://www.ee.umd.edu/~taylor/frame4.htm.

[UCO+98] Ueno S., Chen C., Ohishi T., Matsuda K., Okada Y., Taenaka Y. and Masuzawa T., "Design of a self-bearing slice motor for a centrifugal blood pump", *Proceedings of the Sixth International Symposium on Magnetic Bearings*, pp. 143-151, MIT, USA, Aug. 1998.

[Wei00] Weir C., TRW Aeronautical Systems, "The all-electric aircraft", *IEE Austin Court Seminar*, Birmingham, UK, 16 Feb. 2000.

[Wil87] Williamson S., National Research Development Corp., "Construction of electrical machines", *United States Patent*, No. 4792710, Filed 20 Feb. 1987.

[WM68] Woodson H.H. and Melcher J.R., "Discussion of saliency in different machine types", *Electromechanical dynamics Part 1: Discrete systems*, USA, John Wiley & Sons, Inc., pp. 156-157, 1968.

APPENDIX A

ASPECTS RELATED TO MAGNETIC BEARINGS

Some aspects of magnetic bearings are discussed here. The first section describes how magnetic forces between a pair of opposing electromagnets can be linearised and how inductance limits the slew rate of the levitation force. This is followed by a brief discussion of how a pair of conical magnetic bearings can provide stability to an independent five degrees of freedom rotor with only four independent differential currents. The effect of eddy currents on magnetic bearings completes the discussion in the appendix.

A.1 Force linearisation and slew rate

Magnetic bearings are inherently non-linear. One of the common methods employed to linearise the relation between a control current and the corresponding force is the bias flux linearisation. This method involves the use of a bias flux in two opposing electromagnets in conjunction with the perturbation currents. The bias flux can be provided either by a bias current or permanent magnets but the former is more common because of its simple construction. We restrict our discussion to the case of using a bias current but a similar derivation can also be done by replacing the bias current with an equivalent MMF produced by a permanent magnet.

Consider an electromagnet illustrated in figure A.1. For simplicity it is assumed that the iron has infinite permeability; fringing and leakage of flux are ignored. Using Ampere's law, the MMF drop in the magnetic circuit can be written as:

$$\oint H.dl = NI$$

$$\frac{B_1 g}{\mu_0} + \frac{B_2 g}{\mu_0} = NI \qquad \text{(A.1)}$$

where B, g, N, I and μ_0 are the flux density, air gap size, number of turns, current and permeability of free space respectively. From the conservation of flux assuming constant pole area,

$$B_1 = B_2 = B \tag{A.2}$$

The force generated as a result of Maxwell tensile stress is:

$$F = \frac{1}{2\mu_0} B^2 A_p \tag{A.3}$$

Substituting equations (A.1) and (A.2) into (A.3) gives the overall vertical force expression in relation to the squared current excitation and air gap:

$$F = \frac{\beta \mu_0 A_p N I^2}{4 g_0^{\,2}} \tag{A.4}$$

$$\text{and } \beta = \cos\theta_h \tag{A.5}$$

θ_h is half the angle between two poles in figure A.1.

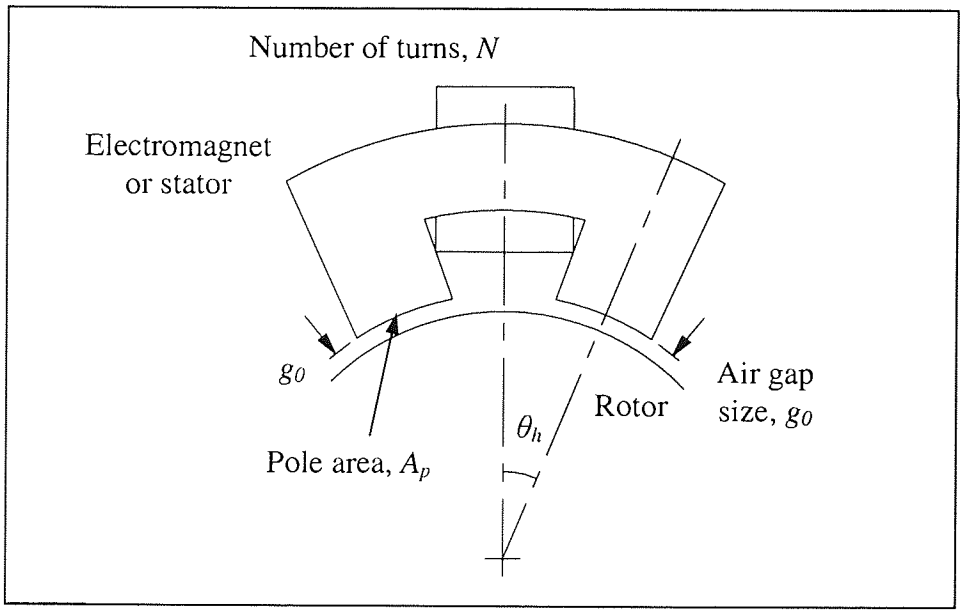

Figure A.1: Geometry of an electromagnet.

Now consider a pair of opposing electromagnets as shown in figure A.2. For such a scheme, the net force generated is:

$$F_y = \frac{\beta \mu_0 A_p N^2}{4} \left[\frac{(I_B + i_p)^2}{(g_0 - \beta y)^2} - \frac{(I_B - i_p)^2}{(g_0 + \beta y)^2} \right] \tag{A.6}$$

where I_B and i_p are the bias and perturbation currents respectively. For linearisation of a non-linear system, we assume that the displacement of the rotor is very small with respect to the concentric position or normal operating condition $\left(y = \overline{y},\ i_p = \overline{i_p}\right)$. Expression (A.6) can then be expanded into a Taylor series about $\overline{y}$, $\overline{i_p}$ neglecting the second and higher order terms:

$$F_y = F\big|_{y=\overline{y},i_p=\overline{i_p}} + \left.\frac{\partial F}{\partial i_p}\right|_{y=\overline{y},i_p=\overline{i_p}} \left(i_p - \overline{i_p}\right) + \left.\frac{\partial F}{\partial y}\right|_{y=\overline{y},i_p=\overline{i_p}} \left(y - \overline{y}\right) + \ldots \qquad \text{(A.7)}$$

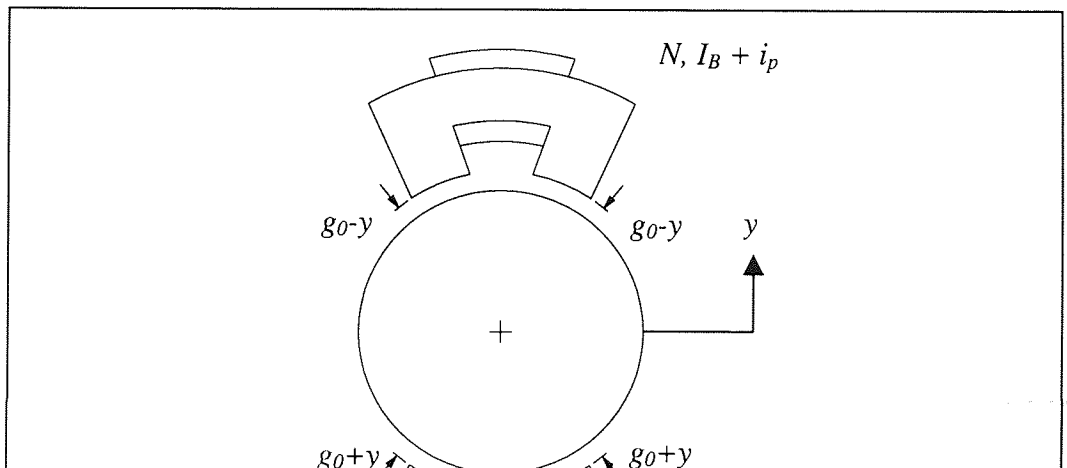

Figure A.2: A schematic of a pair of opposing electromagnets.

Here the actuator gain is defined as:

$$K_i = \left.\frac{\partial F}{\partial i_p}\right|_{y=\overline{y},i_p=\overline{i_p}} \qquad ;\text{let } y = 0$$
$$= \frac{\beta \mu_0 A_p N^2 I_B}{g_0^{\,2}} \qquad \text{(A.8)}$$

and the open loop or negative stiffness is:

$$K_y = \left.\frac{\partial F}{\partial y}\right|_{y=\bar{y},i_p=\bar{i}_p} \qquad \text{;let } y=0,\ i_p=0$$

$$= -\frac{\beta^2 \mu_0 A_p N^2 I_B{}^2}{g_0{}^3} \tag{A.9}$$

Therefore force expression (A.7) can be rewritten as:

$$F_y = F_0 + K_i\left(i_p - \bar{i}_p\right) + K_y\left(y - \bar{y}\right) + \ldots \tag{A.10}$$

Slew rate is a measure of how rapidly the current can change in a coil. Practical magnetic bearings have limited force slew rate due to the inductive nature of the coil and the fact that the power supply driving the amplifier is at a fixed voltage [MHSH89]. The effect of slew rate limitation is to reduce the stiffness and damping of the magnetic bearing.

The rate of change of current in the coil dictates how rapid the bearing force can vary i.e.

$$\frac{dF_y}{dt} = K_i \frac{di_p}{dt} \tag{A.11}$$

For an amplifier driving a coil, the electric circuit equation is:

$$V = \left(I_B + i_p\right)\left(R_c + R_e\right) + L_c \frac{di_p}{dt} \tag{A.12}$$

where V, R_c, R_e and L_c are the supply voltage, coil resistance, amplifier and external circuitry resistances and coil inductance respectively. Further manipulation of equations (A.11) and (A.12) gives the largest possible slew rate:

$$\left.\frac{dF_y}{dt}\right|_{\max} = K_i \frac{\left[V - \left(I_B + i_p\right)\left(R_c + R_e\right)\right]}{L_c} \tag{A.13}$$

The component of impedance due to the resistance is usually very small when compared to the inductance, and so the supply voltage dominates over the potential drop across (R_c+R_e). This suggests that it is possible to increase the force slew rate by simply increasing the

voltage supply. In practice, however, there is a limit to which the voltage can be increased because of the thermal efficiency requirements in the bearing and amplifier.

A.2 Controlling the stability of a five degree-of-freedom rotor with a pair of conical magnetic bearings

Conical magnetic bearings have the characteristics of both lateral and axial magnetic bearings: the control force is split into lateral and axial components by the inclined angle of the pole faces [FK92], [LL98]. For a five degree-of-freedom magnetic bearing, five differential control currents are necessary to control a pair of lateral electromagnets and a thrust electromagnet. Since conical bearings provide both lateral and axial force components, four independent differential currents are sufficient to provide stability to a rigid rotor. The underlying concept in its control system is that the axial displacement of the rotor is controlled by both bearings at the end whereas the lateral displacement is controlled by two diametrically opposing electromagnets in a conical bearing [JKL94], [LJ96]. General expressions for force and control currents of a pair of 8-pole conical bearings are derived as follows.

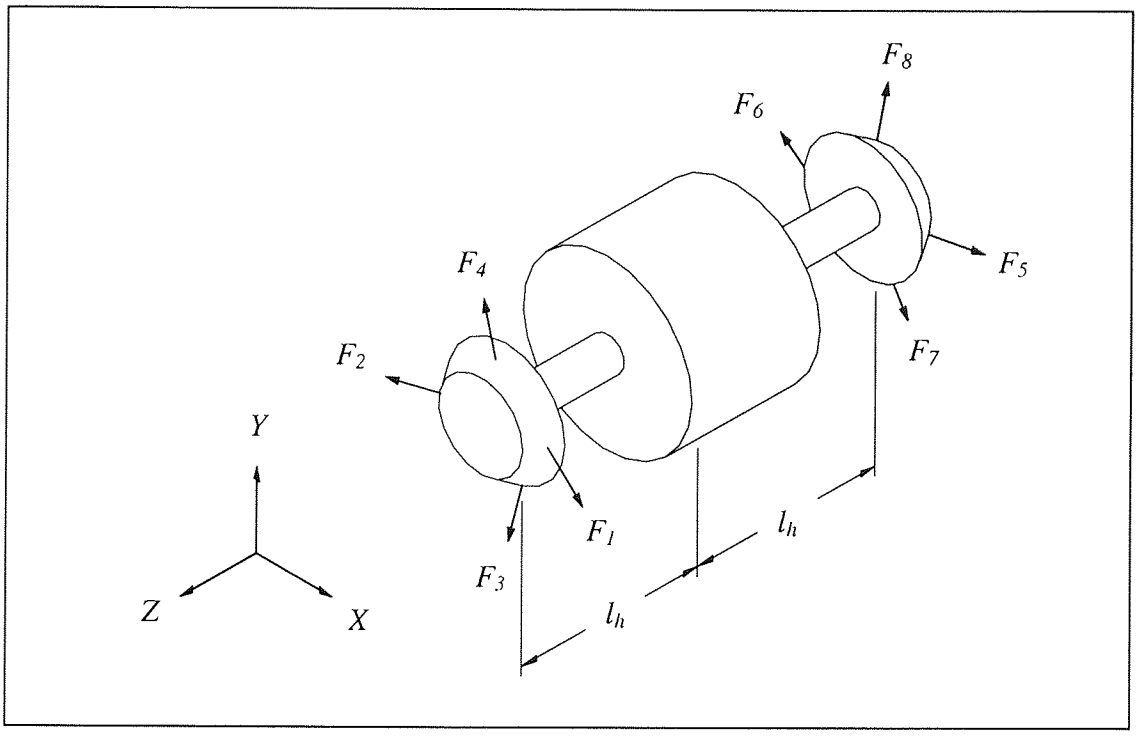

Figure A.3: A model of an active conical rotor-bearing system.

Figure A.3 shows a rotor with conical angle α at each end. The distance between the centre of the rotor and the centre of the inclined surface is denoted l_h. It is assumed that each conical bearing has two pairs of opposing electromagnets producing forces F_1, F_2, F_3, F_4 at one end and F_5, F_6, F_7, F_8 at the other end. These forces are exerted mainly perpendicularly to the cone surface. The changes in the air gap size as the magnetic forces between a pair of opposing magnets vary are depicted in figure A.4. For small motions of rotor, the changes in the air gaps at the locations corresponding to forces F_1, F_2, F_3, F_4, F_5, F_6, F_7 and F_8 can be represented by:

$$
\begin{aligned}
g_1 &= g_0 - \beta z \sin\alpha - \beta(x + l_h\theta_y)\cos\alpha \\
g_2 &= g_0 - \beta z \sin\alpha + \beta(x + l_h\theta_y)\cos\alpha \\
g_3 &= g_0 - \beta z \sin\alpha - \beta(y - l_h\theta_x)\cos\alpha \\
g_4 &= g_0 - \beta z \sin\alpha + \beta(y - l_h\theta_x)\cos\alpha \\
g_5 &= g_0 + \beta z \sin\alpha - \beta(x - l_h\theta_y)\cos\alpha \\
g_6 &= g_0 + \beta z \sin\alpha + \beta(x - l_h\theta_y)\cos\alpha \\
g_7 &= g_0 + \beta z \sin\alpha - \beta(y + l_h\theta_x)\cos\alpha \\
g_8 &= g_0 + \beta z \sin\alpha + \beta(y + l_h\theta_x)\cos\alpha
\end{aligned}
\qquad \text{(A.14)}
$$

where g_0 is the nominal air gap size and β is the sensitivity of the air gap to rotor displacement given by:

$$\beta = \frac{\partial g}{\partial y} \qquad \text{(A.15)}$$

The attractive force for a single electromagnet is proportional to the square of the current and inversely proportional to the square of the air gap, i.e. from (A.4):

$$F = \frac{\beta \mu_0 A_p N^2 I^2}{4 g^2}$$

Therefore, we can write the set of forces produce by the electromagnets as:

$$F_1 = \frac{\beta \mu_0 A_p N^2 \left(I_{0L} + i_{pxL\_1}\right)^2}{4\left(g_0 - \beta z \sin\alpha - \beta(x + l_h\theta_y)\cos\alpha\right)^2} \qquad F_5 = \frac{\beta \mu_0 A_p N^2 \left(I_{0R} + i_{pxR\_1}\right)^2}{4\left(g_0 + \beta z \sin\alpha - \beta(x - l_h\theta_y)\cos\alpha\right)^2}$$

$$F_2 = \frac{\beta\mu_0 A_p N^2 \left(I_{0L} + i_{pxL\_2}\right)^2}{4\left(g_0 - \beta z\sin\alpha + \beta(x + l_h\theta_y)\cos\alpha\right)^2} \qquad F_6 = \frac{\beta\mu_0 A_p N^2 \left(I_{0R} + i_{pxR\_2}\right)^2}{4\left(g_0 + \beta z\sin\alpha + \beta(x - l_h\theta_y)\cos\alpha\right)^2}$$

$$F_3 = \frac{\beta\mu_0 A_p N^2 \left(I_{0L} + i_{pyL\_1}\right)^2}{4\left(g_0 - \beta z\sin\alpha - \beta(y - l_h\theta_x)\cos\alpha\right)^2} \qquad F_7 = \frac{\beta\mu_0 A_p N^2 \left(I_{0R} + i_{pyR\_1}\right)^2}{4\left(g_0 + \beta z\sin\alpha - \beta(y + l_h\theta_x)\cos\alpha\right)^2}$$

$$F_4 = \frac{\beta\mu_0 A_p N^2 \left(I_{0L} + i_{pyL\_2}\right)^2}{4\left(g_0 - \beta z\sin\alpha + \beta(y - l_h\theta_x)\cos\alpha\right)^2} \qquad F_8 = \frac{\beta\mu_0 A_p N^2 \left(I_{0R} + i_{pyR\_2}\right)^2}{4\left(g_0 + \beta z\sin\alpha + \beta(y + l_h\theta_x)\cos\alpha\right)^2}$$

(A.16)

where I_{0L} and I_{0R} are bias currents of the left and right end bearings respectively. i_p is the perturbation current where the subscripts x and y indicate the directions in the orthogonal axes and L and R refer to the left and right end bearings respectively.

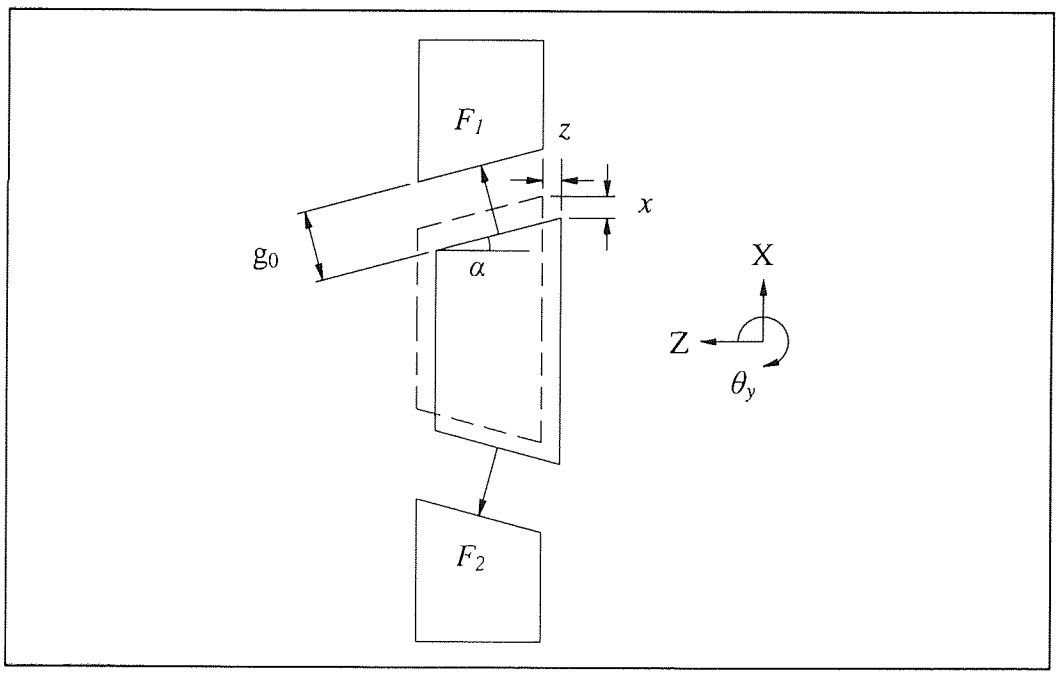

Figure A.4: Displacement of rotor between a pair of opposing electromagnets.

To exert a lateral force in one direction between a pair of opposing electromagnets, the bias currents are perturbed by a differential current. Consider a net lateral force $(F_1\text{-}F_2)$ to be exerted on the rotor in the direction of F_1. From expressions (A.6), the perturbation currents required are of the same magnitude but in opposing direction, i.e.

$$i_{pxL\_1} = -i_{pxL\_2}$$
$$\text{or } i_{pxL\_1} = i_{pxL} \text{ and } i_{pxL\_2} = -i_{pxL} \tag{A.17}$$

Similarly, the perturbation currents for producing lateral forces in other electromagnets are:

$$\begin{aligned} i_{pyL\_1} &= i_{pyL} \text{ and } i_{pyL\_2} = -i_{pyL} \\ i_{pxR\_1} &= i_{pxR} \text{ and } i_{pxR\_2} = -i_{pxR} \\ i_{pyR\_1} &= i_{pyR} \text{ and } i_{pyR\_2} = -i_{pyR} \end{aligned} \tag{A.18}$$

To exert a net axial force, perturbation currents at one end of bearing are made positive with respect to the other end. This is analogous to the principle of lateral force production where both ends of conical bearings are regarded as a pair of opposing electromagnets. We can consider the axial force control to be independent of the control of lateral force. If a net axial force is required toward the left end bearing, then positive perturbation currents must be supplied to left side electromagnets and negative perturbation currents on the right. Thus, the axial perturbation currents are:

$$\begin{aligned} i_{pxL\_1} &= i_{pz} \text{ and } i_{pxL\_2} = i_{pz} \\ i_{pyL\_1} &= i_{pz} \text{ and } i_{pyL\_2} = i_{pz} \\ i_{pxR\_1} &= -i_{pz} \text{ and } i_{pxR\_2} = -i_{pz} \\ i_{pyR\_1} &= -i_{pz} \text{ and } i_{pyR\_2} = -i_{pz} \end{aligned} \tag{A.19}$$

Combining the results from (A.17), (A.18) and (A.19) yields a set of four differential currents required to provide full stabilisation to a five degree-of-freedom rotor. Current relationships are tabulated in table (A.1). The schematic diagram of the control system is shown in figure A.5. Here only the force control in x- and z-directions are shown as an example, but the same schematic can also be used to account for y-direction control.

	Axial force control Z-axis	
Lateral force Control	Left side conical bearing	Right side conical bearing
X-axis	$i_{pxL\_1,2} = i_{pz} \pm i_{pxL}$	$i_{pxR\_1,2} = -i_{pz} \pm i_{pxR}$
Y-axis	$i_{pyL\_1,2} = i_{pz} \pm i_{pyL}$	$i_{pyR\_1,2} = -i_{pz} \pm i_{pyR}$

Table A.1: Four differential currents control for a pair of conical magnetic bearings.

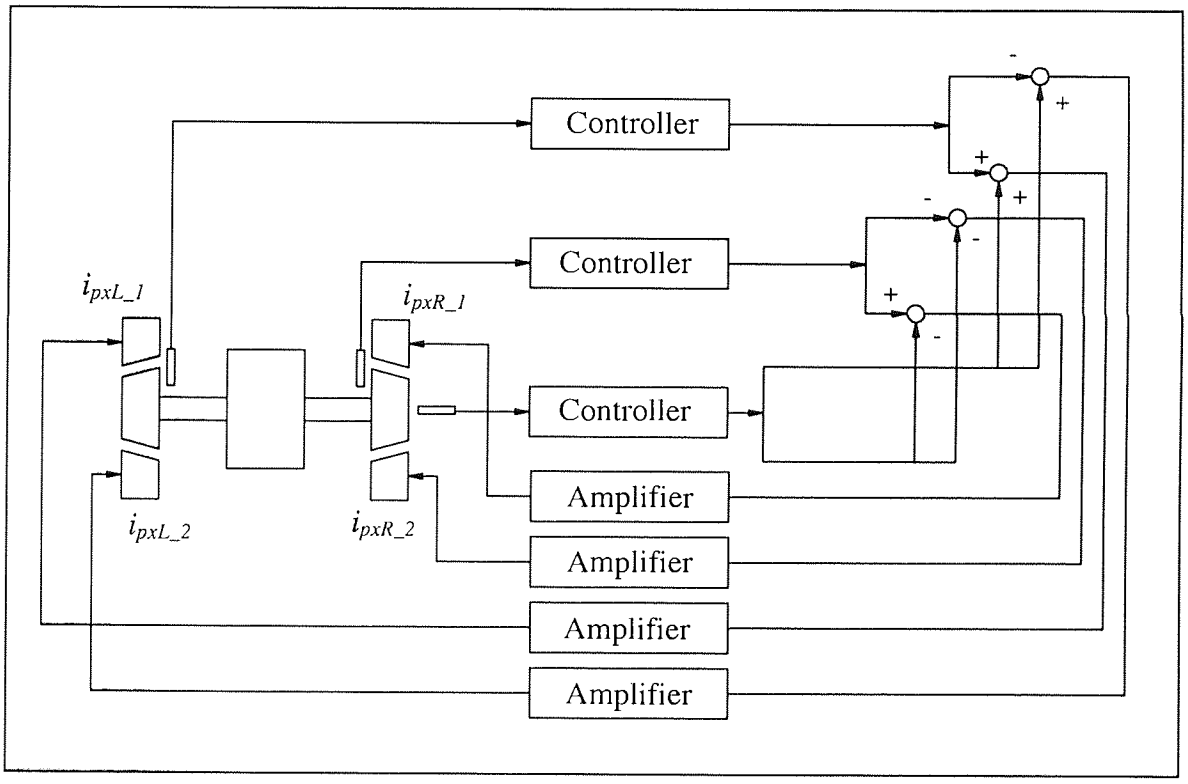

Figure A.5: Conical magnetic bearings control system.

Using the linearisation method described in section A.1, expressions (A.16) can be augmented to obtain a net lateral force between two opposing electromagnets. Consider a pair of electromagnets which produce the lateral component of forces F_1 and F_2. Denoting $g_x=(x+l_h\theta_y)cos(\alpha)$ and $g_z=z.sin(\alpha)$, the net lateral force is:

$$F_{net(1,2)} = \frac{\beta\mu_0 A_p N^2 \left(I_{0L} + i_{pxL}\right)^2}{4g_1^{\,2}} - \frac{\beta\mu_0 A_p N^2 \left(I_{0L} - i_{pxL}\right)^2}{4g_2^{\,2}}$$
$$= \frac{\beta\mu_0 A_p N^2 \left(I_{0L} + i_{pxL}\right)^2}{4\left(g_0 - \beta g_z - \beta g_x\right)^2} - \frac{\beta\mu_0 A_p N^2 \left(I_{0L} - i_{pxL}\right)^2}{4\left(g_0 - \beta g_z + \beta g_x\right)^2} \tag{A.20}$$

The actuator gain is then:

$$K_{i_{pxL}} = \left.\frac{\partial F_{net(1,2)}}{\partial i_{pxL}}\right|_{g_x=0, g_z=0, i_{pxL}=0}$$
$$= \frac{\beta\mu_0 A_p N^2 I_{0L}}{g_0^{\,2}} \tag{A.21}$$

and the open loop stiffnesses are:

$$K_{xL} = \left.\frac{\partial F_{net(1,2)}}{\partial g_x}\right|_{g_x=0, g_z=0, i_{pxL}=0}$$
$$= -\frac{\beta^2\mu_0 A_p N^2 \left(I_{0L}\right)^2}{g_0^{\,3}} \tag{A.22}$$

$$K_{zL} = \left.\frac{\partial F_{net(1,2)}}{\partial g_z}\right|_{g_x=0, g_z=0, i_{pxL}=0} \tag{A.23}$$
$$= 0$$

Therefore, the linearised lateral component of force becomes:

$$F_{net(1,2)} = K_{i_{pxL}} i_{pxL} + K_{xL} g_x$$
$$= K_{i_{pxL}} i_{pxL} + K_{xL}\left(x + l_h\theta_y\right)\cos\alpha \tag{A.24}$$

In a similar manner, the axial component of force, for e.g. between F_1 and F_5 can be derived as:

$$F_{net(1,5)} = K_{i_{pz}} i_{pz} + K_z g_z$$
$$= K_{i_{pz}} i_{pz} + K_z . z \sin\alpha \qquad \text{(A.25)}$$

where $K_{i_{pz}}$ and K_z are the axial actuator gain and axial open loop stiffness respectively.

A.3 Eddy current effect on magnetic bearings

Eddy currents are an electromagnetic phenomena associated with a time-varying magnetic flux in an electrically conducting material. Eddy currents circulate in the core opposing the change in flux density and giving rise to ohmic heating. As such, the rate of change of flux is attenuated and the levitation force of the magnetic bearing is reduced. In addition, eddy currents also cause a tangential force on the rotor, thus creating a retarding torque. Cross coupling of the X- and Y-axes control also arises due to the tangential force and this further complicates the overall stabilising control of the system.

When a rotor is rotated in an 8-pole lateral bearing with alternating N-S polarities, the journal of the rotor will experience 8 times of flux change per revolution. Flux lines are essentially located and traversing on the same plane as the rotor's rotation plane. As the shaft speed increases the rate of change of flux will also increase. This leads to an undesirable increase of the induced eddy currents in the ferromagnetic material. For an axial magnetic bearing, however, the change of flux will not be seen by the rotating disc because the plane of rotation of the disc is orthogonal to the plane where the flux lines flow. Thus the eddy currents effects are insignificant in the axial bearing from the aspect of disc rotation. The effects of eddy currents are more pronounced when the rotor vibrates in the axial direction. The frequency of the perturbation currents must be varied in order to generate a time-varying magnetic field to counteract the axial vibrations. By this means, eddy currents are induced in the axial bearing.

To reduce the effects of eddy currents, core materials are usually made of stacked laminations of magnetic material. Each lamination is electrically insulated from the other and they are aligned in the direction of the field lines. To further reduce the eddy currents heating, high electrical resistance material can be employed for constructing the stator and rotor.

To see the effect of eddy currents on the flux that can be induced in a laminated structure, a useful relationship is given for example by Meeker et al. [MMN96]:

$$B = B_0 \frac{\tanh\left(\sqrt{s\sigma\mu}\,\frac{d}{2}\right)}{\left(\sqrt{s\sigma\mu}\,\frac{d}{2}\right)} \tag{A.26}$$

where B is the average flux density in the lamination; B_0 is the flux density adjacent to the insulation between laminations; σ, μ and d are the electrical conductivity, magnetic permeability and lamination thickness respectively; and $s = j\omega$.

This relation assumes that the flow of flux is parallel and identical at any cross section of the lamination. Also, it is assumed that the laminations are made of homogeneous material and that saturation, hysteresis and end effects are negligible.

The expression relating the force and flux density is given in (A.3). Substituting (A.26) into (A.3) yields

$$\begin{aligned} F &= \frac{{B_0}^2 A_p}{2\mu_0}\left[\frac{\tanh\left(\sqrt{s\sigma\mu}\,\frac{d}{2}\right)}{\left(\sqrt{s\sigma\mu}\,\frac{d}{2}\right)}\right]^2 \\ &= F_0 \frac{\left[\tanh\left(\sqrt{\frac{j2\pi f\mu_0\mu_r}{\rho}}\,\frac{d}{2}\right)\right]^2}{\left(\frac{j2\pi f\mu_0\mu_r}{\rho}\right)\left(\frac{d}{2}\right)^2} \end{aligned} \tag{A.27}$$

$$\text{where resistivity } \rho = \frac{1}{\sigma}. \tag{A.28}$$

Therefore,

$$\frac{F}{F_0} = \frac{\left[\tanh\left(\sqrt{\frac{j2\pi f\mu_0\mu_r}{\rho}}\,\frac{d}{2}\right)\right]^2}{\left(\frac{j2\pi f\mu_0\mu_r}{\rho}\right)\left(\frac{d}{2}\right)^2} \tag{A.29}$$

For a magnetic material with 0.5mm lamination thickness, relative permeability of 2000 and resistivity of 0.22E-6 Ωm, expression (A.29) becomes:

$$\frac{F}{F_0} = \frac{\left[\tanh\left(\sqrt{jf} \times 6.698E-2\right)\right]^2}{(jf)(4.486E-3)} \qquad \text{(A.30)}$$

Expressions (A.30) and $F = K_i I$ can be represented in a block diagram as depicted in figure A.6.

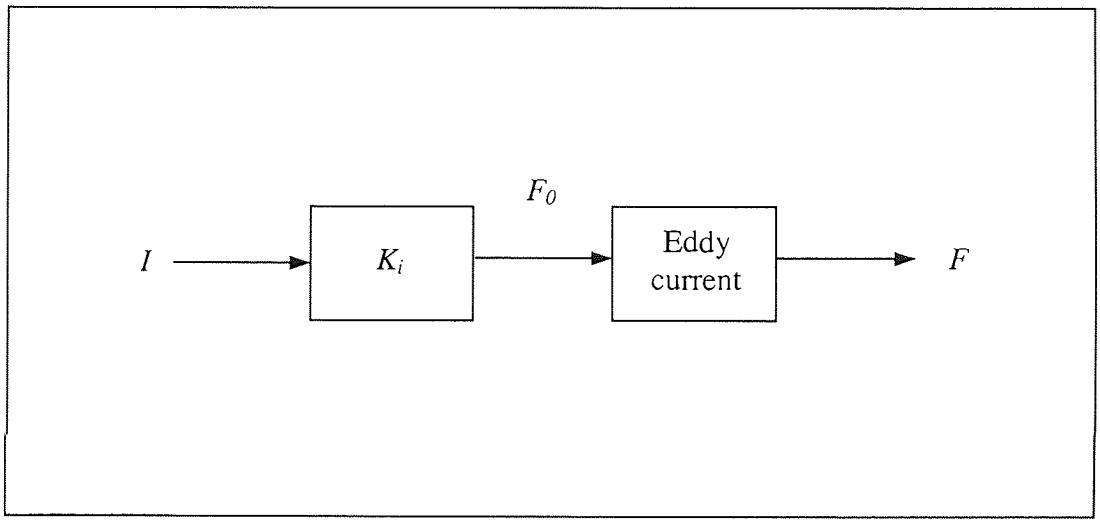

Figure A.6: A block diagram relating force and eddy currents.

A plot of magnitude variation of force (F/F_0) with increasing frequency f is shown in figure A.7. It is evident that as the frequency increases (induced eddy currents increase), the resulting force F is severely reduced for a given force F_0. The roll-off in force production is expected at frequencies beyond 1kHz. At lower frequencies however, eddy currents have negligible effect on force production.

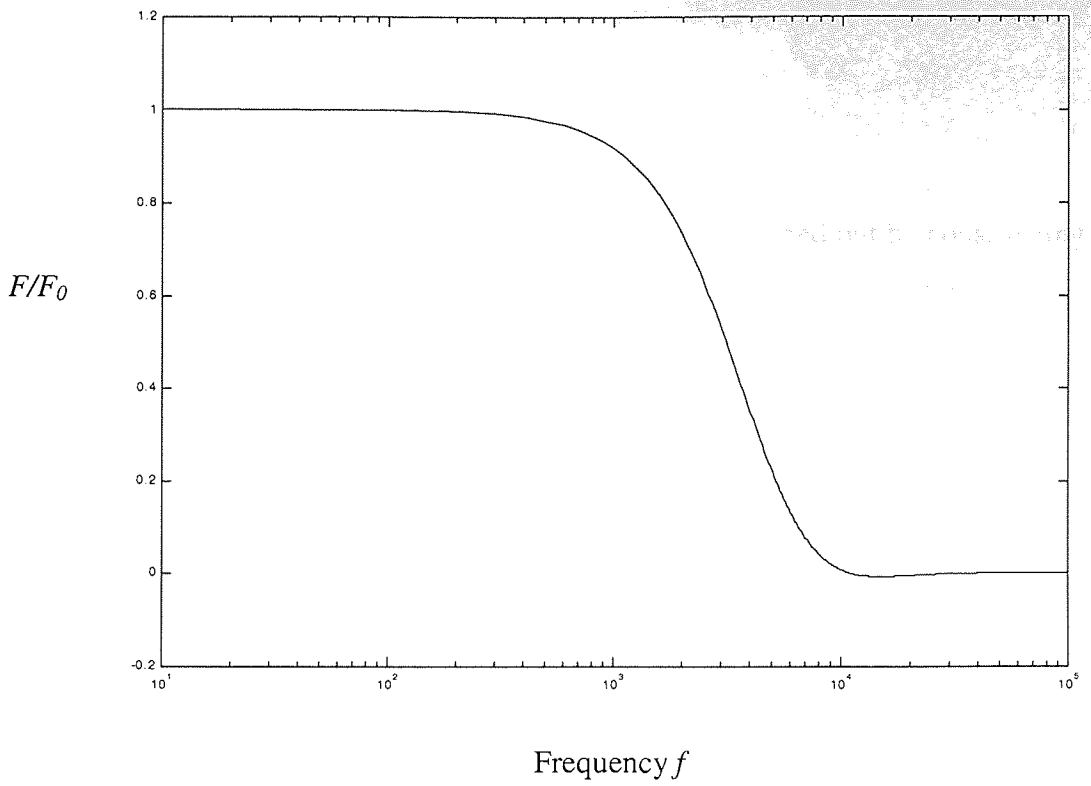

Figure A.7: The effect of eddy current on F/F_0 as frequency f increases.

APPENDIX B

SUGGESTIONS FOR EXPERIMENTAL WORK

This appendix outlines how an experimental work may be carried out by constructing a two degree-of-freedom prototype at the outset and moving forward to a full implementation of a five degree-of-freedom self-bearing motor.

B.1 Operating the self-bearing motor with both rotor ends constrained

A prototype consisting of one stator and a rotor supported by mechanical bearings is first tested to confirm that the self-bearing motor is capable of producing torque. This simple test rig is set up as shown in figure B.1. One end is supported by a ball bearing that will for later experiment allow the shaft to swivel about the bearing whereas the other end is constrained. It is preferable to build separate supporting stands on the mounting base so that they can be retrofitted conveniently in later stages. A shaft encoder or resolver is attached at the swivelled end for sensing the rotor speed and position (resolver only). The encoder or resolver needs a spring tether to mount on the stand so that the shaft is allowed to vibrate or move sideways or up and down. This "floating" mount configuration is common in conventional motor applications to eliminate bearing loads, wear and maintenance.

The shaft of the self-bearing motor is mechanically coupled to a standard dynamometer to facilitate measurement of speed, current and torque. Any conventional control systems can be used to drive the motor. However, the information about speed, rotor orientation and motor current or motor flux density must be made available for lateral force control in the next phase of the experiment. Only after a successful test on torque production should its lateral force capability be examined.

The control system described in chapter 8 can be used to investigate the lateral force production of the bridge connection. At the stator end strain gauges or load cells are attached to the mechanical bearing assembly so that force generated by the stator can be measured. Static force production should be first assessed by injecting levitation currents in relation to the rotor orientation and the corresponding force is measured. No motor current is provided at this point and force is generated by utilising the field contributed by the

permanent magnets alone. Since the rotor is fixed by the bearings, the feedback loop for rotor stabilisation control is not needed.

A net lateral force in any arbitrary direction at any rotor orientation must be also tested. Another useful experiment to be conducted is to fix the magnitude and phase of the lateral force currents while the running the machine as a motor. This causes the generated force to whirl around the bearing and the locus of this whirling force measured by the strain gauges could provide information about the characteristics of the self-bearing motor.

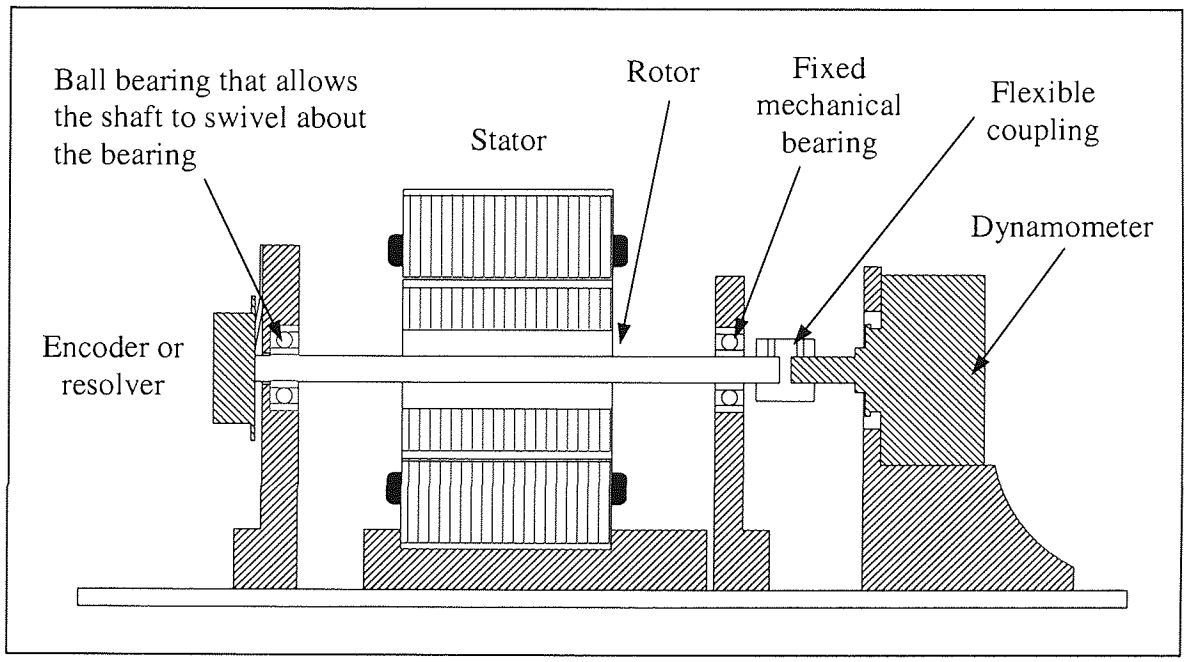

Figure B.1: Test rig for testing the speed and torque of the prototype self-bearing motor.

B.2 A two degree-of-freedom self-bearing motor

The reasons for constructing a two degree-of-freedom prototype are: to familiarise and validate the preliminary design before proceeding to the actual five degree-of-freedom self-bearing motor. Figure B.2 illustrates a two degree-of-freedom self-bearing motor. One end of the rotor is constrained by the ball bearing mentioned earlier while the other is free to move within the air gap limited by the backup mechanical bearing. A backup bearing has a smaller clearance than the air gaps of the self-bearing motor and is used to prevent the rotor from making contact with the stator during catastrophic failure of the control system. Proximity sensors for measuring the rotor displacement are located at the stator end. The philosophy behind this arrangement is that if one stator can operate as a self-bearing motor, then in principle, the full machine with two separate stators will also work.

This particular assembly must be verified to have the characteristics of a self-bearing motor i.e. active control of lateral force and torque is executed simultaneously. A feedback control scheme suggested in chapter 7 may be employed for this purpose. Implementation of a PID controller is preferable at the early stage of control system design. Once the simple controller performs adequately, advanced control methods may be attempted. Experimental tests should include: running the machine unloaded; with static load; and with transient load. Mechanical load can be put on the motor in several ways. An impeller for a bearingless pump might be mounted on the end of the shaft in an overhanging fashion. Alternatively a flexible coupling could be used to connect to a dynamometer or other load with fixed conventional or magnetic bearings. The flexible coupling may give some support to the shaft but that support may be low enough.

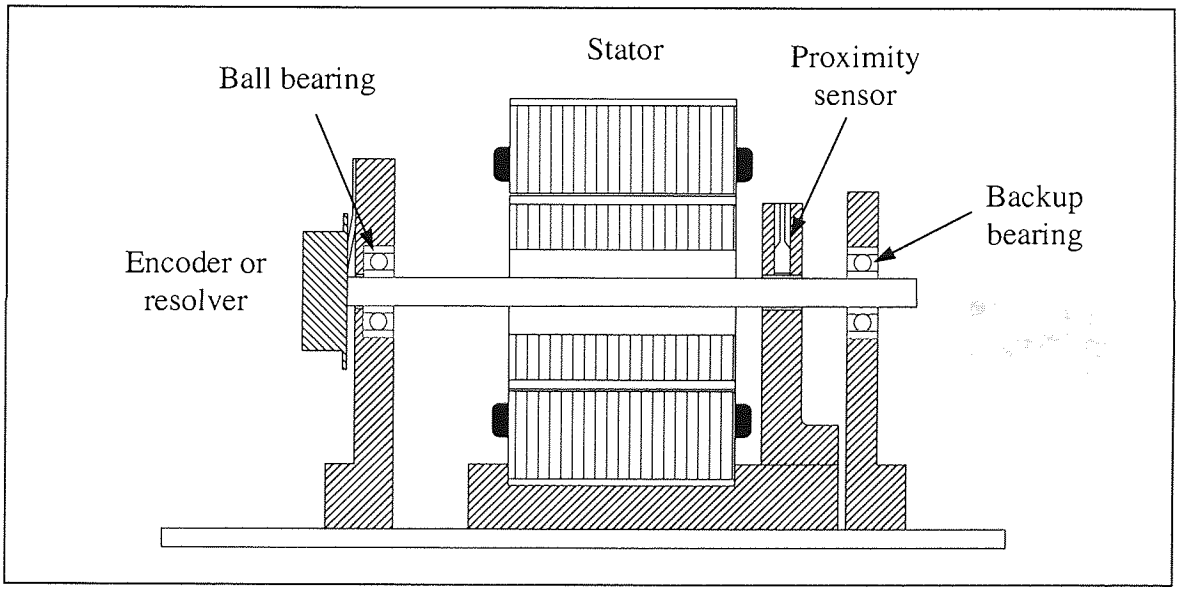

Figure B.2: A two degree-of-freedom self-bearing motor.

B.3 A five degree-of-freedom self-bearing motor

Having constructed and tested the two degree-of-freedom test rig, it can then be augmented into a five degree-of-freedom self-bearing motor. The whole assembly comprises two separate self-bearing stators, a single shaft with two segments of rotor and an axial magnetic bearing. Alternatively, a passive method may be employed to control the movement of the rotor in the axial direction. One stator can be offset angularly by half a pole pitch with respect to the other to reduce the effect of cogging torque.

Both stators of the self-bearing motor can be connected in parallel to a single motor inverter or, if two units of motor inverter are required, then both must be synchronised to produce the same torque. The control of lateral force, however, requires two sets of bearing inverters so that both stators can be controlled independently. Torque performance of the machine can be evaluated by employing a dynamometer as before. Likewise, the lateral force control strategy accomplished in the previous test rig can be also implemented in the present self-bearing motor assembly.

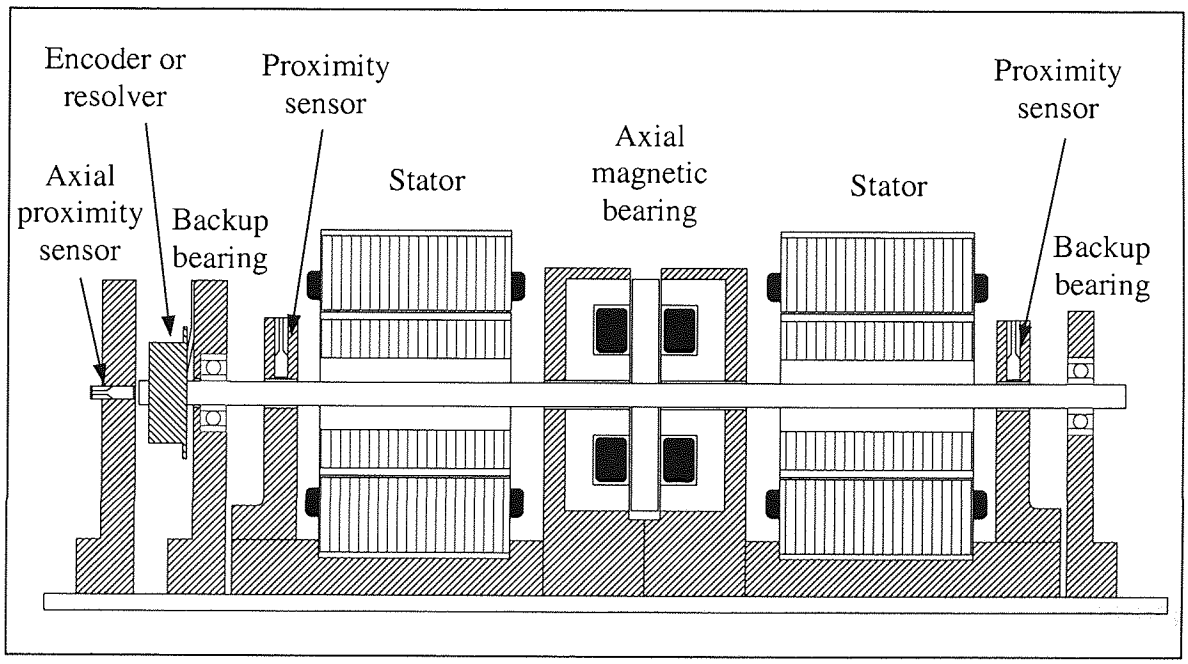

Figure B.3: A five degree-of-freedom self-bearing motor.

APPENDIX C

MORE FINITE ELEMENT RESULTS

This appendix supplements the finite element results discussed in the main chapters and covers: torque ripple; lateral force ripple and cogging torque; 2D flux plots of a rotating rotor; flux density contour plots; and force due to saliency.

C.1 Torque ripple

Torque ripple arises as a result of the interaction between the magnet and the space-harmonics of the winding arrangement and the current harmonics from the power supply. Such an electromagnetic torque fluctuation is undesirable because it generates vibration, acoustic noise and speed fluctuation in the motor. By definition,

$$\text{Torque ripple} = \frac{T_{Max} - T_{Min}}{T_{Max}} \qquad \text{(C.1)}$$

Figure C.1 shows the simulated torque ripple of a self-bearing motor without considering the effect of eddy currents. The resulting torque ripple is about 13.5 %.

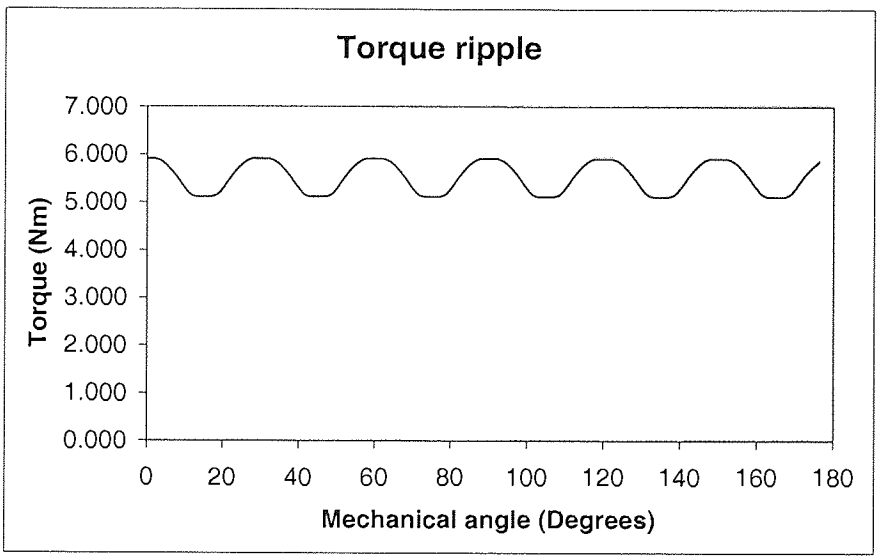

Figure C.1: Torque ripple.

C.2 Lateral force ripple

Force ripple occurs in self-bearing motors when there is a variation in the air gap permeance due to the slotting effect of the stator and rotor. It can be evaluated by taking the difference between the minimum and maximum force divided by the maximum force, i.e.

$$\text{Force ripple} = \frac{F_{Max} - F_{Min}}{F_{Max}} \tag{C.2}$$

In figure C.2 for example, the force ripple is 5.37 %.

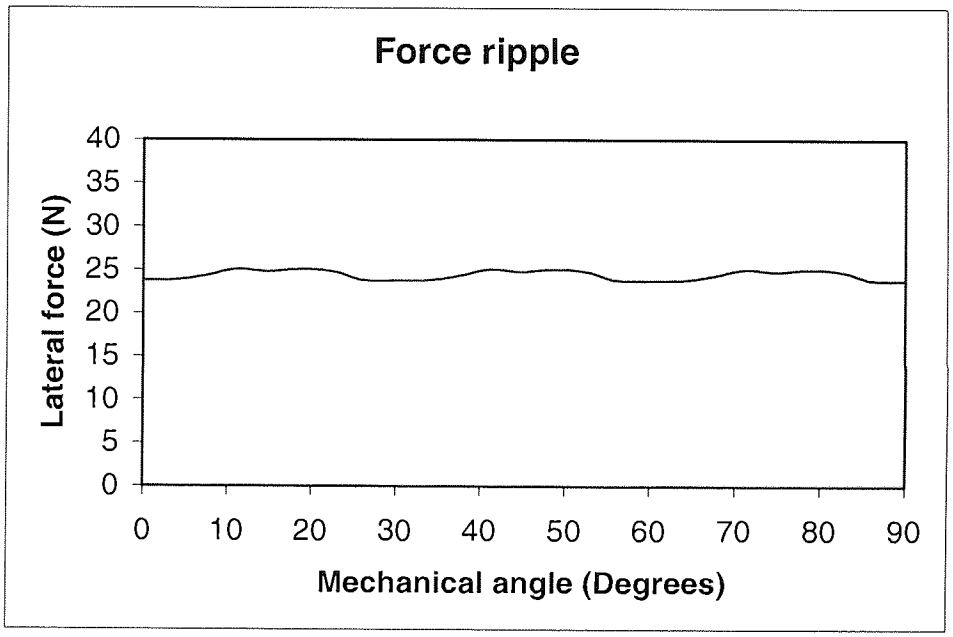

Figure C.2: Force ripple.

C.3 Cogging torque

Cogging torque is an oscillatory effect caused by the interaction of the permanent magnets and the slotted electromagnetic structure. There exists a natural tendency for the rotor to align itself to the stator in a particular direction so as to maximise the permeance experienced by the magnets. Figure C.3 shows the computed cogging torque for the self-bearing motor studied in this thesis. Accordingly the maximum cogging torque is found to be 0.186 Nm.

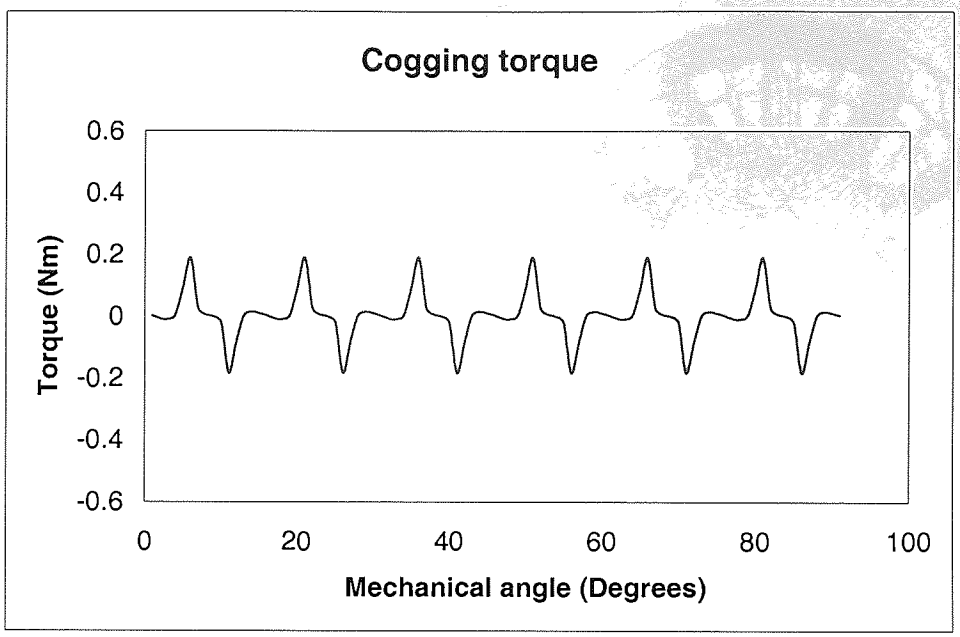

Figure C.3: Cogging torque.

C.4 2D flux plots of a rotating rotor

Some examples of how flux varies when there is relative angular displacement between the stator and the rotor are shown below for reference in figures C.4 – C.6. At present there is no performance indication deducible from examination of these diagrams.

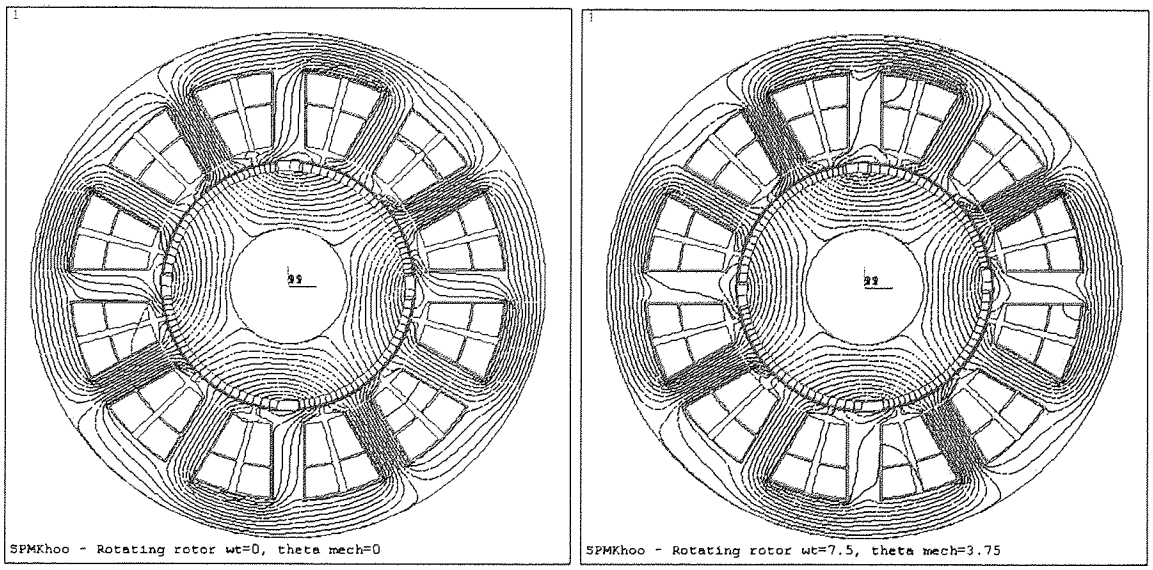

Figure C.4: 2D flux plot at rotor positions 0° and 3.75°.

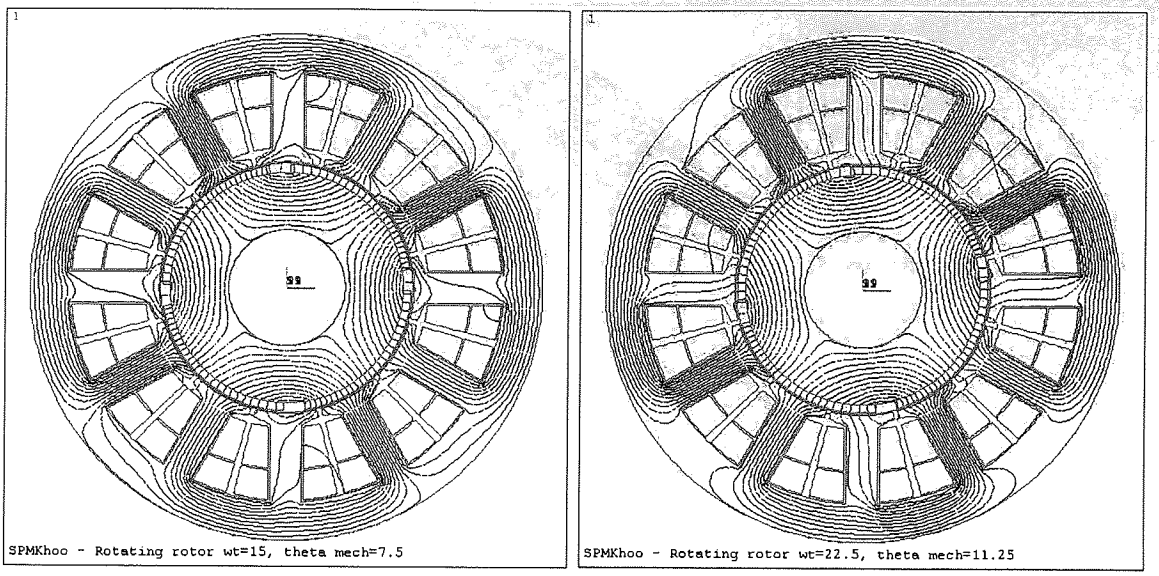

Figure C.5: 2D flux plot at rotor positions 7.5° and 11.25°.

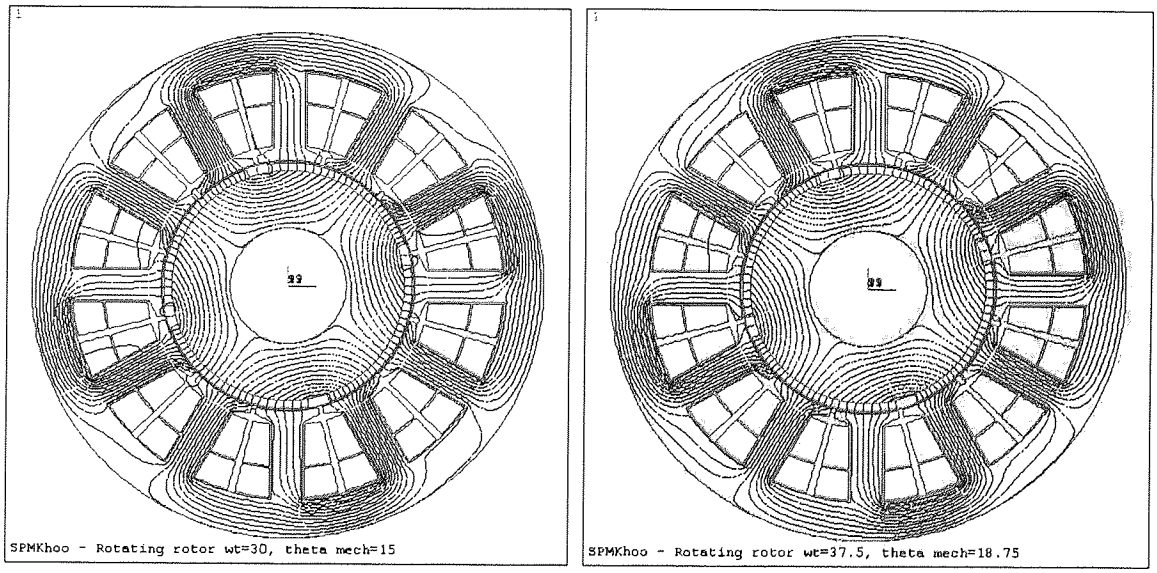

Figure C.6: 2D flux plot at rotor positions 15° and 18.75°.

C.5 Flux density contour plots

In chapter 5 the FEA results show that force and torque computed in the linear analyses are greater than that of non-linear analyses. It is evident from figures C.7 and C.8 that there is a considerable discrepancy between a linear and a non-linear flux density contour plot although both have the same excitation. The maximum flux density in the former is about 4 T whereas the latter is approximately 1.8 T. This difference is due to the fact that magnetic saturation is neglected in the linear analyses.

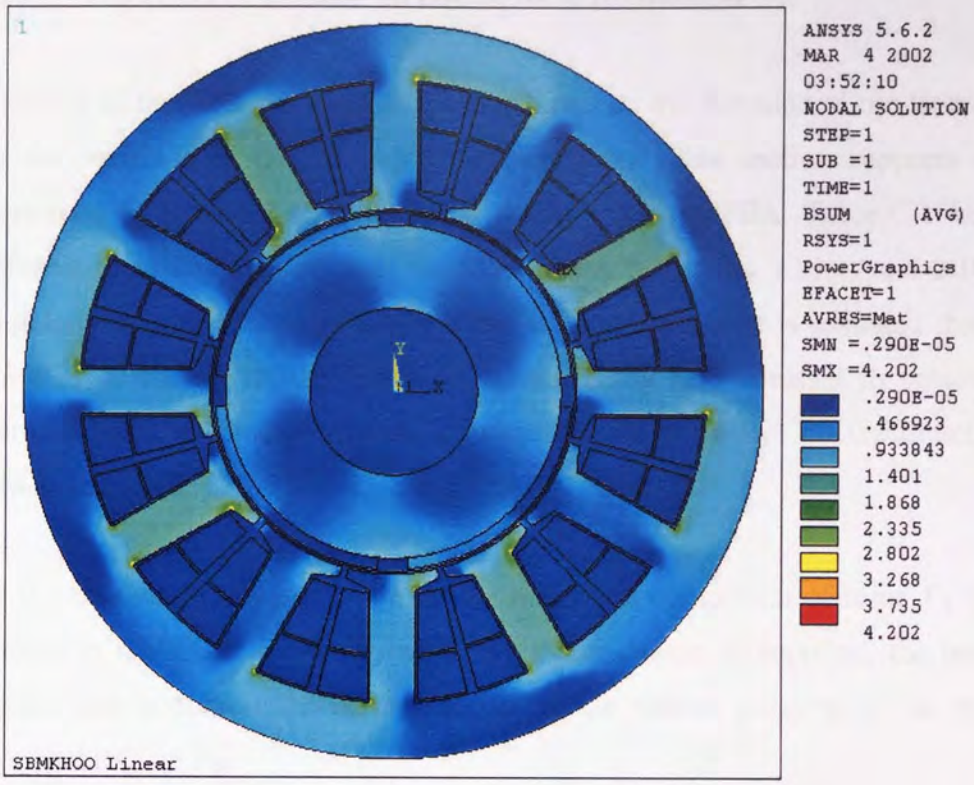

Figure C.7: Flux density contour plot of a linear analysis with 12 A motor current and 0.3A levitation current.

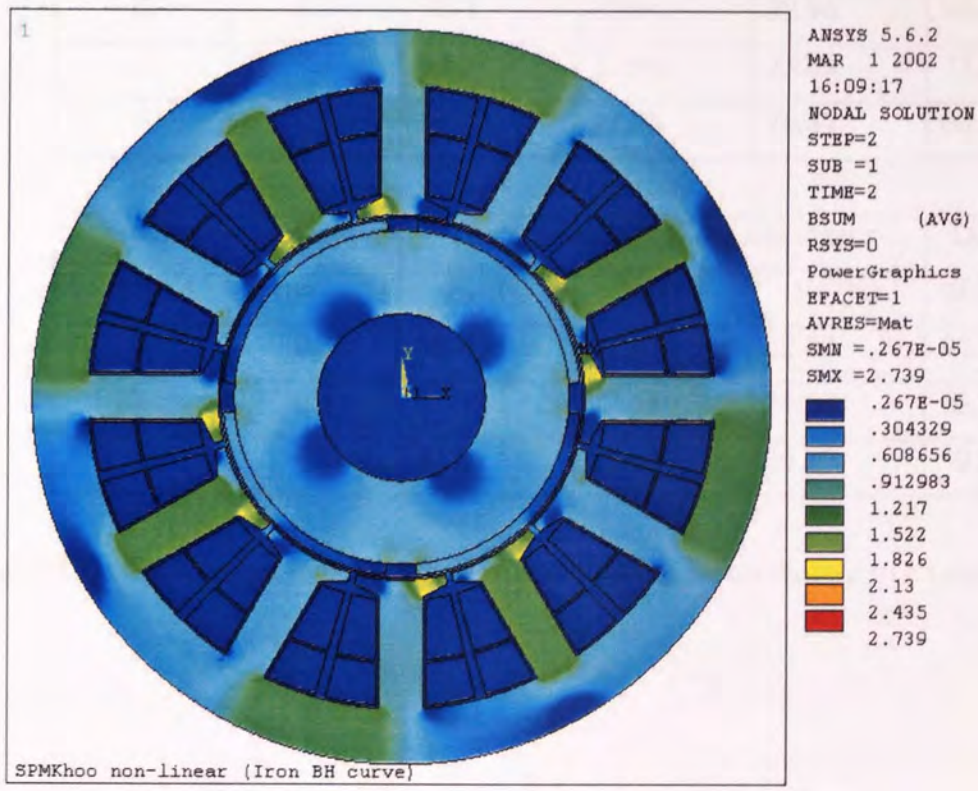

Figure C.8: Flux density contour plot of a non-linear analysis with 12 A motor current and 0.3A levitation current.

C.6 The effect of saliency on lateral force production

Saliency in the rotor can have an adverse effect on the direction of the lateral force because of the variation in the air gap reluctance paths. This section supports what has been described in section 3.4.2 with some results from the FEA. Table C.1 below should be referred to in conjunction with the illustrations in figures 3.10(a) and 3.10(b). The rotor angular position is fixed throughout the simulations and it is assumed that a net vertical force is desired. With the levitation current being held constant to achieve the required vertical force, the motor current is increased and the effect on the direction of force is observed.

In the absence of the motor current the horizontal component of force F_X is negligible, as shown in table C.1. However, when the motor current is supplied, the interaction of the motor and levitation fluxes that occurs at the salient poles give rise to a substantial horizontal force F_X.

Motor current (A)	Levitation current (A)	Force by virtual work method			Direction of force (°)
		F_X (N)	F_Y (N)	F_R (N)	
0	0.3	5E-4	22.96	22.96	90.00
2	0.3	6.603	22.96	23.89	73.96
4	0.3	13.205	22.96	26.87	60.10

Motor current (A)	Levitation current (A)	Force by Maxwell's stress tensor			Direction of force (°)
		F_X (N)	F_Y (N)	F_R (N)	
0	0.3	5E-4	22.63	22.63	90.00
2	0.3	6.535	22.63	23.50	73.89
4	0.3	13.07	22.63	26.29	59.99

Table C.1: Variation of force direction with increasing motor current in a salient pole rotor.

APPENDIX D

FINITE ELEMENT SIMULATION USING ANSYS

A brief description of how a self-bearing motor may be modelled in 2D using ANSYS is described. While the techniques presented here may not be the most efficient, they sufficed to produce the results presented in this thesis. Major steps commonly used in FEA include model creation, boundary conditions, solution and post-processing. Working with ANSYS is flexible where simulations can be performed through composing macros or using a graphical user interface (GUI) or a combination of both methods.

D.1 Model creation

Keypoints are first defined in the global co-ordinate system. They are then connected by lines to form areas. It is possible to bypass the creation of keypoints and lines by creating the areas at the outset. Various ways of creating the areas may be employed. One way is to create pieces of area overlapping on top of one another and forming the overall geometry of the motor. A preferred method is to create a slice of the motor first which is then reflected and copied in a polar manner to form a complete geometry. To facilitate the rotation of the rotor relative to the stator, both components are created as separate entities with the air gap serving as the sliding interface.

Before meshing is executed, the areas must be assigned with the appropriate material properties listed in table 9.3 of chapter 9. This includes the real constants of the coils such as cross-sectional area, number of turns, length, direction of current and coil fill factor. If a non-linear analysis is required then B-H curves, such as the one shown in figure 5.8, must be defined for the materials. Typically, B-H curves for ferromagnetic materials are a necessity but for rare earth magnets, a linear approximation may be assumed where only the relative permeability and coercive force (a vector quantity) are needed. The manner in which the magnet is magnetised is determined by its coordinate system and direction of coercive force. For radially magnetised magnets, a single element coordinate system and two material numbers are required to account for radially inwards and radially outwards magnetisation. If parallel magnetisation is required, a single material number may be used but each magnet must have its own element coordinate system.

Meshing can be generated through the automatic smartsizing option or custom defined by the user. Figure D.1 shows examples of the generated mesh. The FEA model on the right has a finer mesh and considerably more elements. Thus, it is more accurate but computationally more expensive than the one in the left. To obtain an accurate result the air gap region must have a finer discretisation in comparison to other areas of the model. The air gap is divided into two circumferential halves by the sliding interface; the inner half is fixed to the rotor while the outer half is fixed to the stator. Each half has two layers of air element thereby giving a total of four layers in the air gap. Both stator and rotor are defined as two separate element components and are joined later so that there is no discontinuity at the sliding interface (See section D.2).

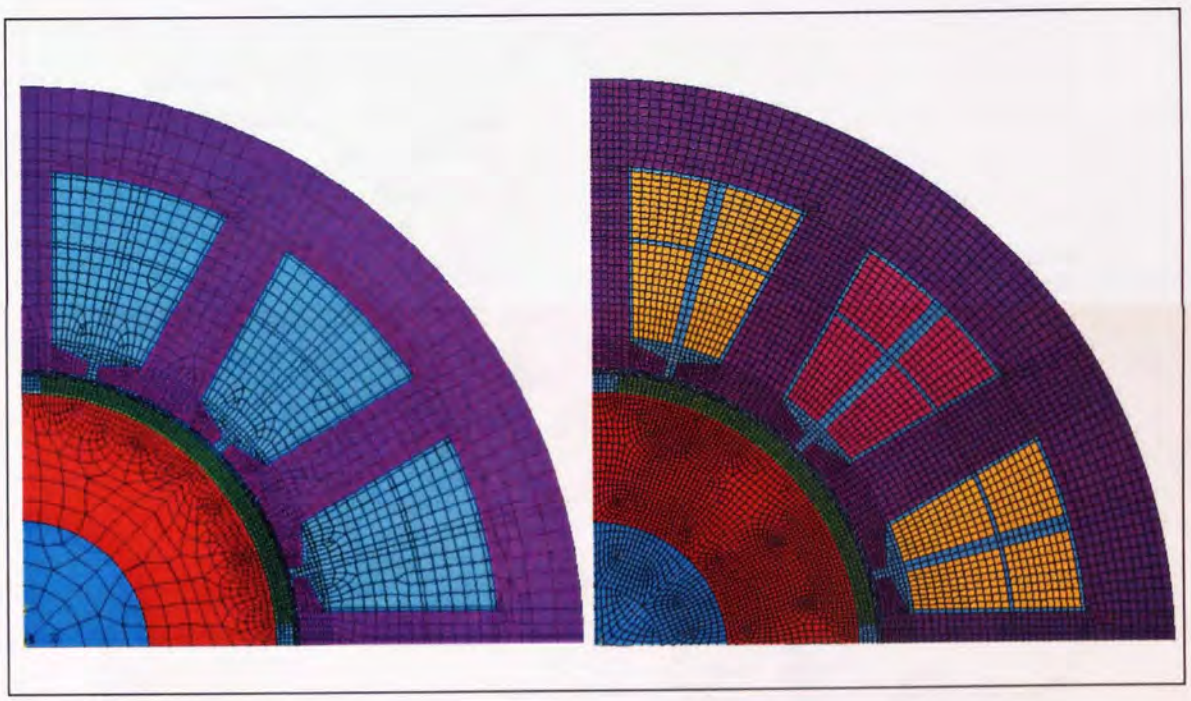

Figure D.1: Examples of finite element mesh.

Irregular shapes can sometimes lead to unsatisfactory meshing and warnings will be generated for serious deformity of areas. If solving proceeds without correcting the poor meshes, the results may be erroneous. Under such a circumstance, it is up to the user to decide whether the results are acceptable. For instance, a meshing warning generated for a few elements in the stator back iron might have negligible effect in the overall computation. However, if the elements in the air gap contain errors then the results might be badly misleading.

To simulate electromagnetic-circuit problems, external electric circuits are directly coupled to the coil areas in the finite element domain. Circuit elements such as stranded coils and current sources are created using the circuit builder. Each stranded coil element is coupled to a single node of each coil side in the FEA domain. This particular node as well as the nodes within each coil side must then be coupled in the current and EMF degrees of freedom to enforce conservation of current and to simulate the uniform distribution of the winding. For example, the simulated self-bearing motor has 48 coil sides in the stator and so a total of 48 coupled coil elements are required as shown in figure D.2. If each coil side requires two coupled set numbers of current and EMF degrees of freedom then a total of 96 unique coupled sets are required. The symbol for couple sets is depicted in figure D.3.

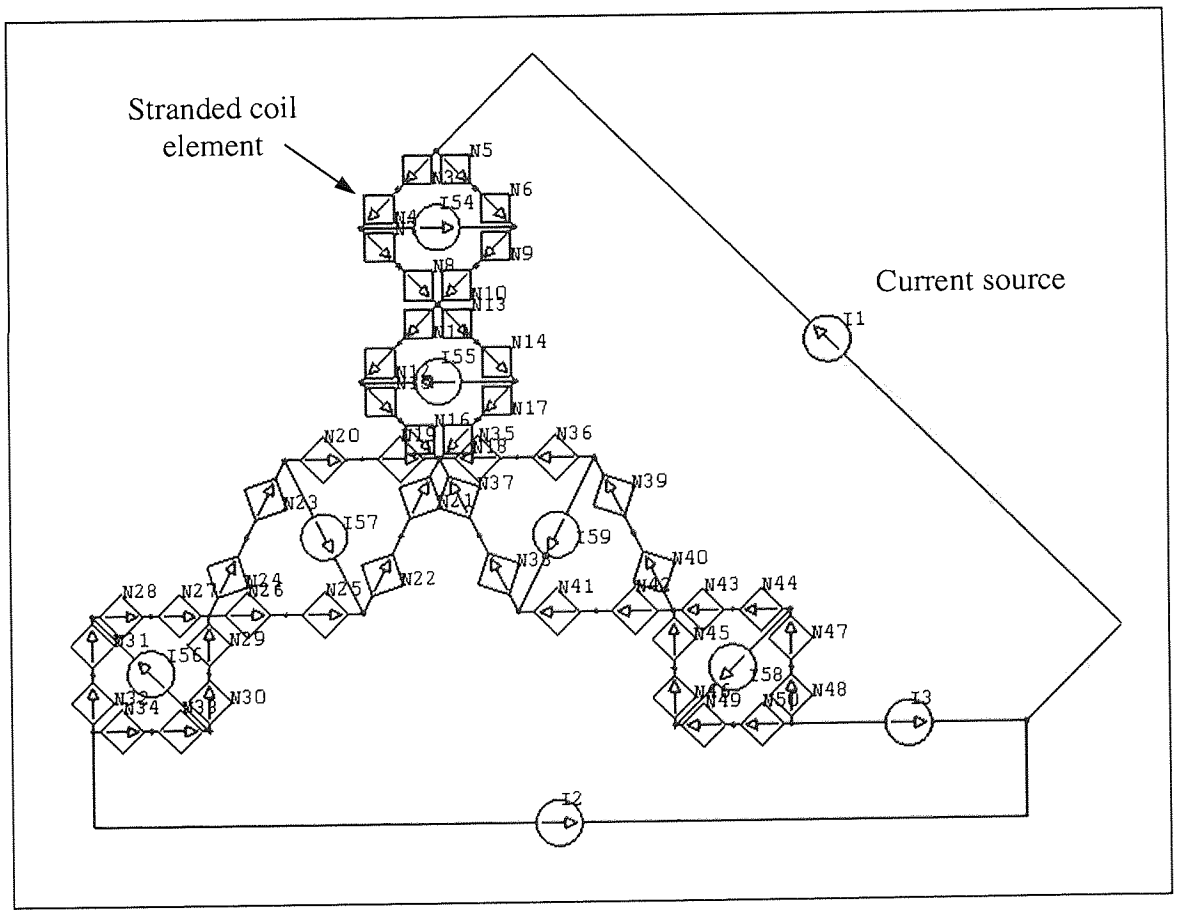

Figure D.2: 2D circuit coupled elements.

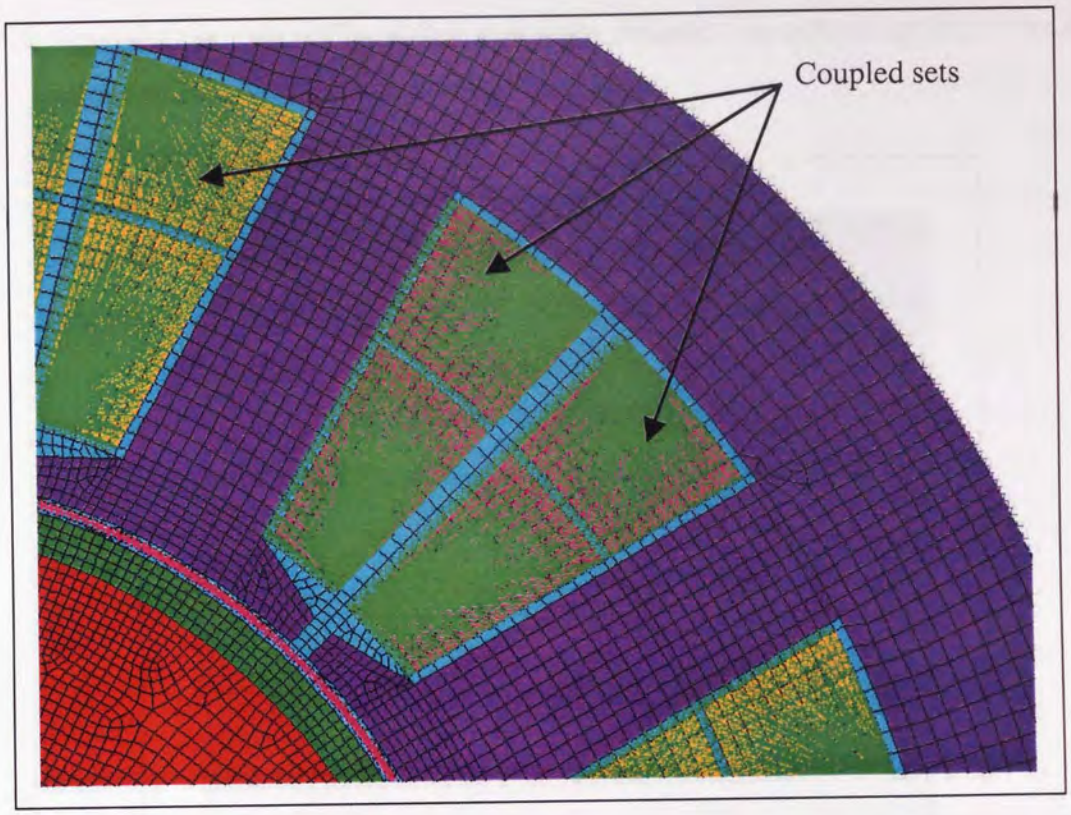

Figure D.3: Current and EMF degrees of freedom coupled sets.

D.2 Boundary conditions and loads

A few boundary conditions are needed in the finite element model before invoking the solution.

- The flux parallel condition must be applied at the exterior of the stator so that flux is forced to flow in parallel to the surface boundary.

- To initiate computation of force and torque, magnetic flags for the virtual work and Maxwell's stress tensor must be applied to the rotor component with its attached air elements removed. A condition to be fulfilled prior to applying the flag is that the rotor component must be surrounded by at least a layer of air gap elements.

- Since the stator and rotor components are built independently, there is a discontinuity of nodes along the sliding interface which prevents the flux from traversing across the air gap. Another boundary condition is required here where the constraint equations generator is used to formally connect the mismatched nodes at

the sliding interface. Figure D.4 shows the constraint equations applied at the stator-rotor interface.

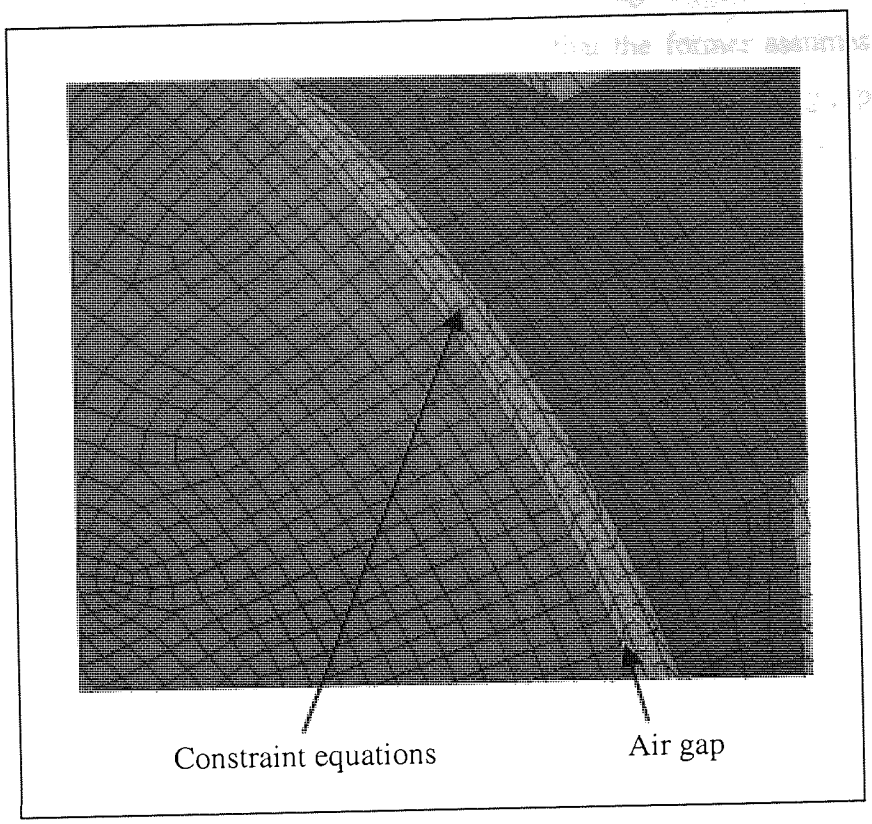

Figure D.4: Constraint equations joining nodes at the mid air gap radius.

Instead of applying the loads in terms of current density in the finite element domain, coupled-field analyses allow loads to be applied directly from the current source elements. Levitation currents are applied according to equation (5.14) whereas motor currents are supplied such that the phase coils produce a flux distribution described by equation (5.4). The final load required is the ground node applied to the circuit.

D.3 Solution

In the solution section, the user specifies the type of analysis required namely, static, harmonic or transient depending on the nature of the problem. By default the frontal solver option is selected (in ANSYS 5.6) irrespective of the type of analysis because it is recommended for most 2D applications. Both linear and non-linear simulations are permitted.

Static magnetic analysis simulates the steady flow of direct currents and does not consider time-varying effects such as eddy currents. On the other hand, harmonic and transient analyses calculate the effects of time-varying current or voltage excitations including eddy currents. The difference between the two, however, is that the former assumes sinusoidal excitations whereas the latter is used for non-sinusoidal inputs, for e.g., pulse width modulation and stepped changes in voltage. Solution control such as frequency range, stepped or ramped loading, etc. must be set for both harmonic and transient analyses before solving. Permanent magnets are not permitted in harmonic analysis. Thus, for calculation of power loss permanent magnets are removed leaving only the air gap between the stator and rotor.

D.4 Post-processing

The final process involves extracting graphical information or numerical results from the finite element analysis. Generated plots such as flux density contour, flux density vector and 2D flux plots are crude but they are a most useful means to check the reasonableness of the solution. Usually, if the boundary conditions or loads were incorrectly specified, the resultant errors can be spotted quickly from a cursory inspection of these plots. A 2D flux plot, for example, is useful to give an overall picture of how flux is flowing or constrained within the model. In addition it also gives clues for estimating leakage flux and calculating leakage permeance. To enhance this observation, a vector plot can display the direction and magnitude of the flux density in the form of arrows with varying colour bands. The contour plot provides coloured filled zones to indicate and pinpointing the level of local saturation in the model. An example of a vector plot is shown in figure D.5 below. More 2D flux plots and flux density contour plots can be found in appendix C.

When the graphical plots are satisfactory we proceed to extract numerical results. As far as a self-bearing motor is concerned the most important results of interest are force and torque; both computed from the virtual work and Maxwell's stress tensor methods. The path operations feature is a powerful tool that allows the user to observe the variation of flux density or intensity along any predefined paths in the model. Flux density plots around the periphery of the air gap in figures 5.9(a)-(c) are plotted using this feature. Other available results include calculation of resistance, power loss, current, EMF, energy, etc. Coil

inductances are computed using a macro called LMATRIX after a nominal solution has been performed about an operating point.

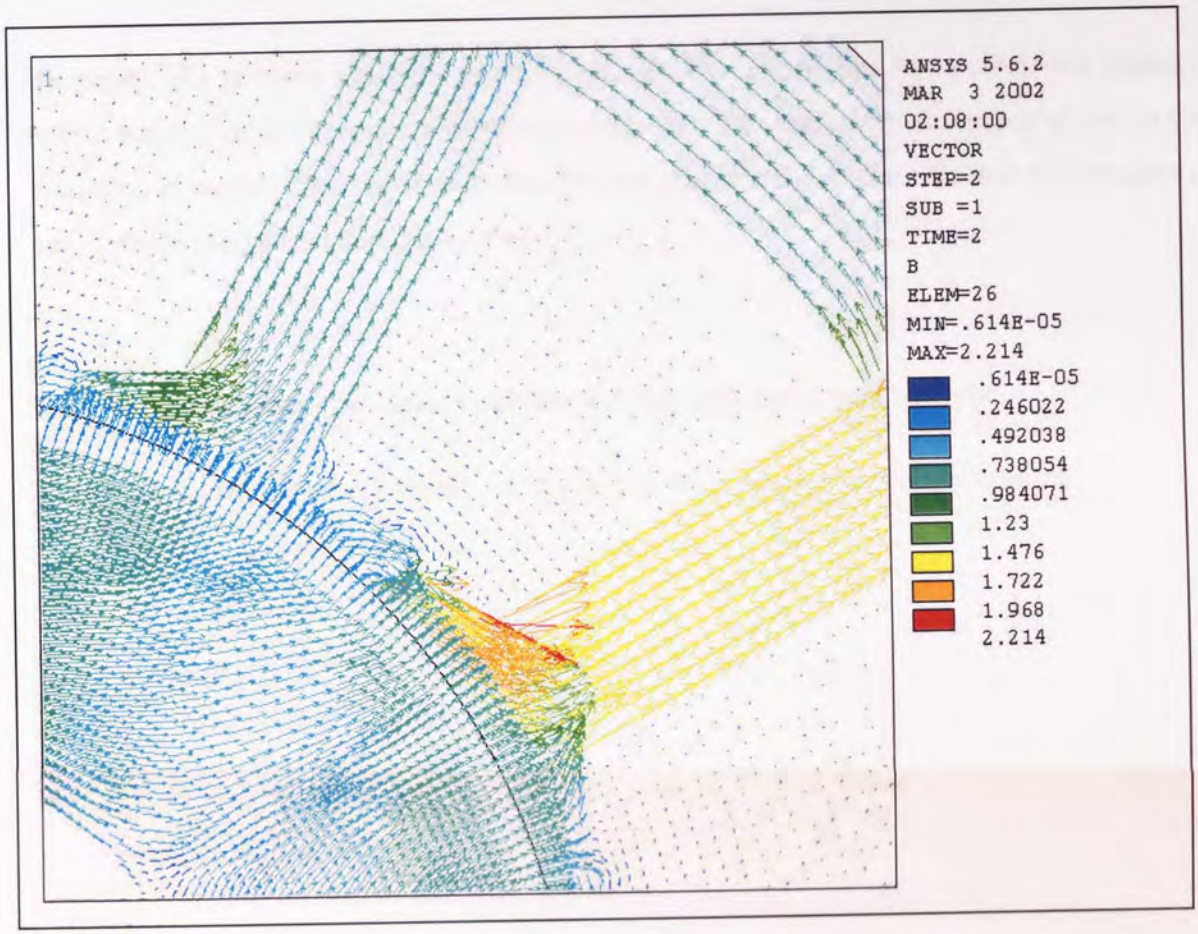

Figure D.5: An example of flux density vectors in a self-bearing motor.

APPENDIX E

MATLAB SCRIPTS FOR CALCULATING FORCE AND POWER LOSS

This appendix contains a sample program listing written in Matlab to calculate the approximate lateral force considering rotor eccentricity and power loss due to the excitation of the motor and levitation currents. The reader is invited to read chapters 5 and 6 for further information about lateral force production and power loss.

E.1 Approximate calculation of lateral force with rotor eccentricity

```
% APPROXIMATE LATERAL FORCE CALCULATION DUE TO ROTOR ECCENTRICITY
% See Chapter 5
% 4-pole motor field and 2-pole levitation field
% 12 slots stator
clear
% Constants
Uo=4*pi*1e-7;           % Permeability of free space
R=0.030;                % Rotor radius
L=0.1;                  % Rotor length
N=60;                   % Number of turns
go=0.8e-3;              % Nominal air gap
%
% Permanent magnet:
Hm=680000;              % Coercive MMF
Lm=0.002;               % Thickness of permanent magnet
Bo=0.95;                % Residual flux
Um=Bo/Hm;               % Permeability of permanent magnet
Ap=2*pi*(R+Lm)*L/12;    % Approximate pole area
%
% Variables:
Immax=3;                % Maximum motor current (parallel)
Ilmax=0.15;             % Maximum levitation current (parallel)
gx=0;                   % Displacement in x-direction
gy=0;                   % Displacement in y-direction
wt=0;                   % w = frequency; t = time
Phi=90;                 % Electrical torque angle (IMPORTANT !!)
Gm=90;                  % Direction of force required
%
% Air gap, g = go - x*cos(theta) - y*sin(theta)
for n=1:1:12;
   g(n)=go-gx*cos((pi/6)*(n+2))-gy*sin((pi/6)*(n+2));
end
%
% Flux due to PERMANENT MAGNET:
%
% Reluctance matrix (PM)
% g(1),g(4),g(7),g(10) - Air gap under phase "a" coils
% g(2),g(5),g(8),g(11) - Air gap under phase "c" coils
% g(3),g(6),g(9),g(12) - Air gap under phase "b" coils
%
for n=1:1:12;
   Rpm(n)=g(n)/Uo+Lm/Um;
```

```
end
%
Reluc_pmA=[Rpm(1)   -Rpm(4)     0          0
           0        Rpm(4)   -Rpm(7)      0
           0          0        Rpm(7)   -Rpm(10)
           1          1          1          1     ];
%
Reluc_pmC=[Rpm(2)  -Rpm(5)      0          0
           0        Rpm(5)    -Rpm(8)     0
           0          0         Rpm(8)   -Rpm(11)
           1          1          1          1      ];
%
Reluc_pmB=[Rpm(3)   -Rpm(6)     0          0
           0         Rpm(6)   -Rpm(9)     0
           0          0         Rpm(9)   -Rpm(12)
           1          1          1          1      ];
%
zero=zeros(4,4);
%
Reluc_pm=[Reluc_pmA     zero       zero
          zero     Reluc_pmC     zero
          zero       zero     Reluc_pmB];

% Equivalent MMF drop
%
for n=1:1:3
   MMFpm_A(n,:)=(2*Bo*Lm/Um)*sin((2*90*n-wt)*pi/180);
   MMFpm_C(n,:)=(2*Bo*Lm/Um)*sin((2*((90*n)+30)-wt)*pi/180);
   MMFpm_B(n,:)=(2*Bo*Lm/Um)*sin((2*((90*n)+60)-wt)*pi/180);
end
MMFpm=[MMFpm_A; 0; MMFpm_C; 0; MMFpm_B; 0];
%
% Flux due to permanent magnets:
Bpmm=inv(Reluc_pm)*MMFpm;
%
% Rearranging the elements according to the defined angle theta
Bpm =[Bpmm(4); Bpmm(8); Bpmm(12); Bpmm(1);
      Bpmm(5); Bpmm(9); Bpmm(2); Bpmm(6);
      Bpmm(10); Bpmm(3); Bpmm(7); Bpmm(11)];
%
figure(1);
plot(Bpm);
title('Permanent magnet flux density (Bpm)')
%
% Flux due to MOTOR CURRENT:
%
% Reluctance matrix (Motor current)
%
for n=1:1:12;
   Rmc(n)=(g(n)+Lm)/Uo;
end
%
Reluc_mcA=[Rmc(1)   -Rmc(4)     0          0
           0         Rmc(4)   -Rmc(7)     0
           0          0         Rmc(7)   -Rmc(10)
           1          1          1          1      ];
%
Reluc_mcC=[Rmc(2)  -Rmc(5)      0          0
           0        Rmc(5)    -Rmc(8)     0
           0          0         Rmc(8)   -Rmc(11)
           1          1          1          1      ];
%
Reluc_mcB=[Rmc(3)   -Rmc(6)     0          0
```

```
            0        Rmc(6)   -Rmc(9)     0
            0         0        Rmc(9)   -Rmc(12)
            1         1         1         1      ];
%
zero=zeros(4,4);
%
Reluc_mc=[Reluc_mcA     zero       zero
            zero     Reluc_mcC     zero
            zero       zero     Reluc_mcB];
% MMF drop
%
for n=1:1:3
   MMFmc_A(n,:)=(4*N*Immax)*sin((2*90*n-wt+Phi)*pi/180);
   MMFmc_C(n,:)=(4*N*Immax)*sin((2*((90*n)+30)-wt+Phi)*pi/180);
   MMFmc_B(n,:)=(4*N*Immax)*sin((2*((90*n)+60)-wt+Phi)*pi/180);
end
MMFmc=[MMFmc_A; 0; MMFmc_C; 0; MMFmc_B; 0];
%
% Flux due to motor currents:
Bmcm=inv(Reluc_mc)*MMFmc;
%
% Rearranging the elements according to the defined angle theta
Bmc =[Bmcm(4); Bmcm(8); Bmcm(12); Bmcm(1);
      Bmcm(5); Bmcm(9); Bmcm(2); Bmcm(6);
      Bmcm(10); Bmcm(3); Bmcm(7); Bmcm(11)];
%
figure(2);
plot(Bmc);
title('Motor flux density (Bmc)')
%
% To find the phase compensation required
Bpmmax=max(Bpm);
Bmcmax=max(Bmc);
%
Pd=(atan2((Bmcmax*sin(Phi*pi/180)),(Bpmmax+Bmcmax*cos(Phi*pi/180))))*180/pi;
%
% Flux due to LEVITATION CURRENT:
%
% Test sign
%
if cos(Gm*pi/180)>-0.0001&cos(Gm*pi/180)<0.0001
      tsign1=0;
   else
      tsign1=sign(cos(Gm*pi/180));
end
if sin(Gm*pi/180)>-0.0001&sin(Gm*pi/180)<0.0001
      tsign2=0;
   else
      tsign2=sign(sin(Gm*pi/180));
end
%
% Maximum levitation flux components:
IlevXm=(Ilmax/sqrt(1+(tan(Gm*pi/180))^2))*tsign1;
IlevYm=(sqrt((Ilmax)^2-(IlevXm)^2))*tsign2;
%
% Reluctance matrix (Levitation current)
% g(1),g(7) - coils A1, g(2),g(8) - coils C2, g(3),g(9) - coils B1,
% g(4),g(10) - coils A2, g(5),g(11) - coils C1, g(6),g(12) - coils B2.
%
for n=1:1:12;
   Rlev(n)=(g(n)+Lm)/Uo;
end
%
```

```
Reluc_levA1=[Rlev(1)  -Rlev(7)
             1          1    ];
%
Reluc_levC2=[Rlev(2)  -Rlev(8)
             1          1    ];
%
Reluc_levB1=[Rlev(3)  -Rlev(9)
             1          1    ];
%
Reluc_levA2=[Rlev(4)  -Rlev(10)
             1          1     ];
%
Reluc_levC1=[Rlev(5)  -Rlev(11)
             1          1     ];
%
Reluc_levB2=[Rlev(6)  -Rlev(12)
             1          1     ];
%
zero=zeros(2,2);
%
Reluc_lev=[Reluc_levA1  zero      zero      zero      zero      zero
           zero   Reluc_levC2  zero      zero      zero      zero
           zero      zero   Reluc_levB1  zero      zero      zero
           zero      zero      zero   Reluc_levA2  zero      zero
           zero      zero      zero      zero   Reluc_levC1  zero
           zero      zero      zero      zero      zero   Reluc_levB2];
%
% MMF DROP
%
% x-direction component:
for n=1:1:6
   MMFlevxx(n,:)=(4*N*IlevXm)*sin(((60+30*n)-wt+Pd)*pi/180);
end
MMFlevx=[MMFlevxx(1); 0; MMFlevxx(2); 0; MMFlevxx(3); 0;
         MMFlevxx(4); 0; MMFlevxx(5); 0; MMFlevxx(6); 0];
%
% Flux due to levitation current in the x-direction:
Blevx=inv(Reluc_lev)*MMFlevx;
%
% Rearranging the elements according to the defined angle theta
Blev_x=[Blevx(8); Blevx(10); Blevx(12); Blevx(1); Blevx(3); Blevx(5);
        Blevx(7); Blevx(9); Blevx(11); Blevx(2); Blevx(4); Blevx(6)];
figure(3);
plot(Blev_x);
title('Levitation flux density (Blev_x)')
%
% y-direction component:
for n=1:1:6
   MMFlevyy(n,:)=(4*N*IlevYm)*cos(((60+30*n)-wt+Pd)*pi/180);
end
MMFlevy=[MMFlevyy(1); 0; MMFlevyy(2); 0; MMFlevyy(3); 0;
         MMFlevyy(4); 0; MMFlevyy(5); 0; MMFlevyy(6); 0];
%
% Flux due to levitation current in the y-direction:
Blevy=inv(Reluc_lev)*MMFlevy;
%
% Rearranging the elements according to the defined angle theta
Blev_y=[Blevy(8); Blevy(10); Blevy(12); Blevy(1); Blevy(3); Blevy(5);
        Blevy(7); Blevy(9); Blevy(11); Blevy(2); Blevy(4); Blevy(6)];
figure(4);
plot(Blev_y);
title('Levitation flux density (Blev_y)')
%
```

```
% Force in the x-direction
   =(Ap/2Uo)*[(Bpm+Bmc)^2+2(Bpm+Bmc)*(Blev_x)+(Blev_x)^2]*cos(theta)
%
for n=1:1:12
   Fx1(n)=((Bpm(n)+Bmc(n))^2)*cos(pi*(n-1)/6);
   Fx2(n)=(Bpm(n)+Bmc(n))*Blev_x(n)*cos(pi*(n-1)/6);
   Fx3(n)=(Blev_x(n))^2*cos(pi*(n-1)/6);
end
Fx_total=(Ap/(2*Uo))*(sum(Fx1)+2*sum(Fx2)+sum(Fx3))
%
% Force in the y-direction %
%  =(Ap/2Uo)*[(Bpm+Bmc)^2+2(Bpm+Bmc)*(Blev_y)+(Blev_y)^2]*sin(theta)
%
for n=1:1:12
   Fy1(n)=((Bpm(n)+Bmc(n))^2)*sin(pi*(n-1)/6);
   Fy2(n)=(Bpm(n)+Bmc(n))*Blev_y(n)*sin(pi*(n-1)/6);
   Fy3(n)=(Blev_y(n))^2*sin(pi*(n-1)/6);
end
Fy_total=(Ap/(2*Uo))*(sum(Fy1)+2*sum(Fy2)+sum(Fy3))
```

E.2 Power loss calculation

```
% POWER LOSS CALCULATION
% See Chapter 6
%
clear
Immax=1;        % Parallel current of a bridge
Ilmax=0.15;     % Parallel current of a bridge
N=60;           % No. of turns
L=0.1133;       % Conductor length
p=0.3e-7;       % Resistivity
Rw=0.4e-3;      % Radius of individual conductor
wt=0;           % Frequency
phi=90;         % Torque angle
Pd=0;           % Phase compensation
Gm=90;          % Direction of force required
Ncs=4;          % No. of coil sides per tooth
%
% n is the tooth number (refer stator diagram)
% Motor current
for n=1:12
   Im(n)=Immax*sin(pi*(n+2)/3+(-wt+phi)*pi/180);
end
% Levitation current
for n=1:12
   Ilev(n)=Ilmax*sin(pi*(n+2)/6+(-wt+Pd+Gm)*pi/180);
end
% Total current
for n=1:12
   I(n)=(Im(n))^2+(Ilev(n))^2-2*Im(n)*Ilev(n)*cos((1-Gm/180+(n+2)/6- ...
        Pd/180+phi/180)*pi);
end
%
% Resistance in one coil side
R=p*L*N/(pi*(Rw)^2);
%
% Total losses
P=I*R*Ncs/2;
fprintf('Total power loss = %d\n', sum(P));
```